Project Final Report

Catalytic Upgrading of Carbohydrates in Waste Streams to Hydrocarbons

Paper Sludge to Fuel Project (PStF)

Federal Agency and Organization	Department of Energy EERE - BETO
Agreement Number:	EE0008498
WBS Number:	2.3.1.210
Project Title:	Catalytic Upgrading of Carbohydrates in Waste Streams to Hydrocarbons
Project PI:	Sunkyu Park, Professor, sunkyu_park@ncsu.edu
Submitting Official:	Sunkyu Park, Professor, sunkyu_park@ncsu.edu
Report Submission Date:	January 31, 2023
Recipient Organization:	NCSU
Project Location:	NCSU, NREL, Yale
Period Covered by Report:	Final report
Approved Project Period:	October 1, 2019 – September 30, 2023
Project Officer/Technology Manager:	Beau Hoffman
Project Monitor:	Seth Menter

Acknowledgements

This material is based upon work supported by the U.S. Department of Energy's Office of Energy Efficiency and Renewable Energy (EERE) under the Bioenergy Technology Office Award Number DE-EE0008498.

Disclaimer

Publication (as of May 2024)

- K. Lan, D. Cruz, J. Li, A. Agyei Boakye, H. Park, P. Tiller, A. Mittal, D. Johnson, S Park, Y. Yao, Life Cycle Assessment of Sustainable Aviation Fuel Derived from Paper Sludge, ACS Sustainable Chemistry & Engineering, Accepted (2024) https://doi.org/10.1021/acssuschemeng.4c00795
- Tiller, H. Park, D. Cruz, E. Carrejo, D.K. Johnson, A. Mittal, R. Venditti, S. Park, Techno-Economic Analysis of Biomass Value-Added Processing Informed by Pilot Scale De-Ashing of Paper Sludge Feedstock, Bioresource Technology, 401: 130744 (2024) https://doi.org/10.1016/j.biortech.2024.130744
- H. Park, D. Cruz, P. Tiller, D. Johnson, A. Mittal, H. Jameel, R. Venditti, S. Park, Effect of ash in paper sludge on enzymatic hydrolysis, Biomass and Bioenergy, 165: 106567 (2022) https://doi.org/10.1016/j.biombioe.2022.106567

Four more publications are in preparation

Keywords

Paper sludge, sustainable aviation fuels, wet organic waste, ash removal, dehydration, pulp and paper.

Executive Summary

This research, funded by the Department of Energy Bioenergy Technologies Office (DOE BETO), aims to understand the barriers and assess opportunities for transforming carbohydrates in paper sludge, a solid lignocellulosic residue from the pulp and paper industry. The goal is to turn the paper sludge into a liquid hydrocarbon product that can be blended into jet fuel, both economically and sustainably. Research groups at North Carolina State University, National Renewable Energy Laboratory, and Yale University collaborated synergistically, leveraging their expertise in pulp and paper operations, biomass deconstruction, and catalytic upgrading to propose a pathway that efficiently captures the energy in paper sludge. Findings from this study could potentially contribute to advancing biomass conversion technologies, aligning with the efforts of the U.S. DOE BETO.

This report documents the experimental and simulation results of a biochemical and catalytic pathway designed to transform paper sludge into a liquid hydrocarbon product. The process involves a sequence of seven steps, including ash removal, carbohydrate enzymatic hydrolysis, sugar dehydration, solvent recovery, aldol-condensation between furans and ketone, hydrogenation, and hydrodeoxygenation to obtain a hydrocarbon blend in the ~C10 range. The experimental efforts from the initiation of the project were guided by techno-economic analysis (TEA) and sensitivity analysis results including around seventy-eight operational parameters. This methodology facilitated the efficient use of resources over time. This study relies on detailed process simulations and TEA to determine the minimum fuel selling price (MFSP) for the hydrocarbon fuel product. Preliminary TEA results led to the evaluation of eight case studies considering alternative dehydration co-solvents, operational settings, and biorefinery layouts. Finally, the life cycle assessment of twenty-eight scenarios, comparing various dehydration co-solvents, fuel sources, chemical feedstock sources, side product utilization, and other process settings, was conducted. Landfilling scenarios with and without landfill gas recovery were also estimated, analyzed, and compared.

Paper sludge, mainly composed of lignocellulosic fibers and ash (e.g., calcium carbonate, etc.), is landfilled at a rate of more than 8 million wet metric tons per year (typically 50% moisture content) in the United States, impacting the use of land and representing a cost for the paper mills (~$30/wet mt). Understanding and overcoming the barriers linked to an economically feasible transformation of this material into liquid fuel could turn the disposal cost into revenues, especially if biorefineries could be co-located on their existing facilities. Removing ash from raw paper sludge becomes the first step of the transformation process. This step is vital to eliminate the herein-proven adverse interaction between ash and enzymes during enzymatic hydrolysis. It has been shown that ash modifies the system's pH, negatively affecting the enzyme activity, thus diminishing the carbohydrate conversion during the enzymatic hydrolysis step. Different screening equipment at the laboratory and pilot scales were employed at NCSU, and their effectiveness in retaining carbohydrates and removing ash was assessed. The pilot-scale Sidehill screening equipment exhibited the best results with carbohydrate retention of 90%, ash removal of 95%, and the potential to process at least 1,500 oven-dry (OD) kg

of paper per day. This provides evidence for the possibility of scaling up this separation stage using readily available and commonly used equipment in the pulp and paper sector. Subsequently, 30 OD kg were screened and sent to NREL for further enzymatic hydrolysis processing. In addition to high ash removal, this study validated the importance of high shear during the enzymatic hydrolysis of deashed sludge to achieve ideal carbohydrate conversion and high C6 and C5 sugar yield. Several enzymatic hydrolysis experiments were performed at NCSU and NREL at a laboratory scale using 1 to 10 OD grams of deashed sludge. This work aimed to assess optimal enzymatic hydrolysis conditions using the studied feedstock and Cellic® CTec2 (Novozymes, USA). Moreover, aiming to produce an adequate amount of sugar solution for the subsequent transformation steps, a pilot-scale paddle reactor was used. The reactor has a capacity of 2.0 OD kg of deashed sludge at a 15% total solids consistency. The enzymatic hydrolysis process was carried out utilizing Cellic® CTec3 (Novozymes, USA), at 50°C, 65 rpm and for 96 hours. These experiments yielded a sugar solution containing 78.2g/L of glucose and 23.2g/L of xylose.

Extensive work was executed at NCSU and NREL using CEM Microwave Synthesizer equipment to determine the best reaction conditions for the dehydration of glucose to 5-hydroxymethylfurfural (5-HMF) and xylose to furfural. This included catalyst loading, reaction temperature, processing time, and co-solvent systems Considering the azeotrope node between 1,4-dioxane and water and the simulation results regarding the heat demand required to recycle this organic solvent, acetone was proposed as a less energy-intensive alternative co-solvent for the dehydration reaction. After evaluating the results from preliminary Techno-economic analysis, acetone was selected as the dehydration co-solvent for the scaled-up production of 5-HMF and furfural. A tubular flow reactor was used at NREL to scale-up the dehydration reaction experiments, obtaining furans from the hydrolysate produced in the paddle reactor. The reaction conditions employed included a temperature of 190°C, a residence time of 7-9min, an acetone to aqueous volume ratio of 2:1, and a catalyst loading of 20 mM $AlCl_3$. These experiments led to a 5-HMF yield of 59.9% and a furfural yield of 71.2%. Approximately 56L of dehydration products containing acetone were generated at NREL. 24L of this material were distilled at the same research facility, producing 8L of aqueous-only furans solution. These materials and the remaining 32L dehydration products containing acetone were then sent to NCSU for further distillation and to perform the aldol-condensation reaction.

An in-house-built multi-stage distillation system was implemented at NCSU based on design specifications estimated using Aspen Plus™ to distill and remove acetone from the remaining 32L of dehydration products containing this organic solvent. The continuous distillation system successfully removed all acetone in the furans solution after 53 hours. As a result, 18.7L of aqueous-only furans solution was then available for the next conversion stage. From the available volume, 13L were used for the large-scale aldol-condensation experiments using 2-butanone (methyl ethyl ketone, MEK, etc.). A 5L batch reactor with an overhead stirrer was employe., The conditions, dictated by a brief local optimal condition experiment, included a furan to MEK molar ratio of 1:2, a temperature of 50°C, pH 13.0, and a reaction time of 10 minutes. The aldol condensation products were extracted using 2-pentanone, and the solvent later evaporated. A total of

218 grams of aldol-condensation products, which is enough to produce approximately 50ml of hydrocarbon blend, were sent to NREL for further hydro treatment. The aldol condensation product was hydrogenated at a low temperature (100°C) to stabilize the intermediates before hydrodeoxygenation (HDO) at a higher temperature (300°C) using a catalyst with an acidic support (Pd/C) to generate the hydrocarbon blend. The hydrocarbon product was then subjected to fuel property analyses executed by the Fuel Performance Group at NREL.

The sugars in the paper sludge hydrolysate were successfully converted into a hydrocarbon (HC) product suitable for blending into jet or diesel fuel, meeting critical fuel property specifications. Analysis of the HC product revealed excellent properties, including surface tension viscosity, flashpoint, and freeze point, aligning with conventional fuel ranges. The dominance of C10 hydrocarbons in the product was attributed to the higher glucose content in the hydrolysate, leading to HMF formation during dehydration. Unexpectedly, the HC product also contained iso-alkanes and small amounts of cyclo-alkanes. Over 50% of the HC product could be blended into jet or diesel fuel, surpassing the 50% target on a GGE basis.

After considering various factors such as biorefinery configuration, financial parameters, and experimental results, the use of acetone during glucose and xylose dehydration emerges as a cost-effective strategy. This method leads to a minimum fuel selling price (MFSP) of $3.4/GGE for the final hydrocarbon blend product from paper sludge. In contrast, systems using 1,4-dioxane yield a MFSP of $5.1/GGE for, even with lower hydrocarbon blend total production in acetone systems (approximately 1MM GGE/year difference). The primary reason for these results is the reduced mass flow across the distillation circuit and subsequent process units when acetone is used. This led to reduced operational expenditure and more critically, reduced overall capital investment for the biorefinery. Finally, the findings herein presented reveal that the Global Warming Potential (GWP) ranges from 35.7 to 41.8 $gCO_2eq\ MJ^{-1}$ SAF when using acetone as a solvent, renewable fuel, and bio-based chemicals. This value can be further reduced to 5.1–11.1 $gCO_2eq\ MJ^{-1}$ if ash is recycled and used for substituting cement. Based on treating 1 dry ton of paper sludge, producing SAF shows a net emission of CO_2 equivalent ranging from -925 to -873 kgCO2eq with ash utilization. This is lower than the emissions that result from landfilling without landfill gas recovery (791 $kgCO_2eq$) and with landfill gas recovery (-294 $kgCO_2eq$).

Table of Contents

Chapter 1: Paper sludge pretreatment

Paper sludge biomass represents an underutilized feedstock rich in pulped and processed cellulose which is currently a waste stream with significant disposal cost to industry for landfilling services. Effective fractionation of the cellulose from paper sludge presents an opportunity to yield cellulose as feedstock for value-added processes. A novel approach to cellulose fractionation is the sidehill screening system, herein studied at the pilot-plant scale. Composition analysis determined ash removal and carbohydrate retention of both sidehill and high-performance benchtop screening systems. Sidehill screening resulted in greater carbohydrates retention relative to benchtop screening (90% vs 66%) and similar ash removal (95% vs 98%). Technoeconomic analysis for production of sugar syrup yielded a minimum selling price of $331/metric ton of sugar syrup including disposal savings, significantly less than a commercial sugar syrup without fractionation. Sensitivity analysis showed that screening conditions played a significant role in economic feasibility for cellulosic yield and downstream processes.

1.1. Introduction

Paper sludge is presently a waste stream from paper mill wastewater treatment systems. Paper sludge from paper mills is primarily comprised of cellulosic fines along with inorganic fillers such as calcium carbonate (Turner et all, 2022, Wiegand and Urwin, 1994, Lark et al, 1996, Lynd et al, 2001). These fines provide valuable cellulose already fractionated from lignin in the pulping process but are lost from the final paper sheet (Duff et al, 1994). Paper sludge is landfilled at a cost of $54 per wet ton (EREF, 2021), resulting in a significant cost to the industry. As of 2023, over four million tons of paper sludge were produced in the United States (FisherSolve Next, 2024). Due to domestic and international legislation protecting the environment, these landfilling costs are forecasted to increase in the future (Turner et al, 2022). In addition, the mill is losing valuable cellulosic feedstock which has already been pulped and conditioned in preparation for bleaching and refining. Paper sludge is produced after the lost fiber is combined with ash from liquor recovery, including dregs, grits, and lime mud, and sent through the mill's effluent treatment clarifier, settling pond, and dewatering screw press (Cherian and Siddiqua, 2019; Turner et al, 2022). As paper sludge fibers are collected from around the mill, there is great variance in the makeup of the feedstock with the two main components being cellulose and calcium carbonate, hereafter referred to as ash. Calcium carbonate is a component common to finished paper products due to its use as a filler within the sheet, enhancing smoothness and appearance. Paper sludge for the current work was collected from a paper mill manufacturing uncoated free sheet and producing over 10 dry tons of paper sludge per day.

Separation and utilization present a chance to recover significant value from paper sludge. Cellulose, the primary component of paper sludge, consists of the cellobiose repeating unit, with 1,4-β-glycosidic bonds forming the backbone of the cellulose (Jalbert et al, 2007). The cellulose found in paper sludge may be hydrolyzed to monomeric sugars via enzymatic hydrolysis. The resulting sugars may then undergo further valorization processes. Studies have been conducted which show that paper sludge is a prime candidate as a feedstock for enzymatic hydrolysis to sugars and bioethanol production

(Dey et al, 2020, Chen et al, 2014a), while others have demonstrated process strategies that show promise for converting paper sludge in high-solids enzymatic hydrolysis (Liu et al, 2015; Yang et al, 2010; Liu et al, 2017), alternative pre-treatment strategies (Sugiharto et al, 2016; Valério et al, 2021; Díaz et al, 2011) and hydrolysis methods (Schroeder et al, 2015). While paper sludge is a highly heterogeneous material, carbohydrates make up roughly two-thirds of its content while the other third is ash, and the small remainder of the mass balance is comprised of acid-soluble lignin and acid-soluble volatile matter (Lynd et al, 2001). It is necessary to remove as much ash as possible to optimize enzymatic hydrolysis yields, as ash will inhibit the enzyme activity (Park et al, 2022a; Mendes et al, 2014). Ash removal is the key performance indicator for screening as ash can greatly affect downstream performance. One such regime for downstream processing is enzymatic conversion of cellulose to sugars for use in bioethanol or other value-added processing regimes.

The screening of usable fibers from the bulk sludge feedstock has been studied in operations at the laboratory scale (Park et al, 2022a; Chen et al, 2014) with ash removal consistently capable of deriving low-ash, high-cellulosic content streams. Additionally, these lab applications have been in the scale of less than one kilogram for each batch. The current study aims to increase the batch mass of screening by roughly 60 times in exploring pilot scale work. While the primary valorization pathway for paper mill sludge so far has been as a feedstock for conversion to geopolymer aggregate in concrete (Cherian and Siddqua, 2019), the goal is to develop a method which can recover cellulose from the sludge for valorization.

Various screening methods are used in paper mills for separating viable cellulose fibers for making the final paper sheet. Paper mills often use screening to reduce fines, shives, and flocs in their pulp streams. One method of screening is sidehill screening. Sidehill, or rundown screens, are used when solids can be easily separated from the liquid phase, such as paper sludge (*SHS & SHP Sidehill Screens*. JWCE, 2022). The sidehill screen uses gravity to allow effluent to flow down the slotted screening media, with solid/liquid separation occurring after the wedge wire. The simplistic and cheap usage of sidehill screens along with the scale of screening they may facilitate makes the sidehill screen an intriguing option for study. There is no current work dedicated to the study of pilot-scale sidehill screening to separate the cellulose fraction in paper sludge.

To optimize the derivation of usable sugars, efficient fractionation of cellulose from paper sludge must be completed (Gurram et al, 2015). There are several methods for concentrating sugars recognized to be effective at large scale. One of the most popular methods is reverse osmosis (RO) (Madaeni et al, 2004; Bichsel et al, 1981; Kumar, 1975) wherein membrane filtration is used to concentrate the sugar solution to target sugar content, usually between 15-30%. An alternative method to membrane filtration is evaporation (Asghar et al, 2020; Leonelli & Mason, 2010) which can entail rotary evaporation or multi-effect evaporators (MEE), especially in large-scale applications. The multi-effect evaporator system of sugar concentration is more energy intensive while being cheaper in capital when related to membranous filtration (Madaeni & Zereshki, 2010). The inputs are low-concentration sugar syrup and high-pressure steam while the

outputs to a multi-effect evaporator train are high-concentration sugar syrup, low-pressure vapor, and condensate.

The current work aims to address a gap in the study of a novel pilot-scale application of the sidehill screen to fractionate paper sludge and yield a carbohydrate-rich fraction. Furthermore, process simulation based on pilot scale findings are used to evaluate industrial-scale technical feasibility for paper sludge conversion to sugars. Techno-economic analysis (TEA) and sensitivity analysis were performed to determine the economic capacity of a technically feasible paper sludge valorization operation.

1.2. Materials and methods

1.2.1. Paper sludge characterization

Paper sludge samples were provided by corporate sponsors on several occasions. The primary paper mill is a fully integrated Kraft pulp mill producing uncoated free sheet. The consistency of the screw-pressed paper sludge was determined in accordance with the NREL/TP-510-42621 method for the determination of total solids in biomass (Sluiter et al, 2008). Variable with paper mill operations, the consistency of the paper sludge had a mean of 33% consistency solids.

Paper sludge before and after sidehill screening fractionation treatment was examined via the NREL/TP-510-42618 method to determine structural carbohydrates and lignin in biomass. This method allowed for the determination of carbohydrates via HPLC after hydrolysis of the biomass sample, acid-insoluble lignin by vacuum filtration, and acid-soluble lignin by UV visual spectroscopy. Partnered with method NREL/TP-510-42622, the ash content in the original biomass was determined (Sluiter et al, 2010). This sequence of methods allows for a general mass balance of the constituent components of the paper sludge biomass collected from the paper mill.

1.2.2. Pilot plant Sidehill screen

The sidehill screening equipment used was in the pilot plant at the Department of Forest Biomaterials at North Carolina State University. A 500-gallon hydropulper connected to municipal water lines facilitated the dilution to target screening consistency and mixing of the paper sludge (PS) feedstock. The sidehill screening equipment is capable of screening at a variety of consistencies ranging from 1% to 5% solids. Roughly 30 oven-dry (OD) kilograms of paper sludge was used for each sidehill screening in the pilot plant. The pilot scale screening setup employed presently may screen up to 1,500 dry kilograms of paper sludge per day.

The screening equipment consisted of the sidehill screen supported by two pumps, one fixed drive Siemens pump (pump #1) and one variable drive Reliance pump (pump #2). After 30 minutes of mixing in the hydropulper to allow for thorough fibrillation, pump #1 sent the diluted sludge to a 2,000-gallon collection tank. From the collection tank, pump #2 pumped the “feed” stream into the headbox of the sidehill screen where it filled the headbox and spilled over the screen. 1.5-inch interior diameter rubber hosing was used as piping for the screening equipment.

"Accepts" from the screen were thickened by the wedge wire separating solids from the liquid phase and fell back into the collection tank. Rejects were ported back to the hydropulper for recirculation back to the collection tank in the closed layout of the system. "Rejects" consisted of very dilute particles that passed through the wedge wire of the screen. In the open layout of screening, the rejects were instead ported into a screening basket for sample collection and disposal. Samples were taken at three-minute intervals for a total of 15 minutes. Accept samples were taken as the screened sludge streamed off the bottom lip of the sidehill screen. Feed samples were taken at the feed pump's sample valve, and rejects samples were taken at the hydropulper in the closed layout and at the screening basket in the open layout. After 15 minutes of running the system closed, the screening was stopped to allow for transition to running open. The system then ran in the open layout for six minutes, collecting samples at three and six minutes. Six minutes of open was chosen due to losing rejects from the system, leading to a continually more diluted system. Samples from screening runs were stored in cold rooms at 2ºC. By way of comparison, screening performance was evaluated against a lab scale centrifugal screening equipment, the Pulmac Masterscreen.

1.2.3. Calculations and data interpretation

The samples from the sidehill screen were collected and used to evaluate both ash removal and carbohydrate retention of the screening system. Carbohydrate retention is a key performance indicator evaluated by Equation 1. Ash removal was calculated for each sample as follows in Equation 2.

(Eq. 1.1) $$Carbohydrate\ Retention = \frac{accepts\ mass_{OD} - accepts\ mass_{ash}}{feed\ mass_{OD} - feed\ mass_{ash}} * 100\%$$

(Eq. 1.2) $$\%Ash\ Content = \frac{ash\ mass}{oven\ dry\ mass} * 100\%$$

The ash removal is calculated for each sample, *i,* based on the incoming ash content in the original paper sludge feedstock as laid out in Equation 3.

(Eq. 1.3) $$\%Ash\ removal_i = \frac{rejects\ ash\ mass_i}{feed\ ash\ in} * 100\%$$

1.2.4. Process simulation

WinGEMS process simulation (Windows General Energy and Material balance System) is a leading software in mass and energy balance programming for the paper industry (Atkins et al, 2010). The present work uses experimental data from pilot-scale de-ashing and process simulation data to model industrial-scale conversion of paper sludge to a value-added material.

To develop an economic profile for simulation and techno-economic analysis, a market had to be assumed for an otherwise underutilized feedstock. Paper sludge was chosen to act as a feedstock for sugar syrup. In the United States, sugar demand was 12.64 million short tons in 2022 (Abadam, 2023). Growth for sugar syrup demand grew 2.4% per capita each year in 2021 and 2022 with the soft drink industry being a major

contributor. The assumed market of sugar syrups yields itself to an assumed process design. **Figure 1.1** shows the process design to valorize paper sludge to sugar concentrate.

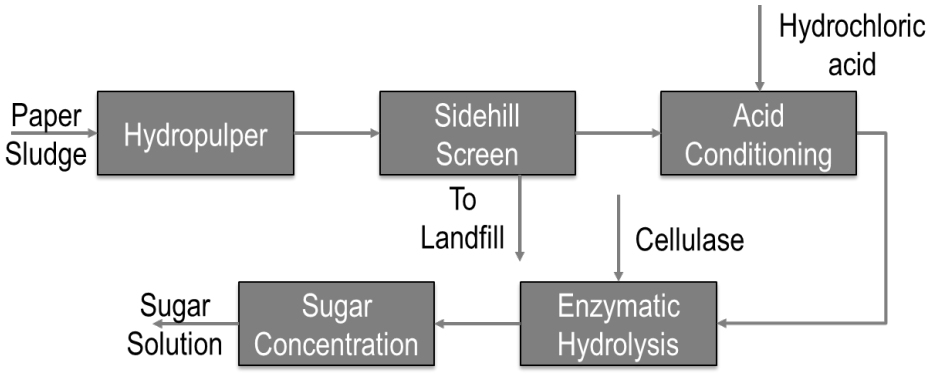

Fig. 1.1. Process map of paper sludge to sugar syrup.

Experimental data collected in pilot scale sidehill screen de-ashing was used to simulate conditions and capabilities for industrial scale screening. Due to the near-industrial scale of pilot plant operations and the use of sidehill screens in industry, it is assumed all experimental data for ash removal and carbohydrate retention are transferrable to the industrial-scale simulation.

Glucose production via enzymatic hydrolysis of lignocellulosic feedstock is a well-studied process (Park et al, 2022a; Jones et al, 2013; Zhang et al, 2018; Chen et al, 2012; Asenjo 1983; Katz et al, 1968). Among feedstocks for enzymatic hydrolysis, paper sludge is a novel feedstock which has gained traction in the body of literature in recent years (Park et al, 2022b; Naicker et al, 2020; Malgas et al, 2020; Zhu et al, 2019; Chen et al, 2014a; Chen et al, 2014b). Prior to enzymatic hydrolysis, an acid conditioning step is required to bring the feedstock pH into the optimal window for enzyme activity. As such, sugar syrup derived from paper sludge cellulosic material may provide an illuminating perspective on costs and revenues.

Agricultural-grade applications of resulting sugar syrup must include removal of contaminants and side products such as xylose and other pentose sugars. While a challenge, there has been much research on separation methods for pentose and hexose monomer fractionation (Roli et al, 2016; Nguyen et al, 2015; Brás et al, 2014; Sjöman et al, 2007; Heikkila et al, 2002) and filtered xylose may be later used for xylitol production as a feedstock for another revenue stream (Guirimand et al, 2019).
Process simulation reflects changing screening capabilities considering both carbohydrate retention and ash removal determined in the pilot scale work. Among the processes present in simulation are pulping of paper sludge, screening, acid conditioning, enzymatic hydrolysis, and sugar concentration to final sugar concentration. The full process simulation scheme may be found in *Supplementary Material*.

1.2.5.Techno-economic analysis

The present TEA is based on the process simulation of large-scale de-ashing, enzymatic hydrolysis, and sugar concentration. The scope of the TEA is to estimate the economic capacity for this process in a long-term operation by assessing revenues and credits levied against operational and capital expenditures across a 30-year lifespan of the project. Capital expenditures are evaluated using quotes from industry paired with engineered sizing and scaling factors for modeled production capacity.

1.3. Results

1.3.1. Sidehill screening of paper sludge

Initial feed consistencies were varied by adding water at the hydropulper. The consistencies of screening runs were varied from 1.7% to 5.0% consistency of initial feed. 3% consistency feed had the best performance for removing ash from the feedstock. Batch sizes were kept uniform with 26±2.0 oven-dried kilograms of paper sludge being introduced at the start of each screening run. Opening the system following 15 minutes of closed running allowed for much greater ash removal to be reached in the system. In comparison to high performance bench scale equipment, as referenced in section 2.2, the sidehill screen removed similar amounts of ash from the feedstock when operated at 3% consistency.

Already mentioned above, the results around the optimal 3% consistency had similar results in the closed system while the higher consistencies had significantly better ash removal performance in the open layout. This is likely a result of the open system becoming gradually diluted, so consistencies lower than 3% became very diluted in the open system. Consequently, the diluted sludge could not aggregate and roll down the screen thus separating the solids less efficiently. Contrastingly, the higher consistencies diluted closer to 3% in the open system, leading to optimal consistency for ash removal as they diluted to 3%. **Figure 1.2** shows that higher consistency resulted in a higher capacity for ash removal than lower consistencies.

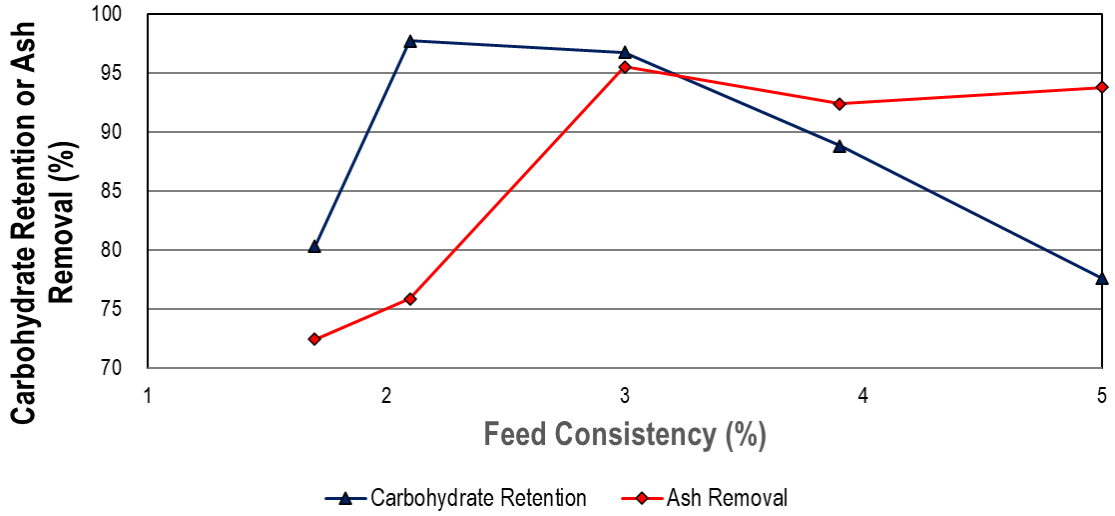

Fig. 1.2. Final ash removal and carbohydrate retention trended against each consistency run completed.

Figure 1.3 serves to summarize the de-ashing and carbohydrate retention performance of all the screening consistencies studied. Each screening run begins with 100% carbohydrate retention. Corroborating **Figure 1.2**, **Figure 1.3** shows that there is an optimal operating window for screening consistency to maximize ash removal. By way of comparison, the performance of the Pulmac Masterscreen lab scale screen is provided in **Figure 1.3.** The 3% consistency screening provides the most selective screening performance. The existence of this performance apex is likely due to this consistency of paper sludge being thick enough to allow for the feedstock to aggregate on contact with the screen and roll down the surface, allowing the ash to separate and filter through the screening media. Meanwhile, this consistency window is not too high in solids as to not have enough free water to allow for fiber-ash separation.

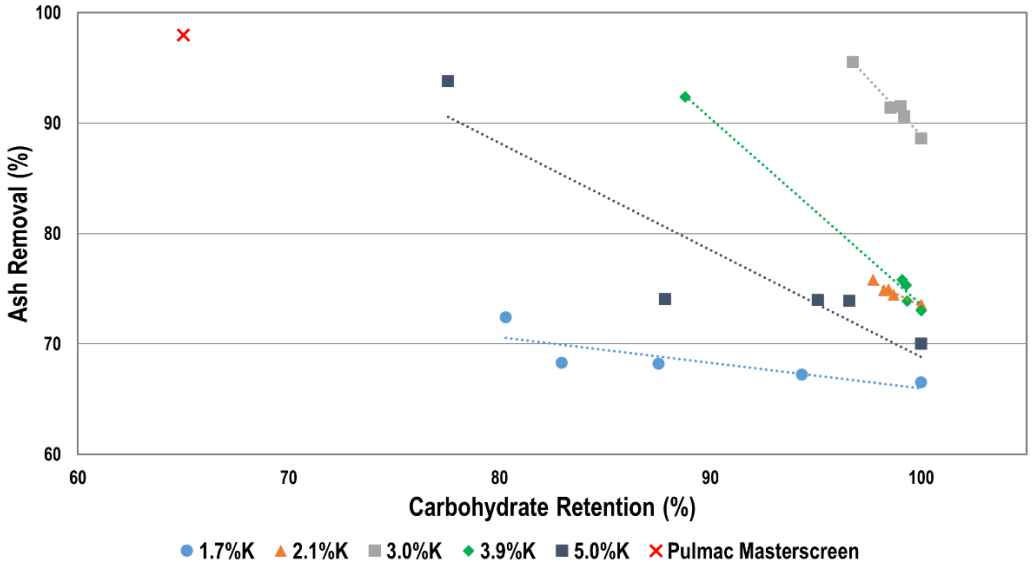

Fig. 1.3. Screening performance indicators carbohydrate retention and ash removal trended from steady state (100% carbohydrate retention) through to final sample collection for each consistency studied.

1.3.2. Biomass composition analysis

The structural component results are presented in **Table 1.1** in addition to a mass balance of final components after screening. This method demonstrated that the raw, supplied sludge was high in ash and carbohydrates Data from **Table 1.1** is derived from carrying out compositional analysis for the 3% consistency screening run and applying that data in conjunction with pilot scale screening yields to model a mass balance. Screening yields were determined by ratio mass of final oven dry accepts and feedstock solids. Data was provided from one run due to the variance of carbohydrate and ash content of sludge samples provided by the mill. It can be seen in the data that the rejects stream is much more concentrated in ash while the accepts stream is much more concentrated in carbohydrates.

Table 1.1. Mass balance via determination of structural carbohydrates and lignin in supplied paper sludge, final aspects, and final rejects of 3% consistency screening.

Properties	ASL (%mass)	AIL (%mass)	Ash (%mass)	Carbohydrates (%mass)
Feedstock	0.5	8	52	38
Accepts	0.4	6	3	87
Rejects	0.5	8	79	8
Mass Balance (*100g basis*)	ASL (g)	AIL (g)	Ash (g)	Carbohydrates (g)
Feedstock	0.5	8	52	38
Accepts (38% mass)	0.1	2	1	33
Rejects (62% mass)	0.4	5	49	5

1.3.3. Process simulation results

Process Simulation of industrial scale sugar production was done to establish the scalability of sidehill screen de-ashing operations from pilot plant scale. Modelling was completed using screening and enzymatic hydrolysis data generated from the present work and work in the literature (Park et al, 2022), while sugar evaporation trends in the literature was also followed (Chantasiriwan et al, 2020).

1.3.3.1. Mass balance, inputs, and outputs

Table 1.2 below shows the critical inputs and outputs of the system under conditions of 100,000 ODMT/year of paper sludge incoming material into the operation. As can be seen, there is a large flow which is landfilled due to the high ash content of the incoming sludge stream. The present work does not consider a potential value-added process for the separated ash. A natural gas boiler provides the steam required for multi-effect evaporation to bring sugar solids to the required concentration.

Table 1.2. Process Simulation Key Inputs and Outputs.

Inputs	Flow	Units
Paper Sludge	21	Wet MT/hr
Fresh Water	2.3	MT/hr
Hydrochloric acid	103	Total kg/hr
Cellulase Enzyme	94	Total kg/hr
Natural Gas	12,000	MJ/hr
60# Steam	8.6	MT/hr
Outputs	Flow	Units
Sugar Syrup (*40%mass*)	2.4	OD MT/hr
Effluent	2.3	MT/hr
Landfilling	10	Wet MT/hr

1.3.3.2. Yields and the effect of screening consistency

Overall yields and process flows are strongly impacted by the effect of screening consistency in the first step of the process. **Table 1.3** shows the relationship between sidehill screening consistency and overall simulated process performance. As can be

seen, the optimal window of screening performance in pilot scale work is exhibited in the process simulation. By optimally carrying cellulosic solids forward through the process, enzyme demands will be increased. The optimal screening window at 3% feed consistency also removes the greatest amount of ash, where greater cellulosic selectivity in screening allows for higher monomeric sugar yields from enzymatic hydrolysis of the separated cellulose. In accordance with the literature (Park 2022a, Park 2022b), the effect of ash included less efficient use of acid for conditioning as well as lower hydrolytic yields.

Table 1.3. Effects of sidehill screen operation on downstream value-added processing areas.

Screening Consistency (%)	Acid Demand (kg/hr)	Enzyme Demand (kg/hr)	Sugar Production (MT/hr)	Sugar Yield from OD Sludge (%)
1.7	115	48	1.3	7.4
2.1	113	77	2.0	11.2
3.0	103	94	2.4	14.1
3.7	97	83	2.2	13.0
5.0	84	77	2.1	11.6

1.3.4. Techno-economic analysis

Techno-economic analysis evaluation of capital expenditure, operational expenditure, revenues, and credits for the system investigated in process simulation. The analysis encompasses both process and expenditure modelling, utilizing process flows from the mass and energy balance to calculate capital and operating costs in 2022 USD. 30-year forecasted analysis of discounted cash flows determine a minimum selling price (MSP) for the final concentrated sugar solution with an IRR of 10%.

1.3.4.1. Capital expenditures

Equipment costs, or capital expenditures, were appropriately chosen and sized in order to facilitate all operations represented in process simulation at the scale of study. The total capital expenditure for the present work was calculated to be $15,700,000 of equipment delivered cost with a total capital investment (TCI) of $53,100,000.

1.3.4.2. Operational expenses

Table 1.4 gives a breakdown of the critical costs associated with the present work. As can be seen, there is a strong influence from the credit for taking on paper sludge from the paper mill producer. This credit is half of the current landfilling cost, resulting in a discount cost to the sludge supplier while diverting the cellulose-rich sludge stream from the landfill. Therefore, this is an attractive opportunity for the paper sludge producer as the rate is less than the trucking and landfilling costs.

Table 1.4. Selected operational expenses for paper sludge valorization.

Stream	Flow (MT/yr)	Cost ($MM/yr)	Price ($/MT)	Water (%Mass)
Paper Sludge	165,000 (wet basis)	*-6.57*	40	67
Fresh Water	15,500	0.02	0.73	·
Hydrochloric Acid	800	0.33	400	63
Cellulase Enzyme	600	0.31	512	99
Wastewater Treatment	15,500	0.02	0.73	·
Landfilling	84,000	3.41	40	60
Natural Gas	1,700	0.56	330	·

Fresh water, effluent treatment, and natural gas costs are established using industrial standard rates for the southeast United States region. Electrical costs are estimated using the process demand of power given from process simulation and utilizing publicly available industrial electricity costs for the region. Hydrochloric acid costs were estimated by extrapolating costs from a lab scale operation due to lack of availability for vendor pricing at the industrial scale. Enzyme operational costs were estimated using Novozymes CTEC3 cellulase. Enzyme costs were based on expense rates of protein mass at small batch enzyme concentration of enzyme provided to the lab.

1.3.4.3. Screening consistency and minimum selling price

Sidehill screening at the pilot scale, as mentioned previously in section 2.2, has the capacity to operate at different consistencies and yield cellulose pulp of varying quality. The outcoming screened product then inherently has different contents of cellulose and ash with each screening consistency. Enzymatic activity is then in turn decreased with increased ash content, so monomeric yields and steam demand are highly dependent on the screening consistency in upstream screening. Screening performance then impacts various operational expenses and yields throughout the process. The evidence of these trends is shown in **Table 1.5** found below. The optimal window of screening performance is supported in economic analysis, with 3% consistency screening showing the greatest ash removal while also showing the greatest economic potential. By way of comparison, sucrose had a global average price of $410/metric ton in 2022 (Worldbank, 2023). After costs of nanofiltration or other filtration methodology, the optimal MSP of $331 per ton potentially makes paper sludge-based sugars an attractive alternative after additional processing costs for end use in agricultural animal feeds. Additionally, no fractionation of paper sludge leads to an MSP over 100% higher than the 3% screening minimum MSP.

1.3.4.4. Sensitivity analysis

Figure 1.4 demonstrates that the most critical items to economic performance are plant capacity, capital expenditure factors, and screening consistency. Consistent with the pilot plant work, it is evident that the ability to screen ash in fractionating the paper sludge feedstock is of high importance to the technical and economic feasibility of a value-added operation aiming to valorize the cellulose in paper sludge.

Table 1.5. TEA minimum selling price of sugar product based on sidehill operational consistency.

Screening Consistency (%)	MSP ($/MT)
1.7	478
2.1	372
3.0	331
3.7	353
5.0	393
No fractionation	679

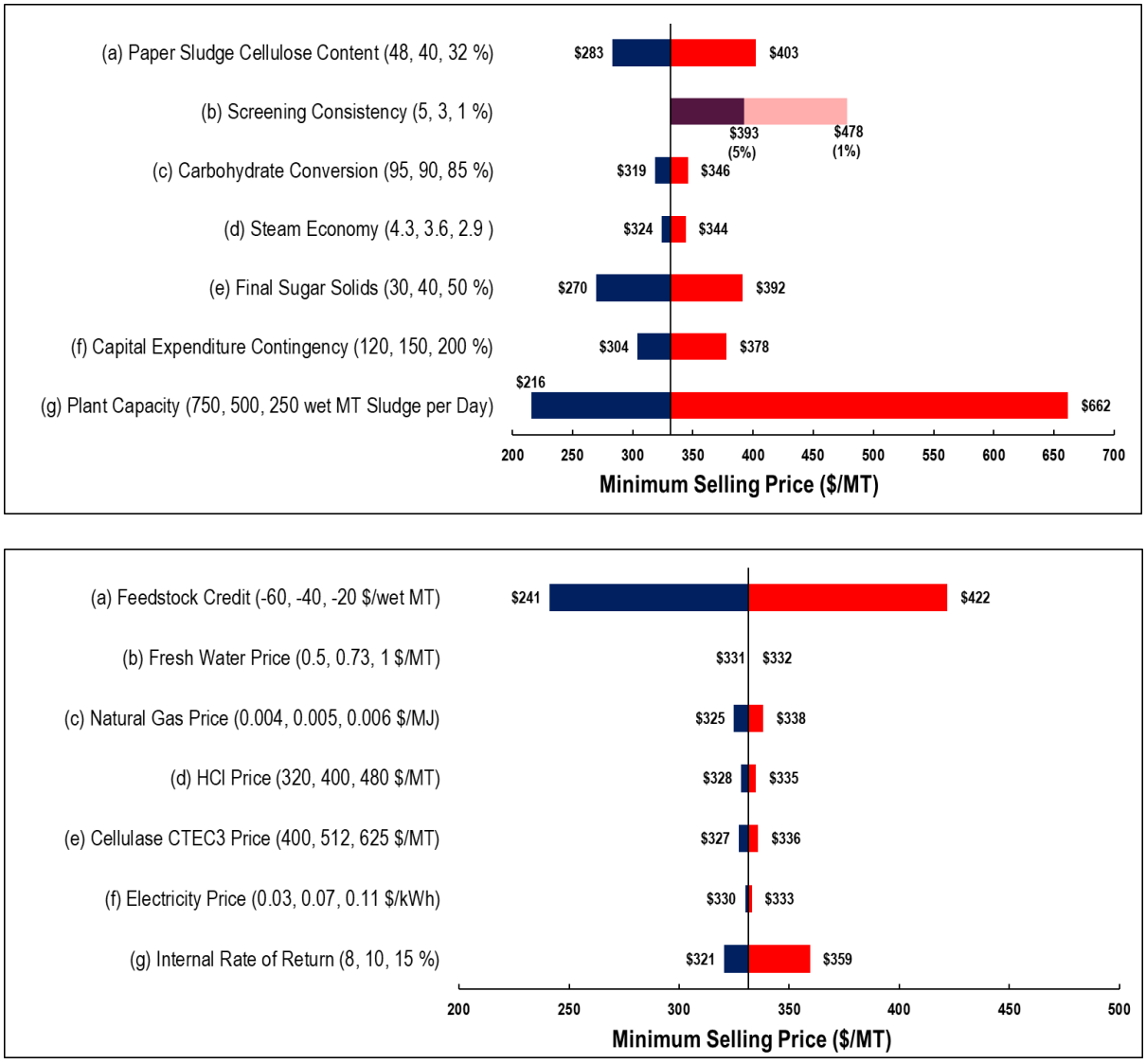

Fig. 1.4. Sensitivity analysis of techno-economic analysis considering internal process capabilities (*top*) and market factors (*bottom*).

1.4. Conclusions

The pilot-plant scale sidehill screen was able to facilitate magnitudes of order greater flow than the Pulmac Masterescreen while also producing improved fractionation performance. Compositional analysis showed that the sidehill screening operation capably increased the content of carbohydrates to roughly 90% mass content. Process simulation of paper sludge valorization to sugars yielded results that maximized sugar yields in the optimal 3% consistency window that was found in pilot scale work. Techno-economic analysis provided a minimum selling price of $331/ton. Techno-economic analysis showed that the most sensitive factors to economic performance are plant capacity, feedstock credit, and screening consistency.

References

1. Abadam, V. (2023). Economic Research Service | Situation and Outlook Report.
2. Asenjo, J. A. (1983). Maximizing the formation of glucose in the enzymatic hydrolysis of insoluble cellulose. In Biotechnology and Bioengineering (Vol. 25, Issue 12, pp. 3185–3190). https://doi.org/10.1002/bit.260251229
3. Asghar, M. T., Yusof, Y. A., Mokhtar, M. N., Yaacob, M. E., Ghazali, H. M., Varith, J., Chang, L. S., & Manaf, Y. N. (2020). Processing of coconut sap into sugar syrup using rotary evaporation, microwave, and open-heat evaporation techniques. Journal of the Science of Food and Agriculture, 100(10), 4012–4019. https://doi.org/10.1002/jsfa.10446.
4. Atkins, Martin & Morrison, Andrew & Walmsley, Michael & Riley, Joesph. (2010). WinGEMS Modelling and Pinch Analysis of a Paper Machine for Utility Reduction. Appita Journal. 63.
5. Brás, T., Guerra, V., Torrado, I., Lourenço, P., Carvalheiro, F., Duarte, L. C., & Neves, L. A. (2014). Detoxification of hemicellulosic hydrolysates from extracted olive pomace by diananofiltration. Process Biochemistry, 49(1), 173–180. https://doi.org/10.1016/j.procbio.2013.09.017
6. Chen, H., Venditti, R. A., Jameel, H., & Park, S. (2012). Enzymatic hydrolysis of recovered office printing paper with low enzyme dosages to produce fermentable sugars. Applied Biochemistry and Biotechnology, 166(5), 1121–1136. https://doi.org/10.1007/s12010-011-9498-2.
7. Chen, H., Han, Q., Daniel, K., Venditti, R., & Jameel, H. (2014a). Conversion of Industrial Paper Sludge to Ethanol: Fractionation of Sludge and Its Impact. Applied Biochemistry and Biotechnology, 174(6), 2096–2113. https://doi.org/10.1007/s12010-014-1083-z
8. Chen, H., Venditti, R., Gonzalez, R., Phillips, R., Jameel, H., & Park, S. (2014b). Economic evaluation of the conversion of industrial paper sludge to ethanol. Energy Economics, 44, 281–290. https://doi.org/10.1016/j.eneco.2014.04.018
9. Cherian, C., & Siddiqua, S. (2019). Pulp and paper mill fly ash: A review. In Sustainability (Switzerland) (Vol. 11, Issue 16). MDPI. https://doi.org/10.3390/su11164394.
10. Dey, P., Rangarajan, V., Nayak, J., Das, D. B., & Wood, S. B. (2021). An improved enzymatic pre-hydrolysis strategy for efficient bioconversion of industrial pulp and paper sludge waste to bioethanol using a semi-simultaneous saccharification and fermentation process. Fuel, 294. https://doi.org/10.1016/j.fuel.2021.120581

11. Díaz, M. J., Cara, C., Ruiz, E., Pérez-Bonilla, M., & Castro, E. (2011). Hydrothermal pre-treatment and enzymatic hydrolysis of sunflower stalks. Fuel, 90(11), 3225–3229. https://doi.org/10.1016/j.fuel.2011.06.040
12. Duff, S. J. B., Moritz', J. W., & Andersen2, K. L. (1994). Simultaneous Hydrolysis and Fermentation of Pulp Mill Primary Clarifier Sludge.
13. Sludge Production by Site, FisherSolve Next. (2024, Quarter 1). Retrieved February 21, 2024.
14. Guirimand, G., Inokuma, K., Bamba, T., Matsuda, M., Morita, K., Sasaki, K., Ogino, C., Berrin, J. G., Hasunuma, T., & Kondo, A. (2019). Cell-surface display technology and metabolic engineering of: Saccharomyces cerevisiae for enhancing xylitol production from woody biomass. Green Chemistry, 21(7), 1795–1808. https://doi.org/10.1039/c8gc03864c
15. Gurram, R. N., Al-Shannag, M., Lecher, N. J., Duncan, S. M., Singsaas, E. L., & Alkasrawi, M. (2015). Bioconversion of paper mill sludge to bioethanol in the presence of accelerants or hydrogen peroxide pretreatment. Bioresource Technology, 192, 529–539. https://doi.org/10.1016/j.biortech.2015.06.010
16. H. Heikkila, M. Manttari, M. Nystrom, M. Lindroos, H. Paananen, O. Puuppo, H. Koivikko, Separation Process, WO02053781, 2002.
17. Jalbert, J., Gilbert, R., Tétreault, P., Morin, B., & Lessard-Déziel, D. (2007). Identification of a chemical indicator of the rupture of 1,4-β-glycosidic bonds of cellulose in an oil-impregnated insulating paper system. Cellulose, 14(4), 295–309. https://doi.org/10.1007/s10570-007-9124-1
18. Jones, B. W., Venditti, R., Park, S., Jameel, H., & Koo, B. (2013). Enhancement in enzymatic hydrolysis by mechanical refining for pretreated hardwood lignocellulosics. Bioresource Technology, 147, 353–360. https://doi.org/10.1016/j.biortech.2013.08.030
19. R. S. Kumar,Ind. J . Technol.1972,10 (4), 142.
20. ark, N., Xia, Y., Cheng-Guo Qin, J., Gongt, C. S., & Tsaot, G. T. (1997). KLUVEROMYCES MARXIANUS (Vol. 12, Issue 2).
21. Leonelli C and Mason TJ, Microwave and ultrasonic processing: now arealistic option for industry.Chem Eng Process.49:885–900 (2010).
22. Liu, Y., Xu, J., Zhang, Y., Yuan, Z., & Xie, J. (2015). Optimization of high solids fed-batch saccharification of sugarcane bagasse based on system viscosity changes. Journal of Biotechnology, 211, 5–9. https://doi.org/10.1016/j.jbiotec.2015.06.422
23. Liu, Y., Zhang, B., Wang, W., He, M., Xu, J., & Yuan, Z. (2017). Evaluation of the solvent water effect on high solids saccharification of alkali-pretreated sugarcane bagasse. Bioresource Technology, 235, 12–17. https://doi.org/10.1016/j.biortech.2017.03.088
24. Lynd, L. R., Lyford, K., South, C. R., van Walsum, P., Levenson Chemical, K., & Program, B. E. (2001). Evaluation of paper sludges for amenability to enzymatic hydrolysis and conversion to ethanol. In TAPPI Journal peer reviewed.
25. Katz And, M., & Reese, E. T. (1968). Production of Glucose by Enzymatic Hydrolysis of Cellulose. In Applied microbiology.
26. Madaeni, S. S., Tahmasebi, K., & Kerendi, S. H. (2004). Sugar syrup concentration using reverse osmosis membranes. Engineering in Life Sciences, 4(2), 187–190. https://doi.org/10.1002/elsc.200401801

27. Madaeni, S. S., & Zereshki, S. (2010). Energy consumption for sugar manufacturing. Part I: Evaporation versus reverse osmosis. Energy Conversion and Management, 51(6), 1270–1276. https://doi.org/10.1016/j.enconman.2010.01.002
28. Malgas, S., Rose, S. H., van Zyl, W. H., & Pletschke, B. I. (2020). Enzymatic hydrolysis of softwood derived paper sludge by an in vitro recombinant cellulase cocktail for the production of fermentable sugars. Catalysts, 10(7). https://doi.org/10.3390/catal10070775
29. Mendes, C. V. T., Rocha, J. M. S., & Carvalho, M. G. V. S. (2014). Valorization of residual streams from pulp and paper mills: Pretreatment and bioconversion of primary sludge to bioethanol. Industrial and Engineering Chemistry Research, 53(50), 19398–19404. https://doi.org/10.1021/ie503021y
30. Naicker, J. E., Govinden, R., Lekha, P., & Sithole, B. (2020). Transformation of pulp and paper mill sludge (PPMS) into a glucose-rich hydrolysate using green chemistry: Assessing pretreatment methods for enhanced hydrolysis. Journal of Environmental Management, 270. https://doi.org/10.1016/j.jenvman.2020.110914
31. Nguyen, N., Fargues, C., Guiga, W., & Lameloise, M. L. (2015). Assessing nanofiltration and reverse osmosis for the detoxification of lignocellulosic hydrolysates. Journal of Membrane Science, 487, 40–50. https://doi.org/10.1016/j.memsci.2015.03.072
32. Park, H., Cruz, D., Tiller, P., Johnson, D. K., Mittal, A., Jameel, H., Venditti, R., & Park, S. (2022a). Effect of ash in paper sludge on enzymatic hydrolysis. Biomass and Bioenergy, 165. https://doi.org/10.1016/j.biombioe.2022.106567
33. Park, Hyeonji, Cruz, David, Tiller, Phoenix, Johnson, David K., Mittal, Ashutosh, Jameel, Hasan, Venditti, Richard, and Park, Sunkyu. Effect of Ash in Paper Sludge on Enzymatic Hydrolysis. United States: N. p., 2022b. Web. doi:10.1016/j.biombioe.2022.106567.
34. Roli, N. F. M., Yussof, H. W., Seman, M. N. A., Saufi, S. M., & Mohammad, A. W. (2016). Separating xylose from glucose using spiral wound nanofiltration membrane: Effect of cross-flow parameters on sugar rejection. IOP Conference Series: Materials Science and Engineering, 162(1). https://doi.org/10.1088/1757-899X/162/1/012035
35. Schroeder, B. G., Zanoni, P. R. S., Magalhães, W. L. E., Hansel, F. A., & Tavares, L. B. B. (2017). Evaluation of biotechnological processes to obtain ethanol from recycled paper sludge. Journal of Material Cycles and Waste Management, 19(1), 463–472. https://doi.org/10.1007/s10163-015-0445-0
36. S. E. Bichsel, A. M. Sondre, Application of Membrane Technology forJuice Concentration,Publ. Tech. Pap. Proc. Annu. Meet. Sugar Ind.Technol.1981,40, 251. SHS & SHP Sidehill Screens. JWCE. (2022, January 28). Retrieved September 14, 2022, from https://www.jwce.com/product/shs/
37. Sjöman, E., Mänttäri, M., Nyström, M., Koivikko, H., & Heikkilä, H. (2007). Separation of xylose from glucose by nanofiltration from concentrated monosaccharide solutions. Journal of Membrane Science, 292(1–2), 106–115. https://doi.org/10.1016/j.memsci.2007.01.019
38. Sluiter, A., Hames, B., Ruiz, R., Scarlata, C., Sluiter, J., Templeton, D., & Crocker, D. (2008). Determination of Structural Carbohydrates and Lignin in Biomass:

Laboratory Analytical Procedure (LAP) (Revised July 2011). http://www.nrel.gov/biomass/analytical_procedures.html
39. Sluiter, J. B., Ruiz, R. O., Scarlata, C. J., Sluiter, A. D., & Templeton, D. W. (2010). Compositional analysis of lignocellulosic feedstocks. 1. Review and description of methods. Journal of Agricultural and Food Chemistry, 58(16), 9043–9053. https://doi.org/10.1021/jf1008023
40. Sugiharto, Y. E. C., Harimawan, A., Kresnowati, M. T. A. P., Purwadi, R., Mariyana, R., Andry, Fitriana, H. N., & Hosen, H. F. (2016). Enzyme feeding strategies for better fed-batch enzymatic hydrolysis of empty fruit bunch. Bioresource Technology, 207, 175–179. https://doi.org/10.1016/j.biortech.2016.01.113
41. The Environmental Research & Education Foundation (2021) “Analysis of MSW Tipping Fees – September 2021”. Retrieved from www.erefdn.org.
42. Turner, T., Wheeler, R., & Oliver, I. W. (2022). Evaluating land application of pulp and paper mill sludge: A review. In Journal of Environmental Management (Vol. 317). Academic Press. https://doi.org/10.1016/j.jenvman.2022.115439
43. Valério, R., Serra, A. T., Baixinho, J., Cardeira, M., Fernández, N., Bronze, M. R., Duarte, L. C., Tavares, M. L., Crespo, J. G., & Brazinha, C. (2021). Combined hydrothermal pre-treatment and enzymatic hydrolysis of corn fibre: Production of ferulic acid extracts and assessment of their antioxidant and antiproliferative properties. Industrial Crops and Products, 170. https://doi.org/10.1016/j.indcrop.2021.113731
44. Wiegand, P. S., & Unwin, J. I. (1994). Solid Waste Management Alternative management of pulp and paper industry solid wastes.
45. Yang, M., Li, W., Liu, B., Li, Q., & Xing, J. (2010). High-concentration sugars production from corn stover based on combined pretreatments and fed-batch process. Bioresource Technology, 101(13), 4884–4888. https://doi.org/10.1016/j.biortech.2009.12.013
46. Zhang, H., Fan, M., Li, X., Zhang, A., & Xie, J. (2018). Enhancing enzymatic hydrolysis of sugarcane bagasse by ferric chloride catalyzed organosolv pretreatment and Tween 80. Bioresource Technology, 258, 295–301. https://doi.org/10.1016/j.biortech.2018.03.004
47. Zhu, S., Sui, J., Liu, Y., Ye, S., Wang, C., Huo, M., & Yu, Y. (2019). Effects of Washing, Autoclaving, and Surfactants on the Enzymatic Hydrolysis of Negatively Valued Paper Mill Sludge for Sugar Production. Energy and Fuels, 33(2), 1219–1226. https://doi.org/10.1021/acs.energyfuels.8b03586
48. World Bank. (2023, October 27). Global Economic Prospects -- June 2023 - World Bank.Worldbank.org. https://openknowledge.worldbank.org/server/api/core/bitstreams/6e892b75-2594-4901-a036-46d0dec1e753/content

Chapter 2: Enzymatic hydrolysis of lignocellulosic fibers in deashed paper sludge

The valorization of paper sludge is a high-potential process to develop renewable fuels and chemicals, which can be integrated with pulp and paper mills. Calcium carbonate is the main ash component in sludge, which plays a role in buffering pH and potentially lowering the conversion during enzymatic hydrolysis. Therefore, it is important to investigate the effect of ash on sugar yields and examine pH change to introduce efficient and economical enzymatic hydrolysis of sludge. Carbohydrate conversion was enhanced when the ash was removed by fractionation. On the other hand, the highest sugar recovery was obtained when the sludge contained 20% ash content. The pH change during enzymatic hydrolysis was influenced by ash and explained why sludge-derived hydrolysate showed lower carbohydrate conversion. Therefore, a high shear process with the increased acid amount is suggested to prohibit the negative effect of ash and enhance the accessibility of cellulase to fibers. This study highlights the feasibility of using wet waste streams generated by the paper industry.

2.1. Introduction

Paper sludge represents solid waste from pulp and paper mills. Sludge sources include rejects, primary sludge, and secondary sludge. Primary sludge is mainly composed of fibers, fines, and fillers, which can be recovered by a sedimentation or flotation process [1]. Landfill, lagoon, and land application as a fertilizer or soil conditioner are the conventional methods of disposing or utilizing the sludge [2]. Since the environmental effects have received increasing attention, the reuse of paper sludge has become a significant issue in the industry. As the primary sludge is fiber-rich, the recovered sludge has been suggested as a source of value-added chemicals [3,4] and ethanol [5–7].

Ash is one of the main obstacles to overcome to increase the effectiveness of converting sludge into chemicals. The amount of ash in sludge ranges from 10 to 50 wt%, depending on the type of mill [1]. Calcium carbonate, the most common component in ash, has been proposed as an inhibitor of enzyme activity [5,8]. Ash may attach to the enzyme since ash has a higher affinity for enzymes than fibers [5]. The inhibition contributes to the increased required dosage of enzyme and additional input of acid in the enzymatic hydrolysis of sludge. Therefore, the fractionation of sludge to remove ash before enzymatic hydrolysis is essential to improve the sugar yield. Chen et al. [5] showed that the fractionation of sludge using a screen increased sugar yield because the enzyme had less chance to adsorb onto acid-insoluble ash. The carbohydrate conversion of the fractionated sludge was 1.2–1.4 times higher than that of the unfractionated case, depending on the sludge components present. Mendes et al. [8] also performed a pretreatment using organic or inorganic acids to remove ash components in sludge. The carbohydrate conversion rate reached 88% when HCl-pretreated sludge was hydrolyzed at a high enzyme dosage (35 FPU/g). Gurram et al. [9] applied an HCl solution to mix primary sludge overnight, followed by washing with distilled water. Through this chemical pretreatment, calcium carbonate can be removed as calcium chloride. Zhu et al. [4] repeated the washing stage to remove ash in sludge, but washing itself did not significantly improve the final sugar yields. It was effective only in reducing the acid usage to neutralize sludge when performing enzymatic

hydrolysis. They proposed the use of nonionic surfactants to improve the enzyme activity rather than only using the washing process.

Conversion yield of sludge to sugars has been investigated depending on the amount of enzyme and the pH adjustment after the fractionation of sludge [5]. Unfractionated sludge achieved higher sugar yield only with the pH adjustment, whereas the fractionated specimen did not need the adjustment. For fractionated sludge, a higher enzyme dosage yielded a higher conversion extent; 8 FPU/g of mixed enzyme dosage resulted in the highest value, 93%. Steffen et al. [10] performed enzymatic hydrolysis of deinking sludge, which had a high content of fiber fines. A sugar yield of 56% was obtained after 6 h at 15 FPU of enzyme dosage. Their results also showed that the longer incubation time adversely affected the yield, but they did not elaborate on the reasons.

In this study, sludge was evaluated to produce sugars such as glucose and xylose in terms of carbohydrate conversion and sugar recovery. Since each type of sludge has a different amount of ash depending on the source of pulp and paper mills, it is important to comprehend the relationship between ash amount and the efficiency of enzymatic hydrolysis. Other studies have proposed that pretreatments enhance the efficiency of enzymatic hydrolysis. However, few studies have shown how different amounts of ash affect the overall process of enzymatic hydrolysis of sludge. Studying the relationship between ash content and the overall efficiency will provide useful concepts to the industries to valorize sludge. For the efficient enzymatic hydrolysis of sludge, a detailed change in pH was observed, and the role of ash in enzymatic hydrolysis was explained. Following by interpreting the impact of ash on enzymatic hydrolysis of sludge, the application of high shear and the addition of hydrochloric acid were also suggested.

2.2. Material and methods

2.2.1. Raw materials

Paper sludge used in this study was obtained from one of the Kraft pulping mills in the USA. The chemical composition of the sludge used in this study is shown in **Table 2.1.** Biomass composition analysis of sludge was performed by the NREL procedure [11], and ash content of sludge was measured by TAPPI standard (T 211 om-02) [12]. Extractions were analyzed by the mixture solvent of benzene and ethanol. In addition, the inorganic component of sludge was analyzed by ICP-MS (Induced coupled plasma–mass spectroscopy, Elan DRC2, PerkinElmer, USA). Cellulase for enzymatic hydrolysis selected Cellic® CTec2 (Novozymes, USA) and its cellulase activity was 139.7 FPU/ml determined by IUPAC standard method [13]. Different amounts of hydrochloric acid (1 M) were used to adjust the optimum pH for the enzyme.

Table 2.1. Composition analysis of paper sludge.

Type	Total carbohydrate	Glucan	Xylan	Arabinan + Mannan	Ash	Lignin	Extractives	Total
Sludge	42.3	30.5	8.5	3.3	43.7[a]	3.1	0	90.2
Deashed sludge	92.6	75.8	13.2	3.4	1.5	1.5	0	95.8

[a] Inorganic compounds of ash in sludge are the following: Ca (93.8%), Al (1.2%), Na (1.4%), Mg (1.0%), S (0.6%), P (0.6%), Fe (0.5%), and K (0.4%).

2.2.2. Fractionation of sludge

Since paper sludge has a high portion of ash, ash removal tends to increase the efficiency of enzymatic hydrolysis [5,8]. A screening (Pulmac Masterscreen, Pulmac Systems International Inc., USA) was performed with different sizes and types of screen: ash removal and carbohydrate retention were calculated after fractionation (Eq. 2.1 & 1.2). Raw sludge was disintegrated using a laboratory Hollander beater prior to the screen fractionation system, and deashed sludge was obtained in the rejected part of the screen, which fraction enriched in fibers and significantly reduced ash content.

(Eq. 2.1) $$Ash\ removal\ (\%) = \left(1 - \frac{Ash\ amount\ in\ deashed\ sludge\ collected\ (g)}{Ash\ amount\ in\ raw\ sludge\ in\ inlet\ (g)}\right) \times 100$$

(Eq. 2.2) $$Carbohydrate\ retention\ (\%) = \frac{Carbohydrate\ amount\ collected\ (g)}{Carbohydrate\ amount\ in\ raw\ sludge\ in\ inlet\ (g)} \times 100$$

2.2.3. Enzymatic hydrolysis of deashed sludge

Enzymatic hydrolysis of deashed sludge was performed in an incubator shaker (New Brunswick Scientific, USA) at 50°C and 150 rpm for 96 h. The total solids content of the stock solution was 5% and Cellic® Ctec2 (Novozymes, USA) was the main cellulase applied to this study. Various amounts of hydrochloric acid were added to control the pH of sample for enzymatic hydrolysis. The pH change during enzymatic hydrolysis was monitored to examine how remained ash would interact with acid and affect the enzyme activity.

In further experiments, the effect of ash amount in paper sludge on carbohydrate conversion was evaluated. Artificial ash was generated by placing raw sludge into the muffle furnace at 550 °C for 4 h. Other components such as cellulose, hemicellulose, and lignin were combusted based on the TAPPI method (T 211 om-02) [12]. Two different shear applications before enzymatic hydrolysis were also compared to enhance the buffering capacity of ash. The one called as high shear was introduced with an overhead stirrer (Eurostar 60, IKA Works, Inc., Germany) at 600 rpm, and the other called as low shear was applied by a horizontal shaker (HS 260 control, IKA Works Inc., Germany).

After enzymatic hydrolysis, sugars in the hydrolyzed solution were measured by HPLC (Agilent 1200, Agilent Technologies, USA). The column for the detection was the Shodex SP0810 sugar column (8.0 mm × 300 mm), the column temperature was 80°C, the RID temperature was 50°C and the flow rate was 0.5 ml/min. This paper refers to glucose and xylose conversion as carbohydrate conversion (Eq. 2.3). The following equation also obtains the total sugar recovery (Eq. 2.4).

(Eq. 2.3) $$Carbohydrate\ conversion\ (\%) = \frac{Sugar\ amount\ in\ hydrolysate\ (g)}{Sugar\ amount\ in\ deashed\ sludge\ (g)} \times 100$$

(Eq. 2.4) $$Sugar\ recovery\ (\%) = \frac{Sugar\ amount\ obtained\ after\ enzymati\ hydrolisis\ (g)}{Sugar\ amount\ in\ raw\ sludge\ before\ fractionation\ (g)} \times 100$$

2.3. Results and discussion

2.3.1. Ash removal of paper sludge

The raw sludge used in this study contains 44% of ash, with a total 29 of inorganic elements detected. The main ash component in sludge is calcium, 94% among all inorganic components. Following the measurement with Fiber Quality Analyzer (FQA, OpTest Equipment Inc., Canada), the average length of fibers in sludge used in this study was 0.77 mm, and the average fines weight percentage was 30.1%. To separate ash from paper sludge, fractionation was performed by a Pulmac Masterscreen using different shapes and sizes of screen plates, and the results in terms of ash removal and carbohydrate retention (Eq. 2.1 & 2.2) are shown in Table S2.1. The smallest size of hole plate, which has 0.2 mm diameter of holes, showed the best performance where the ash content was reduced to 1.5%, while obtaining carbohydrate retention of 63% on average. Even though the slot-type screen still achieved high ash removal (98%), carbohydrate retention was much lower than the screen with holes. In other words, a hole-type screen appears to be better fractionation efficiency than a slot-type screen [14]. Therefore, the fractionation using 0.2 mm size of hole screen was decided to prepare deashed sludge for enzymatic hydrolysis.

2.3.2. Enzymatic hydrolysis of raw and deashed sludge

Enzymatic hydrolysis of sludge was investigated in this part by comparing raw sludge and deashed sludge as a starting material. Previous studies have applied mechanical and chemical pretreatment to remove ash [5,9] for enzymatic hydrolysis or acid-pretreatment with high enzyme dosage to obtain a high sugar yield [4,8]. Since these methods may require additional use of chemicals such as acid or surfactant, this study introduces performing enzymatic hydrolysis using only hydrochloric acid in distilled water rather than a buffer solution. The HCl usage enables to provide an adequate pH environment for cellulase and remove the residual ash at the same time. First, raw sludge was prepared at 5% consistency, followed by adding HCl without the mechanical treatment to remove ash. This treatment enabled most of ash in sludge to be sufficiently dissolved so that cellulase effectively hydrolyzed the substrate during enzymatic hydrolysis. After mixing samples and HCl, cellulase (Cellic® CTec2) was added at 5 FPU/g oven dried (o. d.) sludge. The results showed that carbohydrate conversion was 72.3% after 96 h of hydrolysis whereas the amount of HCl addition was 107.7 mg/g o. d. sludge. The carbohydrate conversion of raw sludge in this study was higher than in other papers, where they used similar properties of raw sludge and achieved 40% [9] and 63% [5] with pH adjustment. In other words, raw sludge has a high potential to produce sugars without taking into account of any fractionation steps, but it demands a high amount of acid. Another side effect is that the salt generated during enzymatic hydrolysis of sludge might have a negative effect on the downstream process or biofuel production (Eq. 2.5).

(Eq. 2.5) $$CaCO_3\,(s) + 2\,HCl\,(aq) \rightarrow CaCl_2\,(aq) + H_2O\,(l) + CO_2\,(g)$$

Deashed sludge, prepared by the fractionation, was subject to enzymatic hydrolysis with 1.5% ash contained. In **Fig. 2.1.**, the changes in pH over time of deashed sludge were investigated while deashed sludge reacted with HCl for 24 h to find the proper HCl amount. Five different amounts of HCl were prepared and added to deashed sludge samples without enzyme. Based on the pH track of deashed sludge (**Fig. 2.1**), it is noted that the first 6 h is the period when a rapid increase in pH was observed at all amounts of

HCl evaluated (0.7–7.2 mg/g o. d. sludge), likely due to most of the calcium carbonate dissolved during this period (Eq. 2.5). Considering the results, a lower concentration of HCl reaches over pH 6.0 in the initial 6 h, so that the pH level is not appropriate to the cellulase activity. Therefore, HCl addition of 7.2 mg/g o. d. sludge was chosen for the enzymatic hydrolysis of deashed sludge to provide the proper pH for cellulase and prevent the inhibition effect of CaCO3 on enzyme activity.

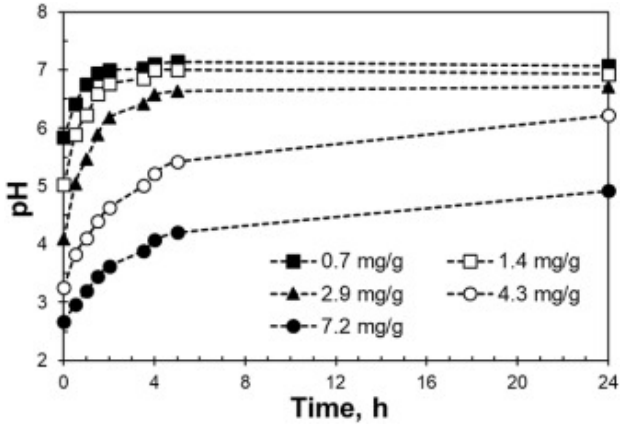

Fig. 2.1. The pH change of deashed sludge with different amounts of HCl. The value of HCl concentration indicates mg HCl/g o. d. sludge. The sample consistency was prepared at 5% and the sample was kept in the incubator shaker (50°C) for all measurements.

Table 2.2. Carbohydrate conversion and pH changes of deashed sludge samples depending on different enzyme dosages. Deashed sludge contained 1.5% of ash. HCl was added at 7.2 mg/g o.d. sludge.

Enzyme dosage	Carbohydrate conversion	Initial pH	Final pH
2.5 FPU/g o.d. sludge	70.9%	3.4	5.9
	75.5%	3.3	5.0
5 FPU/g o.d. sludge	87.4%	2.4	3.9
	88.2%	3.5	5.3
	91.5%	3.0	3.9
	92.6%	2.7	4.1
	93.4%	2.5	4.6
7.5 FPU/g o.d. sludge	98.1%	3.1	4.0
	99.5%	3.1	3.5

Table 2.2. shows the representative results of carbohydrate conversion starting around pH 3.0 by adding HCl of 7.2 mg/g o. d. sludge. The deashed sludge and HCl were agitated under high shear (600 rpm), and then enzyme was added. Based on Eq. 2.5, 70% of CaCO3 (mol based) was reacted with HCl and converted to CaCl2. The average carbohydrate conversion showed 90 (±2.7)% at 5 FPU/g o. d. sludge. As ash in deashed

sludge lowered compared to raw sludge, HCl addition required much lower. The following results are similar to the enzymatic hydrolysis under a buffer system reported by other papers [[5], [6], [7]]. Chen's results showed that the sugar conversion of fractionated sludge was 91.5% at pH 4.8 and 4 FPU/g substrate dosage of mixed enzyme cocktail [5]. As the enzyme dosage increased, as shown in **Table 2.2**, almost 99% of carbohydrate conversion was achieved at 7.5 FPU/g o. d. sludge.

The summary of this part is described in **Fig. 2.2.** When most of the ash was removed by fractionation, high agitation and a small amount of acid added to the matrix prior to enzymatic hydrolysis resulted in reducing the negative effect of ash on enzyme activity and increasing carbohydrate conversion. In contrast, it has a negative impact on sugar recovery since fibers were lost in fractionation. Without fractionation, sugar recovery increased, however, a significant amount of acid was required and the salt generated by CaCO3 and HCl should be considered to design the downstream process. The criteria about how much ash is removed are important to be considered for the enzymatic hydrolysis efficiency of sludge. Following experiments are designed in order to reduce the excess required amount of acid and enhance the accessibility of cellulase to fibers.

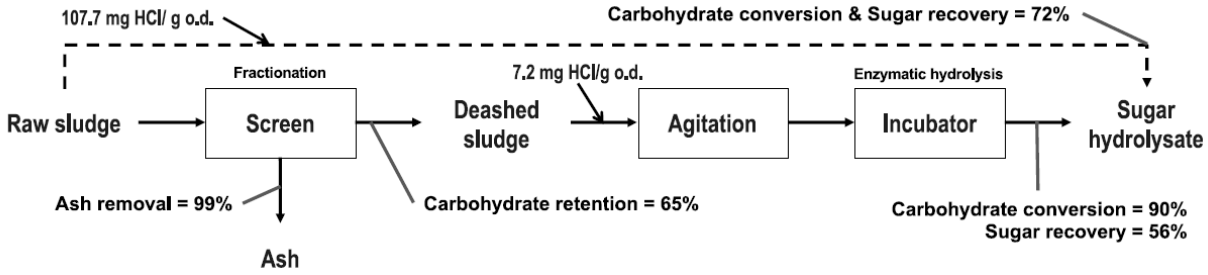

Fig. 2.2. Schematic diagram of an effective process of producing sugars from sludge. Carbohydrate conversion, sugar recovery, and HCl usage (mg HCl/g o. d. sludge) were compared between raw sludge and deashed sludge.

2.3.3. Enzymatic hydrolysis of sludge depending on ash content

Carbohydrate conversion, sugar recovery, and acid requirement varied depending on the ash content of starting materials based on **Fig. 2.2.** Consequently, the effect of ash content on enzymatic hydrolysis is required to be investigated in terms of carbohydrate conversion and sugar recovery, as well as the required amount of HCl. Many papers proposed the pretreatment of sludge before enzymatic hydrolysis to minimize the negative effect of ash on sugar yield and enhance carbohydrate conversion, such as using a screen [5] or HCl soaking overnight [8,9]. However, a definite study on the relationship between enzymatic hydrolysis yield and ash content has been lacking. It is important to acknowledge that each sludge sample contains different amounts of ash depending on the process at the pulp and paper mills manufacturing facility. Therefore, this part suggests the minimization of pretreatment steps by not removing all the ash for the economic valorization of paper sludge. The ash amount was controlled, ranging from 1.5% to 45%, by adding artificial ash in deashed sludge containing 1.5% of ash. Each sample fixed the enzyme dosage at 5 FPU/g o. d. sludge (10.4 mg cellulase/g cellulose). The initial pH was controlled by adding different amounts of HCl, and the amount of HCl

used was the one that resulted in the best conversion from each sample, as shown in **Fig. 2.3a**. Before adding enzyme (Cellic® Ctec2, Novozymes), the sludge sample was agitated with a certain amount of HCl to convert most of CaCO3 to CaCl2, consequently, attaining the desirable pH for cellulase.

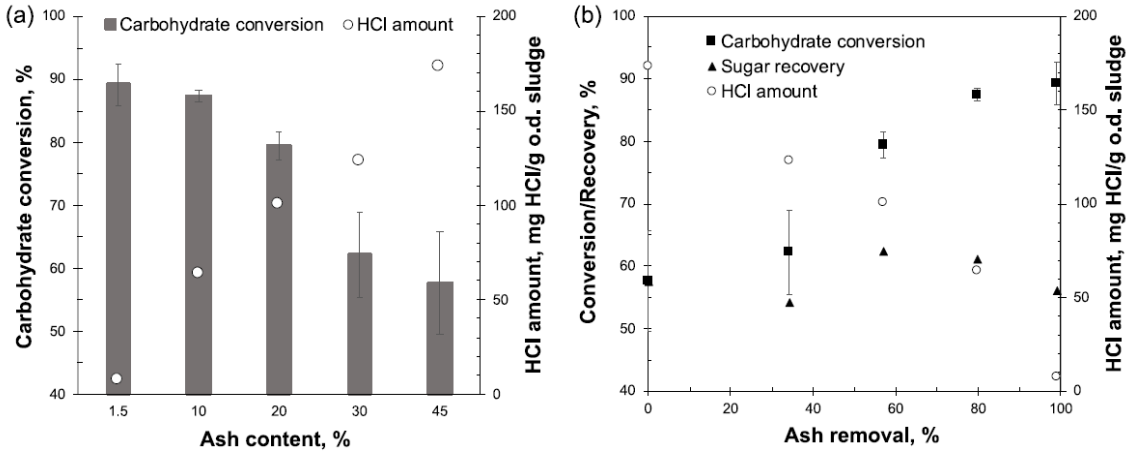

Fig. 2.3 (a) Carbohydrate conversion at 5 FPU/g o. d. sludge and demanded HCl amount depending on ash content. HCl amount was determined as the amount in which the carbohydrate conversion was maximum with 5 FPU/g o. d. sludge. Ash content was adjusted by adding synthesis ash to the deashed sludge. **(b)** Carbohydrate conversion and sugar recovery at 5 FPU/g o. d. sludge and demanded HCl amount depending on ash removal. HCl amount was determined as the amount in which the carbohydrate conversion was maximum with 5 FPU/g o. d. sludge. Ash removal was calculated by dividing the ash amount that remained in deashed sludge, which came from the adjusted ash amount from **Fig. 2.3a**, divided by the ash amount in sludge (Eq. 2.1).

Fig. 2.3a describes carbohydrate conversion and the amount of HCl addition needed for the best results of carbohydrate conversion depending on the ash amount in sludge. As the ash content in sludge increased, more HCl addition was required for the proper pH. Nevertheless, carbohydrate conversion decreased as the ash amount increased because the negative effect of remaining CaCO3 on enzyme activity had more influence than the buffering effect of CaCO3. On the other hand, it is noted that carbohydrate conversion at the ash content of 10% in sludge samples showed similar to the one at the ash content of 1.5%. **Fig. 2.3a** signifies that when raw sludge has a low portion of ash it can be directly put into use to produce sugars without separating the ash and fibers.

Fig. 2.3b explains sugar recovery and carbohydrate conversion in the view of ash removal. In this part, the ash removal rate is considered another critical factor in total sugar recovery. The assumption in **Fig. 2.3b** is that ash removal was calculated by Eq. 2.3. using each ash content (**Fig. 2.3a**) as ash amount in deashed sludge collected and raw ash content (45%) as ash amount in raw sludge in the inlet. While the highest conversion presented 89% at ash removal of 99%, the highest sugar recovery showed 62% at ash removal of 60%. Considering both carbohydrate conversion and sugar recovery based on ash removal in **Fig. 2.3b**, it is not necessary to remove most of the ash in sludge to effectively produce sugars. In other words, ash removal of 80% not only

retains most of the fibers after deashing but also produces a considerable amount of sugars, while CaCO3 is eliminated during enzymatic hydrolysis. On the other hand, when HCl addition and carbohydrate conversion are considered significant, intense ash removal is required. Both the fractionation of sludge and the dissolution of remaining ash by HCl contribute to higher carbohydrate conversion since there is less chance of CaCO3 prohibiting enzyme activity. Although the sample in which most ash is removed showed the highest carbohydrate conversion, the sugar recovery was not the highest. This was attributed to the loss of carbohydrates during the deashing step, where the carbohydrate retention after deashing with the smallest hole of screen indicated 63%.

2.3.4. Factors on enzymatic hydrolysis of sludge – pH adjustment

This part investigates the factors that are affected by different ash content in sludge samples: pH adjustment and shear application. As discussed in **Fig. 2.1**, it was proved that a higher amount of acid was required to create a pH environment that resulted in the highest yield of carbohydrates from sludge. It is necessary to comprehend precisely how the pH condition yields higher carbohydrate conversion of sludge controlled by adding HCl. Two experiments on pH adjustment were designed. First, three different pH of acetate buffers were prepared for the enzymatic hydrolysis of deashed sludge (**Table 2.3**) to confirm which pH range would result in higher sugar yields. It is noted that the initial pH of all samples rose compared to set the intended pH of buffer solution due to the remaining calcium carbonate in deashed sludge. The results confirmed that the acetate buffer solution of pH 3.7 should be prepared, when deashed sludge contained 1.5 wt% of ash. This condition eventually led to pH 5.0 of deashed sludge samples, which is the suggested pH range by Novozymes and resulted in higher carbohydrate conversion (98%) with 5 FPU/g o. d. sludge. The result corresponds with the previous results that a higher amount of HCl is required for the higher sugar yield shown in **Fig. 2.1.** In other words, a higher concentration of acid in buffer solution reacted with the remaining ash in deashed sludge, where the desired pH for the cellulase was reached, and the inhibition of CaCO3 effect on cellulase was prevented.

Table 2.3. Carbohydrate conversion and pH description by three different conditions of buffer solution resulted from enzymatic hydrolysis of deashed sludge (Parenthesis indicates the standard deviation.). Enzyme dosage was at 5 FPU/g o.d. sludge.

Buffer condition	Carbohydrate conversion	Sugar recovery	Initial pH	Final pH
Acetate buffer pH 3.7	97.5 (0.4)%	61.2%	4.86 (0.16)	4.82 (0.16)
Acetate buffer pH 5.2	68.6 (2.1)%	43.1%	6.12 (0.02)	6.07 (0.01)
Acetate buffer pH 5.8	65.3 (3.3)%	41.0%	6.53 (0.04)	6.46 (0.01)

Previous research suggested the additional use of sulfuric acid in buffer solution or increasing the enzyme dosage to achieve higher carbohydrate conversion of sludge

samples when they contained ash [5,8,9]. Gurram and the team [9] mixed primary sludge into acid solution (1 M HCl, 10 w/v%) overnight and additionally pretreated the samples with H2O2 before enzymatic hydrolysis. The pH adjustment happened by using H2SO4 to improve the enzymatic hydrolysis yield, especially in the case of raw sludge [5]. Also, Mendes and the team [8] suggested sludge samples mixed with an acid solution for a few minutes and adding 35 FPU/g carbohydrate, which was much higher than the enzyme dosage used in this study. On the other hand, using lower pH of acetate buffer or adding a higher amount of acid is suggested in this study to overcome the negative effect of ash on enzymatic hydrolysis of sludge and provide the proper pH range. It is also efficient in eliminating the extended period of pretreatment step or lowering the enzyme dosage.

The second experiment was conducted to demonstrate how pH conditions efficiently influence sugar yield by monitoring pH changes during the enzymatic hydrolysis of deashed sludge at several conditions. **Fig. 2.4a** represents the pH monitoring for 96 h of enzymatic hydrolysis of deashed sludge and southern bleached hardwood kraft pulp (SBHK) additionally containing 1.5% CaCO3. The first part where pH change occurs during the initial 6 h in most of the conditions is critical to increasing pH to approximately 6.0 where most of CaCO3 was dissolved by HCl. According to the reference sheet provided by Novozymes (USA), the optimum pH for cellulase (Cellic® Ctec2, Novozymes) is between 5.0 and 5.2, and the pH range of 5.0–6.0 gives 80–100% of relative performance. When deashed sludge performed enzymatic hydrolysis for 24 h, pH of the matrix was maintained at 6.0, and carbohydrate conversion showed 60–70%. Afterward, deashed sludge samples mostly kept the pH range of 5.0–6.0, which resulted in the carbohydrate conversion of 90% at the end. Therefore, the change in pH during enzymatic hydrolysis points out that the dissolution of CaCO3 is necessary to alleviate the negative effect of CaCO3 on cellulase at the beginning of enzymatic hydrolysis.

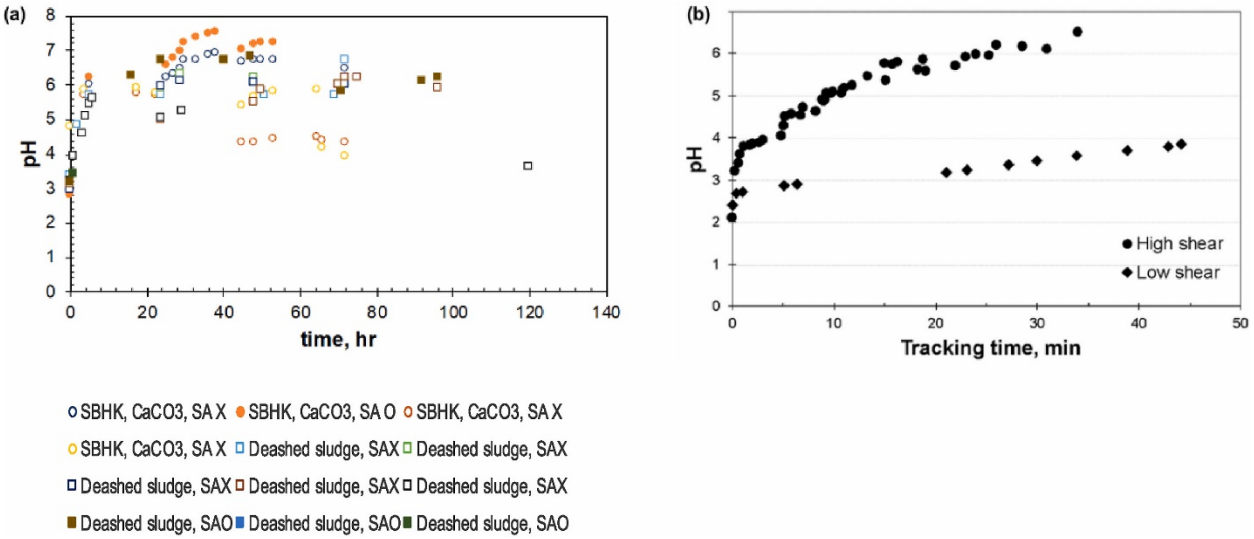

Fig. 2.4. (a) The change in pH during enzymatic hydrolysis: Southern bleached hardwood kraft pulp (SBHK, symbol ○) including 1.5% of calcium carbonate (CaCO3) and deashed sludge (symbol □) with (SAO, filled symbol)/without (SAX, empty symbol) sodium azide (SA). Each pH detail of the sample is described in Fig. S2.2. (b) The change in pH of

deashed sludge which contains 1.5% of ash in depending on the magnitude of shearing. Acid was added at 7.2 mg HCl/g o. d. sludge in sludge samples.

In **Fig. 2.4a**, the pH effect on enzymatic hydrolysis is also investigated depending on the addition of sodium azide. The microbial growth is reported to occasionally have an impact on decreasing the pH during enzymatic hydrolysis. Autoclaving of sludge [6,15] or the use of antibiotics [15,16] has been used for biomass samples before the enzymatic reactions. Kang's team [6] observed some microorganisms' growth during the enzymatic hydrolysis of sludge, so they compared the released sugar amount between each method of using antibiotics and autoclaving the samples. One of their conclusions was that the antibiotics addition lowered the yield by 10%, but they did not mention the reason specifically. In **Fig. 2.4a**, the pH change from the samples containing sodium azide illustrated why the addition of sodium azide lowered the sugar yield. **Fig. 2.4a** shows that the pH of both SBHK and deashed sludge samples with sodium azide increased to 6.0 in the first 6 h. After 6 h, pH went slightly over pH 6.0 for both samples, which was not the preferable pH for the cellulase. As a result, the sugar released inevitably dropped down compared to the samples without sodium azide. The aid of sodium azide can prevent the microbial growth during enzymatic hydrolysis, but it resulted in pH not optimal for the efficient performance of the cellulase, which led to the lower sugar yields.

2.3.5. Factors on enzymatic hydrolysis of sludge – shear application

Our studies observed that the optimal enzymatic hydrolysis of deashed sludge required a higher acid addition in the early hydrolysis stage. This desired condition will maintain the optimum pH for cellulase by HCl consuming CaCO3 and inhibit the affinity of CaCO3 to the enzyme. To provide the desired condition, the faster consumption of CaCO3 by HCl should be achieved during enzymatic hydrolysis. Thus, the relationship between the accessibility of CaCO3 in deashed sludge to HCl and sugar yield is further investigated in terms of shear magnitude. Two simulation experiments were performed to verify if CaCO3 can act as a barrier to the accessibility of cellulase to fibers. The first set of experiments (A) includes two steps. The first step is that enzyme and CaCO3 were added to distilled water, and this sample was agitated for an hour. The second step is that deashed sludge and HCl were added to the sample and agitated for 5 h more. The second set of experiment (B) is prepared by agitating the sample containing all enzyme, CaCO3, HCl, and deashed sludge simultaneously. The carbohydrate conversion of B (21.8%) presents much higher than that of A (5.3%). The presence of CaCO3 disturbs the accessibility of the enzyme to fiber [7,17]. Importantly, we should consider not only how much ash is in the sample but how fast calcium carbonate is accessible to acid rather than enzyme in sludge samples.

Consequently, the shear is proposed to help increase the accessibility of the enzyme to fibers and expedite the dissolution of CaCO3 by HCl. **Fig. 2.4b** represents the pH change by using the different magnitude of shear applied to the 5% consistency of the deashed sludge sample. High shear was applied by the overhead stirrer (Eurostar 60, IKA Works, Inc., Germany), and low shear was applied by the horizontal shaker (HS 260 control, IKA Works, Inc., Germany). As shown in **Fig. 2.4b**, the pH of the sample applied to high shear rapidly increased. In other words, high shear made the accessibility of CaCO3 easier to

HCl than low shear did. In the case of low shear, it took 3 h to reach pH 6.0. This result confirms that high shear is the important step before the enzymatic hydrolysis of sludge. For this reason, the continuous process should include the application of high shear to deashed sludge samples and agitation of deashed sludge with HCl followed by enzymatic hydrolysis, as described in **Fig. 2.2.** After high shear and agitation, carbohydrate conversion of deashed sludge was 90% on average with a relatively lower enzyme consumption. This process also provided an advantage of increasing the accessibility of enzyme to fibers while CaCO3 was dissolving by HCl.

2.4. Conclusions

Carbohydrate conversion and sugar recovery were examined during enzymatic hydrolysis of paper sludge with different ash contents. Removing ash in sludge enhanced carbohydrate conversion, while the highest sugar recovery was achieved when the sludge contained 20% ash. The pH change in enzymatic hydrolysis of deashed sludge indicates that ash is the main factor affecting pH and enzyme activity. Therefore, the acid addition and high shear application were suggested to prevent the negative effect of ash on enzyme. These results provide useful information on the valorization of paper sludge generated by the paper industry.

References

1. P. Bajpai, Management of Pulp and Paper Mill Waste, Springer International Publishing, Cham, 2015, https://doi.org/10.1007/978-3-319-11788-1.
2. T. Mahmood, A. Elliott, A review of secondary sludge reduction technologies for the pulp and paper industry, Water Res. 40 (2006) 2093–2112, https://doi.org/10.1016/j.watres.2006.04.001.
3. N.K. Budhavaram, Z. Fan, Production of lactic acid from paper sludge using acidtolerant, thermophilic Bacillus coagulan strains, Bioresour. Technol. 100 (2009) 5966–5972, https://doi.org/10.1016/j.biortech.2009.01.080.
4. S. Zhu, J. Sui, Y. Liu, S. Ye, C. Wang, M. Huo, Y. Yu, Effects of washing, autoclaving, and surfactants on the enzymatic hydrolysis of negatively valued paper mill sludge for sugar production, Energy Fuel. 33 (2019) 1219–1226, https://doi.org/10.1021/acs.energyfuels.8b03586.
5. H. Chen, Q. Han, K. Daniel, R. Venditti, H. Jameel, Conversion of industrial paper sludge to ethanol: fractionation of sludge and its impact, Appl. Biochem. Biotechnol. 174 (2014) 2096–2113, https://doi.org/10.1007/s12010-014-1083-z.
6. L. Kang, W. Wang, Y.Y. Lee, Bioconversion of kraft paper mill sludges to ethanol by SSF and SSCF, Appl. Biochem. Biotechnol. 161 (2010) 53–66, https://doi.org10.1007/s12010-009-8893-4.
7. L.R. Lynd, K. Lyford, C.R. South, Evaluation of paper sludges for amenability to enzymatic hydrolysis and conversion to ethanol, Tappi J. 84 (2001) 19.
8. C.V.T. Mendes, J.M.S. Rocha, M.G.V.S. Carvalho, Valorization of residual streams from pulp and paper mills: pretreatment and bioconversion of primary sludge to bioethanol, Ind. Eng. Chem. Res. 53 (2014) 19398–19404, https://doi.org/10.1021/ie503021y.
9. R.N. Gurram, M. Al-Shannag, N.J. Lecher, S.M. Duncan, E.L. Singsaas, M. Alkasrawi, Bioconversion of paper mill sludge to bioethanol in the presence of

accelerants or hydrogen peroxide pretreatment, Bioresour. Technol. 192 (2015) 529–539, https://doi.org/10.1016/j.biortech.2015.06.010.
10. F. Steffen, R. Janzon, B. Saake, Enzymatic treatment of deinking sludge – effect on fibre and drainage properties, Environ. Technol. 39 (2018) 2810–2821, https://doi.org/10.1080/09593330.2017.1365948.
11. J.B. Sluiter, R.O. Ruiz, C.J. Scarlata, A.D. Sluiter, D.W. Templeton, Compositional analysis of lignocellulosic feedstocks. 1. Review and description of methods, J. Agric. Food Chem. 58 (2010) 9043–9053, https://doi.org/10.1021/jf1008023.
12. TAPPI (US Technical Association of Pulp and Paper Industry), Test Methods T 211 Om-02 Ash in Wood, Pulp, Paper and Paperboard: Combustion at 525◦C, Tappi Press, Atlanta, GA, USA, 2002.
13. T.K. Ghose, Measurement of cellulase activities, Pure Appl. Chem. 59 (1987) 257–268, https://doi.org/10.1351/pac198759020257.
14. J.A. Olson, Fibre length fractionation caused by pulp screening, slotted screen plates, J. Pulp Pap. Sci. 27 (2001) 255–261.
15. J. Serate, D. Xie, E. Pohlmann, C. Donald, M. Shabani, L. Hinchman, A. Higbee, M. Mcgee, A. La Reau, G.E. Klinger, S. Li, C.L. Myers, C. Boone, D.M. Bates, D. Cavalier, D. Eilert, L.G. Oates, G. Sanford, T.K. Sato, B. Dale, R. Landick, J. Piotrowski, R.G. Ong, Y. Zhang, Controlling microbial contamination during hydrolysis of AFEX-pretreated corn stover and switchgrass: effects on hydrolysate composition, microbial response and fermentation, Biotechnol. Biofuels 8 (2015), https://doi.org/10.1186/s13068-015-0356-2.
16. D.J. Schell, N. Dowe, K.N. Ibsen, C.J. Riley, M.F. Ruth, R.E. Lumpkin, Contaminant occurrence, identification and control in a pilot-scale corn fiber to ethanol conversion process, Bioresour. Technol. 98 (2007) 2942–2948, https://doi.org/10.1016/j.biortech.2006.10.002.
17. S. Marques, L. Alves, J.C. Roseiro, F.M. Gírio, Conversion of recycled paper sludge to ethanol by SHF and SSF using Pichia stipitis, Biomass Bioenergy 32 (2008) 400–406, https://doi.org/10.1016/j.biombioe.2007.10.011.

Chapter 3: Dehydration of carbohydrates to intermediate furans

Biofuels are emerging as replacements for petroleum-based fuels, especially for sustainable fuels for aviation. Feasible sustainable feedstocks are being sought to reduce greenhouse gas emissions from carbon-based fuels. This study focuses on a wet waste stream generated from pulp and paper mills, paper sludge, as a sustainable feedstock from which to produce platform chemicals and jet fuel. Furan chemicals are significant platform chemicals, which can be formed by the dehydration of sugar monomers. Impurities initially contained in paper sludge and generated in enzymatic hydrolysis can impede the high yield of furan chemicals. Herein, the importance of understanding the role of impurities on the dehydration process has been addressed. Optimization of dehydration of sludge-derived hydrolysate is described and the effect of impurities on product yield clarified. Paper sludge valorization utilizes a renewable feedstock and decreases the need for waste disposal.

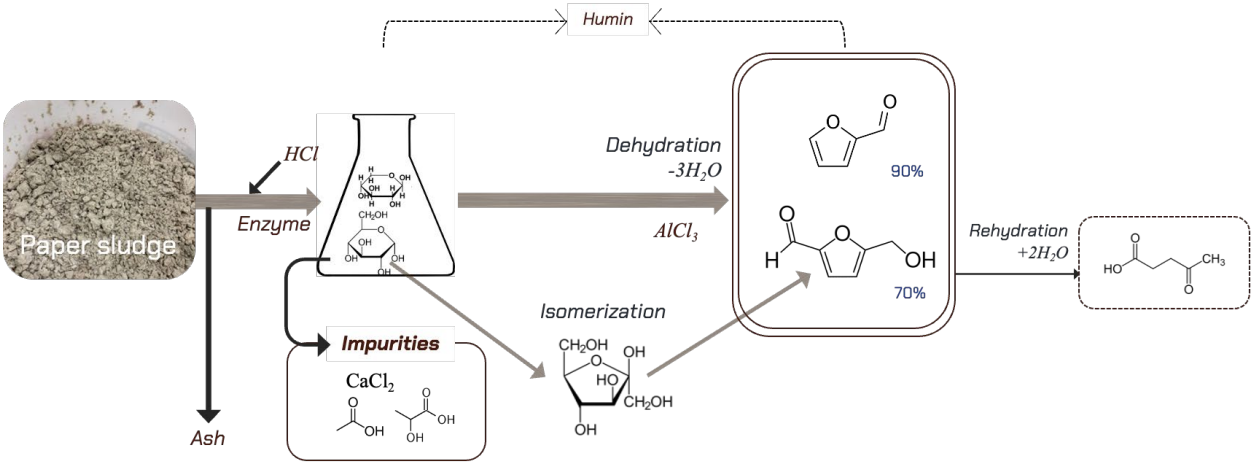

Fig. 3.1. Overall reaction pathway to produce sludge-derived furan chemicals.

3.1. Introduction

The reduction of CO_2 emissions has been pointed out as one of the most serious and important issues we are currently facing and one that needs to be addressed immediately. The Carbon Offsetting and Reduction Scheme for International Aviation (CORSIA) mentioned the necessity of reducing CO_2 emissions from the aviation industry [1]. Hence, the production and use of sustainable aviation fuel (SAF) has been highlighted with one of the criteria being production of SAF from feedstocks such as woody biomass, waste resources, and agricultural residues [2-4].

The Pulp and Paper (P&P) industry has gained a spotlight to lead the future global carbon challenges. The P&P industry is recognized as one of the five largest industries under the category of energy use [5]. Management of the P&P industry has been highlighted as one needing to eliminate negative environmental impacts, including waste management [6]. A solution to waste management can be waste valorization. Waste valorization involves converting waste materials into useful products considering the environmental issues and carbon cycle. Wet waste streams generated in the P&P industry have a high potential to

be converted into useful products such as bio-based materials[7], chemicals [8-10], or energy [11-14].

Paper sludge is one of the major waste streams generated by the P&P industry [15]. The conventional way to dispose of paper sludge in the mill includes landfill, lagoon, incineration, or land application. Since all wet waste streams are collected into a primary clarifier, paper sludge contains a lot of ash, whose content varies depending on the mill type, as well as the fibers to be recovered. Sludge fractionation to remove ash could allow recovery of cellulosic fibers which can be valorized. Our previous study investigated the effect of ash on enzymatic hydrolysis of paper sludge to efficiently and effectively produce sugars [16]. The results showed that it was not necessary to remove all of the ash for effective sludge valorization. To valorize paper sludge into the essential platform chemical, mainly furan chemicals, an understanding of the effect of impurities contained in paper sludge and generated during chemical reaction processes is necessary.

Attempts have been made to use biomass-derived carbohydrates or cellulose to produce liquid alkanes for fuel applications [17-20]. 5-hydroxymethylfurfural (HMF) is an important precursor to produce bio-based chemicals such as 2,5-furandicarboxylic acid (FDCA) and 2,5-dimethylfuran (DMF) or to be converted into hydrocarbons for use in jet fuel [21][22]. Both HMF yield and selectivity are dependent on feedstock selection. Comparing fructose and glucose, glucose has been reported to result in a more limited and sensitive HMF yields [23]. By-products such as humin and levulinic acid or formic acid should be suppressed to gain high selectivity to furan chemicals. Several methods have been introduced to improve the glucose dehydration process, such as the use of solvents [24-26], bi-phasic systems [17], and reactors [27][28]. The use of an ionic liquid (IL) as a solvent during dehydration increased HMF yield to over 90% but IL is an expensive solvent and easily deactivated by small amounts of water so that it cannot be applied to the industrial scale [24]. Bi-phasic systems have also been tried to separate HMF from the aqueous reaction system that give relatively high HMF yield (80%). The huge advantage of this system is the prevention of self-degradation or hydration of HMF [17]. The drawbacks of this system are the difficulty in reutilizing homogeneous catalysts and the use of salts with heterogeneous catalysts [24].

The selection of catalyst and solvent is fundamentally important to provide a better HMF yield from glucose. Acid-base catalysts, metal catalysts, ion-exchange, or salt catalysts are representative for the dehydration of carbohydrates [29][30]. Ordomsky et al. investigated the effect of metals on glucose dehydration over different phosphates [31]. Increasing acid strength enhanced glucose conversion and, the ratio of Brönsted to Lewis acid sites also had a great impact on the selectivity for HMF. Adversely, strong-to-moderate Lewis acidity was reported to promote humin polymerization from glucose, fructose, and HMF [32]. Therefore, the concentrations of both Brönsted and Lewis acid sites are the important factor for glucose dehydration to HMF [33]. Aluminum chloride ($AlCl_3 \cdot 6H_2O$) has been shown to be a good catalyst for glucose dehydration since it is effective for both glucose isomerization and fructose dehydration [34][35]. The effect of solvent on the dehydration of glucose is highly related to the types of catalysts used in

the reaction. When using solid catalysts with an aid of HCl, organic solvents such as DMSO and dioxane work efficiently in terms of HMF yield and selectivity [36].
Fundamental research on catalysts and solvents can bring more opportunities in the use of renewable biomass materials. Considering the chemical pathways for glucose dehydration, glucose can be dehydrated directly from HMF [33][37] or isomerized to fructose followed by dehydration [38-40]. Still, the pathways are under debate due to the difficulty in obtaining clear results from glucose dehydration and the sensitivity of experimental results to the catalyst or solvent used. Undesirable reactions involving rehydration or polymerization result in by-products such as levulinic acid, formic acid, or humins.

Considering both the peculiarity of sludge and the ongoing debate on the mechanism and pathways of catalytic glucose dehydration, it is highly important to scrutinize the existing mechanisms and consider them in the dehydration of sludge-derived hydrolysate. Therefore, the present study focuses on the optimization of dehydration of sludge-derived hydrolysate into furan chemicals with a detailed understanding of the effect of impurities on product yield. Calcium chloride, derived from ash contained in paper sludge, and organic acid, produced after enzymatic hydrolysis, were the impurities mainly focused on in this study. Good selectivities and yields of furan chemicals were obtained from a mixture of dioxane and sludge-derived hydrolysate with aluminum chloride as the main catalyst using a microwave reactor compared to pure glucose and xylose solution. This study is important for the conversion of a wet waste stream generated from the P&P industry into furan chemicals which can then be used to make SAF.

3.2. Materials and Methods

3.2.1. Raw materials

Paper sludge was obtained from the Kraft pulping mill located in the USA (NC, USA). Paper sludge samples were frequently obtained at different times to confirm the uniformity of experiment results. Cellulases were selected for enzymatic hydrolysis of paper sludge, Cellic® CTec2 and CTec3 (Novozymes, USA). Hydrochloric acid (1 M) was added to meet the optimum pH for each cellulase. Dioxane (99.8%, Sigma-Aldrich®) and aluminum chloride (Hexahydrate, 99%, Thermo Scientific™) were used for the dehydration experiment. Glucose and xylose were also purchased from Sigma-Aldrich for comparison with dehydration of sludge-derived hydrolysate.

The composition of the paper sludge was analyzed (NREL procedure [41]) to determine the amount of carbohydrates, lignin, and ash. The inorganic components in ash were determined by ICP-MS (Inductively coupled plasma-mass spectroscopy, Elan DRC2, Perkin Elmer, USA).

3.2.2. Ash fractionation

In this study, the removal of ash from paper sludge was performed with two different screens. Pulmac Masterscreen (Pulmac Systems International Inc., USA) (0.2 mm hole diameter) was used, which can manage up to 100 g oven-dried (o.d.) of material. A Sidehill screen (0.5 mm hole diameter) was also used with a hydrapulper connected, and

20 kg o.d. of sludge. Deashed sludge was collected after most of the ash in paper sludge was removed. The amount of ash in the deashed sludge was also calculated.

3.2.3. Enzymatic hydrolysis of deashed sludge

Enzymatic hydrolysis of deashed sludge was performed in two different ways. The first method used an incubator shaker at 50ºC and 140 rpm for 96 hours at 5% consistency. The amount of deashed sludge for the first method ranged 1 to 10 o.d. grams. The other method was to adapt a paddle reactor operated at 50ºC and 65 rpm for 96 hours with higher consistency (15% total solids). This method can handle a larger scale of enzymatic hydrolysis up to 2 kg o.d. of deashed sludge. The sludge-derived hydrolysate was obtained after either centrifugation or filtration. Sugar concentrations (glucose and xylose) were determined by HPLC (Agilent 1260, Agilent Technologies, USA) using an RID detector (45ºC). The column was an Aminex HPX-87H (Biorad, 300 × 7.8 mm, pH range 1 – 3) operated at 50ºC with a flow rate of 0.7 ml/min of 0.005 M sulfuric acid.

3.2.4. Dehydration of sludge-derived hydrolysate and pure sugar solutions

Dehydration experiments were performed using a microwave reactor (Discover 2.0, CEM, USA). Aluminum chloride ($AlCl_3$) was used as the main catalyst, and 1,4-dioxane was mixed with the sugar solutions or sludge-derived hydrolysates. Reactions were performed for different times and temperatures. The pre-stirring option was chosen for 10 sec before the reaction, and the cooling was operated until a temperature of 50ºC was reached. The magnetic stirring was turned on at the medium level of speed setting during the reaction as well. Products (hydroxylmethylfurfural (HMF), furfural (FF), levulinic acid, glucose, and fructose) were analyzed by HPLC with using RID and VWD detectors.

3.3. Results and Discussion

3.3.1. Properties of paper sludge and sludge-derived hydrolysate

Paper sludge samples used in this study were obtained at the same mill (D mill, USA). The properties of each paper sludge were analyzed whenever paper sludge was obtained. **Table 3.1** shows the composition of sludge and deashed sludge depending on the fractionation equipment. Sludge composition and ash content varied depending on where and when the sludge was obtained. **Table 3.1** implies different composition of samples even though they were collected at the same mill but the different time when acquired. Ash is known as an inhibitor for valorization of sludge into useful products[13]. Ash content was dramatically decreased using the Pulmac Masterscreen and sidehill screen. Since ash is the significant component to be controlled for sludge valorization, ash properties were further analyzed with ICP-MS in our previous study [16] and the results show that the major ash component is calcium carbonate.

Deashed sludge was enzymatically hydrolyzed with different conditions based on how much ash it contained. For enzymatic hydrolysis of deashed sludge, HCl was added to the sample to adjust pH rather than using a buffer solution. **Table 3.2** shows the different amounts of HCl added (mg/g o.d. sludge) added each deashed sludge sample to meet the proper pH for the cellulase. Sample A, B, and C were prepared by different methods Enzymatic hydrolysis was performed in either an incubator shaker (50ºC, 150 rpm) or a

paddle reactor (50ºC, 70 rpm). Samples A and B had ash removed using the Pulmac Masterscreen and were then hydrolyzed enzymatically in an incubator shaker. The enzyme for A and B was Cellic® CTec2. Sample C was prepared by the following method. The ash in the sludge was removed by a sidehill screen and the deashed sludge was then hydrolyzed in a paddle reactor. The enzyme for C was Cellic® CTec3.

Table 3.1. Results of biomass composition analysis for each sludge and deashed sludge.

Sample No.*	Carbohydrate		Lignin, %	Ash content, %
	Glucan, %	Xylan, %		
A	31.5	8.6	3.8	43.1
B	21.7	3.9	2.7	68.5
C	N.A.			
A-1	75.6	13.1	1.7	1.4
B-1	69.7	11.2	1.2	2.6
C-1	66.4	10.8	1.9	9.0

*X samples (e.g., A, B, C) are obtained at different times, and X-1 indicates deashed sludge from the X sample. A and B samples were fractionated by Pulmac Masterscreen, and C samples were fractionated by sidehill screen. (N.A.: Not available).

The final sludge-derived hydrolysate, prepared after ash removal and enzymatic hydrolysis, was used to produce HMF and FF. HPLC analysis of the sludge-derived hydrolysate detected glucose, xylose, organic acids (lactic acid and acetic acid), and barely any oligomers. The concentrations of glucose and xylose (**Table 3.2**) varied due to different initial enzymatic hydrolysis conditions. Various concentrations of organic acids were detected in the hydrolysate. Additionally, the amount of $CaCl_2$ in the hydrolysate was calculated by equation (Eq. 3.1) based on the remaining $CaCO_3$ in each deashed sludge sample and the HCl added to the hydrolysate.

$$CaCO_3\ (s) + 2HCl\ (aq) \rightarrow CaCl_2\ (aq) + H_2O\ (l) + CO_2\ (g) \qquad \text{(Eq. 3.1)}$$

Table 3.2. Properties of sludge-derived hydrolysate prepared from samples A, B, and C (Table 3.1).

Sample No.	Ash content, %	Consistency of EH, %	Enzyme, mg cellulase/ g cellulose	HCl, mg/g o.d. sludge	Carbohydrate conversion, %	Glucose, g/L	Xylose, g/L	Initial pH	Final pH
A-2	1.4	5.0	9.8	7.3	98.1	42.4	5.6	3.1	4.0
B-2	2.6	5.0	16.0	7.3	88.0	38.9	9.7	4.8	4.0
C-2	9.0	15.0	15.0	58.4	85.0	78.2	23.2	5.4	4.0

3.3.2. Microwave-assisted dehydration of sludge-derived hydrolysate

3.3.2.1. Effect of time, catalyst amount, and hydrolysate concentration

In this part, sludge-derived hydrolysate was prepared by the method described for B (**Table 3.1** & **3.2**). The deashed sludge contained 2.6% of ash before enzymatic hydrolysis. After enzymatic hydrolysis, the liquid part was separated by a centrifugation. The effect of sludge-derived hydrolysate concentration on dehydration performance was investigated. Techno-economic analysis (TEA) analysis, which was performed in our previous study, determined that hydrolysis consistency for had an important effect on the

minimum selling price of final products[42]. Different hydrolysate concentrations were prepared by evaporating water with a rotary evaporator (IKA Works, Inc., Germany). The glucose and xylose concentrations were measured after evaporation by HPLC analysis. The dehydration performance was investigated in the microwave reactor at different times, catalyst amounts, and three different hydrolysate concentrations. Aluminum chloride ($AlCl_3 \cdot 6H_2O$) was the main catalyst and dioxane was the co-solvent selected based on the previous research with corn stover hydrolysate[43]. To achieve high HMF and FF yields, each hydrolysate concentration required a different catalyst amount.

The effect of different hydrolysate concentrations on glucose conversion, final product yield, and byproduct yield is summarized in **Figure 3.2**. The lowest and middle range of concentration in **Figure 3.2** required lower $AlCl_3$ (10 mM) and a shorter time (3 min) to produce the highest product yield (76% HMF, 89% FF). In the case of the highest glucose and xylose concentration, 12.5 mM of $AlCl_3$ resulted in the highest HMF (65%) and FF (78%) yields at 3 min reaction. At higher $AlCl_3$ concentrations above the optimum, HMF and FF were prone to be degraded into levulinic acid[44]. However, at lower $AlCl_3$ concentrations not all of the glucose and xylose were not converted into HMF. A similar behavior was observed at different reaction times. At longer reaction times HMF yields decreased by 8% when 12.5 mM of $AlCl_3$ was added. **Figure 3.2** shows that efficient dehydration occurred giving higher HMF and FF yields and lower levulinic acid from sludge-derived hydrolysate with the added co-solvent (dioxane).

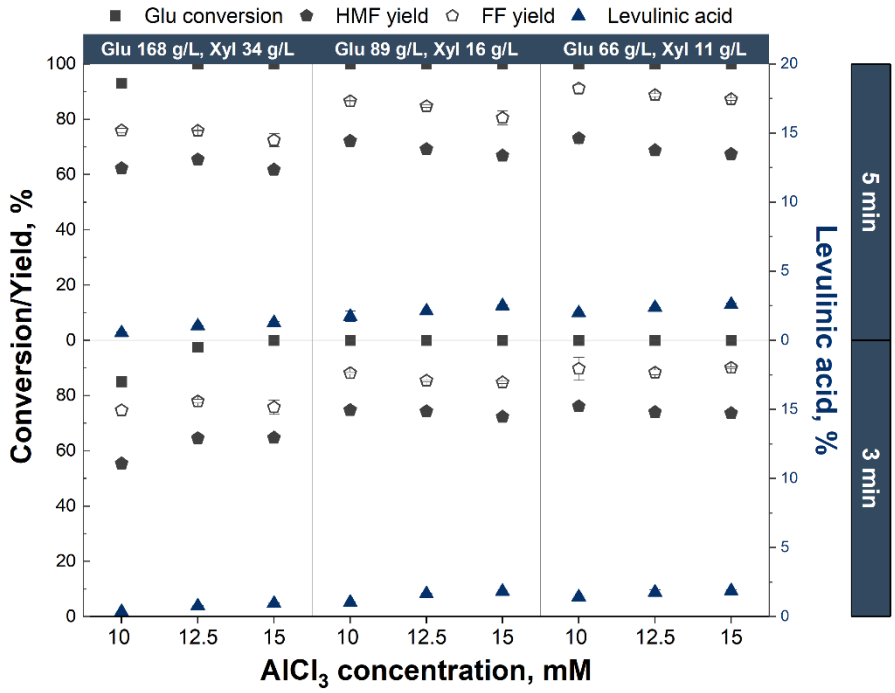

Figure 3.2. Dehydration performance at different reaction times (3 and 5 min), $AlCl_3$ concentrations, and hydrolysate concentrations.

3.3.2.2. Effect of different sludge properties

Several sludge-derived hydrolysate samples were prepared in order to determine if each would require different conditions for effective dehydration. In **Table 3.3**, samples B-2 and C-2 were prepared by the same methods as described in **Table 3.2**. Results of B-2 in **Table 3.3** were listed in **Figure 3.2**. For sample C-2, the sludge-derived hydrolysate contained 78.2 g/L of glucose and 23.2 g/L of xylose. The pH of hydrolysate was 4.0 and sodium azide was added to prevent microorganism growth. **Table 3.3** shows the dehydration performance depending on different concentrations of catalyst ($AlCl_3$).

While Sample B-2 showed good dehydration performance with 10 mM $AlCl_3$ (condition 1), the first three conditions of sample C-2 (condition 4-6) had lower HMF and furfural yields at similar $AlCl_3$ amounts due to the higher pH in sample C-2 hydrolysates. pH is a critical factor in determining the yields of furan chemicals, and ideally the pH should range between 2 and 3 $AlCl_3$[38,43]. To improve the conversion and yields from sample C-2, the amount of $AlCl_3$ was increased to 20 mM or 5 mM HCl was added to the 15 mM $AlCl_3$. Both conditions showed much higher HMF (73-74%) and FF (79-81%) yields. These conditions also resulted in increased levulinic acid production although it remained relatively low. These results show that a different amount of $AlCl_3$ is maybe needed for each sludge-derived hydrolysate if the residual ash content of sludge varies and effects the pH of the dehydration reaction solution.

Further investigation was continued to discover why each sludge-derived hydrolysate sample had different pH levels after adding catalyst and solvent. One factor might be the residual ash content of the deashed sludge or other impurities. The ash content of deashed sludge varied from 1.5% to 11% depending on the properties of raw sludge and types of deashing equipment used in this study. The main difference which resulted from different ash content remaining in deashed sludge resulted in different amounts of $CaCl_2$ generated in the sludge-derived hydrolysate. The calculated amount of $CaCl_2$ in the sludge-derived hydrolysates ranged from 3.7 mM to 30 mM based on Eq.3.1. The effect on pH of $CaCl_2$ in the hydrolysate was demonstrated by adding $CaCl_2$ to a pure glucose solution containing $AlCl_3$. The overall result showed a difference in pH between 5 mM and 30 mM $CaCl_2$ in glucose solution. A pure glucose solution with 7.5 mM $AlCl_3$ gave a pH of 3.5. When 5 mM $CaCl_2$ was added, the pH increased to 3.7. As $CaCl_2$ addition increased to 30 mM, the pH increased to 3.8. With 20 mM $AlCl_3$ the pH decreased to 3.3 and much higher yields of HMF and FF were obtained. pH could also be affected by organic acids (lactic and acetic acid) produced during enzymatic hydrolysis.

3.3.3. Effect of impurities in sludge-derived hydrolysate on dehydration

Compared to pure glucose and xylose solution, sludge-derived hydrolysate was confirmed to contain impurities. The following experiments were performed to identify which components affect the dehydration performance of sludge-derived hydrolysate compared to pure sugars. The differences between pure sugar solution and sludge-derived hydrolysate are (a)remaining $CaCO_3$, (b)$CaCl_2$, (c)lactic acid, (d)acetic acid, and (e)oligomers, which can be recognized as impurities. **Table 3.4** contains results from the dehydration of a pure sugar solution with different levels of $AlCl_3$ and in the presence of various additives. The reaction temperature and time for each condition were fixed at

195ºC for 3 min. The concentrations of glucose and xylose were similar to those in the sludge hydrolysate prepared in the paddle reactor.

Table 3.3. Results from dehydration of several sludge-derived hydrolysate samples with different $AlCl_3$ concentrations and initial pH.

Condition					Glucose conversion, %	HMF yield, %	Furfural yield, %	Levulinic acid, %
No	Type	$AlCl_3$, mM	Adjustment	Initial pH				
1	B-2	10	-	3.0	100	76.1	89.8	1.4
2	B-2	12.5	-	3.0	100	74.0	88.4	1.8
3	B-2	15	-	3.0	100	73.6	90.1	1.9
4	C-2	5	-	4.9	82.1	4.8	9.1	0
5	C-2	7.5	-	4.6	74.9	6.3	11.6	0
6	C-2	15	-	3.6	67.6	28.7	35.7	0
7	C-2	15	HCl 5 mM	3.2	98.6	73.2	79.0	0.2
8	C-2	20	-	3.3	100	74.5	81.2	0.4

*B': Sludge 2021, Pulmac masterscreen, Incubator shakers, Concentrated to Glucose 65.7 g/L & Xylose 11.4 g/L, C': Sludge 2022, Sidehill screen, Paddle reactor, Glucose 78.2 g/L & Xylose 23.2 g/L.

In **Table 3.4**, the first set of experiments the concentration of $AlCl_3$ was varied from 2.5 to 20 mM without any additional chemicals (conditions 1-5). At this concentration of glucose and xylose solution, 5 mM of $AlCl_3$ gave the highest HMF and FF yields and lowest amount of levulinic acid. Above 5 mM $AlCl_3$ more degradation of the furans occurred to produce more levulinic acid[44]. The next experiments modified the initial pH of the starting material by adding different acid types (i.e., HCl, CH_3COOH) with 2.5 mM $AlCl_3$ to inspect their effect on the dehydration performance (conditions 6-8). The hydrochloric acid addition showed better efficiency than the acetic acid addition despite a similar starting pH. The addition of HCl to the solution may have increased the efficiency of $AlCl_3$-catalyzed glucose dehydration by influencing the equilibrium of $AlCl_3$ in water[35,38]. From conditions 9 to 14, variables were selected based on the characterization of sludge-derived hydrolysate, by addition of calcium chloride, and lactic acid. Two concentrations of lactic acid (33, 133 mM) were tried, which were concentrations detected in two of the hydrolysates. Additionally, two concentrations of $CaCl_2$ were selected based on calculating the $CaCl_2$ likely to have been present in two of the hydrolysates. No matter how much lactic acid was included, it did not negatively affect the final product yield. Alternately, having 30 mM $CaCl_2$ and 133 mM lactic acid with 5 mM $AlCl_3$ (condition 11) enhanced the final product yield compared to adding only 5 mM $AlCl_3$ (condition 2).

Table 3.4 concluded that components, which can be recognized as impurities in sludge-derived hydrolysate, had no negative impact on its dehydration. More experiments were

designed in the next section to determine if these impurities improved HMF and FF yields or can replace $AlCl_3$.

Table 3.4. Results from dehydration of pure glucose and xylose solutions with $AlCl_3$ containing various additives. Glucose 73 g/L and xylose 17 g/L in a dioxane and water mixture (2:1 volume ratio).

Condition				Glucose conversion,%	HMF yield, %	Furfural yield, %	Levulinic acid, %	pH
No	$AlCl_3$, mM	$CaCl_2$, mM	Acid, mM					Initial
1	2.5	-	-	80.7±2.3	51.1±1.3	73.1±1.1	0.3±0.4	3.0
2	5	-	-	98.7	64.6±0.5	76.6±0.8	2.4±0.5	3.0
3	10	-	-	100	65.0±0.1	76.3±0.4	5.5±0.2	3.0
4	15	-	-	100	60.9±0.1	71.2±0.4	8.3±0.6	3.0
5	20	-	-	100	57.5±0.5	72.3±0.1	9.8±0.1	3.0
6	2.5	-	HCl 5	97.4±0.7	65.2±0.7	81.3±2.8	2.5±0.4	2.2
7	2.5	-	Ace 25	79.5±3.6	51.8±5.6	4.54±0.6	0.2±0.1	4.0
8	2.5	-	Ace 1000	88.3±0.7	53.4±0.9	73.4±1.7	0	3.0
9	15	-	L 33	100	62.5±1.3	74.9±2.4	7.7±0.4	2.0
10	15	-	L 133	100	64.6±0.6	76.7±2.5	6.0±1.3	1.5
11	5	30	L 133	100	69.9±1.1	78.7±2.9	1.9	3.0
12	15	30	L 133	100	61.9±0.1	73.6±2.2	6.5±0.3	2.5

* Results are the average of duplicate experiments. The solvent was a mixture of dioxane and water (2:1 volume ratio). L stands for lactic acid, HCl for hydrochloric acid, and Ace for acetic acid.

3.3.4. Effect of calcium chloride and lactic acid on the improvement of glucose dehydration performance

3.3.4.1. Effect of $CaCl_2$ on glucose dehydration

Since sludge-derived hydrolysate contained a certain amount of $CaCl_2$, the effect of $CaCl_2$ on glucose solution was first investigated. The effect of $CaCl_2$ as a co-catalyst has been studied and a plausible mechanism follows the direct route of glucose dehydration without forming fructose as an intermediate[33,37,45]. When Gracia-Sancho et al.[37] and Torres-Olea et al.[33] used the catalysts for glucose dehydration, such as Nb_xZr_y and ZrO_2, that did not possess the strong Brönsted acid sites, the calcium cation promoted the replacement of the β form with the α form of glucose, followed by the formation of HMF without the isomerization. On the other hand, a catalyst with both Bronsted and Lewis acid sites, such as Nb_2O_5, followed the isomerization and dehydration steps even in the presence of $CaCl_2$ [33]. Also, the single use of $CaCl_2$ such as a molten salt hydrate was suggested to promote the glucose isomerization in another study[46].

In **Figure 3.3**, the presence of $CaCl_2$ had no negative impact on HMF yield. HMF yield slightly increased when $CaCl_2$ was added. It has been reported that $CaCl_2$ enhanced glucose conversion as well as HMF yield with acid alumina (Al-a) catalyst at 175ºC[37]. Therefore, the next experiment was designed to replace $AlCl_3$ with $CaCl_2$. **Table 3.5** presents the effect of varying $AlCl_3$ and $CaCl_2$ concentrations on glucose dehydration. When only $CaCl_2$ was used, lower HMF and FF was resulted due to the high initial pH. In this experiment, it can be seen that $CaCl_2$ resulted in glucose isomerization to fructose at 68% selectivity. The effect of $CaCl_2$ on glucose isomerization has also been reported in other works, where $CaCl_2$ had the best efficiency for transformation of glucose to fructose[33,46]. Lin's work proved that the $CaCl_2$ role was clearly shown by NMR evidence[46]. It was inferred that the coordination between C1/C2 sites of the β-glucopyranose and Ca^{2+} was formed so that a 1,2-intramolecular hydride shift occurred. However, the reduction of $AlCl_3$ in the presence of $CaCl_2$ was ineffective in improving glucose conversion and HMF yield.

Figure 3.4 provided two approaches to lower the pH of glucose solution and enhance dehydration efficiency, achieved by using a reduced amount of $AlCl_3$ (2.5 mM) with $CaCl_2$ presence. **Figure 3.4a** indicates dehydration results depending on three different concentrations of $CaCl_2$. The increase in $CaCl_2$ until 10 mM helped increase glucose conversion followed by an increase in HMF yield, compared to only 2.5 mM $AlCl_3$ condition. The byproduct yield showed stable with any $CaCl_2$ conditions. The higher HMF selectivity by the addition of $CaCl_2$ in glucose solution was also proven in Combs' work[45]. Another comparison supported to this evidence that improved HMF yield but not promoted the HMF rehydration is between the mixture of 5 mM $AlCl_3$ and 2.5 mM $CaCl_2$ and the mixture of 2.5 mM $AlCl_3$ and 2.5 mM $CaCl_2$ (Table S3.1). **Figure 3.4b** shows the results obtained by increasing HCl addition to 5 mM in the presence of 2.5 mM $AlCl_3$ and 5 mM $CaCl_2$. Hence, it is fundamental to emphasize the importance of a balanced Brönsted and Lewis acid site for the glucose dehydration to HMF[33], a concept widely accepted in previous studies.

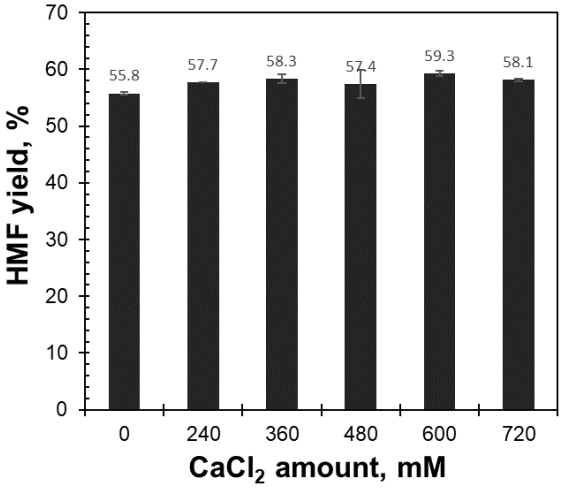

Figure 3.3. Dehydration of glucose with different addition of $CaCl_2$ at 195ºC for 5 min. Initial glucose concentration 80 g/L and 4 mM $AlCl_3$ in the mixture of dioxane and water (2:1 volume ratio).

Table 3.5. Glucose dehydration with different concentrations of $AlCl_3$ and $CaCl_2$. Glucose concentration was 33 g/L (195ºC for 3 min).

Catalyst condition		Glucose conversion		HMF yield, %	Levulinic acid, %
$AlCl_3$, mM	$CaCl_2$, mM	to product, %	to fructose, %		
7.5	5	100	0	61.6 (2.1)	7.6
5	5	97	0	61.4 (0.8)	3.7
2.5	5	79	0.4	50.9 (1.3)	0.9
0	5	39	24	0	0

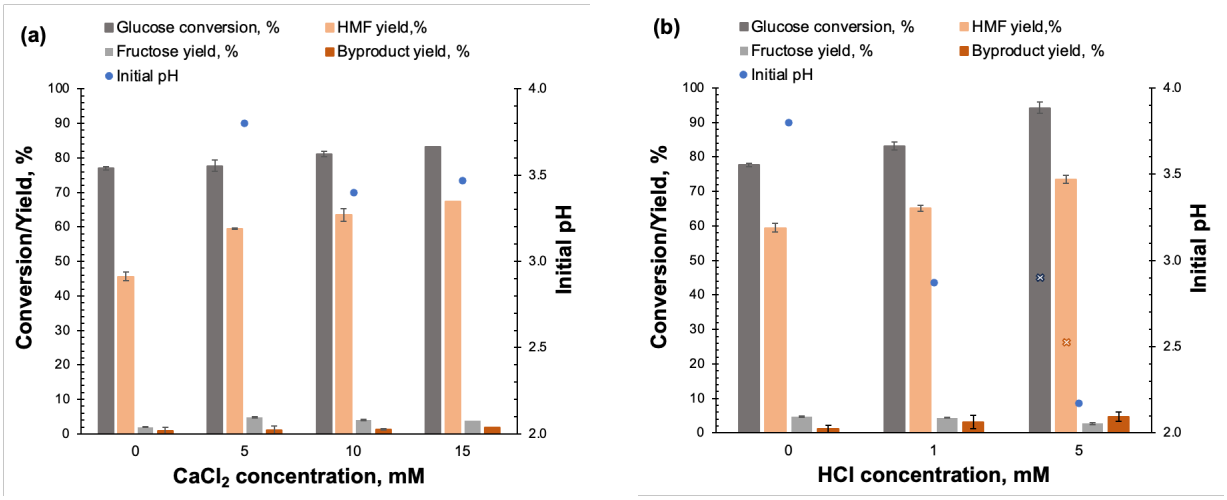

Figure 3.4. Glucose dehydration in the presence of $CaCl_2$. $AlCl_3$ amount was fixed to 2.5 mM (195ºC for 3 min, and dioxane:water 2:1 volume ratio). (a) was depending on different $CaCl_2$ concentration, and (b) was with 5 mM $CaCl_2$. In (b), each cross symbol means glucose conversion and HMF yield under 5 mM $CaCl_2$ and 5 mM HCl with the same conditions of the rest as others.

3.3.4.2. Effect of organic acid on glucose dehydration

Other components in sludge-derived hydrolysate were found to be organic acids such as acetic acid and lactic acid. Acetic acid and lactic acid were found to range from 0 to 20 mM; the average concentrations were 4.5 mM for acetic acid and 6.1 mM for lactic acid. Therefore, this part of the investigation focused on the effect of organic acids on glucose dehydration with various concentrations of different types of organic acids. Organic acids with two carboxylic acid groups at each end, such as maleic acid and oxalic acid, have been applied with a metal catalyst for a greener approach to HMF production[47–52]. This approach has the advantage of using biomass-derived and biodegradable solvents, while some combinations (i.e., maleic acid-$AlCl_3$) showed a slower dehydration reaction[48]. Use of organic acids was expected to lower humin generation even though the total reaction is slower than other catalyst combinations. Zhang et al. (2015) compared the dehydration efficiency between $AlCl_3$-maleic acid and $AlCl_3$-HCl using glucose as a starting material[48]. The same team (2016) further proposed an isomerization mechanism when $AlCl_3$ was used with maleic acid to catalyze conversion of glucose in aqueous media[47]. They mainly suggested the isomerization of glucose to fructose via an acyclic mechanism, where the

hydride shift from C1 to C2 resulted in a new carbonyl group on C2. Yu et al. (2018) also suggested the possible coordination with Cr(III) and maleic acid similar to Al(III)-maleic acid to retard humin generation[49]. However, they pointed out that when Lewis acidity decreased to an extent HMF yield lowered.

The first experiment shown in **Figures 3.5** illustrates the comparison between HCl and acetic acid. Many researchers have used mineral acids (e.g. HCl) for Brönsted acid in glucose dehydration [53], while the possibility of organic acid as a cocatalyst with metal catalyst has been confirmed in recent literature [74-49][54]. **Figures 3.5** show the use of acetic acid resulted in as much HMF production as HCl. **Figure 3.5a** shows glucose conversion, HMF and levulinic acid yield depending on the reaction time in the microwave reactor comparing adding HCl or CH_3COOH with $AlCl_3$. A reaction time of 2-3 min gave the best HMF yields for both cocatalyst reactions and the reaction behavior was similar for both conditions.

Figure 3.5b shows the glucose dehydration performance at different concentrations of cocatalyst with the same amount of $AlCl_3$, reaction temperature, and time from **Figure 3.5a.** It is noted that at higher concentrations of acetic acid levulinic acid production slowed down and HMF yield was maintained. This finding indicates that HMF yield could be stable when sludge-derived hydrolysate contains high levels of impurities such as organic acids. The addition of organic acid in the metal catalyst system has shown less humin generation in other studie [48][52]. In Zhang's study, organic acids such as maleic acid showed less humin generation compared to the rehydration of HMF to levulinic acid with $AlCl_3$ in glucose dehydration while HCl combination with $AlCl_3$ was more prone to rehydrate HMF to generate levulinic acid[48]. Their hypothesis was that maleic acid stabilized the intermediate during glucose dehydration. The reduction of humin generation was also observed in Yu's work[52]. While maleic acid with $AlCl_3$ retarded glucose isomerization, with higher selectivity toward HMF and less humin generation. The high selectivity was ascribed to the regulated Lewis acidity of $AlCl_3$ by the organic acid. Therefore, the understanding of the effect of organic acids on dehydration provided the rational reason why sludge-derived hydrolysate resulted in a considerable amount of HMF yield.

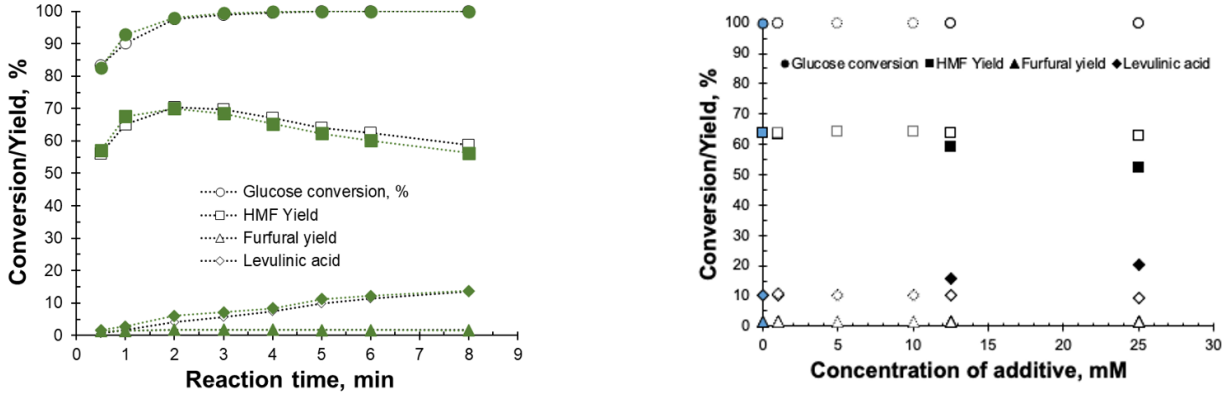

Figure 3.5. Dehydration of glucose (13 g/L), in dioxane:water=2:1, at fixed $AlCl_3$ 7.5 mM, and 195ºC. Filled symbols are for is HCl 25 mM and unfilled symbols are for CH_3COOH

25 mM. Dehydration results depending on the reaction time (a) and concentration of additive (b).

3.4. Scaling-up production of HMF and furfural by dehydration of PStF hydrolysates in a flow reactor

The scaled-up production of HMF and furfural at NREL was continued by conducting dehydration experiments in a continuous flow reactor. Dehydration was conducted on PStF sugars hydrolysate generated in two batches of high-solids enzymatic hydrolysis conducted in a 30-L Paddle Reactor located at IBRF, NREL. Dehydration of PStF sugars was conducted in a tubular flow reactor using glass-lined tubing (GLT), ½ inch outer diameter (0.065-inch wall thickness) with 25 inches in length of the heating zone under the optimum reaction conditions, i.e., 190°C and residence time of 7-9 minutes using AlCl3 at 20 mM, obtained previously to maximize the yields of HMF and furfural. The glucose and xylose conversions of more than 90% were obtained with dehydration of sludge hydrolysate under these reaction conditions. The HMF and furfural yields obtained are reported in **Table 3.6.** The results show that HMF yields of 57-60% were achieved, however, lower furfural yields (~69-71%) were obtained. One possibility of low furfural yields is due to furfural loss through the formation of adducts between furfural and acetone under acidic conditions which was confirmed by a peak appearing at around 4.6 min determined by reverse-phase HPLC (C-18 column with a DAD detector). A further optimization of reaction conditions will be performed to further maximize the HMF and furfural yields.

Table 3.6. Dehydration reaction conditions and HMF and furfural yields from dehydration of deashed sludge hydrolysate using acetone to aqueous ratio of 2:1 with 20 mM AlCl3 in a flow reactor (glass-lined tubing (GLT), ½ inch outer diameter (0.065-inch wall thickness) with 20 inches in length of the heating zone). Effects of varying flow rate at a constant temperature of 190°C and AlCl3 20 mM.

Flow rate, mL/min	Res Time, min	HMF Yield (%)	Furfural Yield (%)
3.0	9	58.0	69.3
3.0	9	59.9	71.2
3.5	7	56.9	68.0
3.5	7	56.9	68.6
3.5	7	58.8	68.6

In this quarter, the total volume of furfurals solution exceeding 50 L was prepared under the optimum reaction conditions mentioned above. The concentrations of HMF and furfural in both furfurals in solution containing acetone/ water, 2:1 (v/v), and in aqueous solution obtained after acetone distillation are provided in **Table 3.7.** From **Table 3.7**, it can be inferred that about 482 g and 83 g of HMF and furfural, respectively (total 565 g of furfurals) were produced and shipped to NSCU to further perform acetone distillation and aldol condensation reactions. To meet our project end goal of producing 1 L of hydrocarbon products, our efforts at NREL to produce furfurals production in a continuous flow reactor will continue to produce at least 30 L of additional furfurals solution in the next quarter and ship it to NSCU to produce aldol adducts.

Table 3.7. Concentrations and amounts of HMF and furfural produced from dehydration of sugars in deashed sludge hydrolysate using acetone to aqueous ratio of 2:1 with 20 mM AlCl3 in a continuous flow reactor at 190°C and a residence time of 7-9 minutes. These furfurals solutions were shipped to NSCU to perform acetone distillation and aldol condensation reactions.

Furfurals Solution	HMF Concentration, g/L	Furfural Concentration, g/L	Volume, L	HMF, g	Furfural, g
Furfurals in acetone/ water, 2:1 (v/v) A	10.07	2.41	24	241.70	57.96
Conc. aqueous #A	27.90	2.91	4	128.81	13.11
Conc. aqueous #B	32.20	3.28	4	111.61	11.65
Total furfurals, g				**482.13**	**82.73**

3.5. Conclusions

This investigation of the effect of impurities contained in sludge-derived hydrolysate facilitates the valorization of paper sludge into value-added products. The present study has shown that impurities, such as organic acids and calcium chloride, do not negatively impact the conversion of sugars into furfurals. The role of each component was further investigated by adding each impurity component into a pure sugar solution. A considerable amount of HMF (76%) and furfural (90%) were obtained in a mixture of dioxane, hydrolysate, and $AlCl_3$ in microwave heated reactions. Paper sludge is expected to be used as a feedstock for conversion into hydrocarbons that could be blended into jet fuel with an economically and environment-friendly controlled process.

References

1. Prussi, M.; Lee, U.; Wang, M.; Malina, R.; Valin, H.; Taheripour, F.; Velarde, C.; Staples, M. D.; Lonza, L.; Hileman, J. I. CORSIA: The First Internationally Adopted Approach to Calculate Life-Cycle GHG Emissions for Aviation Fuels. Renew. Sustain. Energy Rev. 2021, 150, 111398. https://doi.org/10.1016/j.rser.2021.111398.
2. Oakleaf, B.; Cary, S.; Meeker, D.; Arent, D.; Farrell, J.; Day, M.; McCormick, R.; Abdullah, Z.; Young, S.; Cochran, J.; Gearhart, C. A Roadmap Toward a Sustainable Aviation Ecosystem; NREL/TP-6A60-83060, 1881303, MainId:83833; 2022; p NREL/TP-6A60-83060, 1881303, MainId:83833. https://doi.org/10.2172/1881303.
3. SAF Grand Challenge Roadmap, 2022.
4. Why, E. S. K.; Ong, H. C.; Lee, H. V.; Gan, Y. Y.; Chen, W.-H.; Chong, C. T. Renewable Aviation Fuel by Advanced Hydroprocessing of Biomass: Challenges and Perspective. Energy Convers. Manag. 2019, 199, 112015. https://doi.org/10.1016/j.enconman.2019.112015.
5. Furszyfer Del Rio, D. D.; Sovacool, B. K.; Griffiths, S.; Bazilian, M.; Kim, J.; Foley, A. M.; Rooney, D. Decarbonizing the Pulp and Paper Industry: A Critical and

Systematic Review of Sociotechnical Developments and Policy Options. Renew. Sustain. Energy Rev. 2022, 167, 112706. https://doi.org/10.1016/j.rser.2022.112706.
6. Faubert, P.; Barnabé, S.; Bouchard, S.; Côté, R.; Villeneuve, C. Pulp and Paper Mill Sludge Management Practices: What Are the Challenges to Assess the Impacts on Greenhouse Gas Emissions? Resour. Conserv. Recycl. 2016, 108, 107–133. https://doi.org/10.1016/j.resconrec.2016.01.007.
7. Peretz, R.; Sterenzon, E.; Gerchman, Y.; Kumar Vadivel, V.; Luxbacher, T.; Mamane, H. Nanocellulose Production from Recycled Paper Mill Sludge Using Ozonation Pretreatment Followed by Recyclable Maleic Acid Hydrolysis. Carbohydr. Polym. 2019, 216, 343–351. https://doi.org/10.1016/j.carbpol.2019.04.003.
8. Budhavaram, N. K.; Fan, Z. Production of Lactic Acid from Paper Sludge Using Acid-Tolerant, Thermophilic Bacillus Coagulan Strains. Bioresour. Technol. 2009, 100 (23), 5966–5972. https://doi.org/10.1016/j.biortech.2009.01.080.
9. Guan, W.; Shi, S.; Tu, M.; Lee, Y. Y. Acetone–Butanol–Ethanol Production from Kraft Paper Mill Sludge by Simultaneous Saccharification and Fermentation. Bioresour. Technol. 2016, 200, 713–721. https://doi.org/10.1016/j.biortech.2015.10.102.
10. Zhu, S.; Sui, J.; Liu, Y.; Ye, S.; Wang, C.; Huo, M.; Yu, Y. Effects of Washing, Autoclaving, and Surfactants on the Enzymatic Hydrolysis of Negatively Valued Paper Mill Sludge for Sugar Production. Energy Fuels 2019, 33 (2), 1219–1226. https://doi.org/10.1021/acs.energyfuels.8b03586.
11. Kang, L.; Wang, W.; Lee, Y. Y. Bioconversion of Kraft Paper Mill Sludges to Ethanol by SSF and SSCF. Appl. Biochem. Biotechnol. 2010, 161 (1–8), 53–66. https://doi.org/10.1007/s12010-009-8893-4.
12. Fan, Z.; South, C.; Lyford, K.; Munsie, J.; vanWalsum, P.; Lynd, L. R. Conversion of Paper Sludge to Ethanol in a Semicontinuous Solids-Fed Reactor. Bioprocess Biosyst. Eng. 2003, 26 (2), 93–101. https://doi.org/10.1007/s00449-003-0337-x.
13. Chen, H.; Han, Q.; Daniel, K.; Venditti, R.; Jameel, H. Conversion of Industrial Paper Sludge to Ethanol: Fractionation of Sludge and Its Impact. Appl. Biochem. Biotechnol. 2014, 174 (6), 2096–2113. https://doi.org/10.1007/s12010-014-1083-z.
14. Lynd, L. R.; Lyford, K.; South, C. R. Evaluation of Paper Sludges for Amenability to Enzymatic Hydrolysis and Conversion to Ethanol. 2001, 19.
15. Bajpai, P. Management of Pulp and Paper Mill Waste; Springer International Publishing: Cham, 2015. https://doi.org/10.1007/978-3-319-11788-1.
16. Park, H.; Cruz, D.; Tiller, P.; Johnson, D. K.; Mittal, A.; Jameel, H.; Venditti, R.; Park, S. Effect of Ash in Paper Sludge on Enzymatic Hydrolysis. Biomass Bioenergy 2022, 165, 106567. https://doi.org/10.1016/j.biombioe.2022.106567.
17. Chheda, J. N.; Dumesic, J. A. An Overview of Dehydration, Aldol-Condensation and Hydrogenation Processes for Production of Liquid Alkanes from Biomass-Derived Carbohydrates. Catal. Today 2007, 123 (1), 59–70. https://doi.org/10.1016/j.cattod.2006.12.006.
18. Cai, C. M.; Zhang, T.; Kumar, R.; Wyman, C. E. Integrated Furfural Production as a Renewable Fuel and Chemical Platform from Lignocellulosic Biomass. J. Chem. Technol. Biotechnol. 2014, 89 (1), 2–10. https://doi.org/10.1002/jctb.4168.

19. Liu, Y.; Li, G.; Hu, Y.; Wang, A.; Lu, F.; Zou, J.-J.; Cong, Y.; Li, N.; Zhang, T. Integrated Conversion of Cellulose to High-Density Aviation Fuel. Joule 2019, 3 (4), 1028–1036. https://doi.org/10.1016/j.joule.2019.02.005.
20. Huber, G. W.; Iborra, S.; Corma, A. Synthesis of Transportation Fuels from Biomass: Chemistry, Catalysts, and Engineering. Chem. Rev. 2006, 106 (9), 4044–4098. https://doi.org/10.1021/cr068360d.
21. Wang, T. Catalytic Conversion of Glucose to 5-Hydroxymethylfurfural as a Potential Biorenewable Platform Chemical. Doctor of Philosophy, Iowa State University, Digital Repository, Ames, 2014, p 5777418. https://doi.org/10.31274/etd-180810-2227.
22. Román-Leshkov, Y.; Barrett, C. J.; Liu, Z. Y.; Dumesic, J. A. Production of Dimethylfuran for Liquid Fuels from Biomass-Derived Carbohydrates. Nature 2007, 447 (7147), 982–985. https://doi.org/10.1038/nature05923.
23. van Dam, H. E.; Kieboom, A. P. G.; van Bekkum, H. The Conversion of Fructose and Glucose in Acidic Media: Formation of Hydroxymethylfurfural. Starch - Stärke 1986, 38 (3), 95–101. https://doi.org/10.1002/star.19860380308.
24. Gallo, J. M. R.; Alonso, D. M.; Mellmer, M. A.; Dumesic, J. A. Production and Upgrading of 5-Hydroxymethylfurfural Using Heterogeneous Catalysts and Biomass-Derived Solvents. Green Chem 2013, 15 (1), 85–90. https://doi.org/10.1039/C2GC36536G.
25. Tsilomelekis, G.; Josephson, T. R.; Nikolakis, V.; Caratzoulas, S. Origin of 5-Hydroxymethylfurfural Stability in Water/Dimethyl Sulfoxide Mixtures. ChemSusChem 2014, 7 (1), 117–126. https://doi.org/10.1002/cssc.201300786.
26. Toftgaard Pedersen, A.; Ringborg, R.; Grotkjær, T.; Pedersen, S.; Woodley, J. M. Synthesis of 5-Hydroxymethylfurfural (HMF) by Acid Catalyzed Dehydration of Glucose–Fructose Mixtures. Chem. Eng. J. 2015, 273, 455–464. https://doi.org/10.1016/j.cej.2015.03.094.
27. Sweygers, N.; Alewaters, N.; Dewil, R.; Appels, L. Microwave Effects in the Dilute Acid Hydrolysis of Cellulose to 5-Hydroxymethylfurfural. Sci. Rep. 2018, 8 (1), 7719. https://doi.org/10.1038/s41598-018-26107-y.
28. Qi, X.; Watanabe, M.; Aida, T. M.; Smith Jr, R. L. Fast Transformation of Glucose and Di-/Polysaccharides into 5-Hydroxymethylfurfural by Microwave Heating in an Ionic Liquid/Catalyst System. ChemSusChem 2010, 3 (9), 1071–1077. https://doi.org/10.1002/cssc.201000124.
29. Rosatella, A. A.; Simeonov, S. P.; Frade, R. F. M.; Afonso, C. A. M. 5-Hydroxymethylfurfural (HMF) as a Building Block Platform: Biological Properties, Synthesis and Synthetic Applications. Green Chem. 2011, 13 (4), 754. https://doi.org/10.1039/c0gc00401d.
30. Zhao, H.; Holladay, J. E.; Brown, H.; Zhang, Z. C. Metal Chlorides in Ionic Liquid Solvents Convert Sugars to 5-Hydroxymethylfurfural. Science 2007, 316 (5831), 1597–1600.
31. Ordomsky, V. V.; Sushkevich, V. L.; Schouten, J. C.; van der Schaaf, J.; Nijhuis, T. A. Glucose Dehydration to 5-Hydroxymethylfurfural over Phosphate Catalysts. J. Catal. 2013, 300, 37–46. https://doi.org/10.1016/j.jcat.2012.12.028.

32. Li, X.; Peng, K.; Liu, X.; Xia, Q.; Wang, Y. Comprehensive Understanding of the Role of Brønsted and Lewis Acid Sites in Glucose Conversion into 5-Hydromethylfurfural. ChemCatChem 2017, 9 (14), 2739–2746. https://doi.org/10.1002/cctc.201601203.
33. Torres-Olea, B.; García-Sancho, C.; Cecilia, J. A.; Oregui-Bengoechea, M.; Arias, P. L.; Moreno-Tost, R.; Maireles-Torres, P. Influence of Lewis Acidity and CaCl2 on the Direct Transformation of Glucose to 5-Hydroxymethylfurfural. Mol. Catal. 2021, 510, 111685. https://doi.org/10.1016/j.mcat.2021.111685.
34. Saha, B.; M. Abu-Omar, M. Advances in 5-Hydroxymethylfurfural Production from Biomass in Biphasic Solvents. Green Chem. 2014, 16 (1), 24–38. https://doi.org/10.1039/C3GC41324A.
35. Pagán-Torres, Y. J.; Wang, T.; Gallo, J. M. R.; Shanks, B. H.; Dumesic, J. A. Production of 5-Hydroxymethylfurfural from Glucose Using a Combination of Lewis and Brønsted Acid Catalysts in Water in a Biphasic Reactor with an Alkylphenol Solvent. ACS Catal. 2012, 2 (6), 930–934. https://doi.org/10.1021/cs300192z.
36. Kim, Y. Prediction of Hydroxymethylfurfural Yield in Glucose Conversion through Investigation of Lewis Acid and Organic Solvent Effects. ACS Catal 2020, 15.
37. García-Sancho, C.; Fúnez-Núñez, I.; Moreno-Tost, R.; Santamaría-González, J.; Pérez-Inestrosa, E.; Fierro, J. L. G.; Maireles-Torres, P. Beneficial Effects of Calcium Chloride on Glucose Dehydration to 5-Hydroxymethylfurfural in the Presence of Alumina as Catalyst. Appl. Catal. B Environ. 2017, 206, 617–625. https://doi.org/10.1016/j.apcatb.2017.01.065.
38. Yang, Y.; Hu, C.; Abu-Omar, M. M. The Effect of Hydrochloric Acid on the Conversion of Glucose to 5-Hydroxymethylfurfural in AlCl3–H2O/THF Biphasic Medium. J. Mol. Catal. Chem. 2013, 376, 98–102. https://doi.org/10.1016/j.molcata.2013.04.016.
39. Wang, T.; Glasper, J. A.; Shanks, B. H. Kinetics of Glucose Dehydration Catalyzed by Homogeneous Lewis Acidic Metal Salts in Water. Appl. Catal. Gen. 2015, 498, 214–221. https://doi.org/10.1016/j.apcata.2015.03.037.
40. Pidko, E. A.; Degirmenci, V.; van Santen, R. A.; Hensen, E. J. M. Coordination Properties of Ionic Liquid-Mediated Chromium(II) and Copper(II) Chlorides and Their Complexes with Glucose. Inorg. Chem. 2010, 49 (21), 10081–10091. https://doi.org/10.1021/ic101402r.
41. Sluiter, J. B.; Ruiz, R. O.; Scarlata, C. J.; Sluiter, A. D.; Templeton, D. W. Compositional Analysis of Lignocellulosic Feedstocks. 1. Review and Description of Methods. J. Agric. Food Chem. 2010, 58 (16), 9043–9053. https://doi.org/10.1021/jf1008023.
42. Cruz, D.; Park, H.; Gonzales, R.; Mittal, A.; Johnson, D.; Park, S. Techno-Economic Analysis of Biofuel Production via Catalytic Upgrading of Carbohydrates in Paper Sludge; NREL/PR-2800-78364; National Renewable Energy Lab. (NREL), Golden, CO (United States), 2020. https://www.osti.gov/biblio/1734547 (accessed 2022-12-08).
43. Mittal, A.; Pilath, H. M.; Johnson, D. K. Direct Conversion of Biomass Carbohydrates to Platform Chemicals: 5-Hydroxymethylfurfural (HMF) and Furfural. Energy Fuels 2020, 34 (3), 3284–3293. https://doi.org/10.1021/acs.energyfuels.9b04047.
44. Choudhary, V.; Mushrif, S. H.; Ho, C.; Anderko, A.; Nikolakis, V.; Marinkovic, N. S.; Frenkel, A. I.; Sandler, S. I.; Vlachos, D. G. Insights into the Interplay of Lewis and

Brønsted Acid Catalysts in Glucose and Fructose Conversion to 5-(Hydroxymethyl)Furfural and Levulinic Acid in Aqueous Media. J. Am. Chem. Soc. 2013, 135 (10), 3997–4006. https://doi.org/10.1021/ja3122763.

45. Combs, E.; Cinlar, B.; Pagan-Torres, Y.; Dumesic, J. A.; Shanks, B. H. Influence of Alkali and Alkaline Earth Metal Salts on Glucose Conversion to 5-Hydroxymethylfurfural in an Aqueous System. Catal. Commun. 2013, 30, 1–4. https://doi.org/10.1016/j.catcom.2012.10.011.
46. Lin, C.; Chai, C.; Li, Y.; Chen, J.; Lu, Y.; Wu, H.; Zhao, L.; Cao, F.; Chen, K.; Wei, P.; Ouyang, P. CaCl 2 Molten Salt Hydrate-Promoted Conversion of Carbohydrates to 5-Hydroxymethylfurfural: An Experimental and Theoretical Study. Green Chem. 2021, 23 (5), 2058–2068. https://doi.org/10.1039/D0GC04356G.
47. Zhang, X.; Murria, P.; Jiang, Y.; Xiao, W.; Kenttämaa, H. I.; Abu-Omar, M. M.; Mosier, N. S. Maleic Acid and Aluminum Chloride Catalyzed Conversion of Glucose to 5-(Hydroxymethyl) Furfural and Levulinic Acid in Aqueous Media. Green Chem. 2016, 18 (19), 5219–5229. https://doi.org/10.1039/C6GC01395C.
48. Zhang, X.; Hewetson, B. B.; Mosier, N. S. Kinetics of Maleic Acid and Aluminum Chloride Catalyzed Dehydration and Degradation of Glucose. Energy Fuels 2015, 29 (4), 2387–2393. https://doi.org/10.1021/ef502461s.
49. Yu, I. K. M.; Tsang, D. C. W.; Su, Z.; Yip, A. C. K.; Shang, J.; Ok, Y. S.; Kim, K.-H.; Poon, C. S. Contrasting Roles of Maleic Acid in Controlling Kinetics and Selectivity of Sn(IV)- and Cr(III)-Catalyzed Hydroxymethylfurfural Synthesis. ACS Sustain. Chem. Eng. 2018, 6 (11), 14264–14274. https://doi.org/10.1021/acssuschemeng.8b02931.
50. Delbecq, F.; Wang, Y.; Len, C. Various Carbohydrate Precursors Dehydration to 5-HMF in an Acidic Biphasic System under Microwave Heating Using Betaine as a Co-Catalyst. Mol. Catal. 2017, 434, 80–85. https://doi.org/10.1016/j.mcat.2017.02.037.
51. Hongsiri, W.; Danon, B.; de Jong, W. The Effects of Combined Catalysis of Oxalic Acid and Seawater on the Kinetics of Xylose and Arabinose Dehydration to Furfural. Int. J. Energy Environ. Eng. 2015, 6 (1), 21–30. https://doi.org/10.1007/s40095-014-0146-9.
52. Yu, I. K. M.; Tsang, D. C. W.; Yip, A. C. K.; Su, Z.; De Oliveira Vigier, K.; Jérôme, F.; Poon, C. S.; Ok, Y. S. Organic Acid-Regulated Lewis Acidity for Selective Catalytic Hydroxymethylfurfural Production from Rice Waste: An Experimental–Computational Study. ACS Sustain. Chem. Eng. 2019, 7 (1), 1437–1446. https://doi.org/10.1021/acssuschemeng.8b05141.
53. Yang, G.; Pidko, E. A.; Hensen, E. J. M. Mechanism of Brønsted Acid-Catalyzed Conversion of Carbohydrates. J. Catal. 2012, 295, 122–132. https://doi.org/10.1016/j.jcat.2012.08.002.
54. Lopes, M.; Dussan, K.; Leahy, J. J. Enhancing the Conversion of D-Xylose into Furfural at Low Temperatures Using Chloride Salts as Co-Catalysts: Catalytic Combination of AlCl 3 and Formic Acid. Chem. Eng. J. 2017, 323, 278–286. https://doi.org/10.1016/j.cej.2017.04.114.

Chapter 4: Analysis of solvent recyclability of acetone versus 1,4-dioxane when used as co-solvents for the dehydration reaction of sugars at intermediate sugar concentration.

This part of the research work was executed to better understand the differences on the recyclability of acetone versus 1,4-dioxane after being used as co-solvents during the dehydration reaction of sugars. Previous experimental results showed better 5-HMF and furfural yields for low-sugar-content dehydration systems (~10%wt.) using 1,4-dioxane in comparison to systems utilizing acetone. Considering the importance for the overall economics, being able to process intermediate to high sugar content throughout the hypothetical biorefinery is of high relevance. For this reason, aqueous solutions of purchased glucose and xylose were prepared at a combined 20%wt., and the sugars were dehydrated using the solvents of interest. The resulting yields for 5-HMF and furfural were used as a reference to prepare representative aqueous furans solutions from purchased materials containing acetone and 1,4-dioxane. Models developed using Aspen Plus™ were used to assess the number of theoretical stages required to separate each organic solvent and to estimate the overall heat duty of the distillation system for each case. Then, the furans solution containing co-solvents were distilled using a customized in-house-built multi-stage continuous distillation system. Finally, after achieving a steady state, the top and bottom products were analyzed, and the results were discussed and compared.

4.1. Introduction

The dwindling reserves of crude oil and natural gas, along with the environmental impacts associated with a fossil-based economy and the increasing global energy demand driven by population growth and economic expansion, have led to a worldwide commitment to transitioning towards a sustainable, energy-efficient, and low-carbon economy [1][2]. Consequently, it is imperative to find alternative, economically viable, and sustainable industrial processes to replace existing fossil-based pathways to produce fine chemicals and fuels from renewable sources. In this context, the abundant carbon-rich lignocellulosic biomass rises as a promising alternative feedstock to produce high-value-added products such as fertilizers, fungicides, pharmaceuticals, polymers, resins, solvents, surfactants, syngas, and liquid fuels [3][4][5][6][7]. Lignocellulose primarily consists of cellulose (30%-50%wt.), hemicellulose (20%-40%wt.), and lignin (10%-45%wt.), with mass content varying depending on the source of crop residue and plant species [1][4][8][9]. Various physical, chemical, and biological approaches have been proposed for the deconstruction of biomass into its fundamental constituents, primarily hexoses, pentoses, and monolignols [10][11][12]. Glucose and xylose are the primary monomeric products after the complete saccharification of cellulose and hemicellulose, which, under appropriate acidic conditions, can be upgraded via dehydration reactions to 5-hydroxymethylfurfural (5-HMF) and furfuraldehyde (furfural) [13][14]. These two intermediate materials have been identified by the U.S. Department of Energy as key biobased C5 and C6 precursor platform molecules for the decarbonization of global economies [15][14].

5-Hydroxymethylfurfural and furfural have been utilized at the laboratory scale as starting materials to produce a wide range of molecules through various conversion strategies, including aldol-condensation, decarbonylation, decarboxylation, hydrogenation, oxidation, etc. [6][16][17][18][19][20]. Among other relevant transformation pathways, the reductive upgrading of 5-HMF can result in 2,5-dimethylfuran (DMF), a high-energy-density liquid fuel with a prospective future in the transportation sector [21][22][23]. In the same way, the oxidative upgrading of 5-HMF can lead to the production of 2,5-diformylfuran (DFF), a precursor to poly-Schiff bases exhibiting anti-tumor properties of relevance for the pharmaceutical industry [24][25][26]. From an economically significant perspective, 5-HMF can yield 2,5-furandicarboxylic acid (FDCA), the precursor of polyethylene furanoate (PEF), a 100% bio-based polymer with the potential to replace polyethylene terephthalate (PET), the second most used polymer worldwide with an estimated annual global market value of $44.1 billion in 2020 [1][2][27][28]. Likewise, more than 80 different chemicals can be synthesized from furfural [1][2][29]. The market size for this furan material was estimated at $520 million in 2021 [30]. Furthermore, the reductive upgrading of this molecular platform can lead to furfuryl alcohol (FFA), representing ~60% of the total furfural market and with an estimated annual global market size of $787 million by 2017 [29][31]. Tetrahydrofurfuryl alcohol (THFA), 2-methyltetrahydrofuran (MTHF), 2-pentanol, and 1,5-pentanediol can also be produced from furfural under reductive conditions. Similarly, the oxidative upgrading of furfuraldehyde can lead to value-added products such as furonic acid, 2-furanone, maleic acid, and succinic acid; this last derivative with an estimated annual global market size of $159 million in 2021, expected to reach $316 million in the upcoming years [32][33][34].

The saccharification of the naturally occurring polymeric carbohydrates in lignocellulosic biomass to the monomeric sugars and precursors of 5-hydroxymethylfurfural and furfural typically involves high amounts of water in both enzymatic and nonenzymatic processes (e.g., acid hydrolysis) [35][36]. It has been reported that the use of low-solids biomass loadings (~5%wt.) yields high carbohydrate conversion to simple sugars (>80%) [37][38]. Conversely, the use of high-solids biomass loadings (15%wt. - 35%wt.) can result in a considerable reduction in carbohydrate conversion (<60%), depending on the nature of the starting substrate and reaction conditions [39][40]. This remarkable reduction has been associated with diverse factors, such as temperature gradients, a deficient enzyme distribution due to the uneven agitation promoted by the viscosity increase in high-solids content systems, and the reduction in enzyme accessibility caused by the binding of lignin on remanent enzyme molecules [39][40]. As anticipated, the saccharification of lignocellulosic biomass often results in a highly diluted sugar solution, which can affect various aspects of industrial scale biorefinery analysis. Therefore, studying the transformation of monomeric carbohydrates to furan materials in aqueous systems containing low to intermediate sugar content is mandatory.

During the acid-catalyzed dehydration of glucose and xylose in aqueous systems, the addition of an organic co-solvent, such as DMSO, MIBK, THF, 1-butanol, etc., has been used to enhance the yield of 5-HMF and furfural. This has been demonstrated to prevent unwanted side reactions, including ring-opening rehydration to formic and levulinic acid [41][42][43], as well as nucleophilic addition, self-condensation, and polymerization

reactions leading to humins, a dark-colored polymeric network of furanic derivatives [2][44][45]. The dehydration of glucose to 5-HMF involves the initial isomerization step to a ketose, typically fructose, followed by the limiting dehydration step to the final furanic product [46][47]. Recent studies have focused on understanding the catalyst and solvent effects on the yield of 5-HMF during the dehydration of fructose using multivariate computational models. These studies suggest that stabilizing the carbocation intermediates formed during the transformation process prevents further reversion and polymerization reactions, becoming crucial for maximizing the yield to 5-HMF. Thus, the use of solvents with high capacity to stabilize intermediate carbocation complexes through hydrogen bonding (high hydrogen-bond basicity) and with low proton transfer activity (e.g., aprotic solvents), such as DMSO, 1,4-dioxane, and acetone are desirable [48][49]. Alternatively, other studies have attributed the enhancement of 5-HMF yield to a reduction in its susceptibility to nucleophilic attacks, resulting from changes in structural and vibrational properties influencing its reactivity due to stronger interactions between the hydroxyl and the carbonyl groups within this furan molecule and the organic co-solvent used [50].

Biorefineries integrate various mechanical, thermo-chemical, and biochemical biomass conversion technologies to produce bioenergy, biofuels, and other valuable bio-based materials [51][52]. Although this concept is not new in industrial settings, modern biorefinery approaches have emerged as promising strategies to address the environmental challenges of a bio-based economy [53][54]. In contrast to the traditional oil-based industry, biorefineries are expected to operate sustainably [55][56]. Therefore, a thorough analysis is required during their conceptual design. Typical biorefinery analysis includes a precise assessment of adequate raw materials, product portfolios, transformation pathways, separation technologies, process intensification opportunities, economic potential, social assessment, environmental impacts, water and energy analysis, etc. [57][54][58][59]. Fractional distillation is one of the conventional separation methods most frequently applied in lignocellulosic biorefinery studies. This well-established technology has been used to recover organic solvents employed during biomass pretreatment and biomass transformation processes for the production and purification of bioethanol, lactic acid, 5-HMF, and furfural [60][61][62][63]. Due to the low thermodynamic efficiency of conventional distillation processes, caused by the intrinsic requirement of high-quality heat input at the reboiler and the low-quality heat readily available at the condenser, optimizing the operational variables associated with this specific separation unit is desirable to minimize both capital and operational expenditure as part of the biorefinery conceptual design before proceeding with the subsequent steps of the particular technology deployment rout [64][65]. The required amount of heat at the reboiler in a distillation system depends on a range of process, operational, and design variables, including the physicochemical properties of the materials to be separated, such as state of segregation, heat capacity, boiling point, etc., the total mass flow to the distillation system, the operating pressure, the location of the feed plate, the reflux ratio, etc. [66][67]. Similarly, other factors can affect the operation of distillation columns, including the presence of solid materials, the thermochemical instability of the processed components, operational-associated safety risks, the occurrence of azeotropic nodes between the chemical of interest and other materials in the processed stream, among

others [68]. This last phenomenon is of great importance for fractional distillation analysis since, in azeotrope mixtures, the affinity and repulsion forces between two or more components and within each other can lead the system to a thermodynamic boundary. Within this boundary, the mass composition of azeotrope species reaches the same value in both the liquid and the vapor phases at a specific equilibrium stage, restricting the purity level of the distilled product when a conventional distillation system is used [69][70].

High carbohydrate conversion rates (92%-100%) and yields of furan products (75%-80%) have been documented in previous studies when 1,4-dioxane is employed as a co-solvent at a high organic solvent-to-aqueous phase volume ratio (5:1) during the dehydration reaction of monomeric sugars (6%wt.-20%wt., sugar aqueous) over Lewis-acid catalysts. This is in contrast to results obtained when using alternative organic co-solvent systems, such as THF, toluene, MIBK, 2-butanol, etc. [71][72][73][74]. These remarkable results suggest that 1,4-dioxane could be suitable for producing C5 and C6 furan platforms with high throughput at industrial-scale settings. However, this aprotic solvent exhibits an azeotrope node with water at approximately 82%wt., with a boiling point of around 87.6°C at 1 atm [75][76]. This thermodynamic restriction adds complexity to its further separation and recovery. Likewise, this organic solvent has been associated with potential genotoxic and harmful biological effects on rodents and other model organisms after chronic high-dose exposure [77][78][79]. Hence, finding an alternative solvent for designing an operationally safe, energy efficient, environmentally conscious, scalable, and economically feasible process to produce large amounts of furans from lignocellulosic feedstocks is imperative.

In this study, the differences in performance between the microwave-assisted dehydration reaction of purchased glucose and xylose towards 5-HMF and furfural over aluminum chloride in the presence of 1,4-dioxane versus acetone, a low boiling point and non-azeotropic solvent with water are examined. Two-step integrated process models were developed to estimate the theoretical heat duty required at the dehydration reactor, the reboiler, and the condenser of a distillation system for both co-solvents analyzed. The resulting theoretical number of separation stages needed and the optimal feed stage for a complete co-solvent recovery were considered during the assembly of an in-house-built continuous multi-stage distillation system. Utilizing the dehydration performance results, two aqueous solutions containing purchased 5-HMF, furfural, and the studied co-solvent system were prepared and processed in the continuous distillation setup. The distilled (top) and heavy (bottom) products from the distillation experiments were evaluated for co-solvent and furan products content. Finally, the dehydration reaction performance results and the organic solvent recyclability parameters, including recovered co-solvent purity, estimated heat duties, and estimated dehydration catalyst makeup results, are discussed, compared, and analyzed.

4.2. Materials and methods

4.2.1. Materials

Analytical reagents including D(+)-glucose (anhydrous, 99%, Thermo Scientific™), D(+)-Xylose (>99%, Thermo Scientific™), Aluminum Chloride (Hexahydrate, 99%, Thermo

Scientific™), 5-Hydroxymethylfurfural (≥99%, Sigma Aldrich®), 2-Furaldehyde (99%, Sigma Aldrich®), acetone (>99.5%, Thermo Scientific™), 1,4-dioxane (99.5%, Thermo Scientific™), Certified Reference Material for the quantification of glucose, xylose, 5-Hydroxymethylfurfural, and furfural (Absolute Standards, Inc), were used as received. Ultra-pure water (Milli-Q® Biocel water system) was utilized in all experiments.

4.2.2. Dehydration of monomeric sugars

An aqueous solution of sugars was prepared using glucose, xylose, and ultra-filtrated water. A total sugar mass content of 20% and glucose-to-xylose mass ratio of 3.6, as it has been typically found in lignocellulose-derived hydrolysate, were used for this preparation [80]. The sugar dehydration experiments employed a volume ratio of organic solvent-to-aqueous sugar solution of 2 to 1. Two different co-solvent systems were studied. Five samples containing 1,4-dioxane and five samples containing acetone were processed for each case. Aluminum chloride ($AlCl_3$), a Lewis acid catalyst, was selected and used for the dehydration of sugars, following previously reported information [9][20][81] at a total catalyst loading of 15milimolar (mM). Dehydration experiments were performed using the CEM Discovery 2.0 Microwave Reactor (CEM Corporation, Charlotte, NC). A reaction method with a setpoint temperature of 185°C, 10 seconds pre-stirring, continuous stirring at medium level during the processing time, and a total holding time of 3 minutes was configured and used. 10ml vials containing 3ml of total sample volume were used for each run. The quantification of the unreacted glucose and xylose after performing the reaction, as well as the produced 5-HMF and furfural, was performed based on NREL procedure [82], using Agilent HPLC 1260 with chromatographic column Bio-Rad, Aminex HPX-87H Organic Acid Analysis and equipped with Diode Array Detector (5-HMF at 284nm and furfural at 277nm) and Refractive Index Detector (Agilent Technologies, Santa Clara, CA).

4.2.3. Process description and process modeling

The two-step biorefinery process flow diagram for the dehydration of glucose and xylose, along with the solvent recovery strategy proposed, is depicted in **Fig. 4.1**. Aqueous sugars solution enters the mixer where this stream is combined with fresh organic solvent (1,4-dioxane or acetone), catalyst supporting the dehydration reaction ($AlCl_3$), and a stream of recirculated solvent. The mixture enters the dehydration reactor operating at 185°C before being fed into a fractional distillation column used to separate and recirculate the organic solvent towards the beginning of the process. Due to the complexity of the transport phenomena occurring at the distillation column, the use of process simulation software is suitable to estimate a realistic heat demand for this unit operation, as well as for the dehydration reactor.

Aspen Plus™ (version 11) is a computer-based modeling and simulation technology, and a powerful tool initially developed by the Massachusetts Institute of Technology (MIT) and the United States Department of Energy. The use of this software has been recommended and applied for the modeling of modern biorefineries handling the conversion of biomass to sugars, furan materials, and others [83][84]. The thermodynamic method as well as the binary interaction parameters sources selected for the process simulation is of extreme importance considering an accurate representation

of the simulation to the real studied systems. According to literature, the Nonrandom Two Liquid (NRTL) method closely reproduces the experimental results of biomass transformations similar to the one studied in this work [85]. In this study, additional thermodynamic methods and binary interaction parameters sources were evaluated aiming to find the best set of thermodynamic equations that can adequately represent the experimental vapor-liquid equilibrium data reported in the literature for the analyzed systems.

The simulation software was used to estimate the mass balance and the heat duty at the different units presented in **Fig. 4.1**. The RStoic model was used to simulate the dehydration reactor and the rigorous RadFrac model, used to simulate multistage vapor-liquid operations was used in the simulation of the fractional distillation column. Experimental data collected after performing the dehydration reaction of sugars (Sugars conversion and yield to furans) were used as input data for the simulation of the dehydration reactor. At the same time, the Theoretical Equilibrium Stages estimated by the simulation software were used to define experimental conditions for the continuous distillation of 1,4-dioxane and furfural (e.g., adequate number of equilibrium stages, optimal feed stage, distillate, and bottom product flows, etc.).

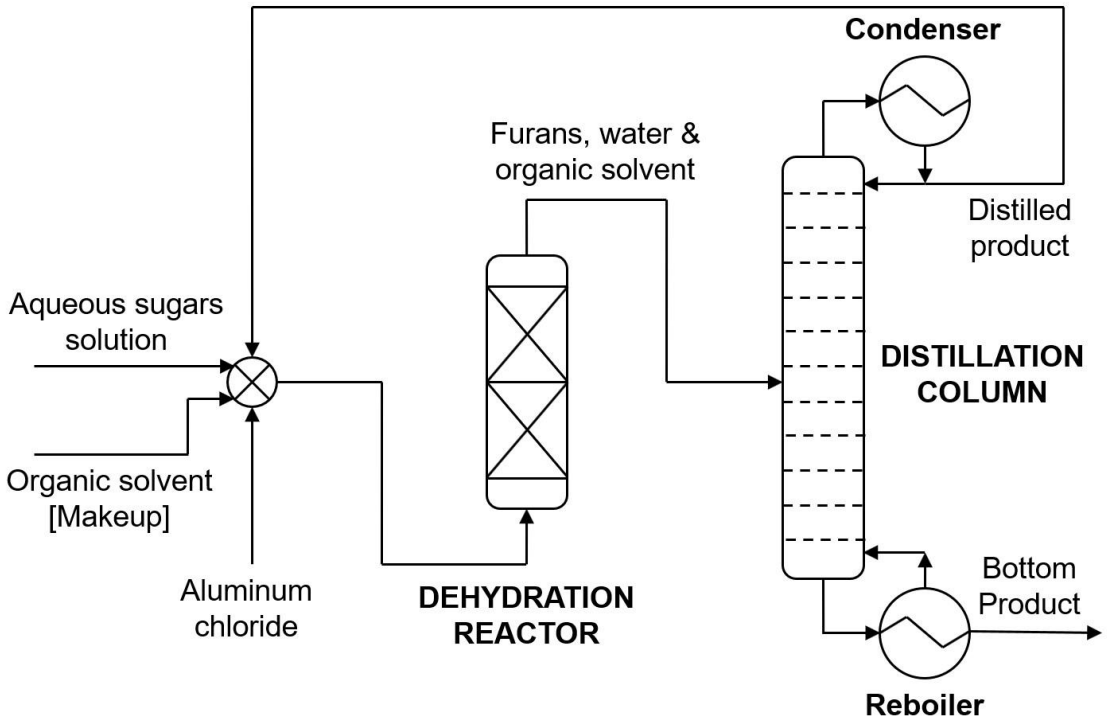

Fig. 4.1. Two-step biorefinery process flow diagram.

4.2.4. Continuous distillation of organic solvents

Commercially available 5-HMF and furfural were used to prepare 300ml of aqueous furans solution containing the corresponding amount of dehydration products dictated by the results of the two sets of experiments of sugars dehydration (1,4-dioxane and acetone systems). Glucose and xylose were added to the solution to simulate the presence of side

products generated during the dehydration reaction. A corresponding volume of organic solvent was added to an organic solvent to aqueous furans solution volume ratio of 2.0. Following the simulation results regarding the number of Theoretical Equilibrium Stages, an in-house-built continuous distillation system was put in place to conduct the distillation experiments.

Two 6-section Snyder columns (ACE Glass Inc, Vineland), a 500ml round bottom flask, and a Graham condenser, were used as a total of 14 Equilibrium Stages systems. A heating mantle with a magnetic stirrer (Fisherbrand™) was used as the source of heat to the reboiler. Two peristaltic pumps were used (Golander LLC, USA). The first one is to feed the furans solution to Equilibrium Stage #8 and the second one is to remove the bottom product from the reboiler. Two temperature controllers (J-Kem Scientific Inc., St. Louis, MO) were used to control the reboiler temperature at 101°C and to avoid the heat loss to the surroundings of the distillation column by maintaining a heating tape wrapped to the distillation column, 2°C below the expected distillate temperature reported in the literature and obtained from the Aspen Plus™ simulation results; 87.6°C [75][76], azeotrope temperature for the 1,4-dioxane/water system, and 56°C, pure acetone boiling point [86]. Finally, a local temperature indicator was installed at Equilibrium Stage #2 to measure and record the temperature at this stage (Sper Scientific LLC, Scottsdale, AZ) The quantification of 1,4-Dioxane and acetone at the distillate and bottom product, was performed using Agilent HPLC 1220 with chromatographic column InfinityLab Poroshell 120 EC-C18, 4.6mm x 100mm and 2.7µm and equipped with Variable Wavelength Detector at 190nm and 266nm respectively (Agilent Technologies, Santa Clara, CA).

4.3. Results and discussion

4.3.1. Microwave-assisted dehydration of sugars at initial intermediate consistency

The results for the conversion of sugars and the yield to furans during the dehydration reaction in 1,4-dioxane and acetone systems are presented in **Fig. 4.2**. Under the studied conditions, the conversion of glucose and xylose reached 100% in all cases. Similar yields to 5-HMF and furfural were obtained when comparing the results for both solvents. These results suggest that in the investigated case studies, replacing 1,4-dioxane with acetone has a neglectable impact on the yield of intended furan products. Furthermore, a reduction in the pH of the solutions after the dehydration reaction was found at the same level for the two analyzed solvent systems (**S5**). This result has been explained before as the consequence of side product formation, including levulinic acid and formic acid as a consequence of the degradation of 5-HMF [20].

4.3.2. Process simulation results

The composition of the liquid and the vapor phases in equilibrium predicted by Aspen Plus™ (version 11) for the binary systems: 1,4-dioxane/water; acetone/water; and acetone/furfural are presented in **Fig. 4.3**, **Fig. 4.4**, and S4.6. From these results, it can be observed how the thermodynamic method NRTL-2 with the Binary Interaction Parameters sources: APV110 VLE-IG and NISTV110 NIST-IG closely represent the experimental vapor-liquid equilibrium data in each case. Thus, validating the use of this set of equations and parameters during the process simulation work herein presented.

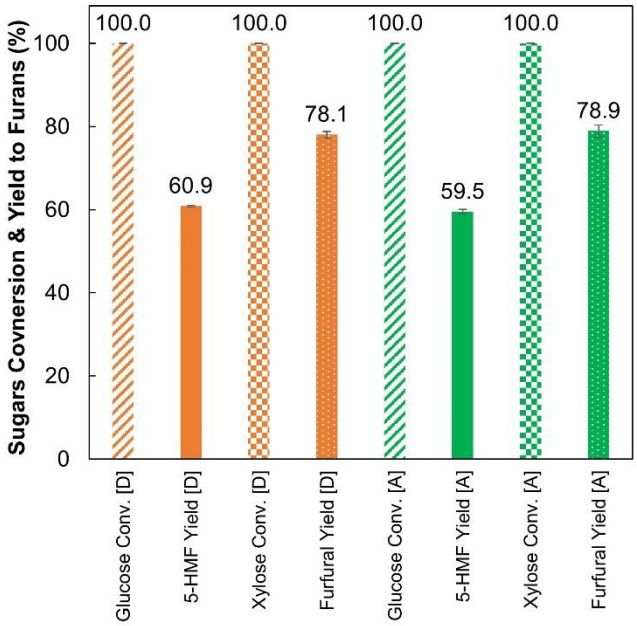

Fig. 4.2. Glucose and xylose conversion and yield to 5-HMF and furfural for 1,4-dioxane [D] and Acetone [A] systems. Experimental conditions: 20%wt. total sugar aqueous solution, 15mM $AlCl_3$, 2.0 organic solvent to aqueous sugar solution volume ratio, 185°C, and 3min holding time.

Two crucial operational parameters needed to be estimated before proceeding with the continuous fractional distillation experiments: the number of Theoretical Equilibrium Stages and the Optimal Feed Stage. For this reason, simulating the two steps of biorefineries prior to performing experimental work was required. The size of the biorefinery was fixed at a processing capacity of 500kg/hr of 20%wt. total sugar aqueous solution. Four different scenarios were analyzed, two for each solvent system: The realistic "closed" scenarios where the solvent is distilled and then recirculated to a mixing unit before reentering the dehydration reactor, and the non-realistic "open" systems where the solvent passes through the distillation column only once, similarly to what can be reproduced at laboratory scale, making these scenarios and results potentially suitable for comparison purposes, but, meaningless from a real industrial settings point of view. Notice that the results of the dehydration experiments were used as input data for the simulation work. Detailed results for the mass balance and the estimated heat duty at each piece of equipment of the hypothetical biorefinery for all four analyzed cases are presented in S4.7.

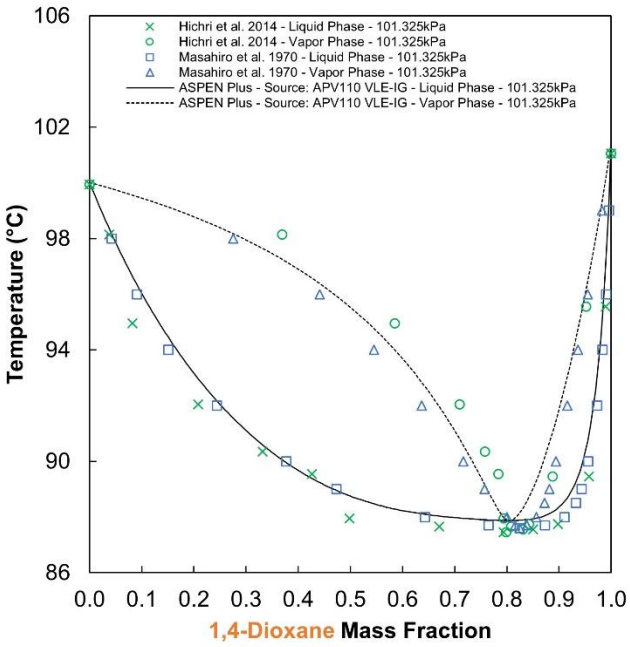

Fig. 4.3. T-x-y diagram for the 1,4-dioxane (1) + water (2) System: X, T-x and ○, T-y for experimental data at 101.325kPa [76]; □, T-x and Δ, T-y for experimental data at 101.3kPa [75]; —, T-x and ---, T-y ASPEN Plus™ NRTL-2 (Binary Interaction Parameters source: APV110 VLE-IG) at 101.325kPa.

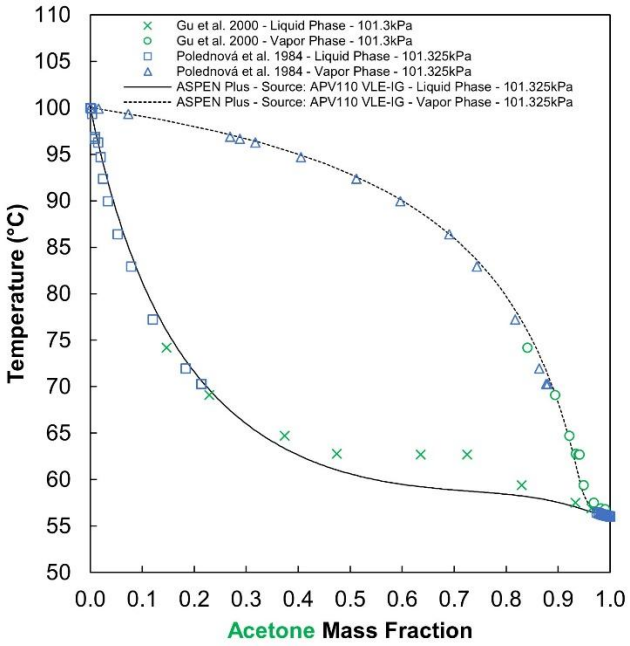

Fig. 4.4. T-x-y diagram for the acetone (1) + water (2) System: X, T-x and ○, T-y for experimental data at 101.3kPa [86]; □, T-x and Δ, T-y for experimental data at 101.325kPa [87]; —, T-x and ---, T-y ASPEN Plus™ NRTL-2 (Binary Interaction Parameters source: APV110 VLE-IG) at 101.325kPa.

Table 4.1. Mass balance and heat duty result in the dehydration of sugars to furans using 1,4-dioxane and acetone as organic solvents: closed (realistic) and open (non-realistic) scenarios.

	1,4-dioxane [Closed]	**1,4-dioxane [Open]**	**Acetone [Closed]**	**Acetone [Open]**
Glucose (kg/h)	78.3	78.3	78.3	78.3
Xylose (kg/h)	21.7	21.7	21.7	21.7
Water (kg/h)	400.0	400.0	400.0	400.0
Sugars Mass Fraction (aq.)	**0.2**	**0.2**	**0.2**	**0.2**
Solvent to Reactor (kg/h)	1,638	825	658	632
Water to Reactor (kg/h)	792	400	416	400
Solvent/Water Mass Ratio to Reactor	2.1	2.1	1.6	1.6
Solvent/Water Volume Ratio to Reactor	**2.0**	**2.0**	**2.0**	**2.0**
Fresh Solvent Make-up (kg/hr)	**32.9**	**825.0**	**13.2**	**632.0**
Solvent Loss (kg/hr) [@ Bottom Product]	32.9	16.6	13.2	12.7
Solvent to the Distillation Column (kg/h)	1,638	825	658	632
Fixed Solvent Loss (%) (Based on Solvent to the DC)	2.0	2.0	2.0	2.0
Total Mass Flow to the Dist. Column (kg/h)	**2,534**	**1,327**	**1,176**	**1,134**
Solvent at Distillate Stream (kg/h)	1,605	808	644	619
Water at Distillate Stream (kg/h)	390.6	197.2	16.0	15.3
Furfural at Distillate Stream (kg/h)	0.42	0.37	0.00	0.00
5-HMF at Distillate Stream (kg/h)	0.0	0.0	0.0	0.0
Total Mass Flow at Distillate Stream (kg/h)	**1,996**	**1,006**	**660**	**635**
Solvent mass fraction at Distillate Stream [organic solvent and water only]	**0.80**	**0.80**	**0.98**	**0.98**
Solvent mass fraction in Distillate Stream [Overall]	0.80	0.80	0.98	0.98
Dehydration Catalyst Makeup ($AlCl_3$)	**4.8**	**2.4**	**2.5**	**2.4**
Glucose Conversion (%) - Experimental	100	100	100	100
Yield to 5-HMF (%) - Experimental	60.89	60.89	59.51	59.51
Xylose Conversion (%) - Experimental	100	100	100	100
Yield to furfural (%) - Experimental	78.07	78.07	78.93	78.93
Recirculated Distillate Stream Temperature (°C)	68*	25*	36*	25*
Total Mass Flow to the Reactor (kg/hr)	**2,534**	**1,327**	**1,176**	**1,134**
Reaction Temperature (°C)	185	185	185	185
Reactor's Heat Duty (MJ/hr)	**3,162**	**1,752**	**1,773**	**1,713**
Reboiler's Heat Duty (MJ/h)	**4,308**	**2,183**	**1,201**	**1,155**
Bottom Product Temperature (°C)	97.4	98.0	93.8	93.8
Condenser's Heat Duty (MJ/h)	**-3,776**	**-1,904**	**-945**	**-908**
Top Product Temperature (°C)	87.9	87.9	56.3	56.4
Reflux Ratio (Mass)	1.5	1.5	1.5	1.5
Distilled Rate (kg/hr)	1,996	1,006	660	635
Total Theoretical Stages	10	10	10	10
Feed Stage Above Stage	5	5	5	5

* In closed systems, these values represent an estimated temperature of the recirculated solvent considering a reduction of 20°C due to heat transfer to the surroundings, integrating a relevant consideration for industrial settings. This temperature is fixed at 25°C (Fresh solvent).

4.3.2.1. Solvent purity at distillate

As expected, the calculated weight percentage of 1,4-dioxane at the distillate stream as well as the top product temperature (S4.7) approached the azeotrope mass fraction and temperature reported in the literature (Results: ~80%wt. and 88°C). Likewise, the simulation model predicted the possibility to distill high-purity acetone (>98%wt.) at a temperature close to the reported boiling point of this organic solvent (Result: 56.4°C).

4.3.2.2. Organic solvent loss

Due to the 18-20%wt. water content at the distillate stream being recirculated in the 1,4-dioxane "closed" system, the amount of organic solvent required in the stream entering the dehydration reactor should be necessarily increased to preserve an organic solvent to aqueous sugars solution volume ratio of 2.0. Since the loss of organic solvent has been fixed at 2.0% of the total solvent fed into the distillation column, the organic solvent makeup in the "closed" scenario for the 1,4-dioxane system is negatively impacted. A fresh organic solvent make-up flow of 32.9kg/hr is estimated for the system using 1,4-dioxane. Whilst a lower make-up flow of 13.2kg/hr is predicted for the system utilizing acetone (**S7**). The replacement of organic solvent could then represent a potential 60% reduction in organic solvent loss, in addition to the reduction in operational cost due to the difference in the price of these materials (1,4-dioxane: $1,150/tonne & acetone: $1,000/tonne) [Pending inserting references].

4.3.2.3. Dehydration catalyst makeup

A dehydration catalyst make-up of almost double (4.8kg/hr) is required for the 1,4-dioxane system (realistic "closed" scenario) when compared to the acetone system (2.4kg/hr). This is because the catalyst loading has been fixed on a concentration basis (15mM), and the flow to the dehydration reactor for the 1,4-dioxane (2.5tonne/hr) is more than double the flow at the same stream for the acetone system (1.2tonne/hr) (S4.7).

4.3.2.4. Heat duty at the dehydration reactor and the distillation column system

In **Fig. 4.5** the heat duty at the reboiler, the condenser, and the dehydration reactor estimated using Aspen Plus™ (version 11) for the two organic solvent systems studied are presented. From these results, it can be noticed that the heat duty required at all units in the 1,4-dioxane system is always higher in comparison to the system utilizing acetone (S4.7). Also, it can be observed how for systems using acetone, the amount of heat required for the separation of the solvent is lower than the heat required for the chemical transformation of the components of interest, contrary to the results obtained for the compared solvent. For the 1,4-Dioxane system, the reboiler heat duty is 3.6 times, the condenser heat duty is 4 times, and the dehydration reactor heat duty is 1.8 times the corresponding values in the acetone system. Two facts mainly explain these results. First, the previously discussed augmented flow entering the dehydration reactor and distillation column in the 1,4-dioxane system, requires supplementary heat addition/removal so the materials can reach adequate process temperatures. Secondly, the difference in boiling point between the binary azeotrope mixture 1,4-dioxane/water (~87.9°C) versus the low boiling point of the distilled high purity acetone (~56.4°C). This fact explains why acetone is less heat-demanding during an evaporation process in comparison to its counterpart.

Under industrial settings, the heat demand at the dehydration reactor and the reboiler are satisfied by the heat released from different fuels that are burned in boilers to produce high-quality steam that can be easily transported to the pieces of equipment demanding energy in the form of heat. Likewise, the heat duty at the condenser, better said, the necessary energy removal to condense the top product, is normally addressed by using cooling water circuits, cooling towers, and other refrigeration systems. For this reason,

minimizing the heat duty at the different pieces of equipment of the biorefinery is a key factor to minimize capital expenditure and operational costs, and to reduce the environmental impacts associated with the operation of the biorefinery through the increase of its energy efficiency.

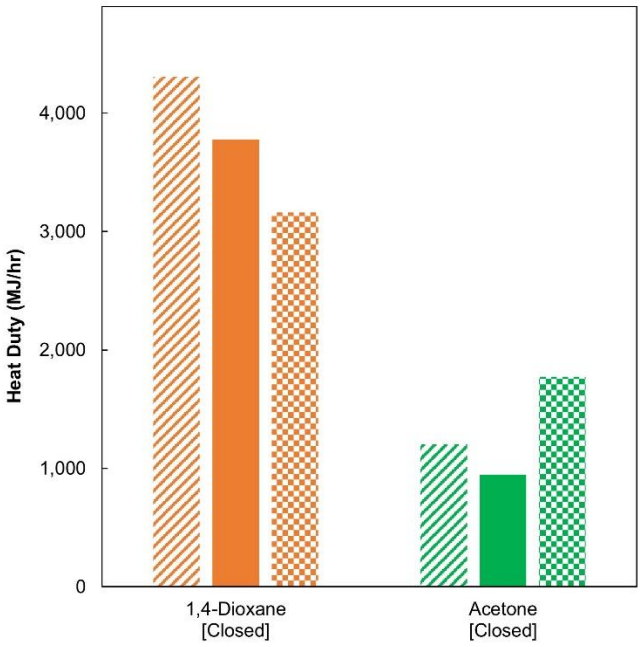

Fig. 4.5. ▨ Reboiler, ■ Condenser, and ▩ Dehydration reactor heat duty for 1,4-dioxane and acetone systems.

4.3.2.5. Distillation column parameters for continuous distillation experiments

According to the simulation results, 10 Theoretical Equilibrium Stages with a Feed Stage over Stage #5 are enough to distill 1,4-dioxane at the azeotrope concentration and nearly pure acetone for each case studied.

4.3.3. Continuous distillation experiments

4.3.3.1. Continuous distillation of 1,4-dioxane from furans solution

Considering the results from the dehydration reaction experiments for the 1,4-dioxane system (**Fig. 4.2**), 300ml of an aqueous solution of purchased furans was prepared containing the correspondent concentration of 5-HMF (6.67%wt.) and furfural (2.17%wt.). 1,4-dioxane was then added to this aqueous solution in a volume ratio of 2.0. After performing several trials, a feed flow to the distillation system depicted in **Fig. 4.6** of 2.0ml/min of solution containing organic solvent was defined as the feed transfer flow. The temperature at the reboiler and the temperature at Equilibrium Stage #2 were recorded. The results presented in **Fig. 4.6** indicate that the thermal equilibrium of the system was achieved at reference process time approximately 44min. The average temperature reached at the reboiler after thermal equilibrium and under the experimental conditions was 97°C±0.1, below the setpoint temperature (101.1°C). Early indicating the

presence of organic solvent at the reboiler stage. An average measured temperature at Equilibrium Stage #2 of 86.4°C±0.1 was close to the expected azeotrope temperature for the 1,4-dioxane/water system (87.8°C [76]). After the thermal equilibrium was achieved, 6 sample sets were taken at different process times (D-R1 to D-R6). Each sample set included a sample of the material from the reboiler and a sample of the distillate collected at Stage #2 using a splitting valve. The volume flow of distillate was also measured using an adapted burette. An average top product flow of 1.5±0.1ml/min was found. An image of the solution fed to the distillation column and the distillation products (top and bottom) are presented in S4.8. The average 1,4-dioxane content in the total twelve samples of distillate and bottoms are presented in **Fig. 4.8**.

A mass percentage of 82.15±0.14%wt. 1,4-dioxane was found in the distilled stream, close to the azeotrope concentration of this organic solvent with water reported in the literature at 82.5%wt. [76]. However, a mass percentage of 13.92±0.81%wt. was found in the reboiler product. More stages are likely needed to completely remove the solvent from the bottom product.

4.3.3.2. Continuous distillation of acetone from furans solution

Considering the results from the dehydration reaction experiments for the acetone system (**Fig. 4.2**), 300ml of an aqueous solution of purchased furans was prepared containing the correspondent concentration of 5-HMF (6.52%wt.) and furfural (2.20%wt.). acetone was then added to this aqueous solution in a volume ratio of 2.0. Similarly, as for the 1,4-dioxane system, a 2.0ml/min solution containing organic solvent was used as the feed transfer flow for this continuous distillation experiment. The results presented in **Fig. 4.7** indicate that the thermal equilibrium of the system was achieved at the reference process time ~approximately 16 minutes. The average temperature reached at the reboiler after thermal equilibrium and under the experimental conditions was 101°C±0.1 (Setpoint temperature 101.1°C). Potentially indicating the absence of organic solvent at the reboiler stage. An average measured temperature at Equilibrium Stage #2 of 55.2°C±0.1 was close to the expected boiling point of pure acetone (56.08°C [88]). After the thermal equilibrium was achieved, 6 sample sets were taken at different process times (A-R1 to A-R6), following similar steps as for the experiments distilling 1,4-dioxane. An average top product flow of 1.4±0.1ml/min was found. An image of the solution fed to the distillation column and the distillation products (top and bottom) are presented in S4.9. The average acetone content in the total twelve samples of distillate and bottoms are presented in **Fig. 4.8**. A mass percentage of 99.98±0.34%wt. acetone was found in the distilled stream and no acetone was detected in the reboiler product. The number of equilibrium stages used was enough to remove all acetone from the bottom product, in contrast with the finding from the 1,4-dioxane system studied.

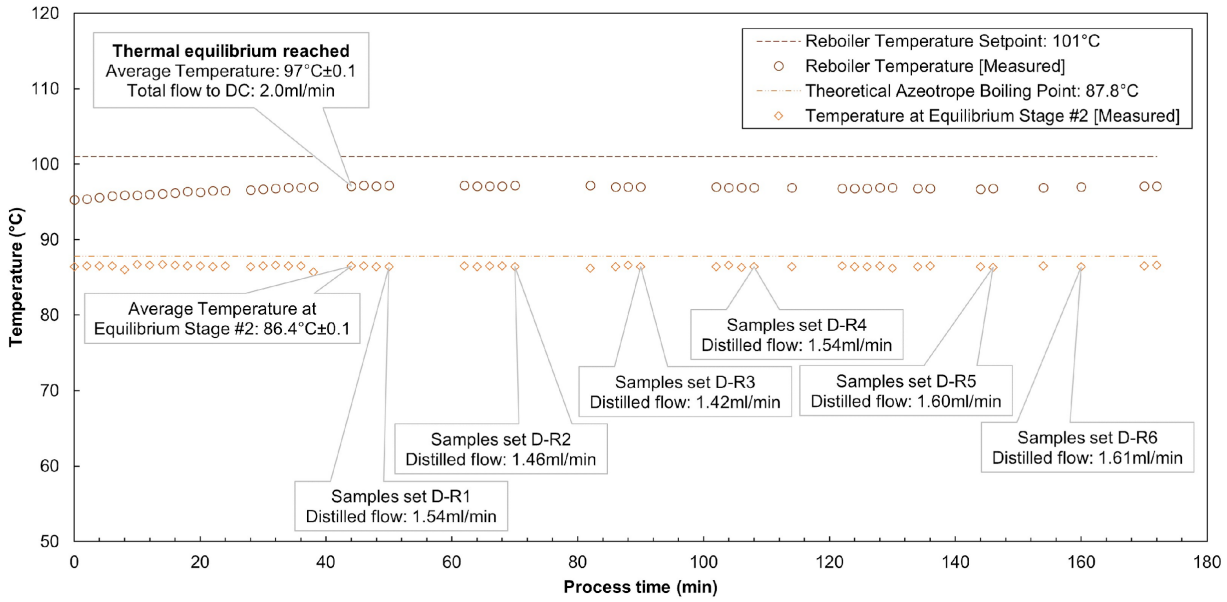

Fig. 4.6. Measured process variables for the continuous distillation of 1,4-dioxane from a 5-HMF, furfural, and sugars solution containing a 2 to 1 volume ratio of organic solvent to aqueous solution - Fixed feed flow: 2.0ml/min and total 14 Equilibrium Stages.

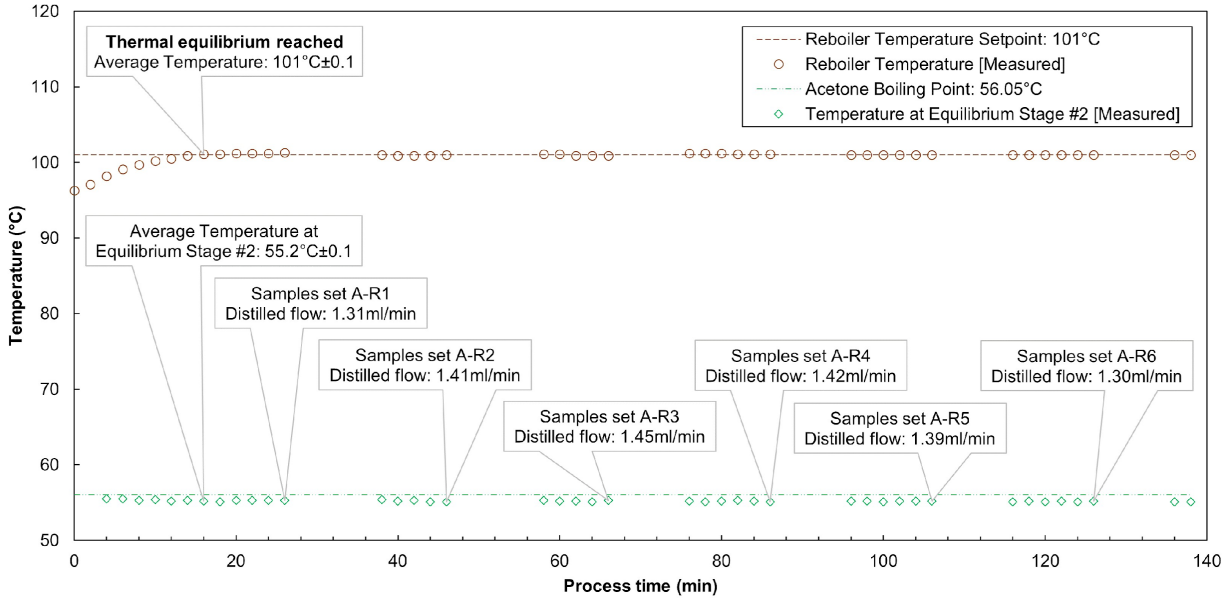

Fig. 4.7. Measured process variables for the continuous distillation of acetone from a 5-HMF, Furfural and sugars solution containing a 2 to 1 volume ratio of organic solvent to aqueous solution - Fixed feed flow: 2.0ml/min and total 14 Equilibrium Stages.

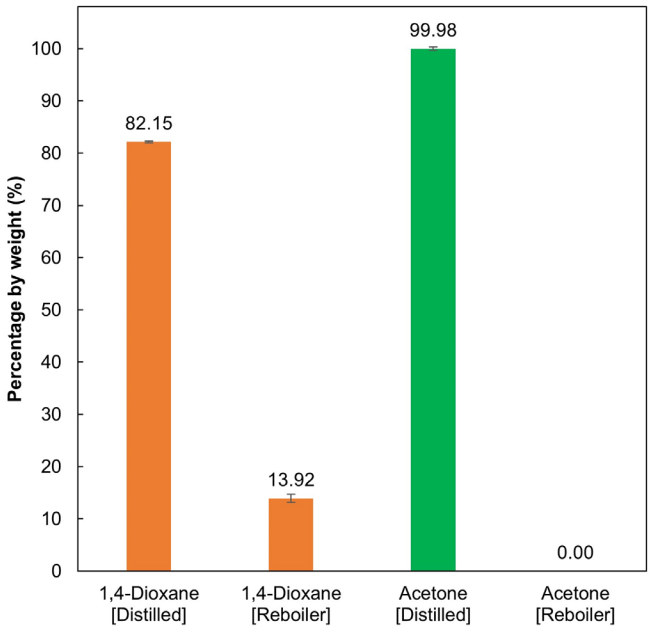

Fig. 4.8. Organic solvent content in the distillate stream and the bottom product as a percentage by weight.

4.3.3.3. Distillation products for 1,4-dioxane and acetone systems

The pH of the resulting distillation products for the two solvent systems studied is presented in S4.10. A lower pH was obtained for the bottom product from the distillation experiment using 1,4-dioxane. This result can be explained due to the concentration effect over the dissolved materials in the solution present in the reboiler, promoted by the removal of water, leaving the system through the distillate stream with the organic solvent at the azeotropic concentration during the distillation operation. As discussed in the literature, it is expected that more acidic conditions and intermediate temperatures could lead to further degradation of 5-HMF [89]. The concentration effect beyond the starting aqueous system values was not appreciated for the system utilizing acetone as an organic solvent, since the distillate was essentially pure acetone (99.98±0.34%wt.). In S4.11, the density of the solutions fed and the resulting products after the distillation process are reported. Consistently, the increase of the density of the furans solution at the reboiler for the 1,4-dioxane system was observed. This aligned with the mentioned effect of water leaving the system at the condensate stream. Furthermore, all samples collected at the distilled stream were analyzed using Agilent HPLC 1260 in search of the presence of furan materials. These results are reported in **Fig. 4.9**. No 5-HMF was detected in the distilled 1,4-dioxane or the distilled acetone. Interestingly, and, opposite to the expected results S4.12, furfural was not only found in the distilled 1,4-dioxane containing ~18%wt. water, but also in the distilled acetone at a rate of 0.25±0.06% and 0.25±0.02% based on the total mass flow fed to the distillation column (**Fig. 4.9**). The presence of furfural in the distillate for the 1,4-dioxane could be possibly promoted by the heterogeneous azeotrope occurring for the binary system furfural/water reported in the literature at 35.46%wt. furfural and 97.75°C [89], also predicted by the utilized simulation software (S.4. 34.95%wt. furfural and 97.98°C, Aspen Plus™). From the results

presented in S4.7, it is clear that with the selected parameters for the simulation, the models from this work failed to predict the presence of furfural at the distillate stream for the acetone system. Additional studies are required to understand the reasons for this observed behavior. Moreover, it is plausible that the number of equilibrium stages was not enough to avoid the presence of furfural within the distilled acetone, and/or, it could be possible that the relative volatility of furfural is being affected by the presence of specific components in the solution, including the concentration of hydrogen ions (pH), etc.

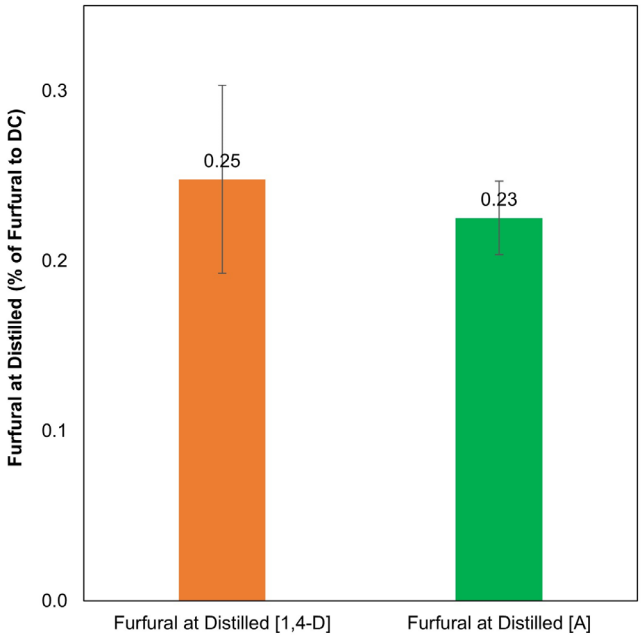

Fig. 4.9. Furfural leaving the system at the distilled stream (open system) as a percentage of furfural being fed to the Distillation Column.

4.4. Conclusions

The reduction of energy consumption as well as minimizing the materials loss and process element make-up are key factors for the economically viable operation of chemical plants, including biorefineries. In this study, several performance and recyclability parameters were compared for two different solvent systems, including the yield to 5-HMF and furfural, the heat duty at the reactor and the distillation column system, the organic solvent make-up, catalyst loss, and the recirculation of process elements. Considering that minor differences were found on the yield to furan components when comparing acetone to. 1,4-dioxane, it can be concluded that, for intermediate sugars concentration systems, using acetone is a more desirable alternative for different reasons. First, there is a lower overall heat demand at the reactor and the reboiler. Second, the lower solvent and catalyst losses of 40%, 41% and 52%, respectively, compared to the corresponding values for the 1,4-dioxane system. Additionally, there are safety concerns associated with the use of 1,4-dioxane to human and environment health, as well as the associated risk of peroxides formation.

References

1. C. Xu, E. Paone, D. Rodríguez-Padrón, R. Luque, and F. Mauriello, “Recent catalytic routes for the preparation and the upgrading of biomass derived furfural and 5-hydroxymethylfurfural,” *Chem. Soc. Rev.*, vol. 49, no. 13, pp. 4273–4306, 2020, doi: 10.1039/d0cs00041h.
2. J. Slak, B. Pomeroy, A. Kostyniuk, M. Grilc, and B. Likozar, “A review of bio-refining process intensification in catalytic conversion reactions, separations and purifications of hydroxymethylfurfural (HMF) and furfural,” *Chem. Eng. J.*, vol. 429, no. September 2021, 2022, doi: 10.1016/j.cej.2021.132325.
3. Y. Zhang and Y. Shen, “Electrochemical hydrogenation of levulinic acid, furfural and 5-hydroxymethylfurfural,” *Appl. Catal. B Environ.*, vol. 343, no. November 2023, 2024, doi: 10.1016/j.apcatb.2023.123576.
4. Z. Song, L. Liu, X. Zhu, Z. Ren, and J. Bai, “Cobalt-based catalysts for catalytic oxidation of biomass-derived 5-Hydromethylfurfural to value-added chemicals,” *Renew. Sustain. Energy Rev.*, vol. 189, no. PB, p. 114003, 2024, doi: 10.1016/j.rser.2023.114003.
5. P. Díaz-Maizkurrena, J. M. Requies, A. Iriondo, P. L. Arias, and R. Mariscal, “5-Methoxymethyl furfural production by acid heterogeneous catalytic etherification of 5-hydroxymethyl furfural,” *Catal. Today*, vol. 426, no. February 2023, 2024, doi: 10.1016/j.cattod.2023.114374.
6. S. Kumaravel *et al.*, “Highly selective catalytic transfer hydrogenation of biomass derived furfural to furfural alcohol over Zr/SBA-15 catalysts,” *J. Phys. Chem. Solids*, vol. 186, no. November 2023, 2024, doi: 10.1016/j.jpcs.2023.111831.
7. C. Park *et al.*, “Biomass gasification: Sub-pilot operation of >600 h with extensive tar cracking property and high purity syngas production at H2:CO ratio ∼2 using moving bed redox looping technology,” *Fuel Process. Technol.*, vol. 252, no. May, 2023, doi: 10.1016/j.fuproc.2023.107966.
8. Z. C. Zhang, *Emerging Catalysis for 5-HMF Formation from Cellulosic Carbohydrates*. Elsevier B.V., 2013. doi: 10.1016/B978-0-444-53878-9.00003-5.
9. X. Zhang, B. B. Hewetson, and N. S. Mosier, “Kinetics of maleic acid and aluminum chloride catalyzed dehydration and degradation of glucose,” *Energy and Fuels*, vol. 29, no. 4, pp. 2387–2393, 2015, doi: 10.1021/ef502461s.
10. S. Liu and G. Cheng, “Industrial Crops & Products Developments and perspectives on lignin-first biomass pretreatment for efficient enzymatic hydrolysis and isolation of lignin with minimized degradation,” *Ind. Crop. Prod.*, vol. 208, no. December 2023, p. 117926, 2024, doi: 10.1016/j.indcrop.2023.117926.
11. E. Yang *et al.*, “Pretreatments of lignocellulosic and algal biomasses for sustainable biohydrogen production: Recent progress, carbon neutrality, and circular economy,” *Bioresour. Technol.*, vol. 369, no. September 2022, 2023, doi: 10.1016/j.biortech.2022.128380.
12. Z. C. Zhang, “Emerging Catalysis for 5-HMF Formation from Cellulosic Carbohydrates,” *New Futur. Dev. Catal. Catal. Biomass Convers.*, pp. 53–71, 2013, doi: 10.1016/B978-0-444-53878-9.00003-5.
13. S. Gupta, A. B. Gambhire, and R. Jain, “Conversion of carbohydrates (glucose and fructose) into 5-HMF over solid acid loaded natural zeolite (PMA/NZ) catalyst,” *Mater. Lett. X*, vol. 13, pp. 0–3, 2022, doi: 10.1016/j.mlblux.2021.100119.

14. L. X. Zhang, H. Yu, H. B. Yu, Z. Chen, and L. Yang, “Conversion of xylose and xylan into furfural in biorenewable choline chloride-oxalic acid deep eutectic solvent with the addition of metal chloride,” *Chinese Chem. Lett.*, vol. 25, no. 8, pp. 1132–1136, 2014, doi: 10.1016/j.cclet.2014.03.029.
15. T. Werpy and G. Petersen, “Top Value Added Chemicals from Biomass Volume I,” *Us Nrel*, p. Medium: ED; Size: 76 pp. pages, 2004, doi: 10.2172/15008859.
16. V. Kumar Vaidyanathan, K. Saikia, P. Senthil Kumar, A. Karanam Rathankumar, G. Rangasamy, and G. Dattatraya Saratale, “Advances in enzymatic conversion of biomass derived furfural and 5-hydroxymethylfurfural to value-added chemicals and solvents,” *Bioresour. Technol.*, vol. 378, no. February, 2023, doi: 10.1016/j.biortech.2023.128975.
17. M. V. Morales, J. M. Conesa, A. J. Galvin, A. Guerrero-Ruiz, and I. Rodríguez-Ramos, “Selective hydrogenation reactions of 5-hydroxymethylfurfural over Cu and Ni catalysts in water: Effect of Cu and Ni combination and the reagent purity,” *Catal. Today*, vol. 423, no. September 2022, 2023, doi: 10.1016/j.cattod.2023.01.028.
18. P. Rapado, L. Faba, and S. Ordóñez, “Selective and stable production of furoic acid by furfural aerobic oxidation at controlled mild-pH conditions,” *Appl. Catal. A Gen.*, vol. 670, no. December 2023, 2024, doi: 10.1016/j.apcata.2023.119536.
19. T. K. Godan *et al.*, “Biotransformation of 5-hydroxymethylfurfural by Acinetobacter oleivorans S27 for the synthesis of furan derivatives,” *Bioresour. Technol.*, vol. 282, no. February, pp. 88–93, 2019, doi: 10.1016/j.biortech.2019.02.125.
20. A. Mittal, H. M. Pilath, and D. K. Johnson, “Direct Conversion of Biomass Carbohydrates to Platform Chemicals: 5-Hydroxymethylfurfural (HMF) and Furfural,” *Energy and Fuels*, vol. 34, no. 3, pp. 3284–3293, 2020, doi: 10.1021/acs.energyfuels.9b04047.
21. H. Wang *et al.*, “Recent advances in catalytic conversion of biomass to 5-hydroxymethylfurfural and 2, 5-dimethylfuran,” *Renew. Sustain. Energy Rev.*, vol. 103, no. January, pp. 227–247, 2019, doi: 10.1016/j.rser.2018.12.010.
22. A. Tuan Hoang, S. Nižetić, V. Viet Pham, A. Tuan Le, V. Ga Bui, and V. Vang Le, “Combustion and emission characteristics of spark and compression ignition engine fueled with 2,5-dimethylfuran (DMF): A comprehensive review,” *Fuel*, vol. 288, no. June 2020, 2021, doi: 10.1016/j.fuel.2020.119757.
23. H. Feng, N. Gao, Z. Nan, and C. Yang, “Effects of molecular structure and active sites of 2,5-DMF and 2-MF on reaction characteristics during auto-ignition,” *Comput. Theor. Chem.*, vol. 1212, no. March, 2022, doi: 10.1016/j.comptc.2022.113687.
24. Q. Li, C. L. Ma, and Y. C. He, “Effective one-pot chemoenzymatic cascade catalysis of biobased feedstock for synthesizing 2,5-diformylfuran in a sustainable reaction system,” *Bioresour. Technol.*, vol. 378, no. March, 2023, doi: 10.1016/j.biortech.2023.128965.
25. S. Hussain and S. Berry, “A review study on green synthesis of chitosan derived schiff bases and their applications,” *Carbohydr. Res.*, vol. 535, no. November 2023, 2024, doi: 10.1016/j.carres.2023.109002.
26. J. Mehta, A. V. Metre, M. S. Bhakhar, D. S. Panwar, and S. Dharaskar, “Biomass-derived 5-hydroxymethylfurfural (HMF) and 2,5-dimethylfuran (DMF) synthesis as promising alternative fuel: A prospective review,” *Mater. Today Proc.*, vol. 62, no. P13, pp. 6978–6984, 2022, doi: 10.1016/j.matpr.2021.12.376.

27. A. E. Amobonye, C. E. Aruwa, and S. Pillai, “Biodegradability and current status of polyethylene terephthalate,” *Biodegrad. Conv. Plast. Oppor. Challenges, Misconceptions*, pp. 155–177, 2022, doi: 10.1016/B978-0-323-89858-4.00011-7.
28. R. Prasad, B. Ashok, P. Oinas, and S. Forssell, “Techno-economic evaluation of a biorefinery to produce g- valerolactone (GVL), 2-methyltetrahydrofuran (2-MTHF) and 5- hydroxymethylfurfural (5-HMF) from spruce,” *Renew. Energy*, vol. 190, pp. 396–407, 2022, [Online]. Available: https://doi.org/10.1016/j.renene.2022.03.128
29. G. Gómez Millán *et al.*, “Furfural production in a biphasic system using a carbonaceous solid acid catalyst,” *Appl. Catal. A Gen.*, vol. 585, no. July, 2019, doi: 10.1016/j.apcata.2019.117180.
30. M. G. A. Vieira, M. A. Da Silva, L. O. Dos Santos, and M. M. Beppu, “Natural-based plasticizers and biopolymer films: A review,” *European Polymer Journal*, vol. 47, no. 3. pp. 254–263, Mar. 2011. doi: 10.1016/j.eurpolymj.2010.12.011.
31. J. Byun, D. Kim, D. Lee, H. J. Kim, and J. Han, “Integrated strategy for concurrent production of furfuryl alcohol and glycerol oxygenates,” *J. Ind. Eng. Chem.*, vol. 73, pp. 268–275, 2019, doi: 10.1016/j.jiec.2019.01.038.
32. W. X. Woo *et al.*, “Bio-based succinic acid production from durian husk: A rising Southeast Asia agricultural waste,” *Ind. Crops Prod.*, vol. 206, no. October, 2023, doi: 10.1016/j.indcrop.2023.117624.
33. J. N. da Cunha *et al.*, “Study of furfural derivatives as a possible green corrosion inhibitor for mild steel in CO2-saturated formation water,” *Corros. Sci.*, vol. 212, no. July 2022, 2023, doi: 10.1016/j.corsci.2022.110907.
34. X. Zhang, S. Xu, Q. Li, G. Zhou, and H. Xia, “Recent advances in the conversion of furfural into bio-chemicals through chemo- And bio-catalysis,” *RSC Adv.*, vol. 11, no. 43, pp. 27042–27058, 2021, doi: 10.1039/d1ra04633k.
35. L. Dong *et al.*, “High-solid pretreatment of rice straw at cold temperature using NaOH/Urea for enhanced enzymatic conversion and hydrogen production,” *Bioresour. Technol.*, vol. 287, no. April, 2019, doi: 10.1016/j.biortech.2019.121399.
36. J. Y. Zhu and X. Pan, “Efficient sugar production from plant biomass: Current status, challenges, and future directions,” *Renew. Sustain. Energy Rev.*, vol. 164, no. January, p. 112583, 2022, doi: 10.1016/j.rser.2022.112583.
37. M. S. Pino, R. M. Rodríguez-Jasso, M. Michelin, and H. A. Ruiz, “Enhancement and modeling of enzymatic hydrolysis on cellulose from agave bagasse hydrothermally pretreated in a horizontal bioreactor,” *Carbohydr. Polym.*, vol. 211, no. January, pp. 349–359, 2019, doi: 10.1016/j.carbpol.2019.01.111.
38. M. S. Pino *et al.*, “Bioreactor design for enzymatic hydrolysis of biomass under the biorefinery concept,” *Chem. Eng. J.*, vol. 347, no. March, pp. 119–136, 2018, doi: 10.1016/j.cej.2018.04.057.
39. Shiva, F. Climent Barba, R. M. Rodríguez-Jasso, R. K. Sukumaran, and H. A. Ruiz, “High-solids loading processing for an integrated lignocellulosic biorefinery: Effects of transport phenomena and rheology – A review,” *Bioresour. Technol.*, vol. 351, no. January, 2022, doi: 10.1016/j.biortech.2022.127044.
40. A. A. Modenbach and S. E. Nokes, “Enzymatic hydrolysis of biomass at high-solids loadings - A review,” *Biomass and Bioenergy*, vol. 56, pp. 526–544, 2013, doi: 10.1016/j.biombioe.2013.05.031.
41. Y. Muranaka, K. Matsubara, T. Maki, S. Asano, H. Nakagawa, and K. Mae, “5-

Hydroxymethylfurfural Synthesis from Monosaccharides by a Biphasic Reaction-Extraction System Using a Microreactor and Extractor," *ACS Omega*, vol. 5, no. 16, pp. 9384–9390, 2020, doi: 10.1021/acsomega.0c00399.
42. L. C. Blumenthal *et al.*, "Systematic Identification of Solvents Optimal for the Extraction of 5-Hydroxymethylfurfural from Aqueous Reactive Solutions," *ACS Sustain. Chem. Eng.*, vol. 4, no. 1, pp. 228–235, 2016, doi: 10.1021/acssuschemeng.5b01036.
43. J. N. Chheda, Y. Román-Leshkov, and J. A. Dumesic, "Production of 5-hydroxymethylfurfural and furfural by dehydration of biomass-derived mono- and poly-saccharides," *Green Chem.*, vol. 9, no. 4, pp. 342–35, 2007, doi: 10.1039/b611568c.
44. J. Esteban, A. J. Vorholt, and W. Leitner, "An overview of the biphasic dehydration of sugars to 5-hydroxymethylfurfural and furfural: A rational selection of solvents using COSMO-RS and selection guides," *Green Chem.*, vol. 22, no. 7, pp. 2097–2128, 2020, doi: 10.1039/c9gc04208c.
45. W. Ouyang, A. M. Balu, Z. A. ALOthman, X. Wang, W. Wang, and R. Luque, "Valorisation of humins to high value-added products: Integrating biorefinery process towards a more sustainable future," *Curr. Opin. Green Sustain. Chem.*, vol. 39, 2023, doi: 10.1016/j.cogsc.2022.100717.
46. N. I. Villanueva and T. G. Marzialetti, "Mechanism and kinetic parameters of glucose and fructose dehydration to 5-hydroxymethylfurfural over solid phosphate catalysts in water," *Catal. Today*, vol. 302, no. November 2016, pp. 100–107, 2018, doi: 10.1016/j.cattod.2017.04.049.
47. S. Meier, "Mechanism and malleability of glucose dehydration to HMF: Entry points and water-induced diversions," *Catal. Sci. Technol.*, vol. 10, no. 6, pp. 1724–1730, 2020, doi: 10.1039/c9cy02567g.
48. Y. Kim *et al.*, "Prediction of hydroxymethylfurfural yield in glucose conversion through investigation of lewis acid and organic solvent effects," *ACS Catal.*, vol. 10, no. 24, pp. 14707–14721, 2020, doi: 10.1021/acscatal.0c04245.
49. Z. Xu, Y. Yang, P. Yan, Z. Xia, X. Liu, and Z. C. Zhang, "Mechanistic understanding of humin formation in the conversion of glucose and fructose to 5-hydroxymethylfurfural in [BMIM]Cl ionic liquid," *RSC Adv.*, vol. 10, no. 57, pp. 34732–34737, 2020, doi: 10.1039/d0ra05641c.
50. G. Tsilomelekis, T. R. Josephson, V. Nikolakis, and S. Caratzoulas, "Origin of 5-hydroxymethylfurfural stability in water/dimethyl sulfoxide mixtures," *ChemSusChem*, vol. 7, no. 1, pp. 117–126, 2014, doi: 10.1002/cssc.201300786.
51. J. Granacher, R. Castro-Amoedo, and F. Maréchal, "Leveraging industrial biorefineries for the energy transition," *J. Clean. Prod.*, vol. 434, no. October 2023, 2024, doi: 10.1016/j.jclepro.2023.139795.
52. E. Arnese-Feffin, P. Facco, D. Turati, F. Bezzo, and M. Barolo, "Hybrid modeling of a biorefinery separation process to monitor short-term and long-term membrane fouling," *Chem. Eng. Sci.*, vol. 283, no. October 2023, 2024, doi: 10.1016/j.ces.2023.119413.
53. J. Moncada B, V. Aristizábal M, and C. A. Cardona A, "Design strategies for sustainable biorefineries," *Biochem. Eng. J.*, vol. 116, pp. 122–134, 2016, doi: 10.1016/j.bej.2016.06.009.

54. J. C. Solarte-Toro and C. A. Cardona Alzate, “Biorefineries as the base for accomplishing the sustainable development goals (SDGs) and the transition to bioeconomy: Technical aspects, challenges and perspectives,” *Bioresour. Technol.*, vol. 340, no. May, 2021, doi: 10.1016/j.biortech.2021.125626.
55. F. Cherubini, “The biorefinery concept: Using biomass instead of oil for producing energy and chemicals,” *Energy Convers. Manag.*, vol. 51, no. 7, pp. 1412–1421, 2010, doi: 10.1016/j.enconman.2010.01.015.
56. V. C. Igbokwe, F. N. Ezugworie, C. O. Onwosi, G. O. Aliyu, and C. J. Obi, “Biochemical biorefinery: A low-cost and non-waste concept for promoting sustainable circular bioeconomy,” *J. Environ. Manage.*, vol. 305, no. December 2021, 2022, doi: 10.1016/j.jenvman.2021.114333.
57. K. Pyrgakis and A. Kokossis, “Total Site Integration as a Process Synthesis and Scheduling Tool in Multiple-feedstock Biorefineries,” *Comput. Aided Chem. Eng.*, vol. 40, pp. 1825–1830, 2017, doi: 10.1016/B978-0-444-63965-3.50306-8.
58. Y. Men, X. Du, J. Shen, L. Wang, and Z. Liu, “Preparation of corn starch-g-polystyrene copolymer in ionic liquid: 1-Ethyl-3-methylimidazolium acetate,” *Carbohydr. Polym.*, vol. 121, 2015, doi: 10.1016/j.carbpol.2014.12.068.
59. V. Aristizábal-Marulanda and C. A. Cardona Alzate, “Methods for designing and assessing biorefineries: Review,” *Biofuels, Bioprod. Biorefining*, vol. 13, no. 3, pp. 789–808, 2019, doi: 10.1002/bbb.1961.
60. Z. Chen *et al.*, “Exploitation of lignocellulosic-based biomass biorefinery: A critical review of renewable bioresource, sustainability and economic views,” *Biotechnol. Adv.*, vol. 69, no. October, 2023, doi: 10.1016/j.biotechadv.2023.108265.
61. L. Hu *et al.*, “State-of-the-art advances and perspectives in the separation of biomass-derived 5-hydroxymethylfurfural,” *J. Clean. Prod.*, vol. 276, 2020, doi: 10.1016/j.jclepro.2020.124219.
62. K. Wiranarongkorn, K. Im-orb, J. Panpranot, F. Maréchal, and A. Arpornwichanop, “Exergy and exergoeconomic analyses of sustainable furfural production via reactive distillation,” *Energy*, vol. 226, 2021, doi: 10.1016/j.energy.2021.120339.
63. M. Martín, M. Taifouris, and G. Galán, “Lignocellulosic biorefineries: A multiscale approach for resource exploitation,” *Bioresour. Technol.*, vol. 385, no. May, 2023, doi: 10.1016/j.biortech.2023.129397.
64. R. de F. D. Milão, O. de Q. F. Araújo, and J. L. de Medeiros, “Second Law analysis of large-scale sugarcane-ethanol biorefineries with alternative distillation schemes: Bioenergy carbon capture scenario,” *Renew. Sustain. Energy Rev.*, vol. 135, no. January 2020, 2021, doi: 10.1016/j.rser.2020.110181.
65. A. A. Kiss and R. Smith, “Rethinking energy use in distillation processes for a more sustainable chemical industry,” *Energy*, vol. 203, 2020, doi: 10.1016/j.energy.2020.117788.
66. Q. Zhang, M. Liu, C. Li, and A. Zeng, “Heat-integrated pressure-swing distillation process for separation of the maximum-boiling azeotrope diethylamine and methanol,” *J. Taiwan Inst. Chem. Eng.*, vol. 93, pp. 644–659, 2018, doi: 10.1016/j.jtice.2018.09.018.
67. M. Skiborowski, “Synthesis and design methods for energy-efficient distillation processes,” *Curr. Opin. Chem. Eng.*, vol. 42, 2023, doi: 10.1016/j.coche.2023.100985.

68. N. Aslam and A. K. Sunol, “Computing all the azeotropes in refrigerant mixtures through equations of state,” *Fluid Phase Equilib.*, vol. 224, no. 1, pp. 97–109, 2004, doi: 10.1016/j.fluid.2004.03.014.
69. J. Abildskov and J. P. O’Connell, “Responses of azeotropes and relative volatilities to pressure variations,” *Chem. Eng. Res. Des.*, vol. 99, pp. 97–110, 2015, doi: 10.1016/j.cherd.2015.06.029.
70. T. Gui and H. Yang, “Experimental investigation and modelling of separation behavior for the Bi–Cu–Pb system in vacuum distillation containing one binary azeotrope,” *Vacuum*, vol. 202, no. May, pp. 1–9, 2022, doi: 10.1016/j.vacuum.2022.111169.
71. T. Yang, D. Chen, W. Li, and H. Zhang, “Efficient conversion of corn stover to 5-hydroxymethylfurfural and furfural using a novel acidic resin catalyst in water-1, 4-dioxane system,” *Mol. Catal.*, vol. 515, no. June, 2021, doi: 10.1016/j.mcat.2021.111920.
72. Q. Guo, L. Ren, S. M. Alhassan, and M. Tsapatsis, “Glucose isomerization in dioxane/water with Sn-β catalyst: Improved catalyst stability and use for HMF production,” *Chem. Commun.*, vol. 55, no. 99, pp. 14942–14945, 2019, doi: 10.1039/c9cc07842h.
73. P. Chen, A. Yamaguchi, N. Hiyoshi, and N. Mimura, “Efficient continuous dehydration of fructose to 5-hydroxymethylfurfural in ternary solvent system,” *Fuel*, vol. 334, no. August 2022, pp. 1–9, 2023, doi: 10.1016/j.fuel.2022.126632.
74. Y. He *et al.*, “1,4-Dioxane intervention enables simultaneous valorization of biomass-based C5 and C6 sugars to furfural over Hβ zeolite,” *Chem. Eng. J.*, vol. 480, no. December 2023, p. 148092, 2024, doi: 10.1016/j.cej.2023.148092.
75. M. Kato, H. Konishi, and M. Hirata, “Apparatus for Measurement of Isobaric Dew and Bubble Points and Vapor-Liquid Equilibria Methanol-Water and Water-Dioxane Systems,” *J. Chem. Eng. Data*, vol. 15, no. 4, pp. 501–505, 1970, doi: 10.1021/je60047a022.
76. M. Hichri, “Isobaric vapour–liquid phase diagram and excess properties for the binary system 1,4-dioxane + water at 298.15 K, 318.15 K and 338.15 K,” vol. 52, no. 3, pp. 373–387, 2014.
77. M. Lafranconi *et al.*, “An integrated assessment of the 1,4-dioxane cancer mode of action and threshold response in rodents,” *Regul. Toxicol. Pharmacol.*, vol. 142, no. March, 2023, doi: 10.1016/j.yrtph.2023.105428.
78. M. Lafranconi *et al.*, “A 90-day drinking water study in mice to characterize early events in the cancer mode of action of 1,4-dioxane,” *Regul. Toxicol. Pharmacol.*, vol. 119, no. June 2020, 2021, doi: 10.1016/j.yrtph.2020.104819.
79. F. Turna Demir and E. Demir, “Potential genotoxic and biological effects of 1,4 dioxane on different model organisms,” *Curr. Opin. Environ. Sci. Heal.*, vol. 35, pp. 1–7, 2023, doi: 10.1016/j.coesh.2023.100502.
80. H. Park *et al.*, “Effect of ash in paper sludge on enzymatic hydrolysis,” *Biomass and Bioenergy*, vol. 165, no. June, p. 106567, 2022, doi: 10.1016/j.biombioe.2022.106567.
81. D. Saang’onyo, S. Parkin, and F. T. Ladipo, “Effect of ancillary (aminomethyl)phenolate ligand on efficacy of aluminum-catalyzed glucose dehydration to 5-hydroxymethylfurfural,” *Polyhedron*, vol. 149, pp. 153–162, 2018,

doi: 10.1016/j.poly.2018.03.035.
82. J. B. Sluiter, R. O. Ruiz, C. J. Scarlata, A. D. Sluiter, and D. W. Templeton, “Compositional analysis of lignocellulosic feedstocks. 1. Review and description of methods,” *J. Agric. Food Chem.*, vol. 58, no. 16, pp. 9043–9053, 2010, doi: 10.1021/jf1008023.
83. Z. Lin, J. Wang, V. Nikolakis, and M. Ierapetritou, “Process flowsheet optimization of chemicals production from biomass derived glucose solutions,” *Comput. Chem. Eng.*, vol. 102, pp. 258–267, 2017, doi: 10.1016/j.compchemeng.2016.09.012.
84. T. Tongtummachat, A. Jaree, and N. Akkarawatkhoosith, “Continuous hydrothermal furfural production from xylose in a microreactor with dual-acid catalysts,” *RSC Adv.*, vol. 12, no. 36, pp. 23366–23378, 2022, doi: 10.1039/d2ra03609f.
85. M. A. Kougioumtzis *et al.*, “Production of 5-HMF from Cellulosic Biomass: Experimental Results and Integrated Process Simulation,” *Waste and Biomass Valorization*, vol. 9, no. 12, pp. 2433–2445, 2018, doi: 10.1007/s12649-018-0267-0.
86. F. Gu and Y. Hou, “Salt effects on the isobaric vapor-liquid equilibrium for four binary systems,” *J. Chem. Eng. Data*, vol. 45, no. 3, pp. 467–470, 2000, doi: 10.1021/je990215s.
87. J. Polednová and I. Wichterle, “Vapour-liquid equilibrium in the acetone-water system at 101.325kPa,” *Fluid Phase Equilib.*, vol. 17, pp. 115–121, 1984.
88. M. G. Myles and T. Ab, “Calculating Activity Coefficients How accurate must your data be ? Experimentally reproducible ?,” vol. 53, no. 3, pp. 219–222, 1961.
89. L. C. Nhien, N. V. D. Long, S. Kim, and M. Lee, “Techno-economic assessment of hybrid extraction and distillation processes for furfural production from lignocellulosic biomass,” *Biotechnol. Biofuels*, vol. 10, no. 1, pp. 1–12, 2017, doi: 10.1186/s13068-017-0767-3.
90. Y. Ma, J. Gao, M. Li, Z. Zhu, and Y. Wang, “Isobaric vapour–liquid equilibrium measurements and extractive distillation process for the azeotrope of (N,N-dimethylisopropylamine + acetone),” *J. Chem. Thermodyn.*, vol. 122, pp. 154–161, 2018, doi: 10.1016/j.jct.2018.03.019.

Chapter 5: Acetone removal from furans solution and aldol-condensation reaction of furans in dehydration products from paper sludge hydrolysate over 2-butanone

5.1. Introduction

This study aims to produce sufficient aldol-condensation products using the dehydration materials from paper sludge hydrolysate synthesized at NREL. Aldol-condensation has been utilized in biorefinery studies to enhance the carbon chain length of furan materials resulting from biomass upgrading [1]. In this specific investigation, acetone was employed as a co-solvent to produce 5-HMF and furfural, as per the considerations outlined in previous chapters of this report. To prevent furan materials from condensing onto acetone instead of onto 2-butanone, which could result in shorter carbon chains in the desired final hydrocarbon product after hydrogenation and hydrodeoxygenation treatments, acetone must be completely removed from the aqueous furans solution. Thus, determining the optimal conditions for the aldol-condensation reaction is crucial, considering the goal to obtain approximately 50ml of hydrocarbon blend for fuel evaluation by the end of the project. A brief study was conducted using dehydration products from paper sludge hydrolysate to determine the optimal conditions for the aldol-condensation reaction. The findings were then utilized to scale up the reaction. Sufficient aldol-condensation products were produced and extracted at NCSU and sent to NREL for further hydrogenation and hydrodeoxygenation treatments.

5.2. Large-scale acetone removal by multi-stage continuous distillation at NCSU

Eight liters of distilled furans solutions were obtained at NREL after distilling the solvent (Acetone) used for the dehydration reaction of sugars from Paper Sludge hydrolysate. This material, together with an additional volume of 32 liters of undistilled solution, was sent to NCSU for processing in the distillation setup displayed in **Fig. 5.1.** The distillation system at NCSU was tuned for a defined feed flow rate of 10ml/min of dehydration products solution containing acetone. A total of 53 hours of stable and continuous operation were required to process the material completely. The goal of removing acetone from the furans solution was successfully achieved. Consistently, RP-HPLC results confirmed the absence of acetone in the resulting product obtained at the reboiler of the distillation system.

Certain difficulties were found during the distillation process. Due to the precipitation of humins (carbon-based macromolecular substances), the distillation system had to be shut down every 4 to 6 hours to proceed with column cleaning (**Fig. 5.2**). This, considering that the feed stage to the distillation column was predetermined at Equilibrium Stage #7 (top to bottom), following simulation results (Optimal feed stage: Stage #7 - Aspen Plus™) and the configuration of commercially available glassware [Condenser + 6 Equilibrium Stages glassware column]. The occurrence of “fouling” on the lower stages of the distillation column during the scaling-up process is relevant for industrial features, where equipment downtime is of concern. The relocation of the feed stage directly to the reboiler could be suitable for the studied arrangement. Moreover, an increase in the overall heat demand is expected.

Fig. 5.1. In-house-built multi-stage continuous distillation setup for dehydration co-solvent recovery at NCSU.

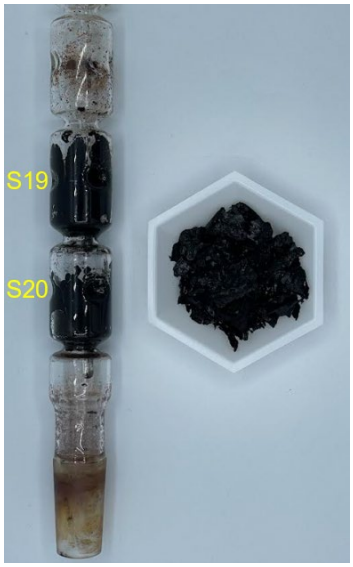

Fig. 5.2. Collected carbon-based material at Stages S19 & S20 of the in-house-built multi-stage continuous distillation setup (Right above the Reboiler or S21).

5.3. Identification of aldol-condensation products

Determining a valid method for clear product identification is required to define optimal conditions for the aldol-condensation reaction (**Fig. 5.3**). RP-HPLC was used for this task after NREL's previous experience with aldol-condensation products analysis (**Table 5.1.**). Purchased 5-HMF, furfural & 2-butanone were used for this series of experiments.

Sample 7083-93-94#8-D (Furans solution from paper sludge hydrolysate after distillation) was used as a reference to be compared with separate 5-HMF and furfural aqueous solutions (31.45g/L of purchased furan) for the individual analysis of condensation products. (**Table 5.2**). All experiments were run in triplicate using a water bath reactor equipped with a temperature control (**Fig. 5.4**). The initial set of reaction conditions used

included: 10ml vials containing 5ml of initial furan solution, a correspondent volume of 5Molar NaOH solution for an initial target pH of 13.0, 80°C, and a reaction time of 60 minutes. After the reaction period, samples were quenched using an ice bath and then neutralized using a 5Molar H_2SO_4 solution to approximate neutral pH (**Table 5.2**).

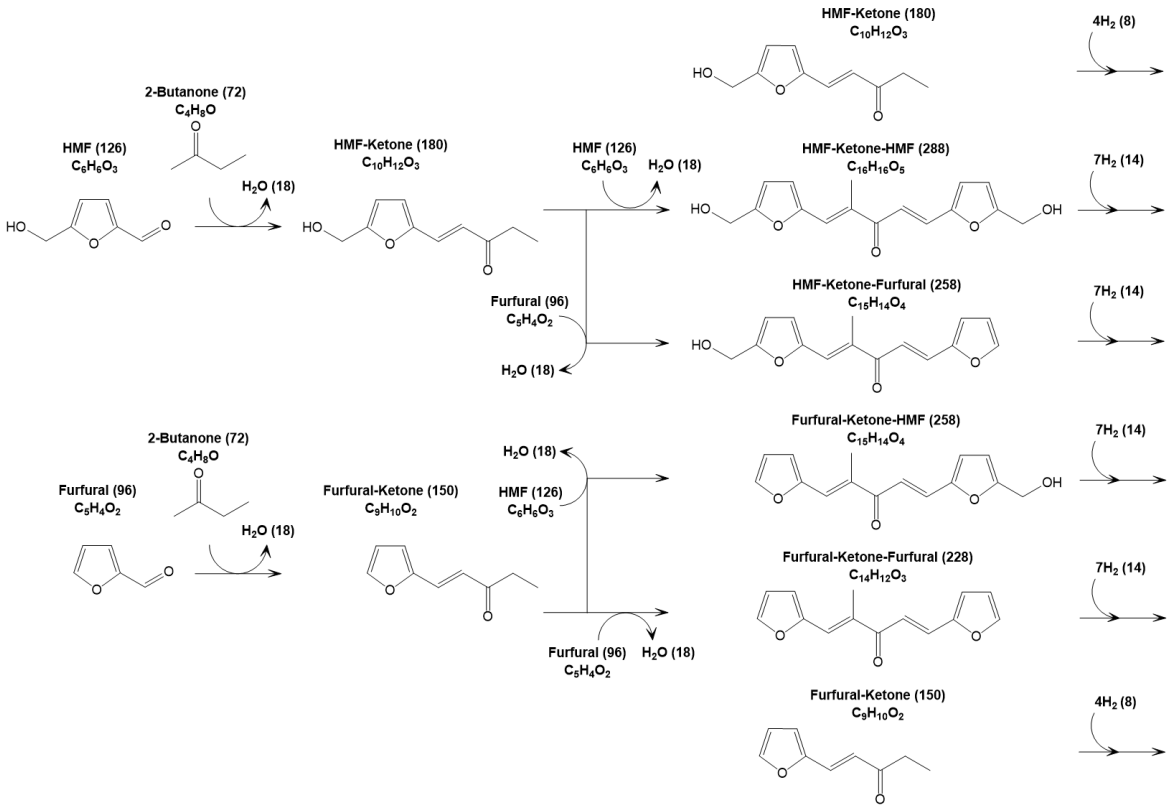

Fig. 5.3. Theoretical aldol-condensation products from the condensation of 5-HMF and furfural over 2-butanone.

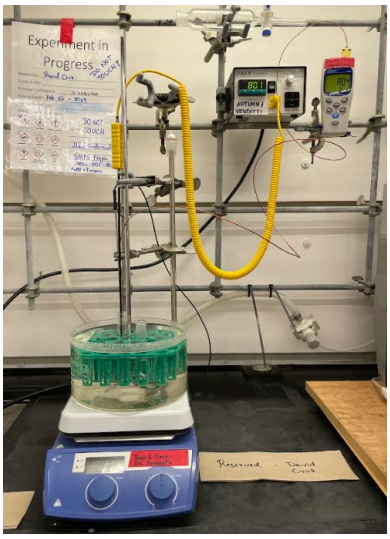

Fig. 5.4. Water bath reactor with temperature controller for local optimal aldol-condensation reactions conditions at NCSU.

Table 5.1. RP-HPLC Analysis method used for the identification of aldol-condensation products.

HPLC	Agilent 1220 (Agilent, Santa Clara, CA)
Analytical Liquid Chromatography Column	InfinityLab Poroshell 120 EC-C18 4.6mm x 100mm & 2.7µm [max. 400bar & pH 2.0-9.0] (@ 40ºC)
Detector	VWD (50ºC)
VWD Spectra	325nm (Optimized value for 5-HMF/MEK condensation products)
Mobile phase	Gradient mode: t0min: A=95% H_3PO_4 0.019M (pH 2.05) & B=5% Acetonitrile t10min: B=100% t20min: B=100% t21min: B=5% t30min: B=5
Sample volume	1.0µL (No Temperature control)
Stop time	30min (95% A & 5%B)
Post time	4min (95% A & 5%B)

Table 5.2. Furan solutions for aldol-condensation products identification and required soda and acid solution for pH targets using a starting volume of 5ml furans solution.

Sample	5-HMF & Furfural (g/L)	*NaOH (5M) volume (µl)	*Target & Measured pH	**H_2SO_4 (5M) volume (µl)	Measured pH (Neutralization)
7083-93-94#8-D	31.45g/L 5-HMF 2.03g/L Furfural	1,200	~13.0	310	9.5 - 8.0
5-HMF	31.45g/L 5-HMF	210	~13.0	100	10.5 - 9.5
Furfural	31.45g/L furfural	160	~13.0	70	7.4 - 6.9

*Volume of 5Molar NaOH solution to achieve the target pH 13.0 for aldol-condensation reaction.
**Volume of 5Molar H_2SO_4 solution to neutralize the resulting aldol-condensation products before RP-HPLC analysis.

5.3.1. 5-HMF & furfural identification

An aqueous solution containing 31.45g/L of 5-HMF and a second solution containing 31.45g/L of furfural were prepared and analyzed individually using RP-HPLC (**Table 5.1**). The corresponding peaks are displayed in the chromatogram (**Fig. 5.5**) at elution times 2.73min (5-HMF) and 3.34min (furfural). Solutions of MEK and Acetone were also analyzed, and no peaks were detected at the wavelength used for this analysis (325nm).

5.3.2. HMF-MEK monoadducts & HMF-MEK-HMF diadduct

As can be inferred from **Fig. 5.3**, one molecule of 5-HMF can condense on the primary or the secondary carbon next to the carbonyl structure of 2-butanone (MEK). The resulting abundance of the two possible mono adducts (HMF-MEK) is expected to depend on the product's stability (kinetic and thermodynamic) under the experimental conditions. At the same time, a second molecule of 5-HMF can condense over the same molecule of MEK on the second available position, forming the corresponding diadduct (HMF-MEK-HMF). Two different molar ratios of 5-HMF to MEK (1 to 2 & 1 to 0.5) were tested for this

experiment. This is to evaluate and compare the results of one scenario having twice the amount of MEK compared to the available 5-HMF molecules (higher likelihood to produce mono adducts) versus having half of MEK molecules compared to the available 5-HMF molecules (higher likelihood to produce diadduct). An aqueous solution containing 31.45g/L of purchase 5-HMF was used to perform this experiment (**Table 5.2**). In **Fig. 5.5**, it can be observed how, when using a molar ratio of 1 to 2 (Blue signal), three prominent peaks appeared on the chromatogram (5.11min, 5.26min & 5.77min). Then, using a molar ratio of 1 to 0.5 (Red signal), two predominant peaks appeared on the chromatogram (5.11min & 5.77). From these results, by reducing the available MEK, the peak at 5.77min increased, which could indicate that this peak corresponds to the diadduct HMF-MEK-HMF. At the same time, when reducing the available MEK, both peaks at 5.11min and 5.26min were reduced, which could indicate that those correspond to the two possible mono adducts HMF-MEK.

Doubts emerged regarding the chemical nature of substances associated with peaks eluding at 5.11min & 5.26min for the described system RP-HPLC Agilent 1220 (**Table 5.1**.). For this reason, a sample containing aldol-condensation products (Reaction conditions: 70°C & 10min) was analyzed using RP-HPLC Agilent 1260 with Diode Arride Detector (DAD) and the same column and conditions referred to in **Table 5.1**. Due to the new geometry of the system (Distance from the sample port to the detector), the elution time was shifted to 6.12min and 6.27min (HMF-MEK mono adducts). As it can be observed on the UV-visible spectra (**Fig. 5.10**), it could be concluded that the nature of the materials eluding at these specific elution times is potentially similar to each other and, at the same time, different from the chemical nature of the material eluding at 6.64min (HMF-MEK-HMF diadduct). Furthermore, when analyzing the same results reported in **Fig. 5.10**. and as it will be discussed later, the chemical nature of materials eluding at 7.76min and 7.82min (F-MEK mono adducts) could also be similar to each other.

Further Hydrodeoxygenation (HDO) experiment and GCMS chromatograms performed at NREL (**Fig. 5.6** & **Fig. 5.7**) suggest that the peak appearing at 5.11min corresponds to the more stable monoadduct where 5-HMF condensed at the primary carbon, which after the HDO would lead to the formation of Decane (straight-chain paraffin). At the same time, the peak appearing at 5.26min is presumed to correspond to a more unstable monoadduct where 5-HMF condensed at the secondary carbon, which after the HDO would lead to the formation of 3-Methyl nonane (branched-chain paraffin). Additional details for this hypothesis will be discussed later in this report (Optimal reaction conditions for aldol-condensation reaction).

Note: The components associated with peaks at 5.57min, 5.91min, 6.11, and 6.28 (**Fig. 5.5**) for the system using a 5-HMF to MEK molar ratio of 1 to 2 (Blue signal) are still undetermined. A solution containing purchased 5-HMF only (31.45g/L) and no MEK and another sample containing only MEK were subjected individually to the aldol-condensation reaction conditions (pH 13.0; 80°C & 60min). No relevant peaks were observed in either experiment (**Fig. 5.8** – Blue and Green signals, respectively).

5.3.3. F-MEK monoadducts & F-MEK-F diadduct

As can be inferred from **Fig. 5.3**, one molecule of furfural can condense on the primary or the secondary carbon next to the carbonyl structure of 2-butanone (MEK). The resulting abundance of each of the two possible mono adducts (furfural-MEK) is expected to depend on the product's stability (kinetic and thermodynamic) under the experimental conditions. At the same time, a second molecule of furfural can condense over the same molecule of MEK on the second available position, forming the corresponding and only possible diadduct (F-MEK-F). Two different molar ratios of furfural to MEK (1 to 2 & 1 to 0.5) were tested for this experiment. This is to evaluate and compare the results of one scenario having twice the amount of MEK compared to the available furfural molecules (higher likelihood to produce mono adducts) versus having half of MEK molecules compared to the available furfural molecules (higher likelihood to produce diadduct). An aqueous solution containing 31.45g/L of purchase furfural was used to perform this experiment (**Table 5.2**). In **Fig. 5.5**, it can be observed how, when using a molar ratio of 1 furfural to 2 MEK (Green signal), three prominent peaks appeared on the chromatogram (6.90min, 6.97min & 8.72min). Then, using a molar ratio of 1 to 0.5 (Magenta signal), several predominant peaks appeared on the chromatogram including the same peaks at (6.90min, 6.97 & 8.72). From these results, by reducing the available MEK, the peak at 8.72min increased, which could indicate that this peak corresponds to the diadduct F-MEK-F. At the same time, when reducing the available MEK, both peaks at 6.90min and 6.97min were reduced, which could indicate that those correspond to the two possible mono adducts F-MEK.

As observed in **Fig. 5.5**, the area below the curve (material abundancy) for the estimated F-MEK monoadducts is similar in both cases (furfural to MEK: 1 to 2 & 1 to 0.5), which potentially means that the instability (kinetic and thermodynamic) of those monoadducts are much similar in comparison to the 5-HMF-MEK monoadducts (as it was previously discussed).

Another relevant finding relates to the appearance of two peaks at 4.19min & 4.61min (**Fig. 5.5**) for the system using a furfural to MEK molar ratio of 1 to 0.5 (Magenta signal). Considering that those peaks appeared only for the system containing furfural and low loading of MEK, a sample containing purchased furfural only (31.45g/L) and no MEK was subjected to the aldol-condensation reaction conditions (pH 13.0; 80°C & 60min). As shown in **Fig. 5.8** (Red signal), two peaks appeared at the expected elution times. This result suggests that the materials associated with the peaks on the chromatogram are correlated with the presence of furfural only. A side reaction seems to occur over furfural under the reaction conditions investigated.

5.3.4. HMF-MEK-F diadducts (heterogeneous diadducts)

In contrast and additionally to the HMF-MEK-HMF and F-MEK-F diadducts. Two heterogeneous condensation products can theoretically be obtained with 5-HMF, furfural & MEK in the reaction media (**Fig. 5.3**). This depends on the furan condensing on the secondary carbon next to the carbonyl group of the MEK. If 5-HMF is condensing on the secondary carbon, and after the HDO reaction, the production of 7-methyltetradecane

could be expected. On the other hand, if furfural condenses on the secondary carbon, and similarly after the HDO reaction, the production of 6-methyl tetradecane is expected.

This experiment utilized 2.5ml of purchased 5-HMF aqueous solution and 2.5ml of purchased furfural. A total furan to MEK ratio of 1 to 0.5 was used to produce heterogeneous diadducts HMF-MEK-F; the results are presented in **Fig. 5.9**. (Blue signal). Considering the previously discussed result, the peaks appearing at 7.06min & 7.15min are presumed to correspond to the heterogeneous diadducts HMF-MEK-F. In the same **Fig. 5.9**, the resulting chromatograms for the aldol-condensation products from furans solution 7083-93-94#8-D (**Table 5.2**) are presented. The presence of HMF-MEK monoadducts (5.11min & 5.26min), and F-MEK monoadduct (6.90min) is clear.

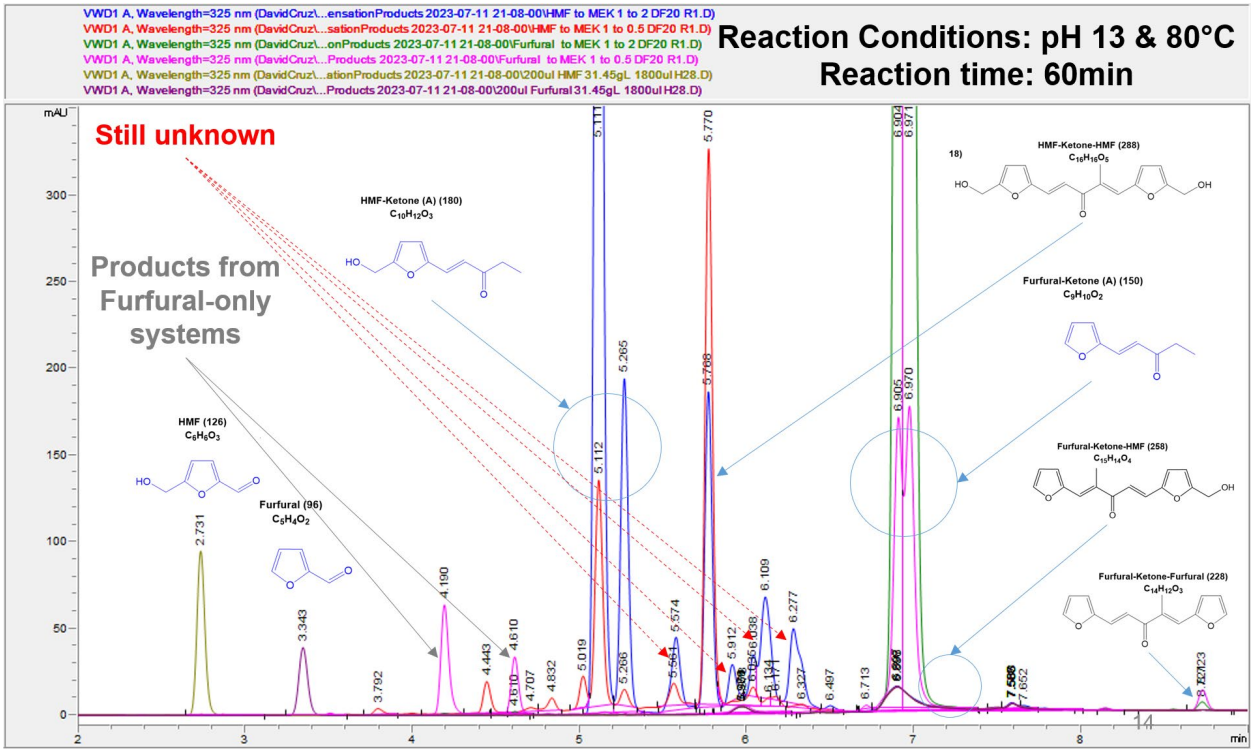

Fig. 5.5. Chromatogram containing peaks for identified aldol condensation products and others.

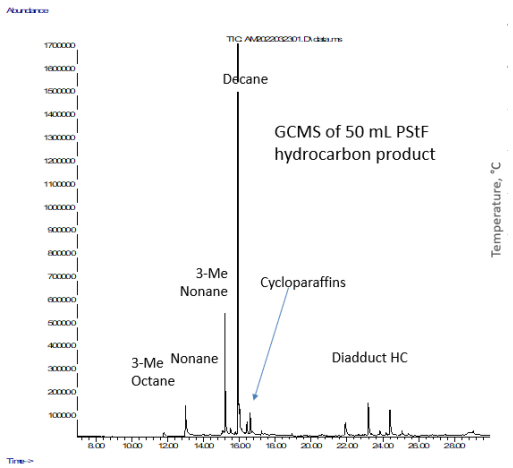

Fig. 5.6. GCMS of hydrocarbon products from PStF hydrolysate using 1,4-dioxane as co-solvent for the dehydration reaction of sugars – Credits to David Johnson (NREL).

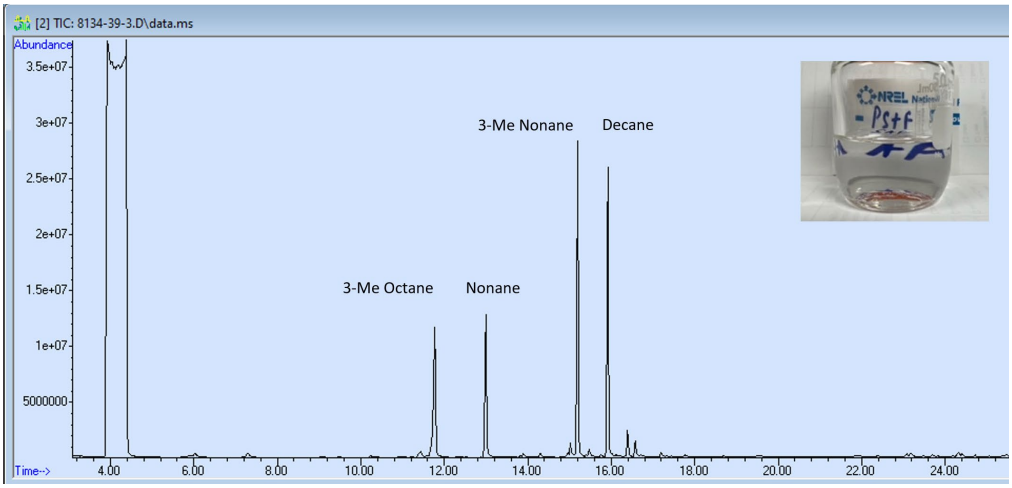

Fig. 5.7. GCMS of hydrocarbon products from PStF hydrolysate using acetone as co-solvent for the dehydration reaction of sugars – Credits to Dr. Ashutosh Mittal (NREL).

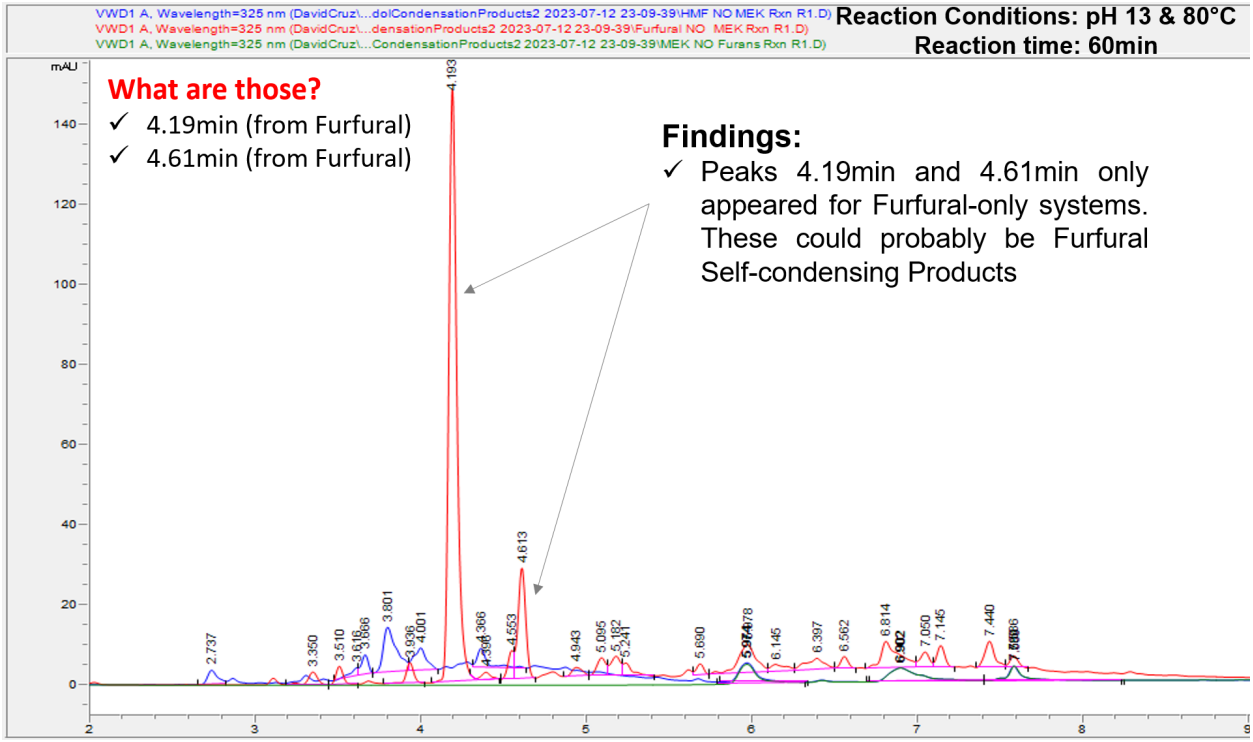

Fig. 5.8. Chromatogram: 5-HMF, furfural and MEK solutions individually subjected to reaction conditions.

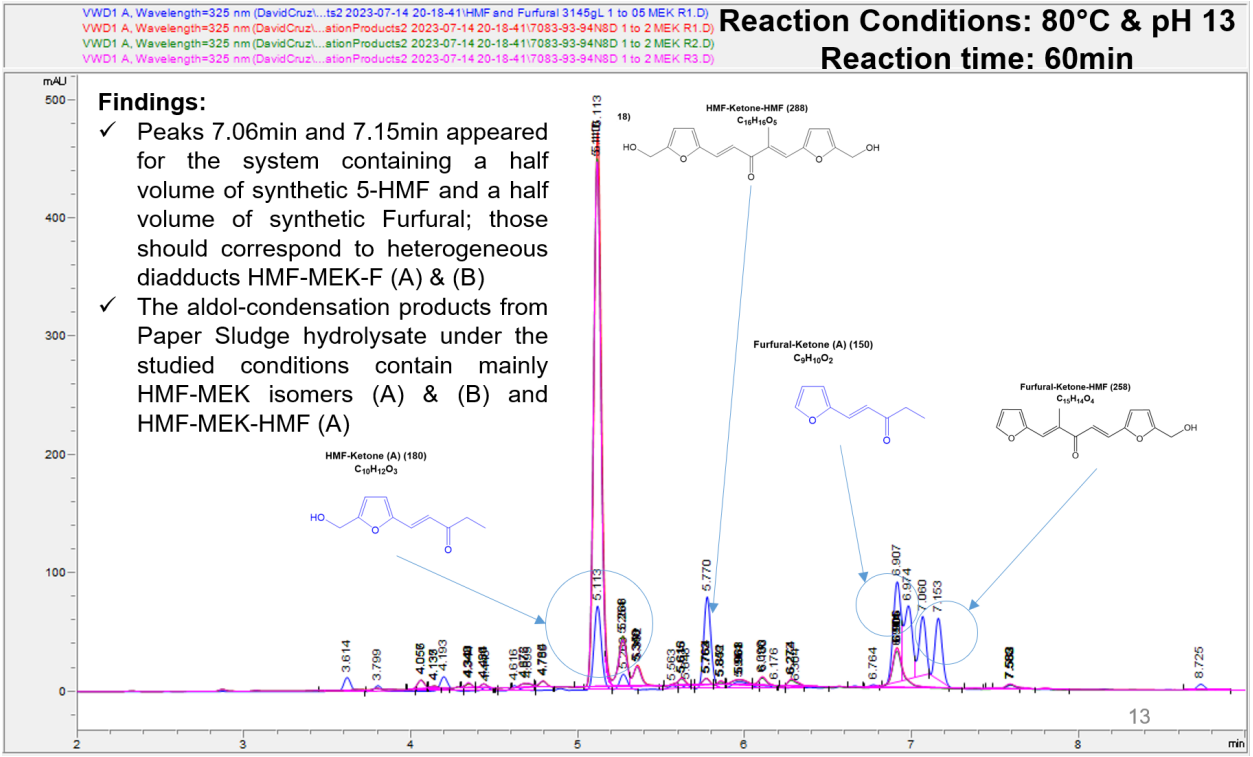

Fig. 5.9. Chromatogram: heterogeneous diadducts & aldol-condensation products from furans solution from paper sludge hydrolysate.

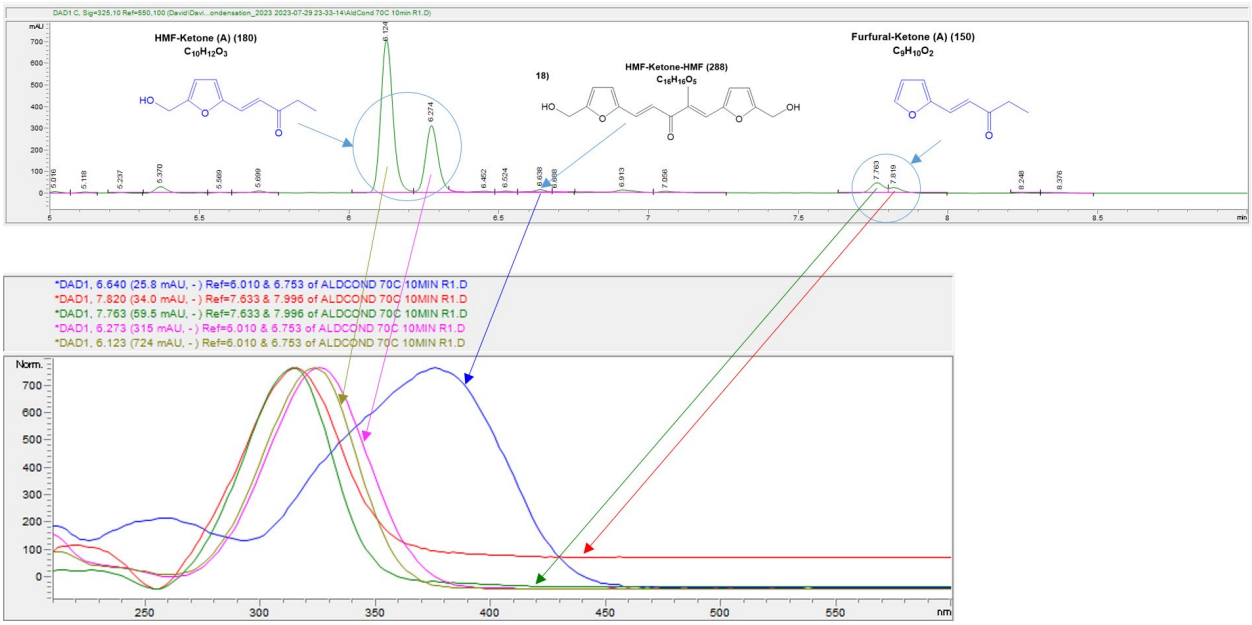

Fig. 5.10. UV-Visible Spectra for relevant peaks: confirming the presumed similarity in chemical nature of monoadducts.

5.4. Brief study to identify local optimal conditions for aldol-condensation reaction (Using furans solution from paper sludge hydrolysate)

Since the studied aldol condensation products are not commercially available, quantifying the reaction results through precise analytical methods (e.g., RP-HPLC, etc.) was not possible. Considering the limited volume of furans solution, a brief study to determine local optimal aldol-condensation reaction conditions was performed based on the maximization of the total area of the previously investigated products of interest.

5.4.1. Experimental parameters to identify local optimal aldol-condensation conditions

Sample 7083-93-94#8-D (Furans solution from paper sludge hydrolysate after distillation) was used for the optimization experiments. All experiments were run by duplicate using a water bath reactor equipped with temperature control (**Fig. 5.4**), 10ml vials containing 5ml of initial aqueous dehydration products solution, a furans to MEK ratio of 1 to 2 (244µL of MEK added to each vial) targeting the production of mono adducts, 1.2ml of 5Molar NaOH solution for an initial target pH of 13.0. Different temperatures ranging from room temperature (23.5°C) to 80°C and a reaction time ranging from 10min to 80min were selected for the experimental work. After the reaction period, samples were quenched using an ice bath and then neutralized by adding 310µL of 5Molar H_2SO_4 solution to approximate neutral pH. Finally, 3ml of 1,4-Dioxane was added to each neutralized sample to homogenize the aldol-condensation products and avoid underestimation due to phase separation.

5.4.2. Local optimal aldol-condensation conditions

The area of relevant peaks (mono and diadducts from aldol-condensation products) was used as the comparison reference to evaluate and determine local optimal conditions.

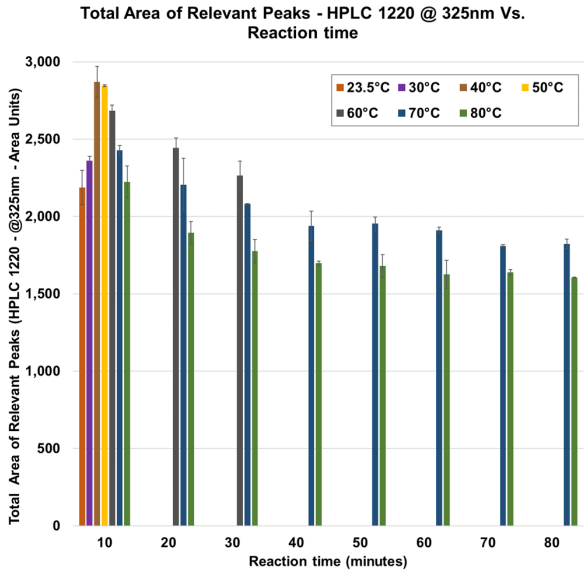

Fig. 5.11. Total area of relevant peaks: Total area of monoadducts and diadducts resulting from the aldol-condensation of furans from paper sludge hydrolysate and MEK [HPLC Agilent 1220 - WVD @325nm].

From the results presented in **Fig. 5.11**, it can be concluded that there is a "Maximum area region" occurring for reactions at 40ºC and 50ºC, both at 10min reaction time. The Total area of relevant peaks reduces when the reaction time is increased for reactions occurring at 60ºC, 70ºC & 80ºC (Baseline: 10min). Additionally, increasing the reaction temperature from 60°C to 80°C negatively impacts the total integrated area of the relevant peaks.

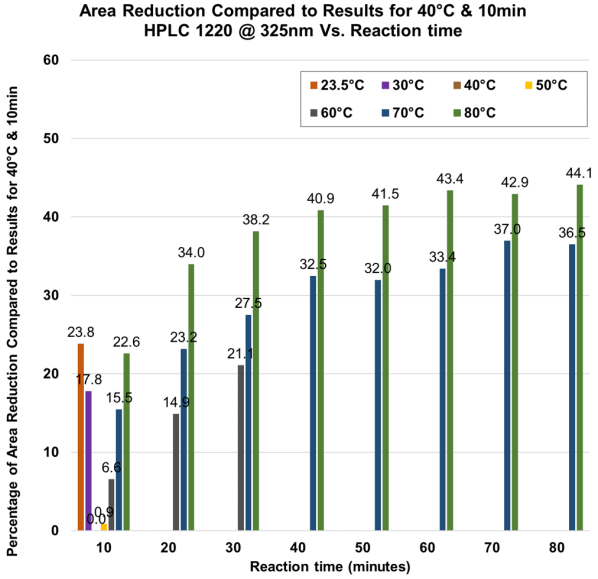

Fig. 5.12. Percentage of area reduction calculated based on the results for aldol-condensation experiments at 40°C & 10min reaction time.

From the results presented in **Fig. 5.12**, it can be concluded that the reduction of the total area of relevant peaks is accelerated by increasing the reaction temperature and the reaction time. Also, when considering the initially defined parameters for the aldol-condensation experiments based on NREL's experience (80°C & 60min), the reduction of the total area is expected to be around 43% compared to the results for the experiments at 40°C & 10min (Highest total area achieved). Finally, running the reaction below 40°C is expected to negatively impact the total area of desired materials.

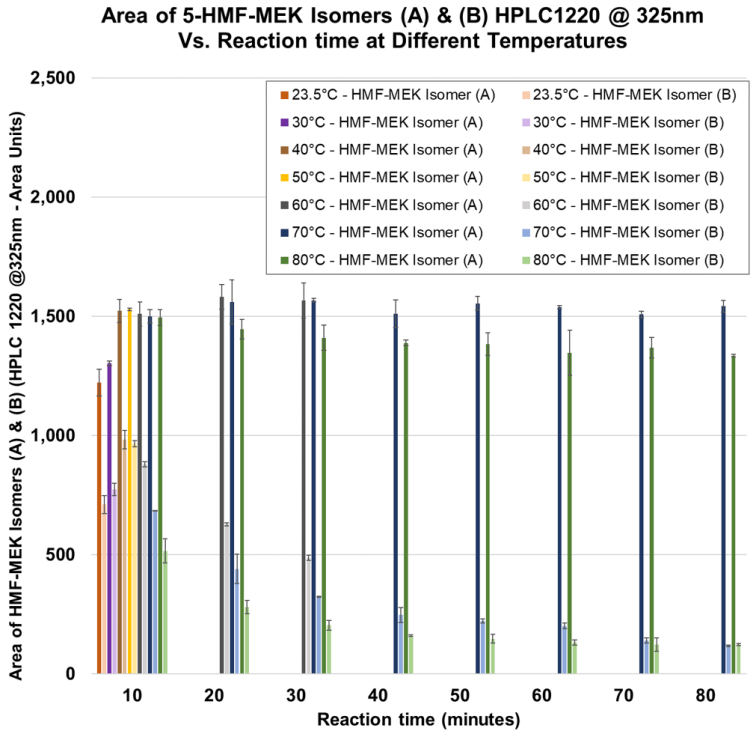

Fig. 5.13. Advance of the area of the peaks on the RP-HPLC chromatogram for the presumed isomers HMF-MEK with changes in reaction conditions.

The advance of the area of the peaks associated with the presumed 5-HMF-MEK isomer mono adducts is presented in **Fig. 5.13**. The displayed results suggest that the reduction in the total area of the relevant peaks seems to be mostly associated with a reduction in the area of the presumed HMF-MEK Isomer (B) [5-HMF condensing on the secondary carbon, next to the carbonyl group of the MEK – Branched isomer]. Also, the HMF-MEK Isomer (A) seems to be thermally stable for experiments up to 70°C compared to experiments at 80ºC. Finally, For the experiment run at 40ºC and 10min, the HMF-MEK Isomer (B) area achieved the maximum value measured. The same occurred with Isomer (A), moreover, the deviation of the duplicate results is higher than the one for experiments at 50ºC and 10min. For this reason and considering the dead-volume and temperature gradients occurring in large-scale experiments, the latest conditions were selected to process the furans solution.

5.5. Scaled-up aldol-condensation experiments using a 5L batch reactor & production of materials for further conversion into hydrocarbon product

5.5.1. Experimental design for the scaled-up aldol-condensation experiments

A 5L reactor with an overhead stirrer was used for the big-scale aldol-condensation reaction experiments. A total of 13L of aqueous furans solution (24.41g/L 5-HMF and 1.44g/L furfural) were reacted in five different batches (2L+3L+3L+3L+2L). Enough MEK was added to each reaction batch to achieve a furans to MEK molar ratio of 1 to 2 in aiming to maximize the production of mono adducts (~31.38g of MEK at 99.5%wt. purity per each 1L of initial furans aqueous solution). The MEK was first added to the furans solution and the mixture heated up to 50°C. Enough 5Molar NaOH solution for a pH target of 13.0 (240ml per each 1L of initial furans aqueous solution) was separately heated up to 50°C and then added to the furan solution containing MEK and kept also at 50°C at time t=0 (zero). An average maximum increase in temperature due to the dissolution heat released after adding the NaOH solution of 6-7°C was recorded for each experiment. Following the local optimal values for the aldol condensation, the reaction media was left under agitation (400RPM) for 10 minutes. After this time, the reactor was placed inside an ice bath to stop the reaction. Enough 5Molar H_2SO_4 solution was added once the reaction media temperature was below 40°C until approximately neutral pH: 6.5 – 7.5 (76ml of 5M acid solution per each 1L of initial furans aqueous solution). The addition of acid solution resulted in the precipitation of a viscous material that was collected at the bottom of the 5L reactor and kept in a separate container after removing the aqueous material inside the reactor. After removing the aqueous fraction from the 5L reactor, this material was equally split into three 2L separation funnels. 100ml of 5-pentanone was added to each separation funnel containing the aqueous fraction from the aldol-condensation products. Each funnel was carefully agitated three times to promote the extraction of organic materials from the aqueous phase to the organic phase (2-pentanone). The aqueous phase was then removed. The organic phase remaining inside the separation funnel was back extracted by adding 100ml of DI water. After backextracting the aqueous phase was collected and preserved. The organic phase was removed, and 12g of $MgSO_4$ (hygroscopic material) was added to remove water that potentially migrated to the organic phase. This step is key for avoiding the presence of water during the HDO, which could deactivate the solid catalyst used for this high-temperature reaction. The organic phase with magnesium sulfate was left sitting for at least one hour before filtrating to remove the hydrated solid material. After removing the precipitated solids, the organic phase was finally preserved for further evaporation (2-pentanone removal). The aqueous phase removed at the end of step #6 was treated following step #7 three more times. From Fig. S5.1 it can be concluded that four total organic extractions are enough to remove the aldol condensation present in the aqueous material left after performing the aldol-condensation reaction. Steps #2 to #8 were performed for each batch of material mentioned in Step #1. All organic extracts from extraction #1 in all five experiments were mixed (**Fig. 5.14** – Organic-rich layer). Organic-rich layers #1 to #4 were evaporated using a Rotary Evaporator and the aldol-condensation materials were collected individually (**Fig. 5.14**). A total mass of 124g (**Fig. 5.14j**) of aldol-condensation products was collected.

5.5.2. Processing of precipitated sludge after aldol-condensation reaction

It was presumed that a portion of the aldol-condensation products were still present in the viscous precipitated material collected in the bottom of the 5L reactor after removing the aqueous materials at each batch. For this reason, the total 570g of "sludge" collected was mixed with 2L of recycled 2-pentanone and shakenfor 24 hours at 80RPM in an orbital shaker. The resulting organic phase was filtered to remove undissolved solid materials. The approximately 2L of the organic phase was split into two 2L separation funnels and backextracted using 1L of DI water added to each separation device. The back extraction was performed twice. RP-HPLC was used to evaluate the presence of aldol-condensation products (Fig. S5.2). Similarly to Step #7, magnesium sulfate was added to the organic phase to remove water from the organic phase. Then filtered, then evaporated. An additional 94g of aldol-condensation products were collected (**Fig. 5.14l**). The aldol condensation products were sent to NREL for further hydrogenation and hydrodeoxygenation treatment.

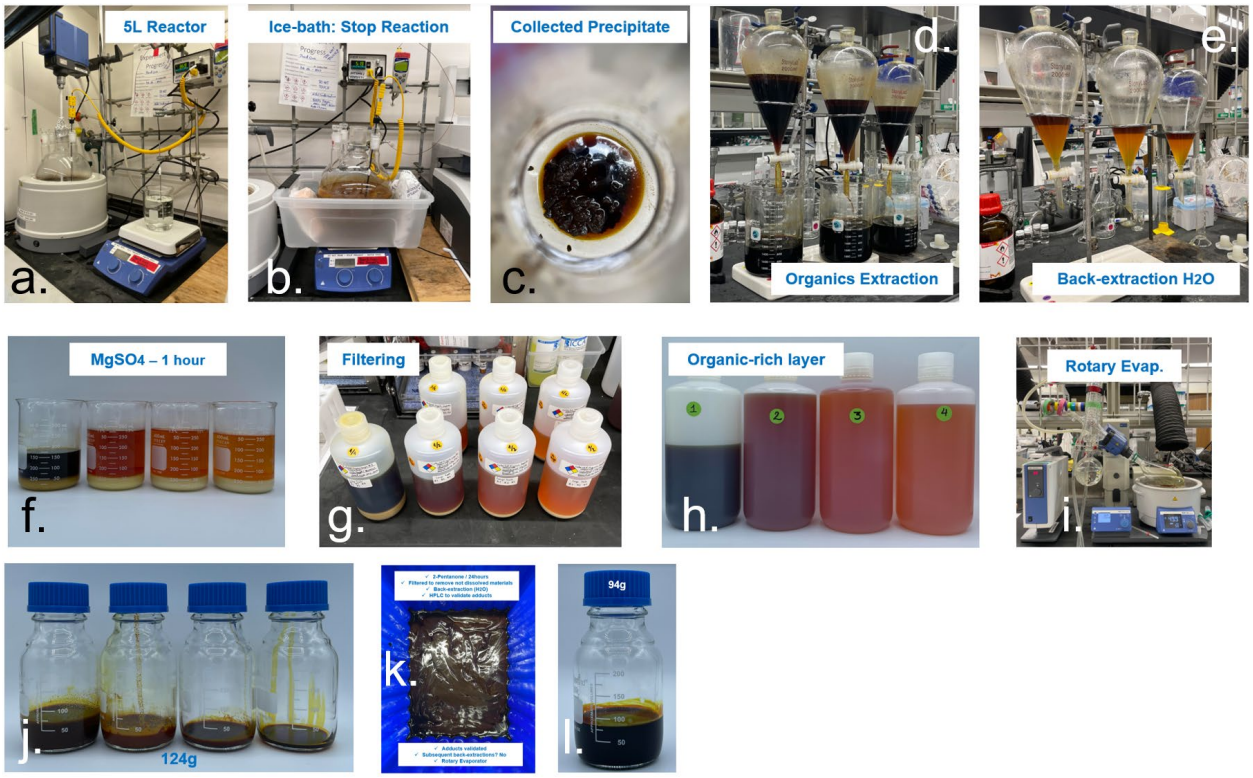

Fig. 5.14. Big-scale aldol-condensation reaction experiments: (a) 5L reactor with overhead stirrer. (b) Ice-bath to stop the reaction. (c) Precipitated sludge left after neutralization of the reaction volume. (d) Organic liquid-liquid extraction using 2-pentanone. (e) Back extraction using DI water. (f) Water removal from organic layer collected during extractions 1 to 4 using $MgSO_4$. (g) Collected organic layers before $MgSO_4$ filtration. (h) Filtrated organic layer from extractions 1 to 4. (i) Rotary evaporator for 2-pentanone removal. (j) Aldol-condensation products collected after 2-pentanone removal. (k) Collected precipitated sludge before 2-pentanone extraction. (l) Additional aldol-condensation products extracted from precipitated sludge.

5.6. Conclusions

The multi-stage continuous distillation system used for this work successfully removed all acetone from the furans solution resulting from the dehydration of paper sludge hydrolysate. Achieving complete acetone removal is crucial to prevent furans from condensing onto acetone instead of onto 2-butanone. The presence of acetone could lead to the formation of aldol-condensation products with one less carbon, which would negatively affect the carbon chain length required in the final product after subsequent hydrogenation and hydrodeoxygenation treatments. Enough aldol-condensation products were obtained at NCSU to proceed with the hydrogenation and hydrodeoxygenation at NREL to generate approximately 50ml of hydrocarbon blend required for further fuel property evaluation.

References

1. Bruno Klein, Ian McNamara, Ryan Davis, Ashutosh Mittal, and David Johnson (2021). Techno-economic assessment for the production of hydrocarbon fuels via catalytic upgrading of furans. NREL/TP-5100-80652.

Chapter 6: Hydrodeoxygenation (HDO) of aldol adducts and fuel property testing of hydrocarbons from aldol adducts obtained from PStF hydrolysates

6.1. Introduction

The purpose of this work is to verify that furfural mixtures made from paper sludge hydrolysates can be converted into HCs, which could be blended in jet or diesel fuel. This was accomplished by converting hydrolysates received from Dr Park's group at NCSU into furfurals at NREL followed by performing aldol condensations of the furfurals with methyl ethyl ketone (MEK) at NCSU and HDO at NREL. The condensations were performed on a sufficiently large scale so that the intermediate material could be used to generate approximately 50 mL of HCs that would be sufficient for fuel property evaluation. Based on BETO's increased interest in developing routes to sustainable aviation fuel (SAF) the condensation reactions were performed under conditions that would favor monoadduct over diadduct formation by increasing the molar ratio of MEK to furfurals. The aldol condensation product was then hydrogenated at a low temperature (100°C) to stabilize the intermediates before hydrodeoxygenation (HDO) at a higher temperature (300°C) using a catalyst with acidic support to generate the HC. The HC product was then subjected to fuel property analyses by the Fuel Performance Group at NREL.

6.2. Hydrogenation of aldol condensation product

After the aldol condensation reaction, the isolated aldol condensation products were then hydrogenated under mild conditions to stabilize the products before being subjected to the more severe conditions necessary for HDO. The hydrogenation was performed in 75 mL stirred Parr batch reactors at 100°C for 2 h with 68 bar of H_2 and Pd/C catalyst (about 7.4 g product/g catalyst). The purpose of this reaction was to hydrogenate the C-C double bonds in the furan rings and the side chain of the adducts. The reaction consumed about 0.28±0.02 g H_2 per g of adduct with most of the H_2 consumed during the heat up of the reactors. The isolated yield of the hydrogenated adduct (H-adduct) from 3 reactions was 95.7±4.4 wt%. ^{13}C NMR

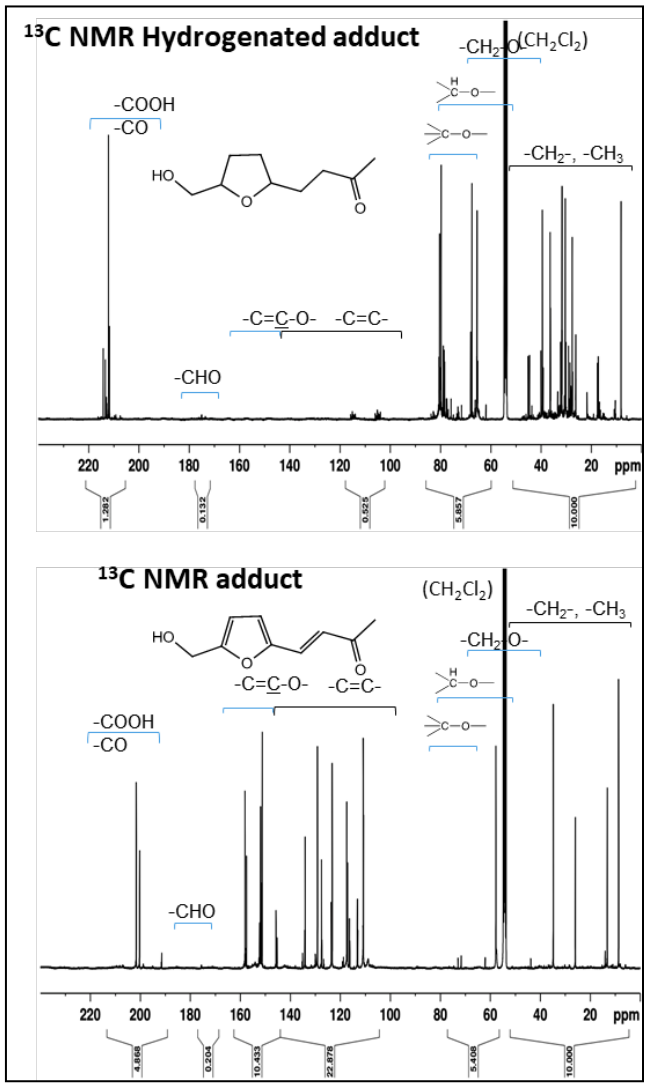

Figure 6.1. ^{13}C NMR of adduct mixture before and after hydrogenation.

(**Figure 6.1**) clearly showed the effect of hydrogenating the aldol condensation product with the disappearance of almost all peaks in the 100 to 160 ppm region, due to unsaturated carbons, with a resulting increase in peaks in the 0 to 90 ppm region because of their conversion to saturated carbons. The spectra also showed that the carbonyls in the adducts were not hydrogenated as shown by retention of the peaks in the 200 to 220 ppm region. RPHPLC GCMS and LCMS analyses of the products confirmed that the C-C double bonds were successfully hydrogenated. CH analysis found that the H/C ratio of the H-adduct increased from 1.26 to 1.73. Hydrogenation of the condensation product made from pure sugars performed very similarly to that made from paper sludge. The amount of H_2 consumed was 0.29 g per g of adduct and the yield of isolated H-adduct was 96.5 wt%. Analyses of the H-adduct showed that it was very similar as well, and CH analysis found that the H/C ratio had increased from 1.23 to 1.69.

6.3. HDO of hydrogenated aldol condensation product

HDO was then performed on the H-adducts in the stirred Parr batch reactors at 300°C for 3 h with 68 bar of H_2 and either a Pd or Pt catalyst on a SiO_2-Al_2O_3 support. The catalyst had 5 wt% of the metal and was made in-house by impregnation of the SiO_2-Al_2O_3 support, which contained 13% Al_2O_3 (W R Grace Davicat 3115). HDO experiments were conducted to examine the effect of using the different metal catalysts and the loading of the H-adduct in the reactors. Overall, the products were successfully converted into the expected HCs (**Figure 6.2**, **Table 6.1**), n-decane, 3-methyl nonane, n-nonane and 3-methyl octane (C8-C10 HC), which are derived from the monoadducts, plus small amounts of hydrocarbons such as 6-methyl tridecane and 7-methyl pentadecane (C13-C16 HC), which are derived from the diadducts. In addition, there were small amounts of cycloalkanes identified in the hydrocarbon product by GCMS, such as ethyl cyclohexane, butyl cyclohexane, and methyl propyl cyclohexane. It appeared that the Pt and Pd catalysts were equally effective, however, an effect was seen based on the loading of the H-adducts in the reactors. At the highest loading (about 7.8 g H-adduct/g catalyst) incomplete deoxygenation was observed by the presence of ketones such as 3-decanone and 3-nonanone and some cyclohexanones in the GCMS analysis. In addition, these products

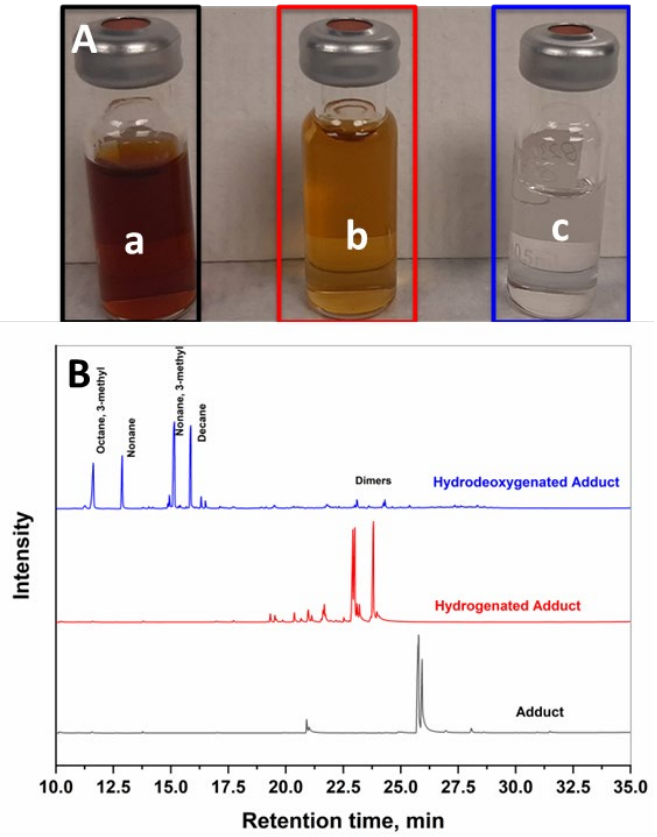

Figure 6.2. (A) Aldol adducts (a), hydrogenated adducts (b), and adducts after HDO (c). (B) GCMS of aldol adduct before and after hydrogenation and adducts obtained after HDO.

were quite dark colored. At lower loadings (3.9 g H-adduct/g catalyst) the concentration of oxygenated products decreased substantially, and the products were much lighter colored (yellow to pale yellow). At the lowest loading, oxygenated products were not detected by GCMS, and the products were colorless (**Figure 6.2 A-C**).

A second set of HDO experiments was performed at the lowest loading but slightly higher concentration of H-adduct in the diluent, methylcyclohexane, to test the reproducibility of the HDO reaction. All reactions were performed with the Pt on the SiO_2-Al_2O_3 catalyst. As shown in **Table 6.2** the HDO reactions reproduced very well in terms of the product distribution and isolated yields. Three of the six reactions did, however, have low concentrations of oxygenated products (mostly ketones) and the products were slightly orange-colored. ^{13}C NMR spectra of the orange-colored products showed small peaks 60-80 ppm range indicating the presence of -CH_2-O carbons in the product, which were absent in colorless products. No carbonyl peaks were observed in the spectra of either product.

Table 6.1. Product distribution from HDO of paper sludge derived H-adduct. (Products concentrations are shown in g/L. nd = not detected).

Catalyst metal	Pd	Pt	Pd	Pt	Pd	Pt
H-adduct/Catalyst weight ratio	7.8	7.8	3.9	3.9	2.0	2.0
H-adduct concn (g/mL)	0.24	0.24	0.14	0.11	0.07	0.07
C8-C10 HC	41.12	17.13	53.50	59.01	36.49	38.28
C13-C16 HC	3.02	-	6.93	7.06	4.00	4.77
Cycloalkanes	8.49	6.05	3.58	2.09	0.39	0.54
Oxygenates	47.30	44.65	4.37	3.06	nd	nd
Isolated yield (Wt%)	67.8%	69.1%	57.5%	54.1%	51.2%	51.4%

Table 6.2. Reproducibility of product distribution from HDO of paper sludge derived H-adduct. (Products concentrations are shown in g/L. nd = not detected).

H-adduct/ Catalyst weight ratio	2.16	2.18	2.16	2.17	2.17	2.18
H-adduct concn (g/mL)	0.11	0.12	0.12	0.12	0.12	0.12
C8-C10 HC	49.92	49.82	49.52	51.93	52.52	52.32
C13-C16 HC	5.17	5.33	5.65	6.66	6.98	6.87
Cycloparaffins	2.08	3.08	3.07	4.02	3.92	3.70
Oxygenates	nd	0.32	nd	nd	0.43	0.65
Isolated yield (Wt%)	54.3%	54.6%	52.9%	53.5%	53.8%	54.7%

A difference was observed in the HDO of the H-adducts made from pure sugars (**Table 6.3**). With H-adducts from pure sugars, complete deoxygenation was achieved at the second-highest loading. Again, little difference was seen between the Pt and Pd catalysts, and no difference in the HC products was seen between the paper sludge and pure sugar-derived HDO products. It appears that something in the paper sludge H-adduct reduced the deoxygenation effectiveness of the HDO catalyst. Analyses are underway to determine if there are differences in the catalysts after being used with the H-adduct from paper sludge compared to pure sugars, and with the unused catalyst.

Table 6.3. Product distribution from HDO of pure sugar derived H-adduct. (Products concentrations are shown in g/L. nd = not detected).

Catalyst Metal	Pd	Pd	Pt	Pt	Pt	Pd
Substrate/ Catalyst weight ratio	7.8	3.9	3.9	2.6	2.0	2.0
Hydrog adduct concn (g/mL)	0.40	0.20	0.20	0.20	0.10	0.10
C8-C10 HC	59.68	55.56	57.11	58.25	34.30	35.89
C13-C16 HC	5.93	6.22	4.96	4.97	3.08	3.86
Cycloparaffins	3.65	1.95	3.35	2.68	0.62	0.56
Oxygenates	25.99	nd	nd	nd	nd	nd
Isolated yield (Wt%)	55.4%	51.4%	51.5%	51.1%	50.5%	49.3%

To make sufficient HC product for fuel property analyses the partially deoxygenated products were combined and put through the HDO process for a second time using the same conditions as previously. This was sufficient to remove all oxygenated species and render the final product colorless (**Figure 6.3**). Overall, the total amount of HC product was 40.0 g, equivalent to 50 mL at a density of 0.80 g/mL. This was split into two aliquots of 25 mL each and was shipped to two independent laboratories: NREL's Fuel Performance Group, and Bioproducts, Sciences, and Engineering Laboratory, Washington State University for all the fuel property tests that were planned.

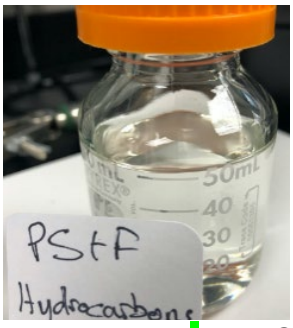

Figure 6.3. HC product generated from paper sludge.

6.4. Analysis of final HC product

6.4.1. GCMS analysis

GCMS and GC X GC analyses showed that the final HC product contained the expected HCs, n-alkanes, and iso-alkanes in the C8-C10 range produced by HDO of the mono adducts formed between furfural and HMF with MEK (**Figures 6.4a and 6.4b**). In addition, there were small amounts of C14-C16 iso-alkanes produced by HDO of the diadducts. The small number of cycloalkanes formed was unexpected, however, these have beneficial fuel properties because of their higher energy density. The presence of both iso- and n-alkanes in similar amounts in the C8-C10 range was a surprise as this indicates the aldol condensation took place at a similar rate at both the methyl and methylene carbon in MEK. Normally a proton on the methylene carbon is slightly more acidic than a proton on the methyl carbon so it would be expected that the condensation reaction would be initiated by the removal of the proton from the methylene carbon, but this was not the case indicating the formation of both methylene and methyl enolate resulting in the formation of both iso- and n-alkanes, respectively in similar amounts.

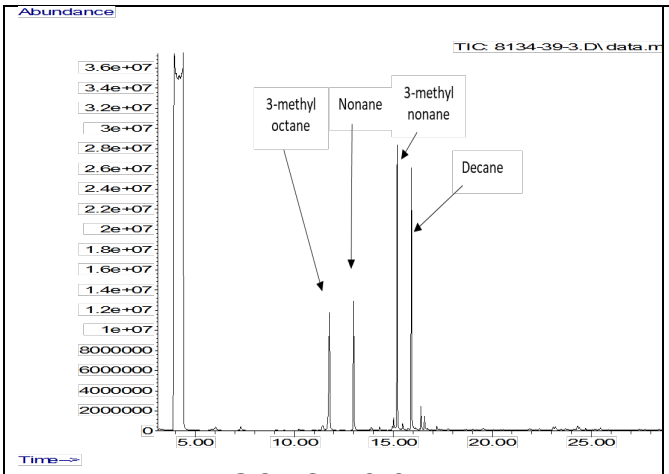

Figure 6.4a. GCMS of final hydrocarbon (HC) product from paper sludge.

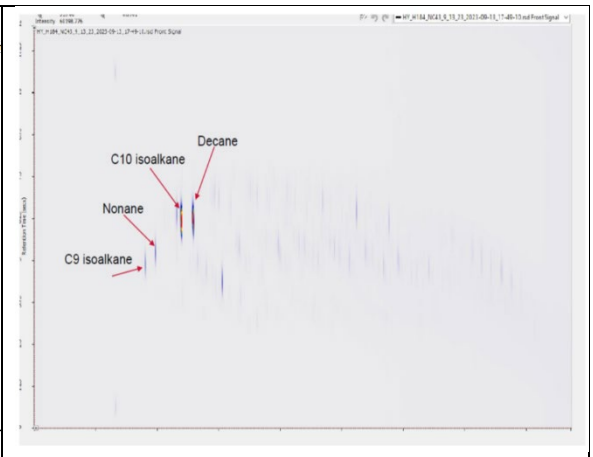

Figure 6.4b. GC X GC of final hydrocarbon (HC) product from paper sludge.

6.4.2. ^{13}C NMR Spectrum

The NMR spectrum of the final HC product (**Figure 6.5**) showed that no peaks appear in -C=O, -C-O- aldehyde (-CHO), and carboxylic acid (-COOH) region. The results indicate that the HDO product was almost completely HC with little to no oxygenated carbons as virtually all the signal intensity was in the 10 to 40 ppm range.

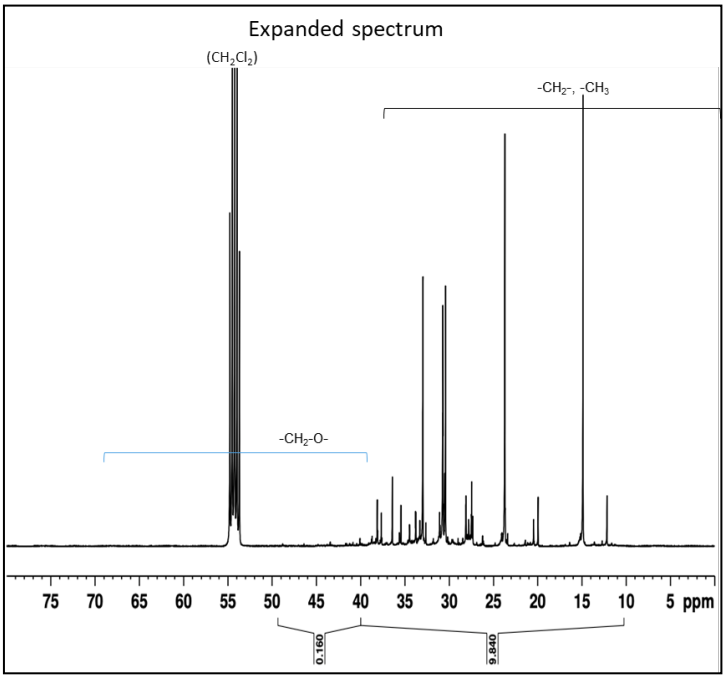

Figure 6.5. ^{13}C NMR spectrum of final HC product from paper sludge.

6.4.3. Fuel property analyses

The fuel properties of the final HC product made from paper sludge were determined by two independent laboratories: NREL's Fuel Performance Group, and Bioproducts, Sciences, and Engineering Laboratory, Washington State University (BSEL-WSU). The fuel properties testing results determined by NREL's Fuel Performance Group are reported in **Table 6.4**. O content was measured by direct analysis and found to be only 0.2 wt% which shows that the hydrocarbon sample had a very small amount of oxygenates. The freezing point for hydrocarbons (-57.1 °C) was within the range for the specifications for jet fuels. The flash point for hydrocarbon product (46.7) also met the specifications for Jet A (Yang, Xin et al. 2019). The density of the hydrocarbon products met commercial fuel specifications, the heating value was above what is required for commercial fuels, and more importantly, the energy density exceeded

the requirement for the jet fuels (46.8 MJ/kg). Overall, the fuel properties indicate that the hydrocarbon product made from PStF hydrolysate could be an excellent fuel blending component for jet fuel.

Table 6.4. Fuel property of hydrocarbons produced by dehydration of PStF hydrolysate.

Fuel Property	Test Method	Test Results	Jet A
Simulated Distillation	ASTM D2887	Distillation Curves	
CH content (wt%)	CHN628	83.67%C 15.53%H	
O content (wt%)	ASTM UOP730-09	0.199 ± 0.003	negligible
n-alkanes	GCXGC	34.2 wt%	
iso-alkanes	GCXGC	43.3 wt%	
cyclo-alkanes	GCXGC	22.3 wt%	
Freezing point (^{o}C)	ASTM D5972	-57.1	-40
Flash Point	ASTM D6450	46.7	38
HHV (MJ/kg)	ASTM D240	46.8	43
Density at 15°C (g/cm^3)	ASTM 7042	0.80	0.82
Energy density (MJ/L)	Calculated	37.4	35

6.4.4. Hydrocarbon distribution

Figure 6.6 shows the HC distribution in the final HC product made from paper sludge determined by BSEL-WSU. It shows that the majority of the product is made up of C10 HC, and this is because the major furfural component was HMF. The C9 HC comes from a reaction of furfural with MEK in the aldol condensation. The HC C>13 is due to the diadducts that formed during the aldol condensation. The final HC product also contained a distribution between n-alkanes (34%), iso-alkanes (43%), and cycloalkanes (22%). This distribution of different types of alkanes is also beneficial for its use as a blendstock in jet and diesel fuels compared to other biofuels which are dominated by a single hydrocarbon.

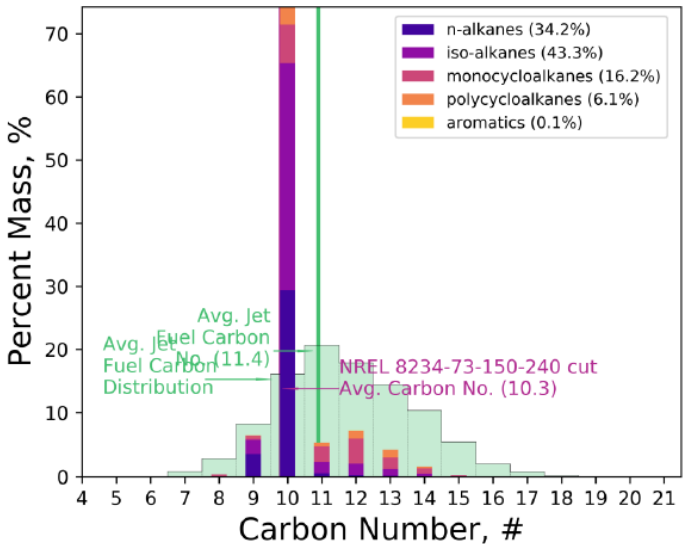

Figure 6.6. Carbon number distribution in final HC product generated from paper sludge.

6.4.5. Simulated Distillation

The result of the simulated distillation analysis, performed by BSEL-WSU according to ASTM D2887, is shown in **Figure 6.7**. The data (black symbols) representing HC products generated from paper sludge are compared against a range of conventional fuels (green-shaded region) (Heyne, Rauch et al. 2021). The results of the simulated distillation analysis indicate that about 44.3% of the hydrocarbons produced from PStF hydrolysate were in the jet fuel boiling range (156 – 293°C) that could be blended into jet fuel. A fraction of HC with a higher boiling point range was in the diesel fuel range. Overall, more than 50% of the final HC product could be blended into jet or diesel fuel.

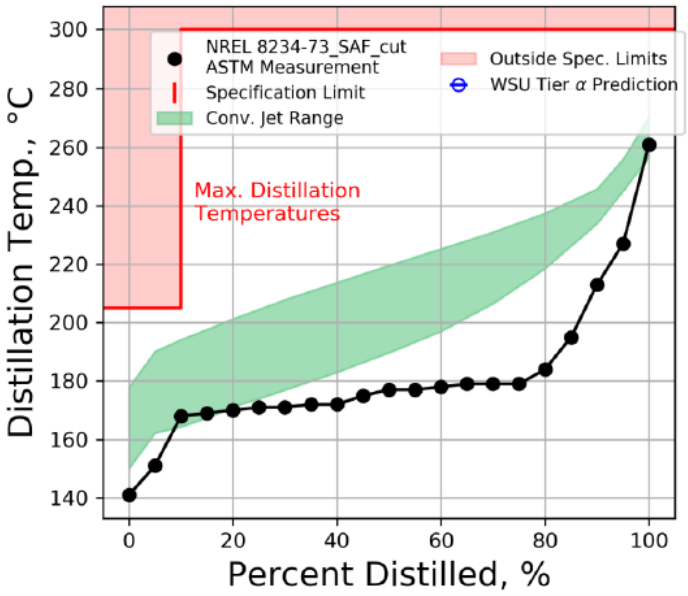

Figure 6.7. Distillation range of final HC product generated from paper sludge.

6.4.6. Property predictions of the HC product generated from paper sludge

Figure 6.8 shows the predictive component of critical properties of the distilled cut of HC product generated from paper sludge determined by BSEL-WSU. The filled black circles represent the measured properties via ASTM test methods and the predicted property range of HC products in conventional fuels is shown in shaded green (Heyne, Rauch et al. 2021). Overall, all the critical properties such as surface tension viscosity (at -20°C (8 cSt) and -40°C (12 cSt)), flashpoint, and freeze point for HC product generated from paper sludge are near or within the range for conventional fuels. Overall, the test results of critical jet fuel properties determined at two independent labs were in good agreement for most of the fuel properties tested.

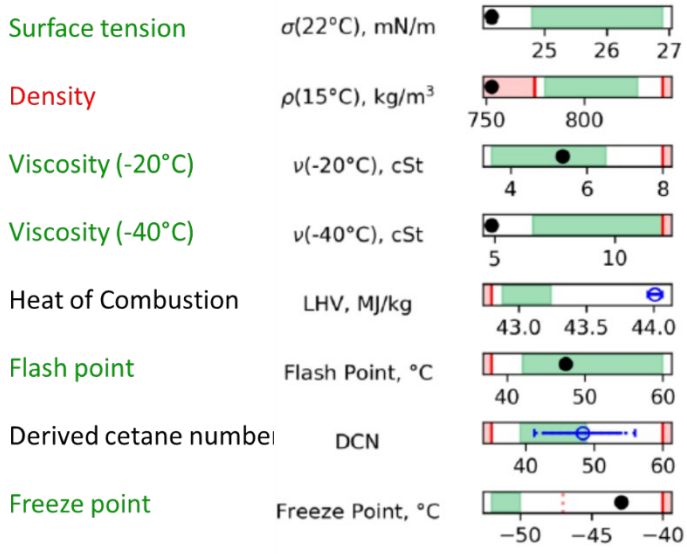

Figure 6.8. Property predictions of the HC product generated from paper sludge.

6.5. Conclusions

Overall, the sugars present in the paper sludge hydrolysate were successfully converted into an HC product that could be blended into jet or diesel fuel. The objective of this work was achieved by the production of sufficient HC so that all planned fuel property analyses could be made. The critical jet fuel properties were determined at two independent labs and the test results obtained were in good agreement for most of the fuel properties tested. The HC product had excellent properties for all the critical properties such as surface tension viscosity (at -20°C (8 cSt) and - 40°C (12 cSt)), flashpoint, and freeze point for HC product generated from paper sludge meeting specifications near or withing the range for conventional fuels. The HC product was dominated by C10 HC because the hydrolysate contained more glucose than other sugars which resulted in the formation of HMF during the dehydration reaction. In addition to n-alkanes, the HC product contained iso-alkanes and small amounts of cyclo-alkanes, which was unexpected. Overall, more than 50% of the HC product could be blended into jet or diesel fuel, exceeding the 50% (GGE basis) target.

There was very little difference observed in the behavior of the paper sludge-derived intermediates, compared to intermediates derived from pure sugars, over the initial steps of the upgrading process, dehydration, condensation, and hydrogenation. However, in the final step, HDO, there was a difference observed as the product derived from the paper sludge proved slightly more difficult to completely deoxygenate. Only at the lowest loading of H-adduct to catalyst loading was complete deoxygenation achieved with the paper sludge-derived H-adduct, whereas at only the highest loading of pure sugar H-adduct were oxygenated products observed after the HDO reaction. Further work is planned to discover the reason for this observation.

References

1. Heyne, J., et al. (2021). "Sustainable aviation fuel prescreening tools and procedures." Fuel **290**: 120004.
2. Yang, J., et al. (2019). "An overview on performance characteristics of bio-jet fuels." Fuel **237**: 916-936.

Chapter 7: Techno-economic and sensitivity analysis for PStF project

7.1. Introduction

A vast amount of Techno-economic and sensitivity analysis models were developed starting from an early stage and throughout the project. Models containing different levels of maturity were executed at different stages of project development. The goal was to identify the more critical variables affecting the overall economics, considering the multiple transformation steps required to convert paper sludge into the final hydrocarbon blend. The minimum fuel selling price (MFSP) of the final liquid fuel product was utilized as the evaluating outcome variable, which resulted from the mathematical models and susceptible to optimization. The results obtained from the TEA and SA analysis guided the laboratory work both at NCSU and NREL, supporting an efficient use of time in both research sites.

Experimental data from each transformation stage, studied and generated at NCSU and NREL, were utilized as input data for the eight case studies developed. Two clear sets of case studies were evaluated. Four of them utilized 1,4-dioxane as a co-solvent for the dehydration reaction of sugars, considering the high yield to furans expected, and four of them used acetone as an organic solvent within this same step, considering the lower heat duty demand during the recycling of this alternative solvent. Additional reasons for this heat intensity difference were explained in Chapter 4. Aspen Plus™, a process development software commonly used in the well-established oil-based industry, was used to estimate the mass balance and the heat demand across the different units in the alternative biorefinery layouts studied. This choice was made given the importance of data reliability and the complexity of the studied biorefinery, especially due to the need for distillation units to recover the co-solvents, etc., Similar economic considerations as those reported in recent NREL's technical reports [1][2][5] were used in the models herein presented.

7.2. Process description

7.2.1. Area100: Feedstock handling

In this area of the plant, paper sludge is received, and stored under a dome reclaim system. 750 tonnes/day of dry paper sludge is the baseline for the biorefinery size used in the simulation.

7.2.2. Area 200: Pretreatment

Before performing chemical transformations on carbohydrates present in paper sludge, the removal of ash is required. High volumes of water, a sidehill screen, and transfer pumps have been used to remove ash from paper sludge at the pilot scale at NCSU (**Fig. 7.1**). Maximizing the retention of carbohydrates is a key parameter for this separation stage.

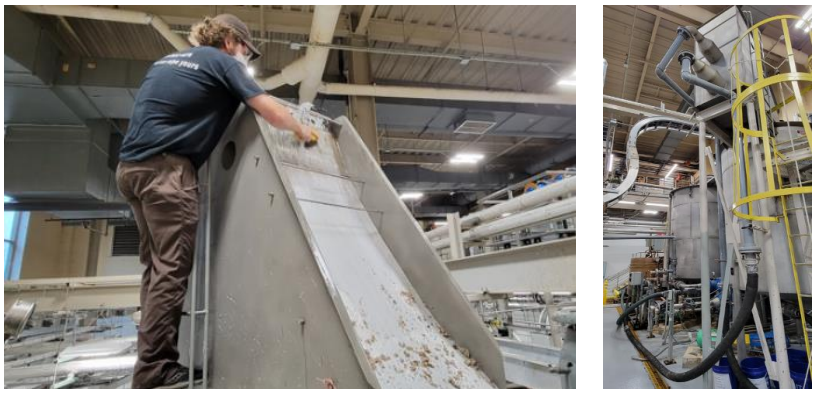

Fig. 7.1. Sidehill screen at NCSU.

7.2.3. Area 300: Enzymatic hydrolysis

The first transformation step occurs in this area of the biorefinery, enzyme (cellulase: Cellic® CTec2, Novozymes, USA) is used to transform glucan and xylan into monomeric sugars, glucose, and xylose. At the pilot scale, a Paddle Reactor at NREL was used to perform this transformation step (**Fig. 7.2**).

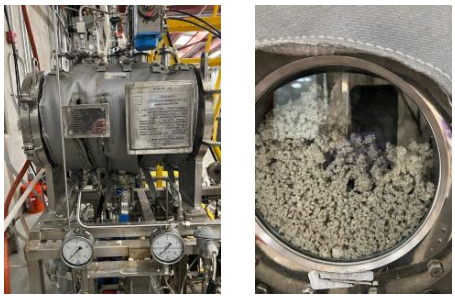

Fig. 7.2. Paddle reactor at NREL.

7.2.4. Area 400: Catalytic conversion and upgrading

This area of the plant comprises most of the equipment required for the transformation of carbohydrates into hydrocarbons. Enzymatic hydrolysis, dehydration of sugars, and solvent recovery are the subsections in this area.

7.2.4.1. Dehydration of sugars to 5-hydroxymethylfurfural and furfural

The second transformation step corresponds to the dehydration of sugars to 5-Hydroxymethylfurfural (5-HMF) and furfural (**Fig. 7.3**) on $AlCl_3$, a Lewis acid catalyst (Catalyst loading: 10miliMolar). The use of an organic solvent is required to achieve high yields of furan materials. Initially, following NREL's previous experience, 1,4-Dioxane was used as a co-solvent for the sugars dehydration reaction, later after determining the Minimum Fuel Selling Prince (MFSP $/GGE) of the final hydrocarbon product in four different case studies as well as the corresponding Sensitivity Analysis (Base case, Alternative Case #2, #3 & #4 / 1,4-Dioxane systems), ten different alternative solvent systems were selected to be investigated based on the; thermodynamic properties of the potential candidates (Boiling point, occurrence of azeotrope nodes with water) and the performance on the dehydration of glucose (major constituent sugar) to 5-HMF. The results are reported in **Fig. 7.4**. Under the experimental conditions, acetone exhibited the

second-best results after 1,4-Dioxane. For this reason, this alternative organic solvent was selected to build new four study cases (Alternative Case #5 to #8 / Acetone systems) and compare the results of the systems using the cancer-associated material, 1,4-Dioxane. As can be observed in **Fig. 7.5**, acetone does not exhibit an azeotrope node with water which means that this material can be potentially recovered at a high purity degree. At the same time, acetone has a lower boiling point (56°C) compared to the boiling point of the azeotropic mixture 1,4-Dioxane/water (82%wt. 1,4-Dioxane at 87.8°C). A ratio of organic solvent to aqueous sugar solution of 1.75 was fixed as a baseline for most of the case studies analyzed.

The study of optimal conditions for the dehydration of glucose to 5-HMF using 1,4-Dioxane vs. Acetone was performed using Microwave Synthesizer (CEM, USA). A sugar solution containing 80g/l of glucose, an organic solvent to aqueous solution of 2.0, and 3 minutes holding time (time after setpoint temperature is achieved) for the reaction were used for all the experiments. Temperatures ranging from 165°C to 205°C and catalyst loads from 5.5miliMolar to 20miliMolar ($AlCl_3$) were evaluated. A maximum yield to 5-HMF of 71.39±0.83% was achieved for the 1,4-Dioxane system (2:1 volume ratio) at a catalyst load of 15mM $AlCl_3$ at 185°C and. On the other hand, the maximum yield to 5-HMF when using acetone as solvent assisting the dehydration reaction (2:1 volume ratio) was 66.22±0.57% at a catalyst load of 7.5mM $AlCl_3$ at 185°C. The corresponding yield to furans values was used for the Base Case and Alternative Cases #2 to #8. The results of these optimization experiments are displayed in **Fig. 7.6**.

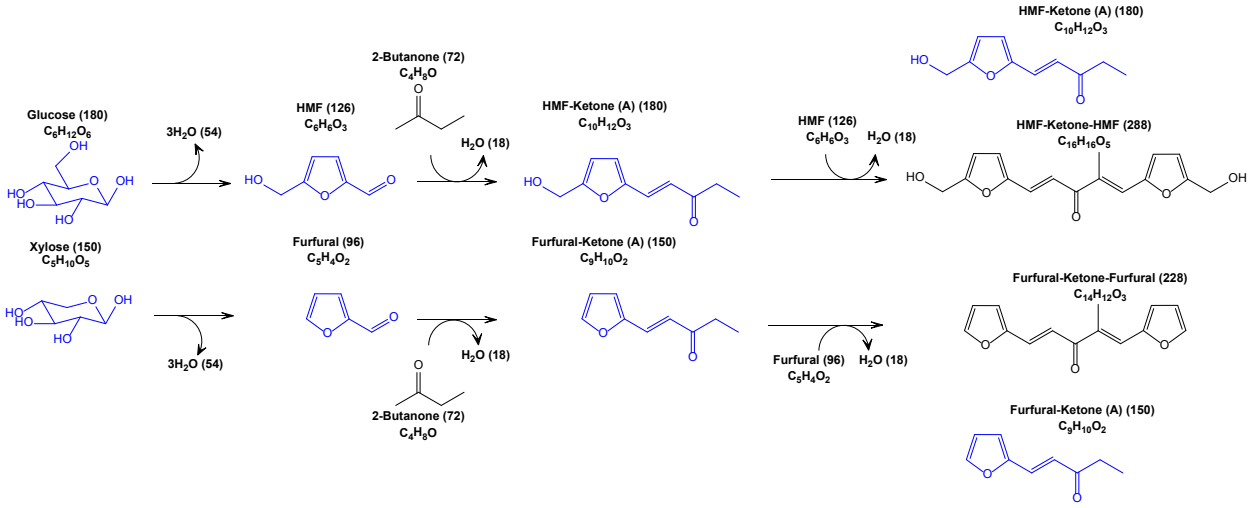

Fig. 7.3. Catalytic transformation of carbohydrates into hydrocarbons: sugars dehydration and aldol-condensation reaction.

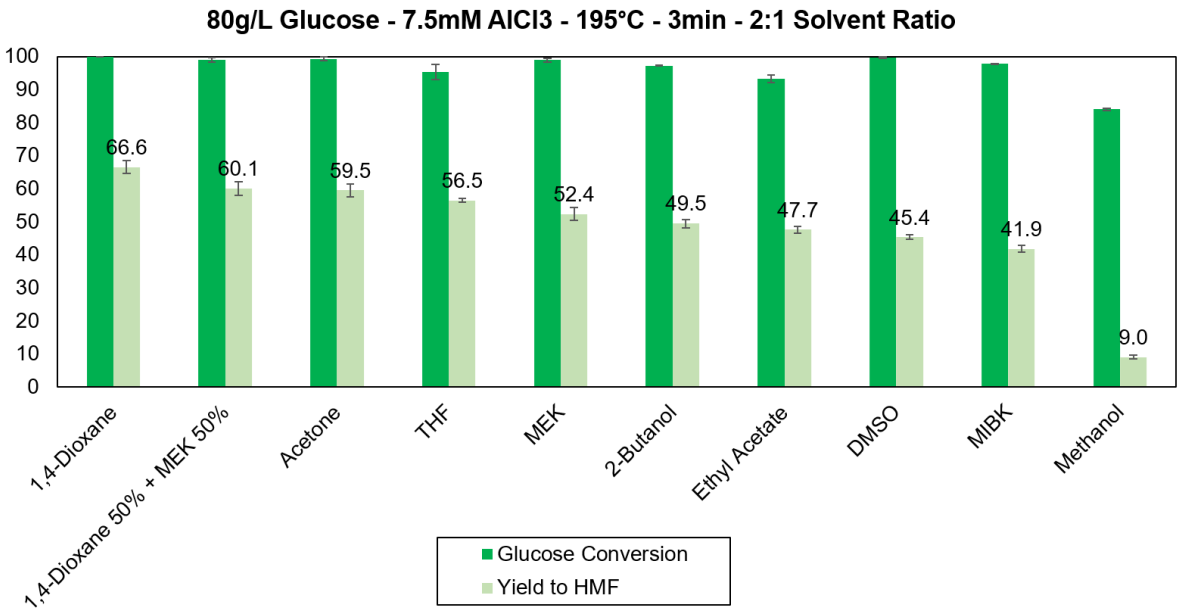

Fig. 7.4. Comparing different organic co-solvent systems during the dehydration of glucose.

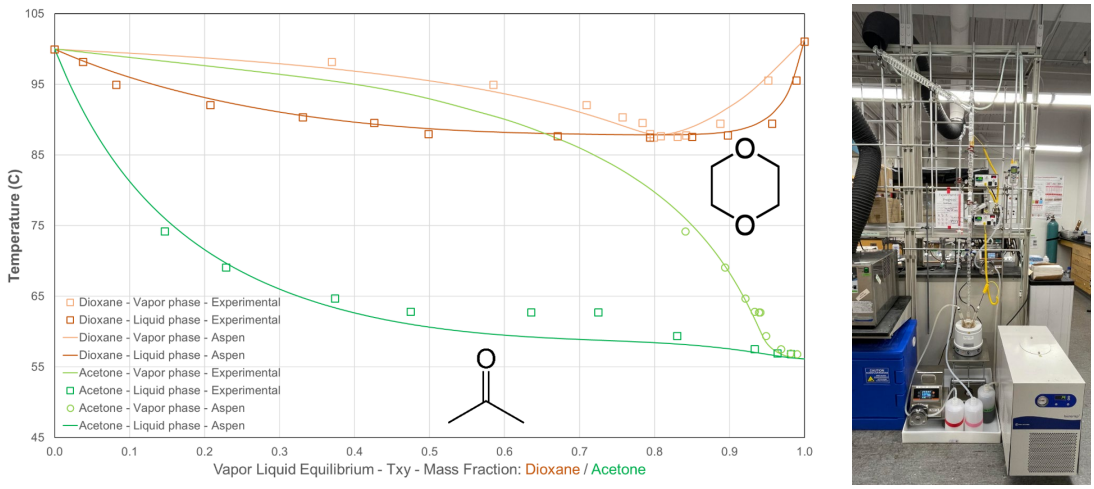

Fig. 7.5. (a) Vapor–liquid equilibrium for the binary system 1,4-dioxane/water and acetone/water from Aspen Plus™ and (b) In-house-built multi-stage continuous distillation system used at NCSU to distill co-solvents from the furan products solution produced at NREL.

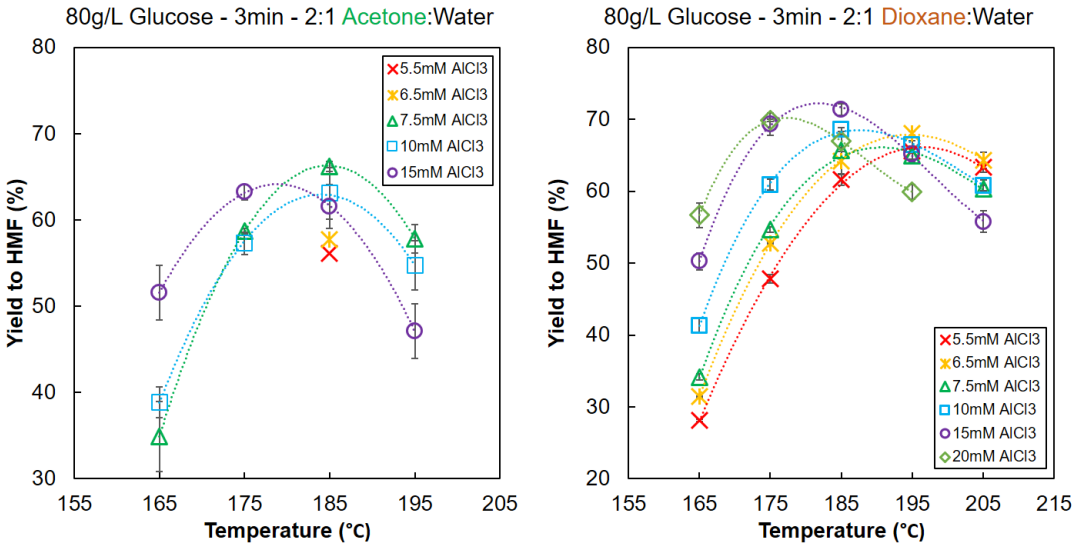

Fig. 7.6. Optimal reaction conditions for the dehydration of glucose to 5-HMF using 1,4-Dioxane vs. acetone as co-solvent.

7.2.4.2. Aldol-condensation reaction

Since the project is targeting the production of a hydrocarbon blend in the Jet fuel range, C9 and C10 alkanes as final products are desired. To achieve this, four additional carbons need to be added to the furan structures obtained from the dehydration reaction. Aldol-condensation, a base-catalyzed condensation reaction occurring between an enolate ion (from 5-HMF and furfural in this case) and a carbonyl compound (2-Butanone) is used to increase the number of carbon in four units. Sodium hydroxide is used as a catalyst in this transformation step. The condensation of 5-HMF and furfural over the structure of the 2-Butanone (Methyl Ethyl Ketone – MEK), can occur on the primary or secondary carbon next to the carbonyl group (**Fig. 7.3**). If only one molecule of furan condenses on the structure of the ketone, the product is commonly referred to as monoadduct. A second molecule of furan material can condense on the same molecule of ketone (e.g. if not enough MEK is present in the reaction medium). The resulting product is referred to in this study as diadduct.

For this project's purpose, maximizing the production of aldol-condensation products, especially mono adducts is desired. Initially, the aldol condensation experiments were performed at NREL in the presence of 1,4-Dioxane, a catalyst load of 1.17 moles of NaOH per mole of furan product (pH ~13.8), and a furan to MEK 0.4 mole ratio at 80°C during 40min. Moreover, new experiments were required considering the highly relevant solvent system modification. As shown in **Fig. 7.8**., for the 1,4-Dioxane system, the distillation column for recovering the organic dehydration-supporting solvent was installed after the hydrogenation reactor. This is because 5-HMF and furfural cannot condense on 1,4-Dioxane during the aldol-condensation reaction. Moreover, in the case of acetone systems, if acetone is preserved in the aldol-condensation reaction media, furans can condense on the structure of this alternative dehydration solvent similarly as they condense on the structure of MEK, resulting in C8 and C9 hydrocarbon products, containing one less carbon than the targeted materials (C9 & C10). For this reason, in

Alternative Cases #5 to #8 (acetone systems), the distillation column had to be relocated right after the dehydration reactor (**Fig. 7.9**). Removing the organic solvent from the dehydration products (for acetone systems only), had an important impact in the starting pH of the furan products used for the aldol-condensation reaction, this increased the NaOH loading. An increased aldol-condensation catalyst loading of 1.80 moles of NaOH per mole of furan product (pH ~13.0) was used for this transformation step in the simulation files for Alternative Case #5 to #8 (acetone systems). As discussed in the "Aldol-condensation report", to maximize the abundance of aldol-condensation products from the furans obtained in the acetone system, mainly governed by the presence of HMF-MEK mono adducts, furans to MEK ratio of 1 to 2 and the local optimal conditions 10 min reaction time and 50°C were used for the 5L scale batch reactor experiments (**Fig. 7.10**).

Notice that in **Fig. 7.3**, only the mono adducts formed after the condensation of furan structures on the primary carbon next to the carbonyl group of MEK are presented. Moreover, as it has been found as part of this project (Aldol-condensation report), the presence of mono adducts from the condensation of furans on the secondary carbon next to the carbonyl group of MEK was confirmed.

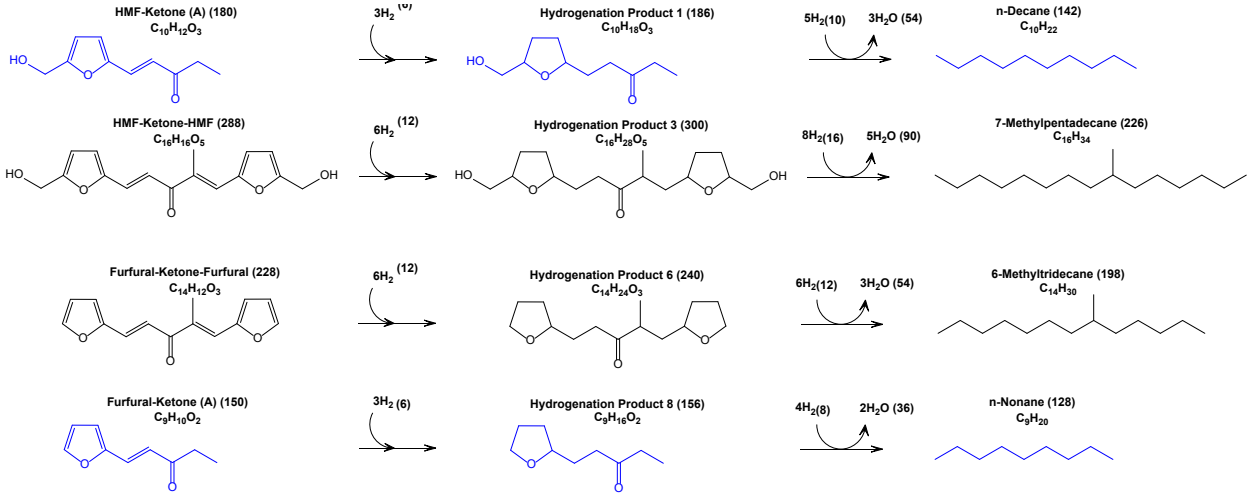

Fig. 7.7. Catalytic transformation of carbohydrates into hydrocarbons: Hydrogenation and Hydrodeoxygenation reactions.

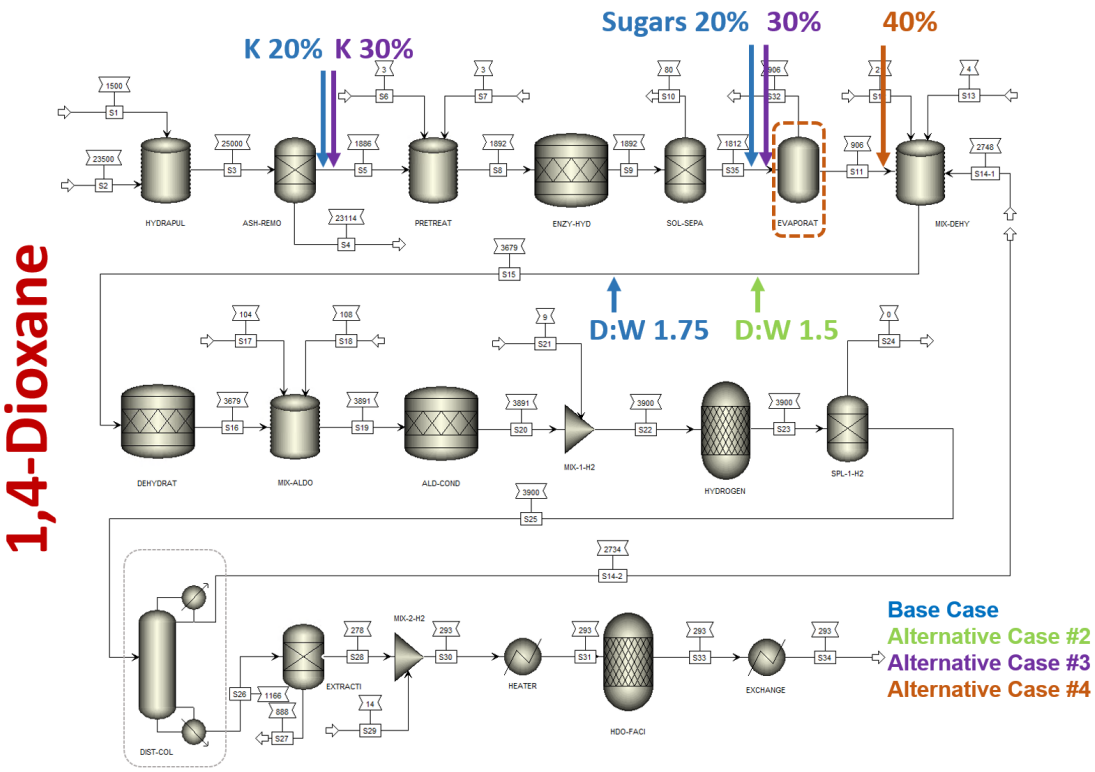

Fig. 7.8. Simplified flow diagram for 1,4-Dioxane case studies.

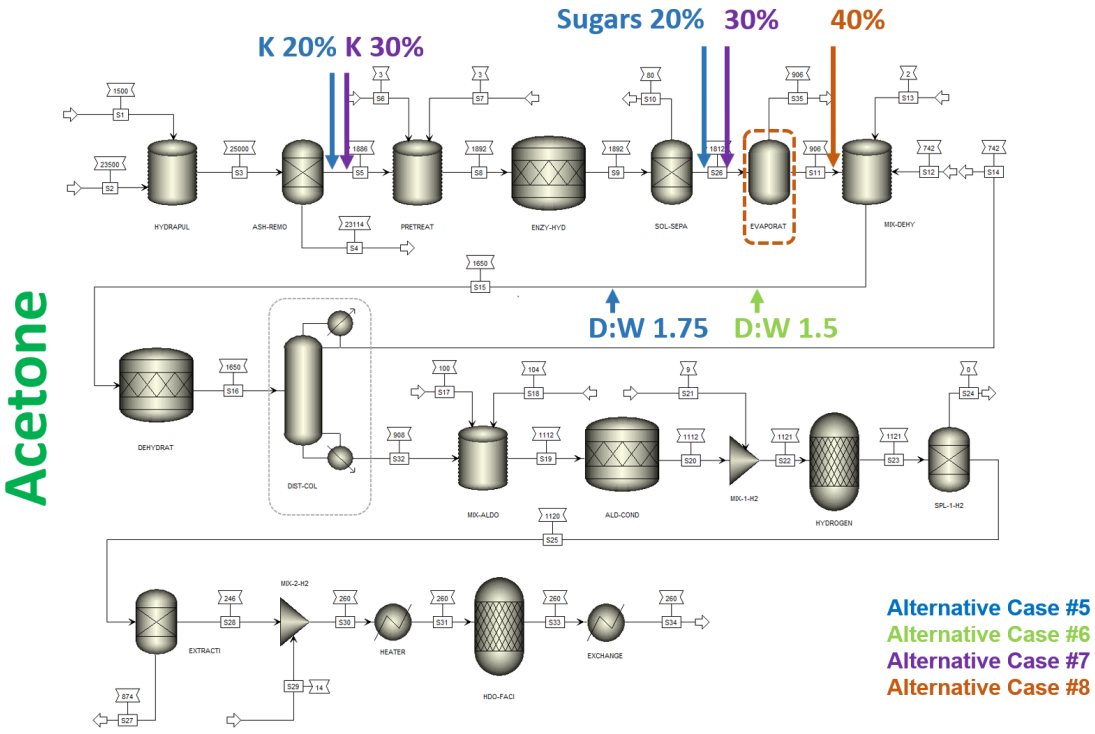

Fig. 7.9. Simplified flow diagram for acetone case studies.

Fig. 7.10. Five-liter batch reactor for aldol-condensation at NCSU.

7.2.4.3. Low-temperature hydrogenation reaction

To stabilize the mono adducts produced after the aldol-condensation products by saturating the carbon-carbon double bonds in these materials by using hydrogen and a carbon/palladium-based catalyst (**Fig. 7.7**), a low temperature hydrogenation reaction was performed at NREL over aldol-condensation samples at 100°C, for 2 hours, using an initial 68bar of Hydrogen and 0.4g 5%Pd/C catalyst.

7.2.4.4. Hydrodeoxygenation reaction (HDO)

The last step in the chemical transformation corresponds to the oxygen removal from the hydrogenation reaction products (**Fig. 7.7**). A hydrodeoxygenation reaction was performed at NREL over hydrogenation products at 300C, for 3 hours using an initial 68bar of Hydrogen and 0.4g 5% Pd/MS-13 catalyst.

Note: Experimental data obtained throughout the experimental work was used as input data for the mass and energy balance simulation work as well as for the sensitivity analysis.

7.2.5. Area 500: Wastewater treatment

This corresponds to the treatment process applied on waste streams generated in the process. The units associated with this area are considered in the calculation of the total capital investment of the biorefinery.

7.2.6. Area 600: Heat and power

In this area, the natural gas power boiler supporting the heat demand of the plant and the steam turbine and power generator systems are considered. Similar than for Area 500, the equipment and support elements associated with this area are considered in the calculation of the total capital investment of the biorefinery.

7.2.7. Area 700: Utilities

In this area, the cooling towers system and the plant air compressors are considered.

7.3. Evaluation methodology

7.3.1. Case studies definition

Two sets of case studies are analyzed. Four cases for systems using 1,4-Dioxane as an organic solvent for the dehydration reaction and four cases for systems using acetone. At the same time, four modifications for each set of studies were proposed and analyzed: As can be observed in **Table 7.1**. and **Table 7.2**., four process variables were modified for the analysis for each solvent system studied: 1) The fiber consistency for enzymatic hydrolysis; 2) The sugars mass fraction to the dehydration reactor; 3) The organic solvent to aqueous sugars solution volume ratio; and, the 4) Presence of an evaporation unit before the dehydration reactor to increase the concentration of sugars at this site up to 40%. The graphical representation of those modifications can also be observed in **Fig. 7.8** and **Fig. 7.9**.

Table 7.1. Base case and alternative case #2 to #4 (1,4-dioxane system).

Process variable for 1,4-dioxane systems	Base Case	Alternative Case #2	Alternative Case #3	Alternative Case #4
Fibers consistency for enzymatic hydrolysis	20%	20%	**30%**	20%
Sugars mass fraction to dehydration reactor	20%	20%	30%	**40%** (Evaporator)
1,4-Dioxane to aqueous sugars solution volume ratio for dehydration reaction	1.75	**1.50**	1.75	1.7
Evaporator before dehydration reactor to increase sugar mass content	No	No	No	**Yes**

Table 7.2. Alternative case #5 to #8 (acetone system).

Process variable for acetone systems	Alternative Case #5	Alternative Case #6	Alternative Case #7	Alternative Case #8
Fibers consistency for enzymatic hydrolysis	20%	20%	**30%**	20%
Sugars mass fraction to dehydration reactor	20%	20%	30%	**40%** (Evaporator)
acetone to aqueous sugars solution volume ratio for dehydration reaction	1.75	**1.50**	1.75	1.75
Evaporator before dehydration reactor to increase sugar mass content	No	No	No	**Yes**

7.3.2. Minimum fuel selling price calculation and sensitivity analysis

The calculation of the Minimum Fuel Selling Price of the resulting hydrocarbon blend as well as the Sensitivity Analysis, comprise the integration of information from multiple sources including; experimental data, information about existing technologies, mass and energy balance results, economic and financial parameters, cost of chemicals, materials and equipment, labor, producer price and plant cost indexes, and specific information for jet fuel. As depicted in **Fig. 7.11**, in this work, the information was collected and integrated using Microsoft® Excel® files.

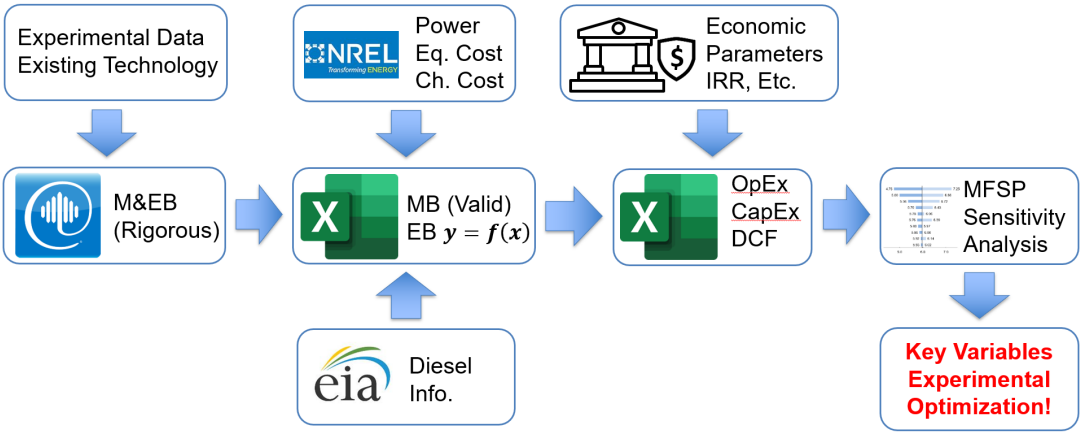

Fig. 7.11. How information flows for estimating MFSP & sensitivity analysis.

7.3.2.1. Mass and energy balance (head demand) and Aspen Plus™

The mass balance was developed using experimental data for reaction conversions and yields. Considering the complexity of the estimation of the heat demand at the reactors and the distillation column system, Aspen Plus™ (version 11), a computer-based modeling and simulation technology, and powerful tool initially developed by the Massachusetts Institute of Technology (MIT) and United States Department of Energy, was used to estimate the energy balance (heat demand) of the studied biorefinery. The use of this software has been recommended and applied for the modeling of modern biorefineries handling the conversion of biomass to sugars, furan materials, and others. The thermodynamic method as well as the binary interaction parameters sources selected for the process simulation is of extreme importance considering an accurate representation of the simulation to the real studied systems. According to literature, the Nonrandom Two Liquid (NRTL) method closely reproduces the experimental results of biomass transformations similar to the one studied in this work. Additionally, and after graphically comparing the experimental results for the Vapor-Liquid Equilibrium (VLE) of the binary systems: 1,4-Dioxane/water; acetone/water; and acetone/furfural to Aspen Plus™ results, the NRTL-2 method and the selected parameter sources were defined for the process simulation. The simulation software was used to estimate the mass balance and the heat duty at the different units presented in **Fig. 7.8** and **Fig. 7.9**. The “RStoic” model was used to simulate the reactors and the rigorous “RadFrac” model, used to

simulate multistage vapor-liquid fractionation operations was used for the simulation of the distillation column system.

7.3.2.2. Total capital investment

For calculating the total capital investment of the plant in each case study, seven process areas are considered and the parameters included are indicated in **Table 7.3.** were used. The cost of land was fixed at $1.8MM. Changes in the parameters marked (**) were included in the Sensitivity Analysis performed for all the case studies. More than 126 units are considered for the calculation of the Installed Equipment Cost (IEC) of the studied biorefineries **Annex A.**

Table 7.3. Total Capital Investment and definitions for baseline of the sensitivity analysis for each case study based on NREL reports [1][2][5].

Process Area	
A100 - Feedstock Handling	
A200 - Pretreatment	
A300 - Enzymatic Hydrolysis	
A400 – Catalytic Conversion and Upgrading	
A500 - Waste Water Treatment	
A600 - Heat and Power	
A700 - Utilities	
Installed Equipment Cost (IEC) = Installed cost of equipment in A100 to a 700	
Warehouse**	4.0% of ISBL*
Site Development**	10.0% of ISBL*
Additional Piping**	4.5% of ISBL*
Total Direct Costs (TDC) = IEC + Warehouse + Site development + Add. piping	
Prorateable Expenses** [a]	10.0% of TDC
Field Expenses** [b]	10.0% of TDC
Home Office & Construction Fee** [c]	20.0% of TDC
Project Contingency** [d]	10.0% of TDC
Other costs (Start-up, permits, etc.)** [e]	10.0% of TDC
Total Indirect Costs (TIC) = a + b + c + d + e	
Fixed Capital Investment (FCI) = TDC + TIC	
Land	$1,848,000
Working Capital**	5.0% of FCI
Total Capital Investment (TCI) = FCI + Land + Working Capital	

*ISBL: Internal Battery Limits (Includes A100 to A700, but it does not include A600).
**Modifications on these values were included as part of the Sensitivity Analysis.

7.3.2.3. Operational Expenditure: variable operating costs and fixed operating costs

In this section, two different groups of costs are considered: the variable operating costs and the fixed operating costs.

7.3.2.4. Variable operating cost

In this section, the cost of raw materials, other waste stream cost, by-products and credits are included. The values used as the base line for each scenario are presented in **Table 7.4**.

Table 7.4. Variable operating cost.

Raw Material	Price per metric ton (2023's $)	Reference
Process makeup water	$0.49/tonne	2018 - NREL/TP-5100-71949 [1]
Enzyme	$6,840/tonne	2018 - NREL/TP-5100-71949 [1]
Hydrochloric acid	$126/tonne	2015 - NREL/TP-5100-62498 [2]
1,4-Dioxane	$1,150/tonne	Chen et al. 2014 [3]
AlCl3 (Dehydration Catalyst)	$812/tonne	Zang et al. 2020 [4]
Methyl Ethyl Ketone (Ketone)	$660/tonne	Biobased MEK 2021 - NREL/TP - 5100 – 80652 [5]
NaOH (Aldol Condensation Cat.)	$590/tonne	2018 - NREL/TP-5100-71949 [1]
Hydrogen	$1,800/tonne	2018 - NREL/TP-5100-71949 [1]
Pt/Al2O3 (HDO Cat.)	$47,800/tonne	2018 - NREL/TP-5100-71949 [1]
Raw Material	**Price per metric ton (2023's $)**	**Reference**
Make up water to the Power Boiler	$0.49/tonne	2018 - NREL/TP-5100-71949 [1]
Boiler chemicals	$7,300/tonne	2018 - NREL/TP-5100-71949 [1]
Cooling water chemicals	$4,400/tonne	2018 - NREL/TP-5100-71949 [1]
Natural Gas	$2.84/MMBTU	www.eia.com / U.S. Energy Information Administration [6]
Credits	**(2023's $)**	**Reference**
Paper sludge disposal credit	$61/tonne (dry)	Typical industrial value
Power	¢6.9/kWh	www.eia.com / U.S. Energy Information Administration / Average Retail Price (Industrial) [6]

Note: No SAF credits have been considered yet for the presented results. Including these credits is expected to contribute to reducing the MFSP of the hydrocarbon product.

7.3.2.5. Fixed operating cost

In this section, the labor and supervision costs as well as the other overhead costs are included.

Table 7.5. Fixed operating cost based on U.S. Bureau of labor statistics [7].

Position	Yearly Salary (2023's $)
Plant manager (1)	$194,000
Plant engineer (1)	$92,000
Maintenance supervisor (1)	$75,400,
Maintenance technician (1)	$53,000
Lab Manager (1)	$74,000,
Lab Technician (1)	$53,000
Shift Supervisor (1)	$63,000
Shift Operators (9)	$53,000 (each)
Yard Employees (1)	$37,000
General Manager (1)	$121,000

Clerks & Secretaries (1)	$43,000
Maintenance	**3.0% of IBL**
Property insurance & tax	**1% of FCI**

7.3.2.6. Minimum fuel selling price and financial parameters (Discounted cash flow rate of return)

The financial and operating parameters in **Table 7.6** were used to estimate the Minimum Fuel Selling Price (MFSP) in dollars per Gasoline Gallon Equivalent ($/GGE) of the hydrocarbon blend product in all cases. Sensitivity analysis was applied to parameters marked (**).

7.3.2.7. Discounted cash flow rate of return: measure of the maximum interest rate that the project could afford just by paying the Total Capital Investment at the end of the project life.

Table 7.6. Financial and operation parameters for DCFROR based on NREL reports [1][2][5]

Financial Parameter	Value	Source
Equity**	40%	Previous NREL Reports
Loan Interest**	8%	Previous NREL Reports
Loan term**	10 years	Previous NREL Reports
Working Capital	5%	Previous NREL Reports
Depreciation Period General Plant	7 years	IRS Pub. 946 - MACRS
Depreciation Period Heat & Power – Utilities	20 years	IRS Pub. 946 - MACRS
Construction Period & Study	3 years (33 years study)	Previous NREL Reports
Start-up time	0.25 years	Previous NREL Reports
Discount Rate: Internal Rate of Return**	10%	Previous NREL Reports
Income Tax Rate**	21%	Previous NREL Reports
Operating time of the year	90%	Previous NREL Reports
Cost year for analysis	2023	Previous NREL Reports

7.4. Results and discussion

7.4.1. Minimum fuel selling price

The MFSP for the final hydrocarbon product for Base Case and Alternative Cases #2 to #8 are presented in **Fig. 7.12**. The results for the Sensitivity Analysis results are displayed in **Annex B** & **Annex C**.

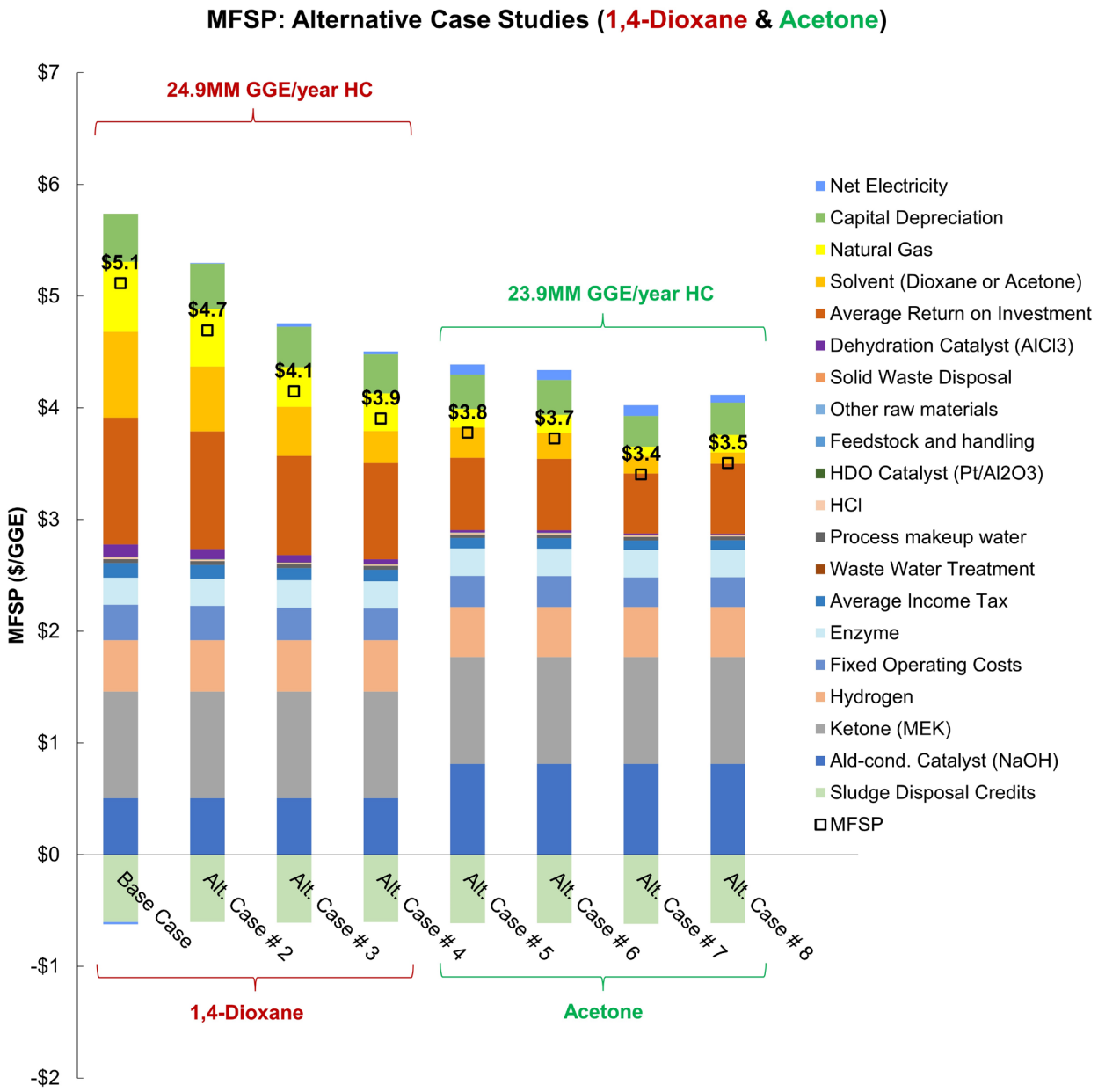

Fig. 7.12. Minimum fuel selling price for base caase and alternative case #2 to #8.

7.4.1.1. Analysis for 1,4-dioxane systems (Base case to alternative case #4 – Only)

✓ The Total Capital Investment (TCI) is consistently reduced throughout all case studies (from Base Case to Alternative Case #4): This, due to the generalized reduction in the mass flow passing through the dehydration reactor, the aldol condensation reactor, the hydrogenation reactor, and the Distillation Column (Equipment size – Capital Investment).

✓ The reduction in flow mentioned before also results in the reduction of the Heat Duty at the dehydration reactor, and the reboiler of the distillation column. For the 1,4-Dioxane solvent systems, the Total Heat Demand (required steam) of the plant is mainly governed by the heat duty at the distillation unit. For this reason, when reducing

the mass flow to the Distillation Column, a reduction in the equipment cost of area A600 Heat & Power (Power Boiler) was achieved (Equipment size - Capital Cost).

- ✓ With the reduction in the Total Heat Demand of the plant, when moving from the Base Case to Alternative Case #4, the demand for Natural Gas is also reduced (Natural gas cost).

- ✓ When moving from the Base Case to Alternative Case #4, the total mass of water getting into the Dehydration reaction circuit is reduced. Due to this, the used/required total mass of Dioxane in the recirculation loop required to satisfy the organic volume to aqueous solution volume ratio is also reduced, and since the loss of solvent is fixed in all cases at 1% of the total 1,4-Dioxane fed to the distillation column, the loss of solvent is reduced with advancing from one studied case to the other (1,4-Dioxane cost).

- ✓ A reduced flow to the Dehydration reactor, achieved when moving from the Base Case to Alternative Case #4, contributes to reducing the amount of dehydration catalyst (Aluminum Chloride - AlCl3), since this material is loaded on a concentration basis of 10mM (Aluminum chloride cost).

- ✓ The reduction in; the Total Heat Demand, the Total Capital Investment (TCI), the demand for Natural Gas, the Loss of solvent (Dioxane), and the required dehydration catalyst (AlCl3), mainly explain the reduction of the contribution of the Average Return of Investment to the Minimum Fuel Selling Price (MFSP) of the hydrocarbon product.

- ✓ Only for the studied Base Case, a surplus of power was estimated. This isdirectly related to the high heat demand of the plant. While passing the required steam through the Steam Turbine Generator, more power was obtained than required to satisfy the power demand of the plant.

7.4.1.2. Analysis for acetone systems (Alternative case #5 to #8 – Only)

- ✓ Similarly, to the “Dioxane Systems”, when moving from Alternative Case #5 to Alternative Case #8 (acetone systems), the total mass of water getting into the Dehydration reaction circuit is reduced (Except for Alternative Case #6). Due to this, the required total mass of Acetone in the recirculation loop is also reduced to preserve the 1.75 volume ratio. The amount of acetone for Alternative Case #6 is also reduced due to the defined 1.5 volume ratio for this specific scenario. Since the loss of solvent is fixed in all cases at 1% of the total acetone fed to the distillation column, the loss of solvent is reduced by advancing from one studied case to the other (acetone cost).

- ✓ When comparing acetone systems only, even when the total flow to the Distillation Column was reduced from Alternative Case #5 (acetone to aqueous volume ratio 1.75) to Alternative Case #6 (acetone to aqueous volume ratio 1.5), the Total Heat Demand of the plant remained almost the same. This is because the mass fraction of Acetone was moved from 0.52 to 0.48. In the second scenario, a slightly higher Reboiler Heat Duty was estimated. Even when some heat demand is saved at the

Dehydration unit, more heat is required at the Reboiler due to an increase in the Reflux Ratio required to achieve a fixed mass purity of 98%.

- ✓ In Alternative Case #7 the lower Total Heat Demand and the lower Total Capital Investment (TCI) were achieved. For this reason, the lower Natural Gas demand and the lower contribution of the Average Return on Investment to the MFSP were estimated. In contrast, in Alternative Case #8, the Total Heat Demand was increased due to the use of an Evaporation unit. This rise led to an increase in Natural Gas demand, the Total Capital Investment (TCI), and consequently, the Average Return of Investment.

7.4.1.3. Analysis for acetone systems (Alternative case #5 to #8) vs. 1,4-dioxane systems (Base case to alternative case #4)

- ✓ Acetone was selected as an alternative solvent for the dehydration reaction because this material does not exhibit an azeotropic node with water. This means that acetone can be completely distilled and separated from the aqueous reaction media, by using a conventional distillation.

- ✓ To avoid the condensation of acetone on the structure of the furan products during the aldol-condensation step, which could lead to a one-less-carbon hydrocarbon product, the distillation unit was relocated after the dehydration reactor.

- ✓ The use of acetone as the organic solvent during the dehydration of sugars promoted the reduction of the yield from Glucose to 5-Hydroxymethylfurfural from 71% to 68% as well as the reduction of the yield from Xylose to Furfural from 84% to 81% (Additional experiments at NREL – Different to the reported in Section 2.4 of this report). Only by modifying these parameters, the estimated annual production of hydrocarbon product reduced from 24.9MM gal/year (1,4-Dioxane systems) to 23.9MM gal/year (acetone systems).

- ✓ As mentioned in Section “2.4 / Aldol-condensation reaction”, for acetone systems, more aldol-condensation catalyst (NaOH) was required (1.80 moles of NaOH per mole of furan product) versus the catalyst loading for systems containing 1,4-Dioxane (1.17 moles of NaOH per mole of furan). This effect, potentially caused by the increase in the concentration of ions explains the difference in the contribution to the MFSP of the product of aldol-condensation catalyst in **Fig. 7.12**.

- ✓ Since almost no water is present in the recirculation loop for the acetone systems, the “solvent dilution effect” occurring for the studied “1,4-Dioxane systems” (Azeotrope: 82% Dioxane & 18% Water) is avoided for acetone systems. This positively reduces the required amount of solvent needed during the dehydration step to preserve the established acetone to aqueous solution volume ratio (1.75 or 1.5).

- ✓ When comparing the “acetone systems” to the “dioxane systems”, a lower flow of solvent required at the recirculation loop, not only represents a lower loss of acetone (fixed at 1% of the total solvent entering the distillation column), but also a lower mass

flow fed into the distillation tower. This, at the same time respresents a reduction in; the Reboiler Heat Duty, the Total Heat Demand of the plant, the demand for natural gas, the cost of area A600 Heat & Power (Power Boiler), the Total Capital Investment (TCI), and consequently, the contribution of the Average Return of Investment to the MFSP of the hydrocarbon blend.

- ✓ The power consumption from the grid increased for all four case studies using Acetone as a dehydration solvent. This can be explained due to the reduction in the Total Heat Demand of the plant for acetone systems. If less service steam is needed to satisfy the plant's demand, also less steam will pass through the Steam Turbine Generator and less power can be produced. Then, more power from the grid is required to satisfy the power demand of the plant.

- ✓ When comparing the "dioxane systems" to the "acetone systems", a substantial Total Capital Investment reduction is achieved when using acetone. This is mainly because of the reduction in the cost of area A600 Heat & Power (Power Boiler). Moreover, this variable is also partially influenced by the reduction in the flow passing through the aldol-condensation and the Hydrogenation units, as a result of the relocation of the distillation column for acetone systems.

- ✓ A maximum potential reduction on the MFSP of the final hydrocarbon product of $1.72/GGE (34% Reduction) from $5.12/GGE (Base Case – 1,4-dioxane) down to $3.40/GGE (Alternative Case #7 – acetone) was obtained from the case studies analyzed.

7.4.2. Sensitivity analysis results

A sensitivity analysis was developed using 76 variants, including 57 operating and 19 financial/economic variables for each case study analyzed. The sensitivity analysis results guided the development of the project from an early stage when the Base Case (1,4-Dioxane) (**Fig. 7.13**) was developed. This tool was successfully used to prioritize the team members' laboratory work and efforts. From the results obtained for the Base Case (1,4-Dioxane), the need to reduce the flow of water to the dehydration reactor was identified, and understood, and became the base to define Alternative Cases #2 to #8. As can be observed in the graphics presented in **Annex B** (1,4-Dioxane), the key process parameters to minimize the MFSP of the final hydrocarbon product were associated mainly with the sugar content entering the dehydration reactor (better said water content in this stream), and different variables associated with the organic co-solvent used during the dehydration (solvent volume ratio, loss of solvent, etc.). After implementing the modifications associated with the organic solvent used for the dehydration reaction and as can be observed in the sensitivity analysis results for Alternative Cases #5 to #8, especially from the results in Alternative Case #7 (**Fig. 7.14**), we can conclude that a new variable raised in importance to minimize the MFSP of the final product; NaOH dosage during the aldol-condensation reaction. From the presented results we propose further work oriented in finding a catalyst for the aldol-condensation reaction that can be easily recovery and reused (solid base catalysts, etc.). This is to address an opportunity to further reduce the estimated MFSP of the produced hydrocarbon blend.

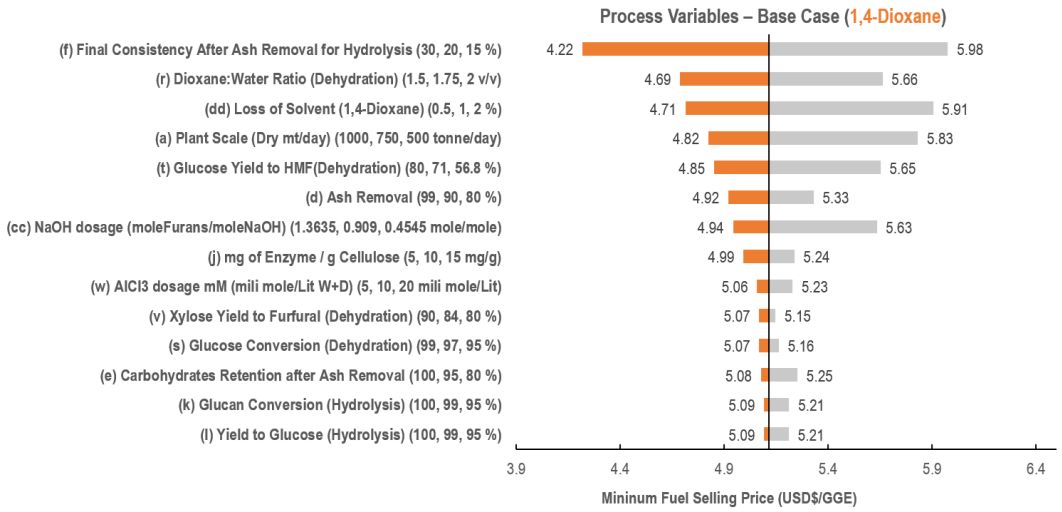

Fig. 7.13. Sensitivity analysis results for process variables – base case (1,4-dioxane).

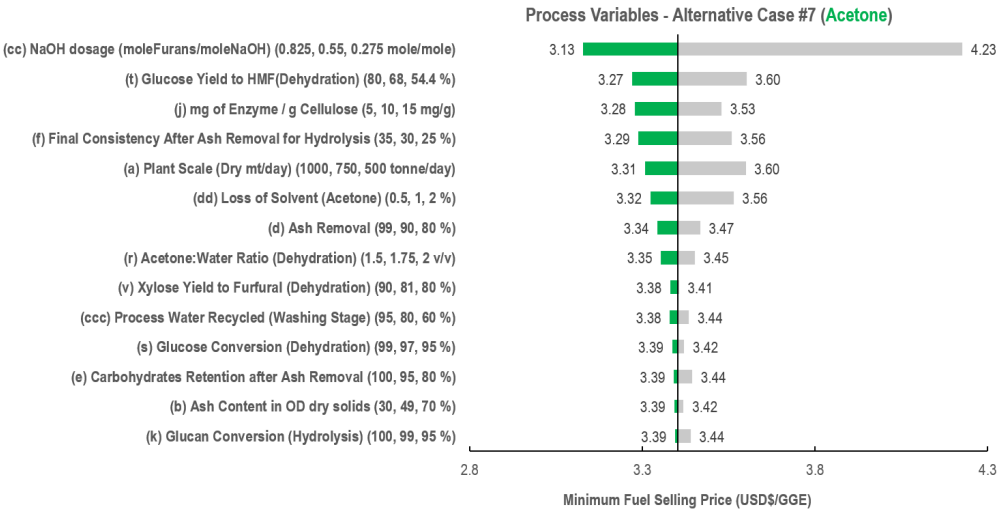

Fig. 7.14. Sensitivity analysis for process variables – alternative case #7 (acetone).

7.5. Conclusions

Under the studied conditions, which include the configuration of the compared biorefineries, financial and economic parameters, along with the experimental and simulation results, it was found that the use of acetone during the dehydration of glucose and xylose can lead to a more competitive minimum fuel selling price (MFSP) for the final hydrocarbon blend product obtained from the catalytic transformation of carbohydrates in paper sludge, compared to systems using 1,4-dioxane. This is observed even when the total production is lower in the studied acetone systems (~1MM GGE difference). The primary driver for the presented results lies in the reduced mass flow running across the distillation circuit and subsequent process units when acetone is employed, which

reduces not only the operational expenditure but, more representatively, a decrease in the overall capital investment for the biorefinery.

References

1. Ryan Davis, Nicholas Grundl, Ling Tao, Mary J. Biddy, Eric C. D. Tan, Greg T. Beckham, David Humbird, David N. Thompson, and Mohammad S. Roni (2018). Process Design and Economics for the Conversion of Lignocellulosic Biomass to Hydrocarbon Fuels and Coproducts: 2018 Biochemical Design Case Update. NREL/TP-5100-71949.
2. R. Davis, L. Tao, C. Scarlata, and E.C.D. Tan (2015). Process Design and Economics for the Conversion of Lignocellulosic Biomass to Hydrocarbons: Dilute-Acid and Enzymatic Deconstruction of Biomass to Sugars and Catalytic Conversion of Sugars to Hydrocarbons. NREL/TP-5100-62498
3. Hui Chen, Richard Venditti, Ronalds Gonzalez, Richard Phillips, Hasan Jameel, Sunkyu Park (2014). Economic evaluation of the conversion of industrial paper sludge to ethanol. Energy Economics 44, 281-290.
4. Guiyan Zang, Ajay Shan, and Caixia Wan (2020). Techno-economic analysis of co-production of 2,3-butanediol, furfural, and technical lignin via biomass processing based on deep eutectic solvent pretreatment. Biofuels, bioproducts and biorefinery. Volume 14, Issue 2, 326-343.
5. Bruno Klein, Ian McNamara, Ryan Davis, Ashutosh Mittal, and David Johnson (2021), Techno-Economic Assessment for the Production of Hydrocarbon Fuels via Catalytic Upgrading of Furans. NREL/TP-5100-80652.
6. U.S. Energy information administration - https://www.eia.gov/
7. U.S. Bureau of labor statists - https://data.bls.gov/cgi-bin/srgate

Chapter 8: Life cycle assessment of sustainable aviation fuel derived from paper sludge

Converting waste paper sludge to sustainable aviation fuel (SAF) offers a unique opportunity to decarbonize the aviation sector while supporting a circular economy by diverting waste from landfills and enhancing material utilization efficiency. This study develops a life cycle assessment (LCA) for converting high-ash paper sludge to SAF in the U.S. using a catalytic sugar upgrading system that consists of ash removal, enzymatic hydrolysis, dehydration, aldol condensation, and hydroprocessing. The LCA study is coupled with a process simulation for an industrial-scale biorefinery based on experimental data. Our results reveal that the Global Warming Potential (GWP) is 38.5–44.9 gCO2eq MJ^{-1} SAF with acetone as a solvent, renewable fuel, and bio-based chemicals; this value is further reduced to 6.1–12.5 gCO2eq MJ^{-1} if ash is recycled and used for substituting cement. On the basis of treating 1 dry t paper sludge, producing SAF shows -814 to -866 kgCO2eq with ash utilization, lower than landfilling without landfill gas recovery (791 kgCO2eq) and with landfill gas recovery (-294 kgCO2eq).

8.1. Introduction

The aviation sector is a crucial industry contributing to the global economy.[1–4] It contributed US$1.7 trillion to the global Gross Domestic Product (GDP) and supported a total of 41.7 million jobs in 2020.[5] Global flights released 0.9 Gt CO_2 in 2019, which accounts for 12% of CO_2 emissions from all transportation sources.[6] Considering all aviation-related Greenhouse Gas (GHG) emissions and atmospheric processes (e.g., N_2O, water vapor, soot particles), the aviation sector contributed to around 1.1 $GtCO_2e$ global warming potential (GWP) in 2019.[7–9] Despite the adverse impacts of the COVID-19 pandemic on travel in recent years,[10] the demand for air transport is estimated to increase by 3% annually over the next 20 years.[5] There are many ongoing efforts to decarbonize the aviation industry to curb the increasing GHGs from air travel[3]. For example, the United Nations International Civil Aviation Organization (UN ICAO) adopted a global net-zero carbon emission target for the aviation sector by 2050.[11] The European Commission set a target to reduce GHG emissions by at least 55% by 2030.[12] The U.S. government recently launched the Sustainable Aviation Fuel (SAF) Grand Challenge aiming at supplying at least 3 billion gallons of SAF annually by 2030 and 35 billion gallons per year by 2050.[13] Among various SAF pathways, bio-based, drop-in SAFs is highly attractive as they do not need engine modification and use renewable resources.[14]

Previous studies have investigated SAF production from various biomass feedstocks[15] (e.g., sugar, starch, algae, and waste cooking oil) via different technologies[16] (e.g., Fischer-Tropsch (FT) synthesis, hydroprocessed esters and fatty acids (HEFA), alcohol-to-jet (ATJ)). Among various feedstocks, paper sludge is promising for SAF production.[17,18] Paper sludge is a waste material from pulp and paper mills. It mainly includes cellulose fibers, fines, and inorganic fillers.[19] Each year, more than 40 Mt of paper sludge are generated globally.[20–22] Common methods of treating paper sludge include landfilling,[23] incineration,[23] pelletizing,[19] and molding into fiber products.[19] To decarbonize industries and accelerate the transition towards a circular economy, upcycling paper sludge to value-added and low-carbon products has become more

pressing in recent years.[19] One option is converting paper sludge into SAF. Unlike other waste biomass streams, paper sludge typifies high ash content, around 10%–50%,[24] along with high moisture content, making it less desirable for thermochemical conversion processes.

Life cycle assessment (LCA) is a standardized tool to evaluate the environmental impacts of a product or a process throughout its life cycle.[25–27] LCA has been widely used to quantify the environmental impacts, especially the carbon intensity, of SAF[4,7,34–38,14,17,28–33] compared to their fossil-based counterparts. For example, Bhatt et al. quantified the life-cycle GHG emissions of SAF produced from waste and biomass feedstocks (i.e., used cooking oil, vegetable oil, fats, municipal solid waste, lignocellulosic biomass) via three technologies, namely HEFA, FT, and ATJ).[14] They found that compared to conventional aviation fuel, HEFA, FT, and ATJ can reduce the life-cycle GHG emissions by 60%–78%, 86%, and 67%, respectively.[14] De Jong et al. employed the LCA to compare the well-to-wake (WTWa) GHG emissions of multiple SAF conversion pathways (i.e., HEFA, FT, ATJ, Hydrothermal Liquefaction (HTL), pyrolysis, and Synthetic Isoparaffinic fuel (SIP)).[37] This study concluded that SAF produced via the FT pathway has the lowest life-cycle GHG emissions.[37] Puschnigg et al. conducted an LCA to analyze SAF converted from softwood residues by using a proposed pathway of enzymatic hydrolysis, fermentation, purification, oligomerization, and hydrogenation.[38] The results showed that the life-cycle GHG emissions ranged from 18.7 to 56 $gCO_2eq\ MJ^{-1}$, depending on the electricity sources and byproduct uses.[38]

Several LCA studies assessed different upcycling pathways for paper sludge to reach lower life-cycle GWP.[20,39–46] For instance, Mohammadi et al. quantified the life-cycle environmental impacts of two alternative anaerobic digestion approaches to processing paper sludge and reported lower life-cycle GWP of the anaerobic digestion pathways compared to traditional incineration and landfilling.[43] A comparative LCA study by Likon and Saarela revealed that producing sorbent material from paper sludge resulted in lower life-cycle carbon intensity compared to landfilling.[42] Few studies have estimated the life-cycle environmental impacts of SAF derived from high-ash paper sludge. Nor have they evaluated the corresponding environmental feasibility of the SAF compared with the fossil-based jet fuel, or the environmental performance of treating paper sludge via producing SAF compared with landfilling.

To address the knowledge gap, this study develops a cradle-to-grave LCA for drop-in SAF produced from carbohydrates in paper sludge in the U.S. The study proposes an integrated conversion process to efficiently deash the feedstock and catalytically upgrade carbohydrates in a pathway characterized by high ash and moisture tolerability, as well as moderate reaction conditions (e.g., lower temperature or pressure compared to thermochemical conversion or hydrothermal liquefaction). In this study, the mass and energy balance needed by the LCA is generated by process models which are substantiated by optimized performance from experimental work. A set of scenarios are assessed to explore factors such as solvent and fuel choices, incorporation of bio-based chemicals, waste recycling, and solvent load. A sensitivity analysis is conducted to identify key drivers influencing the results. This research introduces a technically feasible

and environmentally friendly method for converting high-ash paper sludge into valuable energy products. The study identifies areas for improvement and provides valuable insights to decision-makers in the pulp and paper and aviation sectors.

8.2. Methods and materials

As summarized in **Figure 8.1**., the paper sludge-to-SAF process encompasses ash removal, enzymatic hydrolysis, dehydration, aldol condensation, and hydroprocessing. In this study, the life cycle inventory (LCI) data of the biorefinery is derived from the mass and energy balance information from the process simulation model built in Aspen Plus™ (Version 11), as shown in **Figure 8.2**. With a daily processing capacity of 750 dry t of paper sludge, the drop-in SAF biorefinery mainly consists of five areas, including pretreatment and ash removal, enzymatic hydrolysis, dehydration and aldol condensation, upgrading, and combined heat and power (CHP) plant. The sections below describe the designed processes, process simulation, LCA, scenario analysis, and sensitivity analysis.

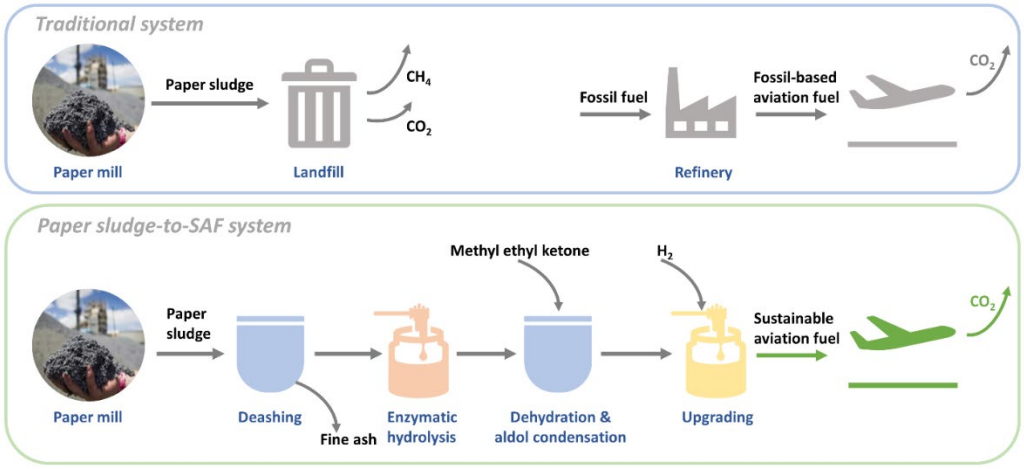

Fig. 8.1. A simplified system diagram of the systems.

8.2.1. Feedstock characterization

The high-ash paper sludge is used as the feedstock for the biorefinery. The compositions of a paper sludge sample collected from a paper mill in the U.S. was analyzed by the U.S. National Renewable Energy Laboratory (NREL).[47] The sample contained 37.7% glucan, 9.3% xylan, 3.8% mannan, 4.0% lignin, and 49.0% ash. The moisture content of paper sludge fed in the biorefinery is 50% (*w.b.*).

8.2.2. Process simulation of the biorefinery

8.2.2.1. Pretreatment and ash removal

After the paper sludge feedstock arrives at the biorefinery, it is fed into the hydrapulper to agitate the slurry to a 3% consistency.[48] Since high ash content in paper sludge can largely reduce the conversion rate in enzymatic hydrolysis, ash removal is essential.[24,49,50] The side-hill screen uses 0.5 mm mesh to deash the pulp from the hydrapulper. The deashing process is simulated based on the results of the pilot-scale experiment conducted by authors. The ash removal rate is 90% with a 95% carbohydrate retention

rate. The reject stream that has a high ash content is then dewatered to separate the ash cake and wastewater.[51] Researchers have previously investigated the possibility of

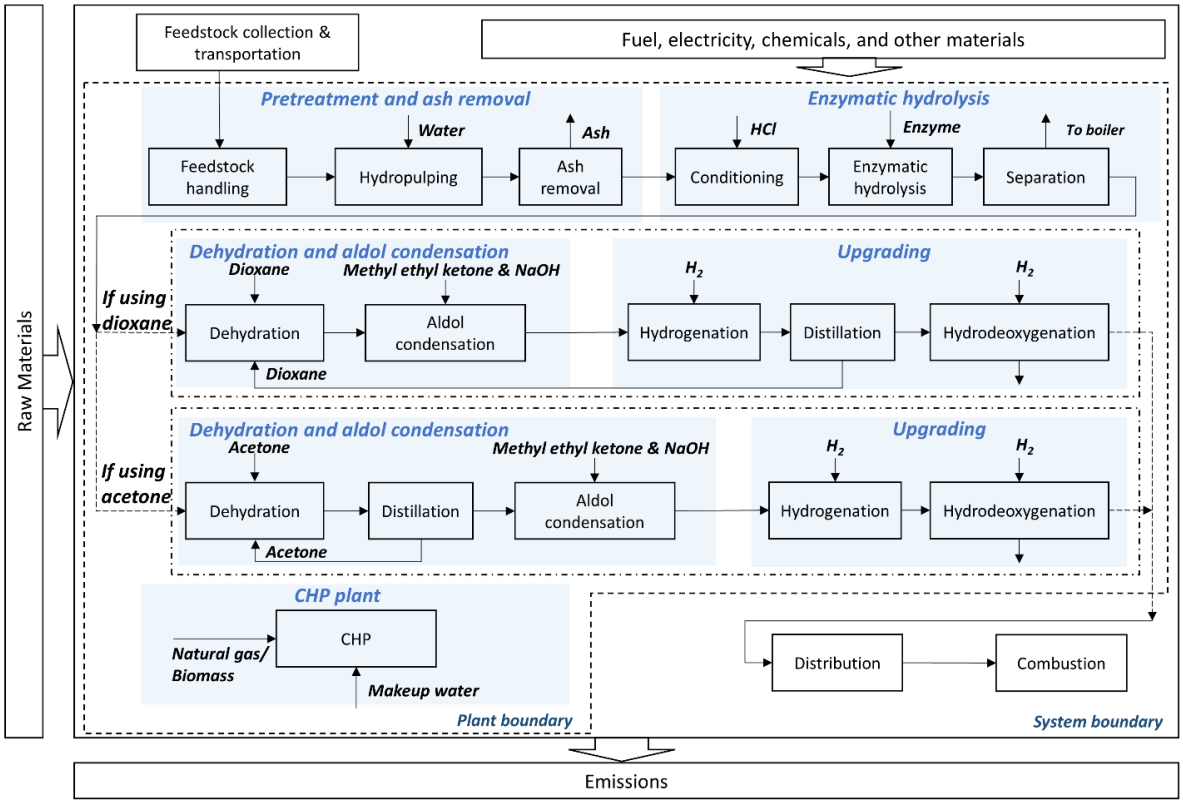

Fig. 8.2. The system boundary of Life Cycle Assessment and the flow diagram of the biorefinery.

Recycling the fine ash generated during the ash removal process to replace traditional cement mortar.[52–55] The potential advantages of this recycling approach are explored by modeling the benefits of using the removed ash as a substitute for U.S. cement, as compared to sending it to a landfill.

8.2.2.2. Enzymatic hydrolysis

The deashed paper sludge is then sent to the enzymatic hydrolysis process step to convert cellulose and hemicellulose to monosaccharides.[49,56] Before enzymatic hydrolysis, the stream is conditioned by adding HCl at a load of 7.3 mg per g dry deashed sludge.[24] Two different consistency cases for enzymatic hydrolysis, 20% and 30%, are explored in this study, (see Section Scenario Analysis). The enzymatic hydrolysis is performed at 50 °C for 96 h starting at pH 4.8 which is adjusted by adding HCl. The cellulase used in this study is Cellic® CTec2 from Novozymes, USA at the load of 10 mg (5 filter paper units (FPU)) per oven dry g cellulose.[24] The conditions, material loads, and conversion rates are based on the authors' previous experimental work.[24] The reactions and conversion rates used in the simulation are shown in **Table 8.1**. At the end of the hydrolysis process, the suspended solids are separated with a filter press.

8.2.2.3. Dehydration and aldol condensation

In the dehydration reaction, the sugars (i.e., pentoses and hexoses) in the hydrolysate are converted to furans as the intermediates, including 5-hydroxymethylfurfural (HMF) and furfural.[57] In order to achieve a high yield of furan, the presence of an organic solvent is required. In this study, two different solvents (i.e., dioxane, acetone) and varied volume ratios of organic solvent to aqueous hydrolysate (i.e., 1.50, 1.75) are explored to understand the life-cycle environmental impacts of the final products (see Section Scenario Analysis). The dehydration process is catalyzed by a Lewis acid catalyst, $AlCl_3$.[58] The hydrolysate is first mixed with the solvent and catalyst and then heated to 190 °C at 14.6 atm. The $AlCl_3$ is added to achieve a 10 mM concentration.[59] Three sugar concentration levels are explored to investigate the impacts of different solvent loads on the results, namely 20%, 30%, and 40% (see Section Scenario Analysis).[58] Then the stream is sent to a reactor for dehydration for 5 min. The main reactions and conversion rates in the dehydration process are shown in **Table 8.1**.

After dehydration, the stream that contains furans and sugars is cooled to 60 °C and its pressure is reduced to 1 atm before aldol condensation. For aldol condensation, this study selects methyl ethyl ketone (MEK) as the reactant and NaOH as the catalyst.[58] MEK reacts with furans to form aldol monoadducts (one MEK molecule reacts with one furan molecule) and aldol diadducts (one MEK molecule reacts with two furan molecules). MEK is loaded at a 5% excessive rate; NaOH is kept at the level of 1.81 mol per 1 mol total furfurals for dioxane cases and 1.10 mol per 1 mol total furfurals for acetone cases. The aldol condensation is conducted for 50 minutes to ensure that furans are converted to aldol condensates. The reactions and conversion rate used in this study are displayed in **Table 8.1**.

Since the aldol condensation process uses a large amount of solvent, it is necessary to recover the solvent to minimize chemical waste. The order of solvent recovery by distillation varied for the two different solvents explored, as shown in **Figure 8.2.** In the dioxane system, the distillation column was placed after the hydrogenation reaction. On the other hand, the distillation column was placed after the dehydration reaction in the acetone system. This is because acetone is expected to undergo aldol-condensation reactions, competing with the desired condensation reactions of MEK and reducing the yield of final hydrocarbon products. Hence, to avoid acetone becoming involved with aldol-condensation, the distillation to recover acetone is needed before aldol-condensation. The distillations were set to recover 99.0% of dioxane and 98.0% of acetone respectively. Under this condition, a purity of 76.6% (near the azeotropic concentration ~80.2% w/w) for the product at the top of the distillation column is predicted for dioxane scenarios, and around 98.0% purity estimated for the acetone scenarios. For the dioxane scenarios, the bottom stream was ducted to the decanter to separate the heavy condensates (aldol monoadducts and diadducts) from the aqueous phase. The heavy condensates were then transported to be upgraded to hydrocarbons.

8.2.2.4. Upgrading

To generate the final hydrocarbons, hydrodeoxygenation is conducted with a Pd catalyst at 300 °C and 98.7 atm.[58] In this study, H_2 is loaded at a 5% excessive rate. This study also assumes that all condensates are hydrotreated to form the final paraffin. The

reactions are shown in **Table 8.1**. The outlet stream of hydrodeoxygenation goes through pressure swing adsorption to recover H_2 at a 95% recovery rate.[58]

8.2.2.5. CHP

To meet the heat demand and power consumption of the biorefinery, a CHP plant is deployed to produce heat and power. The design of the CHP plant follows the U.S. DOE fact sheets for a medium-size CHP plant.[60] The CHP boiler generates high-pressure steam at 42 atm and 302 °C with an 80% boiler efficiency.[60] The final outlet steam after power generation is 11 atm and 185 °C.[60] Two fuel sources are included: natural gas and wood-residue-derived pellets.

Table 8.1. Main reactions and conversion rate used in this study.

Process	Reactions	Conversion rate in dioxane cases	Conversion rate in acetone cases
Enzymatic hydrolysis	$(Glucan)_n + n\ H_2O \rightarrow n\ Glucose$	99%	
	$(Xylan)_n + n\ H_2O \rightarrow n\ Xylose$	99%	
Dehydration	$Glucose \rightarrow HMF + 3\ H_2O$	69%	66%
	$Xylose \rightarrow Furfural + 3\ H_2O$	80%	79%
Aldol condensation	$HMF + MEK \rightarrow HMF\text{-}MEK + H_2O$	95%	
	$2HMF + MEK \rightarrow HMF\text{-}MEK\text{-}HMF + 2\ H_2O$	4%	
	$Furfural + MEK \rightarrow Furfural\text{-}MEK + H_2O$	95%	
	$2\ Furfural + MEK \rightarrow Furfural\text{-}MEK\text{-}Furfural + 2\ H_2O$	4%	
Hydrotreating	$HMF\text{-}MEK + 8\ H_2 \rightarrow C_{10}H_{22} + 3\ H_2O$	70%	
	$HMF\text{-}MEK\text{-}HMF + 14\ H_2 \rightarrow C_{16}H_{34} + 5\ H_2O$	70%	
	$Furfural\text{-}MEK + 7\ H_2 \rightarrow C_8H_{20} + 2\ H_2O$	70%	
	$Furfural\text{-}MEK\text{-}Furfural + 12\ H_2 \rightarrow C_{14}H_{30} + 3\ H_2O$	70%	

8.2.3. Life cycle assessment

A cradle-to-grave LCA (or well to wake[4,61]) was conducted following ISO Standard 14040 series[62,63] to evaluate the life-cycle environmental impacts of the drop-in jet fuel produced from paper sludge. The system boundary is displayed in **Figure 8.2**, including paper sludge collection and transportation, production, distribution, and combustion. The upstream burdens of producing chemicals, materials, fuels used in foreground processes, and fuel combustion are included. The functional unit is 1 MJ of biofuel produced which is a common functional unit used in LCA studies of SAF.[25,37] To compare the results of different end-of-life (EOL) treatment methods of paper sludge, another functional unit 1 dry t paper sludge basis is included.

The LCI data of the foreground processes in the biorefinery was generated from the process simulation model described above. The LCI data of background processes,

including upstream production and fuel combustion, were obtained from literature,[64] the ecoinvent cut-off 3.7 database,[65] and GREET 2022.[66] The ecoinvent processes used in this study are listed in Supporting Information Table S8.1. In this LCA study, the upstream burdens of generating the paper sludge are cut-off.[67] The cradle-to-gate life-cycle environmental impacts of bio-based MEK were evaluated based on the study by Klein et al.[58] and the ecoinvent cut-off 3.7 database.[65] The GHG emissions of the distribution and combustion of the produced jet fuel follow GREET 2022 values.[66]

To understand the environmental impacts of conventional waste treatment methods, the GHG emissions of landfilling paper sludge (mainly CH_4 and CO_2) were modeled following the Intergovernmental Panel on Climate Change (IPCC) First Order Decay (FOD) method for the 100-year decay process (see Supporting Information Section 1 and Table S8.2 for details).[68] Landfill gas (LFG) recovery is becoming increasingly popular in the U.S., according to the Landfill Methane Outreach Program by the U.S. EPA,[69] given the high energy value and climate change contribution of CH_4 (non-fossil CH_4 contributes 27 times as high as CO_2 to global warming based on GWP-100 factor).[69,70] With this in mind, we include two counterfactual scenarios: landfilling paper sludge with and without LFG recovery to explore how this would affect landfilling.

For life cycle impact assessment (LCIA), this study adopts GWP-100 factors from the IPCC AR6 report (fossil CO_2 1.0, fossil CH_4 29.8, non-fossil CH_4 27.0, N_2O 273.0) and TRACI 2.1 by the U.S. Environmental Protection Agency (US EPA) to assess other life-cycle environmental impacts of the SAF produced from paper sludge.[71,72] The LCIA impact categories include GWP, acidification, human health-carcinogenics, human health-non-carcinogenics, eutrophication, fossil fuel depletion, ozone depletion, smog formation, ecotoxicity, and respiratory effects.[71,72] The biogenic and fossil-based carbon flows in the system are tracked separately based on the sources of materials and fuels used.

8.2.4. Scenario analysis

In this study, 4 scenarios and 28 cases were established to explore the impacts of different enzymatic hydrolysis consistency levels, solvent-to-hydrolysate ratios, sugar concentrations in dehydration, fuel sources, fossil or bio-based MEK, and ash utilization. **Table 8.2** displays the scenario settings for the combination of the scenarios. As mentioned in Section 2.2., Scenarios 1–4 describe the various combinations of enzymatic hydrolysis consistency levels, solvent-to-hydrolysate ratios, and sugar concentrations in dehydration. In each scenario, wood pellets (denoted as “W”) are selected as the alternative fuel source for the CHP plant for decarbonization purposes and compared with natural gas (denoted as “N”). For the solvent, as discussed in Section 2.2.3., acetone (denoted as “A”) is chosen to compare with dioxane (denoted as “D”). Since a part of the carbon in produced SAF is originally from MEK, this study also explores two cases related to carbon sources, namely fossil-based MEK (denoted as “F”) and bio-based MEK (denoted as “B”). Finally, to discover the impact of utilizing the separated ash to substitute cement, another case of ash utilization is added (denote as “U”).

Table 8.2. Scenario settings.

Scenarios*	Fuel source (W or N)	Solvent (D or A)	Fossil- or bio-based MEK (F or B)	Ash utilization (U)	Solvent : hydrolysate	Enzymatic hydrolysis consistency	Sugar concentration in dehydration
1-NDF	Natural gas	Dioxane	Fossil-based MEK	No	1.75	20%	20%
2-NDF					1.5	20%	20%
3-NDF					1.75	30%	30%
4-NDF					1.75	20%	40%
1-NAF		Acetone	Fossil-based MEK		1.75	20%	20%
2-NAF					1.5	20%	20%
3-NAF					1.75	30%	30%
4-NAF					1.75	20%	40%
1-WDF	Wood pellets	Dioxane	Fossil-based MEK	No	1.75	20%	20%
2-WDF					1.5	20%	20%
3-WDF					1.75	30%	30%
4-WDF					1.75	20%	40%
1-WAF		Acetone	Fossil-based MEK		1.75	20%	20%
2-WAF					1.5	20%	20%
3-WAF					1.75	30%	30%
4-WAF					1.75	20%	40%
1-WDB	Wood pellets	Dioxane	Bio-based MEK	No	1.75	20%	20%
2-WDB					1.5	20%	20%
3-WDB					1.75	30%	30%
4-WDB					1.75	20%	40%
1-WAB		Acetone	Bio-based MEK		1.75	20%	20%
2-WAB					1.5	20%	20%
3-WAB					1.75	30%	30%
4-WAB					1.75	20%	40%
1-WABU	Wood pellets	Acetone	Bio-based MEK	Yes	1.75	20%	20%
2-WABU					1.5	20%	20%
3-WABU					1.75	30%	30%
4-WABU					1.75	20%	40%

* In scenario names, W or N stands for wood pellets or natural gas; D or A stands for dioxane or acetone; F or B stands for fossil-based or bio-based MEK; U stands for ash utilization.

8.3. Results and discussion

8.3.1. Life-cycle GWP of 1 MJ hydrocarbon product

Figure 8.3 shows the life-cycle GWP of 1 MJ SAF produced from paper sludge in 20 cases (i.e., NDF, WDF, WAF, WAB, and WABU). The results of the other 8 cases and the source data of **Figure 8.3** are available in Supporting Information Table S8.3 due to a similar trend. The diamond markers record the total cradle-to-grave GWP. The negative values represent the biogenic carbon in the biofuel produced from either the paper sludge or bio-based MEK, and the potential substitution benefits for utilizing paper sludge ash. The mass and energy balances of scenarios are available in Supporting Information Section 2 and Table S8.4.

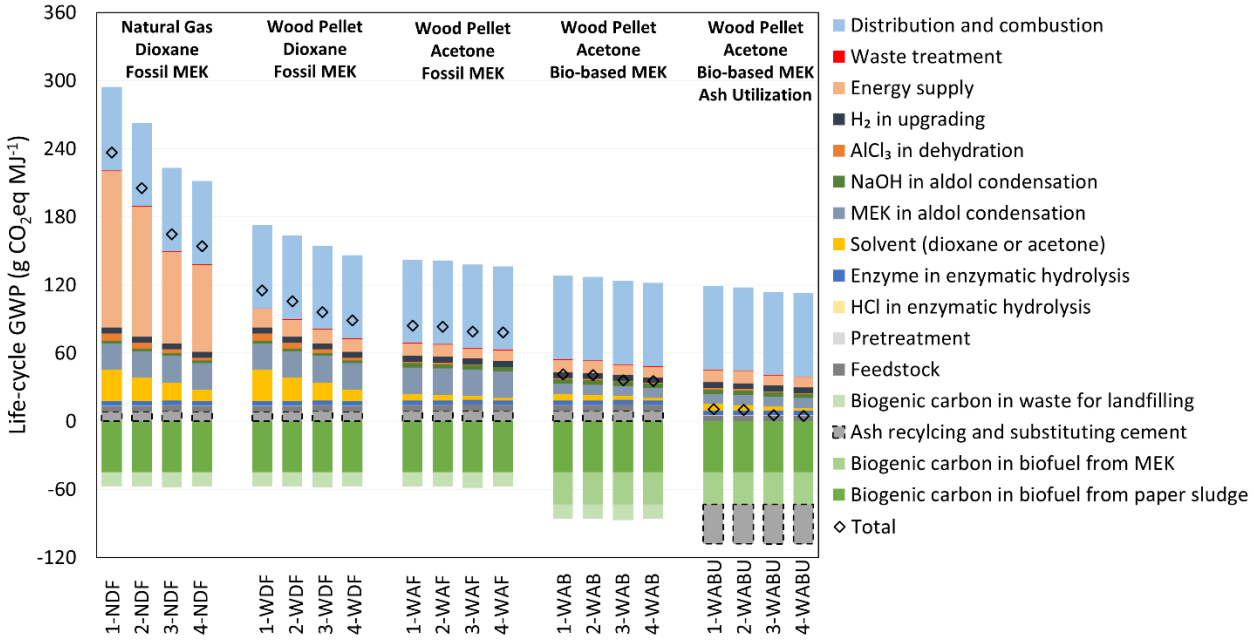

Figure 8.3. Life-cycle Global Warming Potential of 1 MJ of SAF produced from paper sludge.

Figure 8.3 identifies a road map for reducing the GWP of paper-sludge-derived SAF by changing energy sources, solvents, chemicals, waste treatment, and operational conditions. The four natural gas-powered scenarios with dioxane and fossil-based MEK (NDF scenarios) show the largest life-cycle GWP (154.4–237.1 $gCO_2eq\ MJ^{-1}$). In NDF scenarios, the largest GHG emission source is the energy supply (including fuel consumption for the CHP plant and electricity consumption). Across NDF scenarios in **Figure 8.3**, energy supply contributes 76.6–137.8 $gCO_2eq\ MJ^{-1}$. Moving from Scenario 1 to Scenario 4 results in a reduction of natural gas consumption (see Supporting Information Table S8.4) due to the lower heat demand of the distillation process caused by the lower solvent to hydrolysate ratio (see Supporting Information Table S8.4 for LCI data). Another plausible way to reduce GHG emissions is fuel switching. Switching to wood pellets decreases the GWP from the energy supply to 11.2–16.5 $gCO_2eq\ MJ^{-1}$ in WDF scenarios, representing 12.6% to 14.3% of the total life cycle GHG emissions (89.1–115.8 $gCO_2eq\ MJ^{-1}$), leaving dioxane solvent (10.4–27.9 $gCO_2eq\ MJ^{-1}$) and MEK (23.3 $gCO_2eq\ MJ^{-1}$) as the main contributors.

Replacing dioxane with acetone in WAF scenarios resulted in further reductions in GWP to 78.6–84.7 $gCO_2eq\ MJ^{-1}$. This reduction is majorly contributed by two aspects. One aspect is that changing to acetone reduces the GWP of the energy supply to 9.2–10.7 $gCO_2eq\ MJ^{-1}$ in WAF scenarios because 1) the solvent load of acetone is smaller than dioxane (see Supporting Information Table S8.4); 2) the heat demand of processing acetone is lower due to reduced stream mass for distillation. The other aspect is that the GWP by the solvent is reduced to 2.2–5.9 $gCO_2eq\ MJ^{-1}$, because carbon intensity of producing 1 kg acetone is lower than 1 kg dioxane.[65]

Another option for reducing the GWP of produced SAF is using bio-based MEK, resulting in 35.7–41.8 $gCO_2eq\ MJ^{-1}$ in WAB scenarios. This reduction is mainly due to the biogenic carbon in biofuel from bio-based MEK (-28.4 $gCO_2eq\ MJ^{-1}$) and the relatively lower GWP of bio-based MEK (8.9 $gCO_2eq\ MJ^{-1}$ compared to 23.3 for fossil-based MEK). In this study, the carbon in SAF has two sources, MEK, and HMF and furfural converted from cellulose and hemicellulose. In the aldol condensation process, HMF and furfural react with MEK to form compounds hydrotreated into SAF. Hence, all the carbon in SAF is biogenic when bio-based MEK is used. In the case of fossil-based MEK, a portion of the carbon in SAF is originally fossil-based. As shown in **Figure 8.3**, across the scenarios, the biogenic carbon in biofuel from paper sludge is -44.7 $gCO_2eq\ MJ^{-1}$. For WAB scenarios, there is additional biogenic carbon from bio-based MEK, -28.4 $gCO_2eq\ MJ^{-1}$. Once we proceed to the SAF combustion stage, the biogenic carbon in SAF is released. The distribution and combustion of SAF (light blue bars) contribute a GWP of 73.4 $gCO_2eq\ MJ^{-1}$, with distribution accounting for only 0.3 $gCO_2eq\ MJ^{-1}$. Hence, with bio-based MEK in WAB scenarios, the biogenic carbon uptake from paper sludge and bio-based MEK nearly cancels out the combustion GHG emissions.

Further recycling ash to substitute cement, as exhibited in WABU scenarios, results in the lowest GWP of SAF, 5.1–11.1 $gCO_2eq\ MJ^{-1}$. Using fine ash in place of cement could reduce the GWP by 30.7 $gCO_2eq\ MJ^{-1}$, highlighting the potential benefits of utilizing ash when producing low-carbon SAF. It is worth noting that the results of WABU scenarios highly rely on the system expansion method and the assumption of substituting carbon-intensive cement material. In the scenarios without ash utilization (i.e., NDF, WDF, WAF, WAB), a portion of paper sludge is sent to the landfill along with ash from the ash removal and filter press processes in the pretreatment stage. This portion of biogenic carbon in waste for landfilling (-13.1– -14.0 $gCO_2eq\ MJ^{-1}$) is managed through a landfill gas recovery process to capture a portion of generated methane from decomposed carbon. The remaining undecomposed biogenic carbon remains at the landfill site after 100 years. Overall, the lowest GWP of 1 MJ of SAF is obtained under WABU scenarios (5.1–11.1 $gCO_2eq\ MJ^{-1}$). Without ash recycling, the lowest GWP is under WAB scenarios, 35.7–41.8 $gCO_2eq\ MJ^{-1}$. Compared to traditional petroleum jet fuel (estimated at 84.5 $gCO_2eq\ MJ^{-1}$),[36,66] the carbon intensity reduction is 86.8%–94.0% for WABU scenarios and 50.6%–57.7% for WAB scenarios. Since the feedstock is paper sludge, there are no environmental impacts from land use changes. According to the U.S. EPA Renewable Fuel Standard (RFS) program, qualified jet fuels need to achieve a 60% GHG emission reduction compared to the traditional baseline fuels.[73] This target can be achieved by WABU scenarios, indicating the importance of incorporating renewable energy resources, biochemicals, proper solvent selection, and waste recycling into SAF production. It is worth noting that, the cradle-to-grave GWP of WAB and WABU scenarios (5.1–41.8 $gCO_2eq\ MJ^{-1}$) in this study is comparable with the SAF produced by other feedstocks (e.g., used cooking oil, willow, corn stover, forest residues) via different pathways (e.g., HEFA, FT, HTL, pyrolysis, ATJ) (0–75 $gCO_2eq\ MJ^{-1}$ when using system expansion method).[37]

Additionally, in 2022, the U.S. published the Inflation Reduction Act that sets the requirement of “at least a 50 percent lifecycle greenhouse gas emissions reduction in

comparison with petroleum-based jet fuel" for SAF to earn the $1.25 per gallon incentive and a supplementary incentive of $0.01 per gallon for "each percentage point by which the lifecycle greenhouse gas emissions reduction percentage with respect to such fuel exceeds 50 percent" (not exceeding $0.5).[74] WAB and WABU meets the life cycle GHG reduction targets.

8.3.2. Life-cycle environmental impacts of 1 MJ hydrocarbon product

Figure 8.4 shows the normalized life-cycle environmental impacts of 1 MJ biofuel produced from paper sludge in 20 cases (i.e., NDF, WDF, WAF, and WAB). The normalization base is the maximum value for each environmental impact category among 28 cases. The detailed values of **Figure 8.4** and the other 8 cases are available in Supporting Information Tables S8.5 and S8.6.

Across all scenarios in **Figure 8.4**, WDF-1 has the highest impacts in all categories except GWP and fossil fuel depletion. Compared to NDF scenarios, using wood pellets for the CHP plant yields a 41.5%–59.3% reduction in GWP and fossil fuel depletion but substantially increases other impact categories, particularly in non-carcinogenic human health which shows a 155.0%–230.3% surge. This is caused by the higher combustion emissions from wood pellets, such as volatile organic compounds and trace contaminants. In NDF and WDF scenarios, transitioning from Scenario 1 to Scenario 4 results in reduced environmental impacts across all impact categories, attributable to the diminished input of dioxane and decreased fuel consumption in the CHP plant.
Upon substituting the dioxane with acetone, a reduction in environmental impacts is observed across all impact categories due to: 1) the acetone load is less than dioxane; 2) acetone has lower environmental impacts in 10 categories than dioxane; 3) the fuel consumption in the CHP is decreased in the acetone scenarios. In WAF scenarios, Scenario WAF-3 exhibits the lowest life-cycle environmental impacts in acidification, ecotoxicity, non-carcinogenic human health, ozone depletion, and smog formation, whereas Scenario WAF-4 presents the lowest impacts in the remaining categories. This result stems from the trade-off between solvent usage (higher in Scenario WAF-3 than WAF-4) and fuel consumption (lower in Scenario WAF-3 than WAF-4).

Using bio-based MEK in WAB scenarios leads to 0.2% to 59.0% reduction in acidification, carcinogenic human health, fossil depletion, GWP, and smog formation compared to WAF scenarios, while ecotoxicity, eutrophication, non-carcinogenic human health, ozone depletion, and respiratory effects experience increases of 0.6% to 35.9%. Further recycling ash in WABU scenarios lowers the environmental impacts by 7.4%–85.8% compared to WAB scenarios. Finally, the normalized environmental impact results (percentage basis shown in **Figure 8.4**) for WAB scenarios range from 2.1% to 81.4% across the various impact categories, where GWP reaches the lowest results of 2.1% to 4.7%.

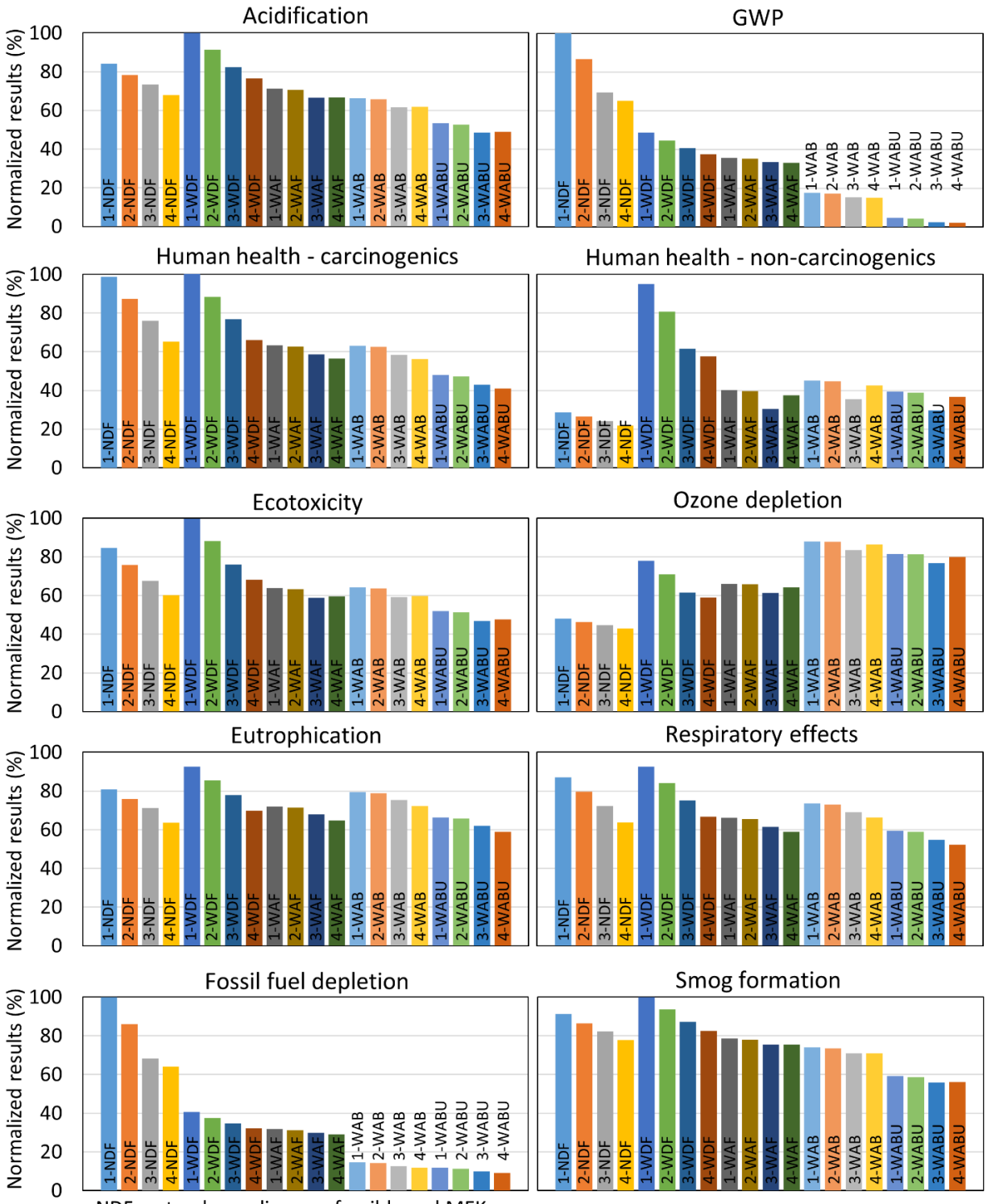

NDF: natural gas, dioxane, fossil-based MEK
WDF: wood pellets, dioxane, fossil-based MEK
WAF: wood pellets, acetone, fossil-based MEK
WAB: wood pellets, acetone, bio-based MEK
WABU: wood pellets, acetone, bio-based MEK, ash utilization

Fig. 8.4. Normalized life-cycle environmental impacts of 1 MJ produced from paper sludge.

8.3.3. Life-cycle GWP of treating paper sludge in different methods

To understand the climate implications of different waste paper sludge treatment methods, this study compares the life-cycle environmental impacts of converting 1 dry t of paper sludge to SAF with current practices, conventional landfilling, and landfilling with landfill gas recovery. **Figure 8.5** shows the life-cycle GWP of treating paper sludge in 20 cases (i.e., NDF, WDF, WAF, WAB, WABU) compared to two landfilling methods. The source data of **Figure 8.5** and the other 8 cases are available in Supporting Information Table S8.7. Since the basis is treating 1 dry t paper sludge, the potential substitution benefit of biofuel (substituting fossil fuels) is listed (dark gray bars) using the system expansion method. Hence, the total life-cycle GWP of WAF, WAB, and WABU scenarios has negative values.

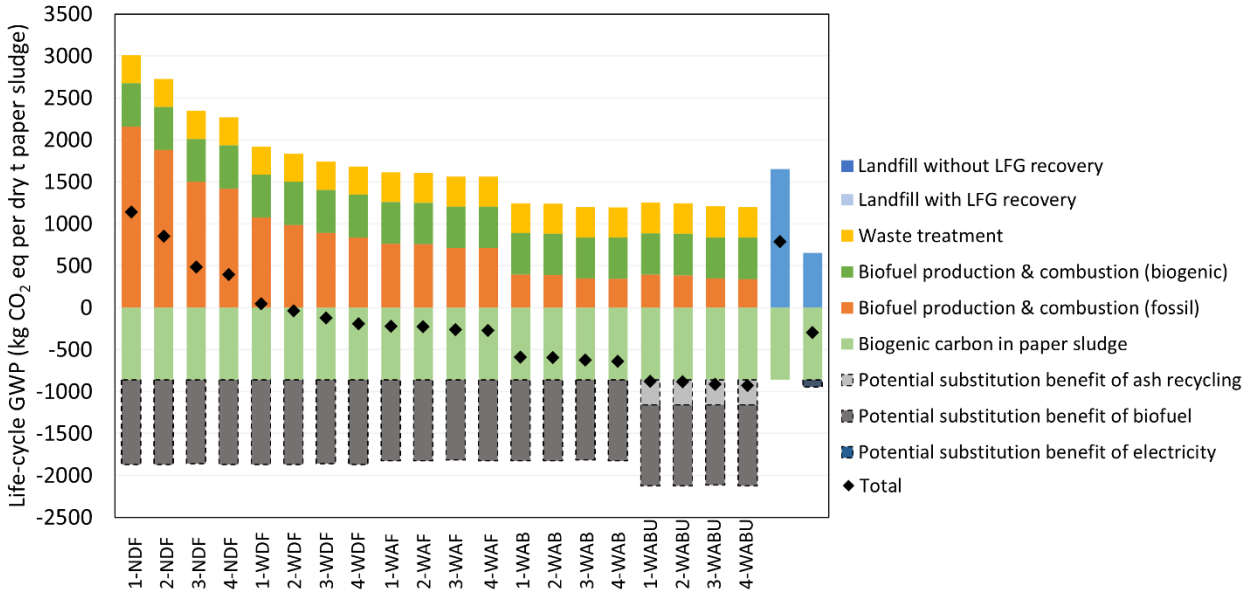

Fig. 8.5. Life-cycle Global Warming Potential of treating 1 dry t of paper sludge. The diamonds show the net total GWP.

As depicted in **Figure 8.5**, landfilling 1 dry t of paper sludge without LFG recovery culminates in the life-cycle GWP value of 791 $kgCO_2eq$. This is predominantly due to the release of methane that possesses a high GWP-100 factor of 27.0. In the landfilling scenario without LFG recovery, the biogenic carbon sequestered in the paper sludge (-860 $kgCO_2$ eq) is partially released as methane (18% of sequestered carbon in paper sludge) and CO_2 (19% of sequestered carbon in paper sludge) with the rest 63% remaining in the landfill site after 100 years. Hence, with the high GWP-100 factor of methane, landfilling paper sludge without LFG recovery shows relatively high GWP results. However, when LFG recovery is implemented for electricity generation, the net life-cycle GWP is reduced to -294 $kgCO_2$ eq per 1 dry t treated paper sludge due to avoided emissions from substituting grid electricity and recovering 75% of the methane in LFG.

In the SAF scenarios, the biogenic carbon sequestered in the paper sludge is released by combusting SAF (dark green bars) and the waste generated by the biorefinery (gold bars). The lowest GWP appears in WABU Scenarios, ranging from -873 to -925 $kgCO_2eq$ per dry t paper sludge fed in. Scenario 4-WABU reduces 1,716 $kgCO_2eq$ from landfilling without LFG recovery and 630 $kgCO_2eq$ from landfilling with LFG recovery when treating 1 dry t paper sludge. The comparative findings of other SAF cases in **Figure 8.5** are consistent with the 1 MJ basis results displayed in **Figure 8.3**. The highest GWP is observed in Scenario 1-NDF (1,140 $kgCO_2eq$). The GWP decreases to -215– -267 $kgCO_2eq$ in WAF scenarios and -584– -636 $kgCO_2eq$ in WAB scenarios. Hence, all SAF scenarios show lower GWP than landfilling without LFG recovery except Scenario 1-NDF and 2-NDF; WAB and WABU scenarios achieve lower GWP than landfilling with LFG recovery. The potential substitution benefits of biofuel to fossil fuels are substantial, 958–1009 $kgCO_2eq$ per dry t paper sludge. In WABU scenarios, the potential substitution benefit of ash utilization is -298 $kgCO_2eq$. In the U.S., there are more than 4 million dry t paper sludge generated every year. This can yield more than 33 million gallons of SAF, resulting in 2.4 to 6.7 million tCO_2eq GWP reduction annually.

8.3.4. Sensitivity analysis

To investigate the effects of parameter variability on the results, a sensitivity analysis is conducted. The variability ranges for the parameters are either sourced from existing literature or assumed (see Supporting Information Table S8.8 for the detailed values). Based on the sensitivity analysis results, parameters with less than 1% influence are not shown.

Figure 8.6 presents the results for Scenario 4-WAB, with the most significant factor being the ash content in the paper sludge. A reduction in ash content to 30% significantly cuts the life cycle GWP value to 33.5 $gCO_2eq\ MJ^{-1}$. A lower ash content results in a higher biofuel yield and consequently a lower burden of feedstock transportation, handling, and pretreatment. Other significant factors include the glucose yield to HMF and the moisture content of paper sludge. The life-cycle GWP decreases to 33.8 $gCO_2eq\ MJ^{-1}$ if the glucose yield to HMF is enhanced from 66% to 79%. When the moisture content went up from 50% to 60%, the life-cycle GWP increases to 38.6 $gCO_2eq\ MJ^{-1}$. Higher moisture content causes lower biofuel yield and higher burdens of feedstock transportation, handling, and pretreatment. Reducing solvent (acetone) loss to 0.5% decreases the GWP by 3.1%. Other opportunities for GWP reduction include lowering enzyme load, increasing enzymatic hydrolysis consistency (also explored in Scenario 3; see **Table 8.2**), and minimizing sodium hydroxide (NaOH) dosage. Altering $AlCl_3$ load demonstrated relatively minor impacts on the GWP (-0.7%/+1.5%).

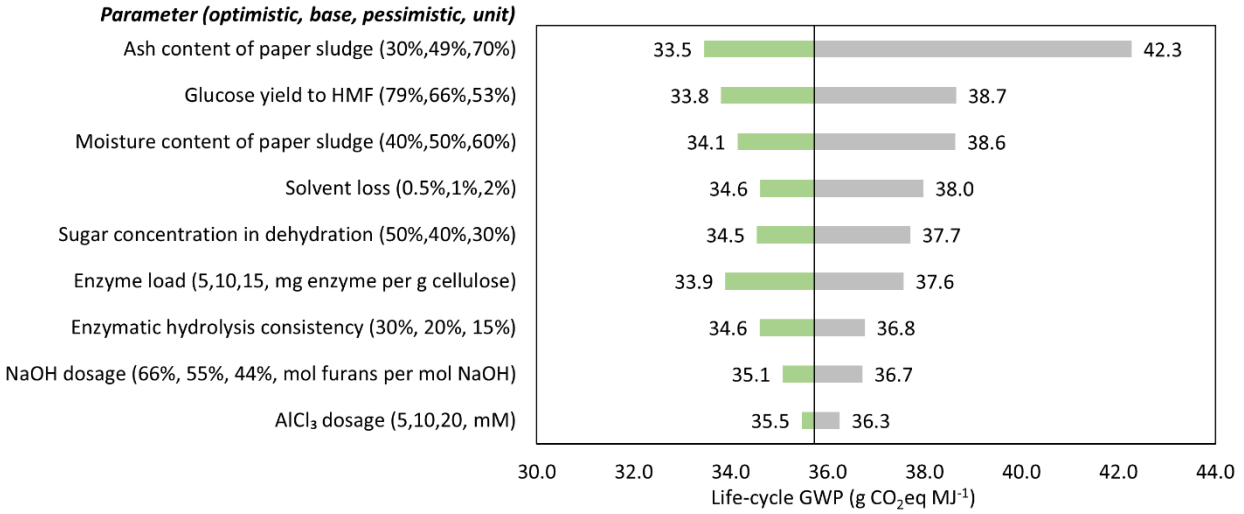

Figure 8.6. Sensitivity analysis of Scenario 4-WAB.

8.4. Conclusions

This study conducted a cradle-to-grave LCA for a SAF biorefinery via a catalytic sugar upgrading pathway in the U.S. The biorefinery valorizes high-ash paper sludge, a commonly landfilled material. In this study, a set of scenarios are developed to explore the effects of solvent choices (i.e., dioxane or acetone) and loads, fuel sources (i.e., natural gas or wood pellets), fossil-based or bio-based chemicals, ash utilization, and process parameters on the environmental impacts. Our study estimates the life-cycle GWP as 35.7–41.8 gCO_2eq per MJ of SAF when using acetone as the solvent, wood pellets as the fuel source, and bio-based MEK. The lower bound of the range, 35.7 $gCO_2eq\ MJ^{-1}$, can be achieved by increasing the sugar concentration in dehydration to reduce the solvent load and heat demand in solvent recycling. The life-cycle GWP range can be further reduced to 5.1–11.1 $gCO_2eq\ MJ^{-1}$ if the separated ash is recycled to replace a portion of high-carbon-intensity cement mortar materials rather than landfilling. This range has a GWP reduction of 86.8%–94.0% compared to petroleum-based jet fuel (84.5 $gCO_2eq\ MJ^{-1}$).[36,66] This highlights the importance of applying industrial ecology and circular economy principles.[75] Our results show that choosing acetone over dioxane, wood pellets over natural gas, and bio-based MEK over fossil-based MEK, can significantly reduce the life-cycle GWP of SAF. Using wood pellets increases environmental impact categories other than GWP and fossil fuel depletion due to the emissions of combusting wood. On the other hand, using bio-based MEK leads to a reduction in all impact categories except for fossil fuel depletion, which experiences a slight increase. This study also compares the GWP of converting 1 dry t paper sludge to SAF with landfilling. The lowest GWP ranges from -584 to -636 $kgCO_2eq$ per dry t of paper sludge without ash utilization and -873 to -925 $kgCO_2eq$ per dry t of paper sludge with ash utilization. These ranges are lower than conventional landfilling without landfill gas recovery (791 $kgCO_2eq$ per dry t of paper sludge) and landfilling with gas recovery (-294 $kgCO_2eq$ per dry t of paper sludge). The result of this study supports sustainability-informed process design and provides industry stakeholders and policy-makers with quantitative information on potential environmental benefits of producing SAF from waste streams.

References

1. Federal Aviation Administration. *The Economic Impact of Civil Aviation on the U.S. Economy*; 2020.
2. Lynd, L. R.; Beckham, G. T.; Guss, A. M.; Jayakody, L. N.; Karp, E. M.; Maranas, C.; McCormick, R. L.; Amador-Noguez, D.; Bomble, Y. J.; Davison, B. H.; Foster, C.; Himmel, M. E.; Holwerda, E. K.; Laser, M. S.; Ng, C. Y.; Olson, D. G.; Román-Leshkov, Y.; Trinh, C. T.; Tuskan, G. A.; Upadhayay, V.; Vardon, D. R.; Wang, L.; Wyman, C. E. Toward Low-Cost Biological and Hybrid Biological/Catalytic Conversion of Cellulosic Biomass to Fuels. *Energy Environ. Sci.* 2022, *15* (3), 938–990. https://doi.org/10.1039/d1ee02540f.
3. Gonzalez-Garay, A.; Heuberger-Austin, C.; Fu, X.; Klokkenburg, M.; Zhang, D.; van der Made, A.; Shah, N. Unravelling the Potential of Sustainable Aviation Fuels to Decarbonise the Aviation Sector. *Energy Environ. Sci.* 2022, *15* (8), 3291–3309. https://doi.org/10.1039/d1ee03437e.
4. Grim, R. G.; Ravikumar, D.; Tan, E. C. D.; Huang, Z.; Ferrell, J. R.; Resch, M.; Li, Z.; Mevawala, C.; Phillips, S. D.; Snowden-Swan, L.; Tao, L.; Schaidle, J. A. Electrifying the Production of Sustainable Aviation Fuel: The Risks, Economics, and Environmental Benefits of Emerging Pathways Including CO2. *Energy Environ. Sci.* 2022, *15* (11), 4798–4812. https://doi.org/10.1039/d2ee02439j.
5. ATAG. *Aviation Benefits beyond Borders*; 2020.
6. ATAG. *Facts & figures*. https://www.atag.org/facts-figures.
7. Seber, G.; Escobar, N.; Valin, H.; Malina, R. Uncertainty in Life Cycle Greenhouse Gas Emissions of Sustainable Aviation Fuels from Vegetable Oils. *Renew. Sustain. Energy Rev.* 2022, *170* (May), 112945. https://doi.org/10.1016/j.rser.2022.112945.
8. Pathak, M.; Slade, R.; Shukla, P. R.; Skea, J.; Pichs-Madruga, R.; Ürge-Vorsatz, D. 2022: Technical Summary. In *Climate Change 2022: Mitigation of Climate Change. Contribution of Working Group III to the Sixth Assessment Report of the Intergovernmental Panel on Climate Change*; Shukla, P. R., Skea, J., Slade, R., Khourdajie, A. Al, Diemen, R. van, McCollum, D., Pathak, M., Some, S., Vyas, P., Fradera, R., Belkacemi, M., Hasija, A., Lisboa, G., Luz, S., Malley, J., Eds.; Cambridge University Press: Cambridge, UK and New York, NY, USA, 2022.
9. Lee, D. S.; Fahey, D. W.; Skowron, A.; Allen, M. R.; Burkhardt, U.; Chen, Q.; Doherty, S. J.; Freeman, S.; Forster, P. M.; Fuglestvedt, J.; Gettelman, A.; De León, R. R.; Lim, L. L.; Lund, M. T.; Millar, R. J.; Owen, B.; Penner, J. E.; Pitari, G.; Prather, M. J.; Sausen, R.; Wilcox, L. J. The Contribution of Global Aviation to Anthropogenic Climate Forcing for 2000 to 2018. *Atmos. Environ.* 2021, *244* (February 2020). https://doi.org/10.1016/j.atmosenv.2020.117834.
10. Yao, Y. How Does COVID-19 Affect the Life Cycle Environmental Impacts of U.S. Household Energy and Food Consumption? *Environ. Res. Lett.* 2022, *17* (3). https://doi.org/10.1088/1748-9326/ac52cb.
11. UN ICAO. *ICAO Advocates for Decarbonization of Aviation at COP 27*; 2022. https://www.icao.int/Newsroom/Pages/ICAO-advocates-for-decarbonization-of-aviation-at-COP-27.aspx.
12. European-Commission. *Stepping up Europe's 2030 Climate Ambition Investing in a Climate-Neutral Future for the Benefit of Our People*; 2020.

13. US DOE; DOT; USDA; EPA. SAF Grand Challenge Roadmap Flight Plan for Sustainable Aviation Fuel. 2021, 1–128.
14. Bhatt, A. H.; Zhang, Y.; Milbrandt, A.; Newes, E.; Moriarty, K.; Klein, B.; Tao, L. Evaluation of Performance Variables to Accelerate the Deployment of Sustainable Aviation Fuels at a Regional Scale. *Energy Convers. Manag.* 2023, *275* (October 2022), 116441. https://doi.org/10.1016/j.enconman.2022.116441.
15. Cabrera, E.; Melo de Sousa, J. M. Use of Sustainable Fuels in Aviation—A Review. *Energies* 2022, *15* (7), 1–23. https://doi.org/10.3390/en15072440.
16. Ng, K. S.; Farooq, D.; Yang, A. Global Biorenewable Development Strategies for Sustainable Aviation Fuel Production. *Renew. Sustain. Energy Rev.* 2021, *150* (May), 111502. https://doi.org/10.1016/j.rser.2021.111502.
17. Kubic, W. L.; Moore, C. M.; Semelsberger, T. A.; Sutton, A. D. Recycled Paper as a Source of Renewable Jet Fuel in the United States. *Front. Energy Res.* 2021, *9* (October), 1–16. https://doi.org/10.3389/fenrg.2021.728682.
18. Royal NLR – Netherlands Aerospace Centre. *Feedstocks for Sustainable Aviation Fuels in the Netherlands*; 2021.
19. Gottumukkala, L. D.; Haigh, K.; Collard, F. X.; van Rensburg, E.; Görgens, J. Opportunities and Prospects of Biorefinery-Based Valorisation of Pulp and Paper Sludge. *Bioresour. Technol.* 2016, *215*, 37–49. https://doi.org/10.1016/j.biortech.2016.04.015.
20. Faubert, P.; Barnabé, S.; Bouchard, S.; Côté, R.; Villeneuve, C. Pulp and Paper Mill Sludge Management Practices: What Are the Challenges to Assess the Impacts on Greenhouse Gas Emissions? *Resour. Conserv. Recycl.* 2016, *108*, 107–133. https://doi.org/10.1016/j.resconrec.2016.01.007.
21. Wang, L.; Wang, J. G.; Littlewood, J.; Cheng, H. B. Co-Production of Biorefinery Products from Kraft Paper Sludge and Agricultural Residues: Opportunities and Challenges. *Green Chem.* 2014, *16* (3), 1527–1533. https://doi.org/10.1039/c3gc41984c.
22. Heinz, K. G. H.; Zanoni, P. R. S.; Oliveira, R. R.; Medina-Silva, R.; Simão, T. L. L.; Trindade, F. J.; Pereira, L. M.; Tavares, L. B. B.; Giongo, A. Recycled Paper Sludge Microbial Community as a Potential Source of Cellulase and Xylanase Enzymes. *Waste and Biomass Valorization* 2017, *8* (6), 1907–1917. https://doi.org/10.1007/s12649-016-9792-x.
23. Mahmood, T.; Elliott, A. A Review of Secondary Sludge Reduction Technologies for the Pulp and Paper Industry. *Water Res.* 2006, *40* (11), 2093–2112. https://doi.org/10.1016/j.watres.2006.04.001.
24. Park, H.; Cruz, D.; Tiller, P.; Johnson, D. K.; Mittal, A.; Jameel, H.; Venditti, R.; Park, S. Effect of Ash in Paper Sludge on Enzymatic Hydrolysis. *Biomass and Bioenergy* 2022, *165* (August), 106567. https://doi.org/10.1016/j.biombioe.2022.106567.
25. Han, J.; Elgowainy, A.; Cai, H.; Wang, M. Q. Life-Cycle Analysis of Bio-Based Aviation Fuels. *Bioresour. Technol.* 2013, *150*, 447–456. https://doi.org/10.1016/j.biortech.2013.07.153.
26. Lan, K.; Zhang, B.; Yao, Y. Circular Utilization of Urban Tree Waste Contributes to the Mitigation of Climate Change and Eutrophication. *One Earth* 2022, 1–14. https://doi.org/10.1016/j.oneear.2022.07.001.

27. Lan, K.; Yao, Y. Feasibility of Gasifying Mixed Plastic Waste for Hydrogen Production and Carbon Capture and Storage. *Commun. Earth Environ.* 2022, *3*, 300. https://doi.org/10.1038/s43247-022-00632-1.
28. Abrantes, I.; Ferreira, A. F.; Silva, A.; Costa, M. Sustainable Aviation Fuels and Imminent Technologies - CO2 Emissions Evolution towards 2050. *J. Clean. Prod.* 2021, *313* (June). https://doi.org/10.1016/j.jclepro.2021.127937.
29. Chao, H.; Agusdinata, D. B.; DeLaurentis, D.; Stechel, E. B. Carbon Offsetting and Reduction Scheme with Sustainable Aviation Fuel Options: Fleet-Level Carbon Emissions Impacts for U.S. Airlines. *Transp. Res. Part D Transp. Environ.* 2019, *75* (August 2019), 42–56. https://doi.org/10.1016/j.trd.2019.08.015.
30. Hayward, J. A.; O'Connell, D. A.; Raison, R. J.; Warden, A. C.; O'Connor, M. H.; Murphy, H. T.; Booth, T. H.; Braid, A. L.; Crawford, D. F.; Herr, A.; Jovanovic, T. The Economics of Producing Sustainable Aviation Fuel: A Regional Case Study in Queensland, Australia. *GCB Bioenergy* 2015, *7* (3), 497–511.
31. Michaga, M. F. R.; Michailos, S.; Hughes, K. J.; Ingham, D.; Pourkashanian, M. *Techno-Economic and Life Cycle Assessment Review of Sustainable Aviation Fuel Produced via Biomass Gasification*; INC, 2021. https://doi.org/10.1016/B978-0-12-820297-5.00012-8.
32. Oehmichen, K.; Majer, S.; Müller-langer, F.; Thrän, D. Comprehensive LCA of Biobased Sustainable Aviation Fuels and JET A-1 Multiblend. *Appl. Sci.* 2022, *12* (7). https://doi.org/10.3390/app12073372.
33. Prussi, M.; Lee, U.; Wang, M.; Malina, R.; Valin, H.; Taheripour, F.; Velarde, C.; Staples, M. D.; Lonza, L.; Hileman, J. I. CORSIA: The First Internationally Adopted Approach to Calculate Life-Cycle GHG Emissions for Aviation Fuels. *Renew. Sustain. Energy Rev.* 2021, *150* (June). https://doi.org/10.1016/j.rser.2021.111398.
34. Bachmann, J.; Hidalgo, C.; Bricout, S. Environmental Analysis of Innovative Sustainable Composites with Potential Use in Aviation Sector—A Life Cycle Assessment Review. *Sci. China Technol. Sci.* 2017, *60* (9), 1301–1317. https://doi.org/10.1007/s11431-016-9094-y.
35. Van Bentem, K. J. P. Techno-Economic Analysis of Sustainable Aviation Fuels by Using Traffic Forecasts and Fuel Price Projections: A Case Study at TUI Aviation. 2021.
36. Yoo, E.; Lee, U.; Wang, M. Life-Cycle Greenhouse Gas Emissions of Sustainable Aviation Fuel through a Net-Zero Carbon Biofuel Plant Design. *ACS Sustain. Chem. Eng.* 2022, *10* (27), 8725–8732. https://doi.org/10.1021/acssuschemeng.2c00977.
37. De Jong, S.; Antonissen, K.; Hoefnagels, R.; Lonza, L.; Wang, M.; Faaij, A.; Junginger, M. Life-Cycle Analysis of Greenhouse Gas Emissions from Renewable Jet Fuel Production. *Biotechnol. Biofuels* 2017, *10* (1), 1–18. https://doi.org/10.1186/s13068-017-0739-7.
38. Puschnigg, S.; Fazeni-Fraisl, K.; Lindorfer, J.; Kienberger, T. Biorefinery Development for the Conversion of Softwood Residues into Sustainable Aviation Fuel: Implications from Life Cycle Assessment and Energetic-Exergetic Analyses. *J. Clean. Prod.* 2023, *386* (December 2022), 135815. https://doi.org/10.1016/j.jclepro.2022.135815.

39. Gaudreault, C.; Samson, R.; Stuart, P. R. Energy Decision Making in a Pulp and Paper Mill: Selection of LCA System Boundary. *Int. J. Life Cycle Assess.* 2010, *15* (2), 198–211. https://doi.org/10.1007/s11367-009-0125-1.
40. Kamali, M.; Gameiro, T.; Elisabete, M.; Costa, V.; Capela, I. Anaerobic Digestion of Pulp and Paper Mill Aastes - an Overview of the Developments and Improvement Opportunities Anaerobic Digestion of Pulp and Paper Mill Wastes. *Chem. Eng. J.* 2018, *298* (January), 162–182.
41. Manda, B. M. K.; Blok, K.; Patel, M. K. Innovations in Papermaking: An LCA of Printing and Writing Paper from Conventional and High Yield Pulp. *Sci. Total Environ.* 2012, *439*, 307–320. https://doi.org/10.1016/j.scitotenv.2012.09.022.
42. Likon, M.; Saarela, J. The Conversion of Paper Mill Sludge into Absorbent for Oil Spill Sanitation - The Life Cycle Assessment. *Macromol. Symp.* 2012, *320* (1), 50–56. https://doi.org/10.1002/masy.201251006.
43. Mohammadi, A.; Sandberg, M.; Venkatesh, G.; Eskandari, S.; Dalgaard, T.; Joseph, S.; Granström, K. Environmental Performance of End-of-Life Handling Alternatives for Paper-and-Pulp-Mill Sludge: Using Digestate as a Source of Energy or for Biochar Production. *Energy* 2019, *182*, 594–605. https://doi.org/10.1016/j.energy.2019.06.065.
44. Sebastião, D.; Gonçalves, M. S.; Marques, S.; Fonseca, C.; Gírio, F.; Oliveira, A. C.; Matos, C. T. Life Cycle Assessment of Advanced Bioethanol Production from Pulp and Paper Sludge. *Bioresour. Technol.* 2016, *208*, 100–109. https://doi.org/10.1016/j.biortech.2016.02.049.
45. Arena, U.; Mastellone, M. L.; Perugini, F.; Clift, R. Environmental Assessment of Paper Waste Management Options by Means of LCA Methodology. *Ind. Eng. Chem. Res.* 2004, *43* (18), 5702–5714. https://doi.org/10.1021/ie049967s.
46. Villanueva, A.; Wenzel, H. Paper Waste - Recycling, Incineration or Landfilling? A Review of Existing Life Cycle Assessments. *Waste Manag.* 2007, *27* (8). https://doi.org/10.1016/j.wasman.2007.02.019.
47. Sluiter, J. B.; Ruiz, R. O.; Scarlata, C. J.; Sluiter, A. D.; Templeton, D. W. Compositional Analysis of Lignocellulosic Feedstocks. 1. Review and Description of Methods. *J. Agric. Food Chem.* 2010, *58* (16), 9043–9053. https://doi.org/10.1021/jf1008023.
48. De Assis, C. A.; Iglesias, M. C.; Bilodeau, M.; Johnson, D.; Phillips, R.; Peresin, M. S.; Bilek, E. M.; Rojas, O. J.; Venditti, R.; Gonzalez, R. Cellulose Micro- and Nanofibrils (CMNF) Manufacturing - Financial and Risk Assessment. *Biofuels, Bioprod. Biorefining* 2017, *12* (2), 251–264. https://doi.org/10.1002/bbb.
49. Chen, H.; Han, Q.; Daniel, K.; Venditti, R.; Jameel, H. Conversion of Industrial Paper Sludge to Ethanol: Fractionation of Sludge and Its Impact. *Appl. Biochem. Biotechnol.* 2014, *174* (6), 2096–2113. https://doi.org/10.1007/s12010-014-1083-z.
50. Gurram, R. N.; Al-Shannag, M.; Lecher, N. J.; Duncan, S. M.; Singsaas, E. L.; Alkasrawi, M. Bioconversion of Paper Mill Sludge to Bioethanol in the Presence of Accelerants or Hydrogen Peroxide Pretreatment. *Bioresour. Technol.* 2015, *192*, 529–539. https://doi.org/10.1016/j.biortech.2015.06.010.
51. Mäkinen, L.; Ämmälä, A.; Körkkö, M.; Niinimäki, J. The Effects of Recovering Fibre and Fine Materials on Sludge Dewatering Properties at a Deinked Pulp Mill. *Resour. Conserv. Recycl.* 2013, *73*, 11–16. https://doi.org/10.1016/j.resconrec.2013.01.011.

52. Smol, M.; Kulczycka, J.; Henclik, A.; Gorazda, K.; Wzorek, Z. The Possible Use of Sewage Sludge Ash (SSA) in the Construction Industry as a Way towards a Circular Economy. *J. Clean. Prod.* 2015, *95*, 45–54. https://doi.org/10.1016/j.jclepro.2015.02.051.
53. Bin Mohd Sani, M. S. H.; Bt Muftah, F.; Ab Rahman, M. Properties of Waste Paper Sludge Ash (WPSA) as Cement Replacement in Mortar to Support Green Technology Material. *3rd ISESEE 2011 - Int. Symp. Exhib. Sustain. Energy Environ.* 2011, No. June, 94–99. https://doi.org/10.1109/ISESEE.2011.5977117.
54. Chen, M.; Zheng, Y.; Zhou, X.; Li, L.; Wang, S.; Zhao, P.; Lu, L.; Cheng, X. Recycling of Paper Sludge Powder for Achieving Sustainable and Energy-Saving Building Materials. *Constr. Build. Mater.* 2019, *229*, 116874. https://doi.org/10.1016/j.conbuildmat.2019.116874.
55. Shubbar, A. A.; Sadique, M.; Nasr, M. S.; Al-Khafaji, Z. S.; Hashim, K. S. The Impact of Grinding Time on Properties of Cement Mortar Incorporated High Volume Waste Paper Sludge Ash. *Karbala Int. J. Mod. Sci.* 2020, *6* (4), 396–403. https://doi.org/10.33640/2405-609X.2149.
56. Humbird, D.; Davis, R.; Tao, L.; Kinchin, C.; Hsu, D.; Aden, A.; Schoen, P.; Lukas, J.; Olthof, B.; Worley, M.; Sexton, D.; Dudgeon, D. *Process Design and Economics for Biochemical Conversion of Lignocellulosic Biomass to Ethanol: Dilute-Acid Pretreatment and Enzymatic Hydrolysis of Corn Stover (No. NREL/TP-5100-47764)*; Golden, CO, 2011. https://doi.org/10.2172/1013269.
57. Mittal, A.; Pilath, H. M.; Johnson, D. K. Direct Conversion of Biomass Carbohydrates to Platform Chemicals: 5-Hydroxymethylfurfural (HMF) and Furfural. *Energy and Fuels* 2020, *34* (3), 3284–3293. https://doi.org/10.1021/acs.energyfuels.9b04047.
58. Klein, B.; Mcnamara, I.; Davis, R.; Mittal, A.; Johnson, D.; Klein, B.; Mcnamara, I.; Davis, R.; Mittal, A.; Johnson, D. *Techno-Economic Assessment for the Production of Hydrocarbon Fuels via Catalytic Upgrading of Furans Techno-Economic Assessment for the Production of Hydrocarbon Fuels via Catalytic Upgrading of Furans*; 2021.
59. Degenstein, J.; Kamireddy, S. R.; Tucker, M. P.; Ji, Y. Oligomer Saccharide Reduction during Dilute Acid Pretreatment Co-Catalyzed with Lewis Acids on Corn Stover Biomass. *Int. J. Agric. Biol. Eng.* 2013, *6* (2), 54–62. https://doi.org/10.3965/j.ijabe.20130602.00?
60. US DOE Office of EERE. *DOE/EE-1334 Combined Heat and Power Technology Fact Sheet Series*; 2016. https://www.energy.gov/sites/prod/files/2016/09/f33/CHP-Steam Turbine.pdf.
61. Seber, G.; Escobar, N.; Valin, H.; Malina, R. Uncertainty in Life Cycle Greenhouse Gas Emissions of Sustainable Aviation Fuels from Vegetable Oils. *Renew. Sustain. Energy Rev.* 2022, *170* (October), 112945. https://doi.org/10.1016/j.rser.2022.112945.
62. ISO. *ISO 14040:2006 Environmental Management — Life Cycle Assessment — Principles and Framework*; 2006. https://www.iso.org/standard/37456.html.
63. ISO. *ISO 14044: Environmental Management, Life Cycle Assessment, Requirements and Guidelines*; 2006.
64. Lee, J. W.; Bhagwat, S. S.; Kuanyshev, N.; Cho, Y. B.; Sun, L.; Lee, Y. G.; Cortés-Peña, Y. R.; Li, Y.; Rao, C. V.; Guest, J. S.; Jin, Y. S. Rewiring Yeast Metabolism

for Producing 2,3-Butanediol and Two Downstream Applications: Techno-Economic Analysis and Life Cycle Assessment of Methyl Ethyl Ketone (MEK) and Agricultural Biostimulant Production. *Chem. Eng. J.* 2023, *451* (June 2022). https://doi.org/10.1016/j.cej.2022.138886.

65. Wernet, G.; Bauer, C.; Steubing, B.; Reinhard, J.; Moreno-Ruiz, E.; Weidema, B. The Ecoinvent Database Version 3 (Part I): Overview and Methodology. *Int. J. Life Cycle Assess.* 2016, *21* (9), 1218–1230. https://doi.org/10.1007/s11367-016-1087-8.
66. Argonne National Laboratory. *The Greenhouse Gases, Regulated Emissions, and Energy Use in Technologies (GREET) Model*; 2022.
67. Gentil, E. C.; Damgaard, A.; Hauschild, M.; Finnveden, G.; Eriksson, O.; Thorneloe, S.; Kaplan, P. O.; Barlaz, M.; Muller, O.; Matsui, Y.; Ii, R.; Christensen, T. H. Models for Waste Life Cycle Assessment: Review of Technical Assumptions. *Waste Manag.* 2010, *30* (12), 2636–2648. https://doi.org/10.1016/j.wasman.2010.06.004.
68. Towprayoon, S.; Ishigaki, T.; Chiemchaisri, C.; Abdel-Aziz, A. O.; Hunstone, M. E.; Jarusutthirak, C.; Ritzkowski, M.; Thomsen, M. Chapter 3: Solid Waste Disposal. In *2019 Refinement to the 2006 IPCC Guidelines for National Greenhouse Gas Inventories*; 2019; Vol. 5, pp 6.1-6.49.
69. US EPA. *Landfill Methane Outreach Program (LMOP)*. https://www.epa.gov/lmop/project-and-landfill-data-state.
70. Anshassi, M.; Sackles, H.; Townsend, T. G. A Review of LCA Assumptions Impacting Whether Landfilling or Incineration Results in Less Greenhouse Gas Emissions. *Resour. Conserv. Recycl.* 2021, *174* (May), 105810. https://doi.org/10.1016/j.resconrec.2021.105810.
71. IPCC. *Climate Change 2021: The Physical Science Basis AR 6 Work Group I*; 2022.
72. Ryberg, M.; Vieira, M. D. M.; Zgola, M.; Bare, J.; Rosenbaum, R. K. Updated US and Canadian Normalization Factors for TRACI 2.1. *Clean Technol. Environ. Policy* 2014, *16* (2), 329–339. https://doi.org/10.1007/s10098-013-0629-z.
73. US EPA. *Renewable Fuel Standard Program*. https://www.epa.gov/renewable-fuel-standard-program.
74. The White House. *Inflation Reduction Act Guidebook*. https://www.whitehouse.gov/cleanenergy/inflation-reduction-act-guidebook/.
75. Muscat, A.; de Olde, E. M.; Ripoll-Bosch, R.; Van Zanten, H. H. E.; Metze, T. A. P.; Termeer, C. J. A. M.; van Ittersum, M. K.; de Boer, I. J. M. Principles, Drivers and Opportunities of a Circular Bioeconomy. *Nat. Food* 2021, *2* (8), 561–566. https://doi.org/10.1038/s43016-021-00340-7.

Chapter 9: Learnings and remarks for future work

9.1. Paper sludge to fuel project learnings

- ✓ Carbohydrates in paper sludge can be converted to hydrocarbons with excellent properties for blending into jet fuel (and diesel)
- ✓ Good flash point, freezing point, energy density, v. low O content, surface tension, viscosity, cetane value.
- ✓ About 35% of the diesel boiling range is above the jet range (overall 80% could be blended into jet and diesel).
- ✓ Properties confirmed at 2 laboratories, tier α and β tests completed.

9.2. How does paper sludge compare to other feedstocks?

- ✓ After ash removal there are few differences – Sidehill screen did an excellent job separating ash from the fiber.
- ✓ Dissolved CaCO3 and CaCl2 required pH adjustment with HCl for effective enzymatic hydrolysis, but this did not affect the yields of HMF and furfural.
- ✓ Yields of HMF and furfural, and aldol condensation products are very similar to pure sugars, corn stover hydrolysate, and paper sludge hydrolysate.
- ✓ Small differences in yields from the HDO step. Oxygenated products were slightly more persistent in paper sludge-derived feed compared to pure sugar feed.

9.3. Changes since intermediate verification

- ✓ Enzymatic hydrolysis can be scaled up into a 30 L paddle reactor.
- ✓ 50 L of furfurals solutions could be produced in a flow reactor.
- ✓ Dehydration solvent could be switched from dioxane to acetone while maintaining yields.
- ✓ Solvent change had a big impact on decreasing costs and CO2 emissions of the process.

9.4. Remarks for future work

9.4.1. Steps for decreasing process costs

- ✓ Increase solids concentration and decrease enzyme used in the hydrolysis step.
- ✓ Increase HMF and furfural yields in the dehydration step (solid catalyst instead of $AlCl_3$).
- ✓ Increase sugar concentration in the dehydration step and reduce the solvent ratio.
- ✓ Purify furfural feed prior to aldol condensation – Impurities increase the amount of NaOH needed, which I think leads to lower adduct yields.
- ✓ Removing impurities could also improve yields from the HDO step and decrease the amount of higher boiling hydrocarbons in the final product.

9.4.2. Steps for decreasing CO_2 emissions from the process

- ✓ Increase overall yield of hydrocarbons from the process.
- ✓ Decrease energy used by the process – Decrease the amount of solvent that needs recycling, increase feed concentrations, and decrease enzyme usage.
- ✓ Change base from NaOH to a solid base, e.g., $Sr(OH)_2$ that is more easily recycled.

- ✓ Look at possibilities of using renewable H_2 and natural gas.
- ✓ Examine the possibility of utilizing the ash instead of disposing of it.

9.4.3. Steps for scaling the process towards commercialization

- ✓ Interest pulp companies in partnering to develop this process.
- ✓ Interest petroleum companies in partnering to develop the process or at least HDO processing.
- ✓ Demonstrate process in pilot scale equipment, deashing, enzymatic hydrolysis, dehydration, aldol condensation, and HDO in a flow reactor.